MODIFICATION OF IRON BINDING LIGANDS IN ISOPENICILLIN N SYNTHASE

by

Malkit Sami

Wolfson College,

Oxford

A thesis submitted to the board of the faculty of Physical Sciences in partial fulfilment of the requirements for the degree of Doctor of Philosophy

Michaelmas Term, 1998

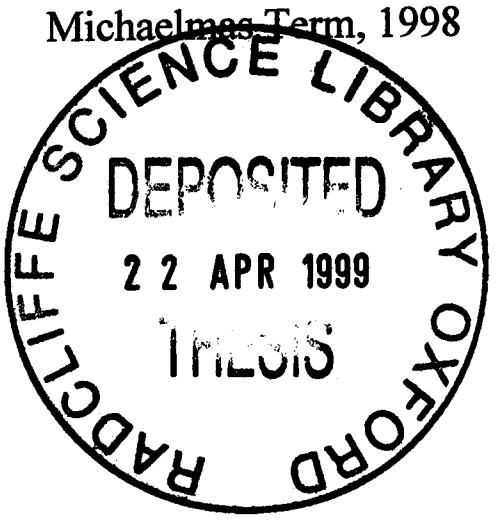

MUTAGENESIS OF IRON BINDING LIGANDS IN ISOPENICILLIN N SYNTHASE

Malkit Sami
Wolfson College

D. Phil. Thesis
Michaelmas Term, 1998

ABSTRACT

Isopenicillin N synthase (IPNS) is a non-haem iron dependent dioxygenase which catalyses the oxidative conversion of δ-(*L*-α-aminoadipoyl)-*L*-cysteinyl-*D*-valine (ACV) to isopenicillin N (IPN). Sequence comparisons between IPNS isozymes reveal the complete conservation of two histidine (His214, His270), one aspartate (Asp216) [also known as the '2-His-1-carboxylate' motif] and one glutamine (Gln330) residue. The crystal structure of IPNS (*Aspergillus nidulans*) active site (in the absence of ACV) revealed an octahedrally coordinated manganese atom surrounded by these four protein ligands and two water molecules.

The role of the four conserved metal binding ligands was investigated using site directed mutagenesis. The results demonstrated that ligation of the iron with Gln330 was not essential for the catalytic activity of IPNS. In contrast, ligation of the iron with the three remaining metal ligands was indispensable for catalytic activity. Additionally, it was demonstrated that the conserved Asp216 residue may be substituted by a glutamate residue (D216E) with significant retention of catalytic activity. Crystallographic and spectroscopic evidence suggested that the D216E mutant bound both iron and ACV in a similar way to wild-type IPNS.

The inactivation of wild-type IPNS was examined under *in vitro* assay conditions. This study showed that inactivation of IPNS results (minimally) from a slow non-oxidative pathway (in buffer alone) and a fast oxidative pathway *via* Udenfriend's chemistry (ferrous iron, ascorbate, and oxygen). The oxidative inactivation pathway was substantially reduced by the inclusion of catalase in the assay mixture, thus indicating that oxidative IPNS inactivation results (in part) from the generation of hydrogen peroxide in solution. Inactivation was also accompanied by a slow fragmentation of intact IPNS into (at least) five oligopeptides (observed by sodium dodecyl sulphate polyacrylamide gel electrophoresis). N-Terminal sequencing analyses confirmed that the fragmentation resulted from at least two cleavage sites within the active site (between Asp216-Val217 and Val272-Lys273).

To Jaswinder, Arvind and Amrit

Table of Contents

Acknowledgements

I would like to thank Professor C. Schofield for his supervision, his constant enthusiasm and continuing stream of ideas throughout this project. I would also like to thank Professor (Sir) J. E. Baldwin for giving me the opportunity to work in this department, initially as a Research Technician and then as a graduate student. I thank B.B.S.R.C. for a postgraduate studentship and O.C.M.S. for financial help with the conference.

I am indebted to many technical and support staff of the Dyson Perrins Laboratory and the O.C.M.S. In particular Wendy Sobey, John Keeping, Jon Pitt, Elizabeth McGuiness, Tony Willis, Steve Lee, Ann Asprey, Sarah Hargreaves and Patrica Knall. I also acknowledge the expertise of Dr Robin Aplin with mass spectrometric analysis and Dr Michael Gross with the CD analysis.

Throughout my time as a graduate student, I was fortunate to work with some good people who provided a sociable atmosphere in the lab as well as outside. Many thanks go to Dr Nicolai Burzlaff who made it possible to do many crystallisation experiments and structural refinements; Drs Matthew Lloyd and Peter Roach with proof reading, HPLC problems and NMR experiments; Dr Alain Dubus (our collaborator from the University of Liege, Belgium) and Toby Brown with kinetic analysis and fruitful discussions about the IPNS project; Ian, Penny, Meng Huee and Li Ching for their help; Dr Rupert Wilmouth (the lab scapegoat) for proof reading and all my computing problems. I also like to thank members of room 30, especially Alex Long, Peter Rutledge for making substrate analogues.

Finally, I owe much to my family (especially my wife Jaswinder) who have put up with my unusual working hours and for their total support during my studies.

Abbreviations

ACA	δ-(*L*-α-aminoadipoyl)-*L*-cysteinyl-*D*-alanine
ACG	δ-(*L*-α-aminoadipoyl)-*L*-cysteinyl-glycine
ACAB	δ-(*L*-α-aminoadipoyl)-*L*-cysteinyl-*D*-α-aminobutyrate
ACC	1-aminocycopropane-1-carboxylate
ACCO	1-aminocycopropane-1-carboxylate oxidase
ACV	δ-(*L*-α-aminoadipoyl)-*L*-cysteinyl-*D*-valine
ADP	adenosine monophosphate
AUFS	absorption units at full scale deflection
BSA	bovine serum albumin
CD	circular dichroism
1,2-CTD	catechol 1,2-dioxygenase
Da	Dalton
DAC	deacetylcephalosporin C
DACS	deacetylcephalosporin C synthase
DAOC	deacetoxycephalosporin C
DAOCS	deacetoxycephalosporin C synthase
dpm	disintegrations per minute
DTT	dithiothreitol
E. coli	*Escherichia coli*
EDTA	ethylenediaminetetraacetic acid
EPR	electron paramagnetic resonance
ESIMS	electrospray ionisation mass spectrometry
FPLC	fast protein liquid chromatography
GC	gas chromatography
GSH	glutathione (γ-glutaminylcysteinylglycine)
HEPES	N-(2-hydroxyethyl)piperazine-N′-(2-ethanesulphonic acid)
HPLC	high performance liquid chromataography
4-HPPD	4-hydroxyphenolpyruvate dioxygenase

IPN	isopenicillin *N*
IPNS	isopenicillin *N* synthase
J	NMR coupling constant
α-KG	α-ketoglutarate
LAA	*L*-α-aminoadipoyl
LB	Luria-Bertani
LMCT	ligand to metal charge transfer
MW	molecular weight
NMR	nuclear magnetic resonance
ODS	octadecylsilyl
PAGE	polyacrylamide gel electrophoresis
ppm	parts per million
3,4-PCD	protocatechuate 3,4-dioxygenase
P-3H	proline 3-hydroxylase
PVDF	polyvinylidene difluoride
rpm	revolutions per minute
SDS	sodium dodecyl sulphate
TEMED	*N,N,N′,N′*-tetramethylethylenediamine
Tris	trishydroxymethylaminomethane
TSP	3-(Trimethyl silyl) propionic acid
2TY	tryptone yeast
TyrOH	tyrosine hydroxylase

CHAPTER 1

Introduction

1.1 Metal ions in biology

The transition metals are the amongst the least abundant metal ions in the sea water from which contemporary organisms are thought to have evolved[1,2]. For many of the transition metals the concentration in the plasma exceeds that in the sea water[3]. Living organisms store and transport transition metals to provide appropriate concentrations for use in metallo-proteins and cofactors to protect themselves against the toxic effects of metal excesses[4,5]. Transition metals for which biological storage and transport is significant, in order of decreasing abundance in organisms, include: iron, zinc, copper, molybdenum, cobalt, chromium, vanadium and nickel. The knowledge for iron storage and transport is more complete than for any other metal in this group[6].

Iron is the most abundant transition metal in the earth's crust and, in general, all life forms. It has been proposed that, under the anaerobic environment of the earth (several billion years ago), the availability of ferrous iron was one of the factors that led to its incorporation into so many metabolic processes of the earliest life forms. In an oxidising environment iron is present in the ferric form which has low solubility at physiological pH [concentration of Fe(III) $\sim 10^{-18}$ M]. Because of the low solubility of ferric ions at physiological pH, micro-organisms have developed numerous ways to overcome this iron deficiency[7]. Some micro-organisms acquire iron by the secretion of high-affinity iron binding compounds called siderophores[8]. The iron uptake rates of these siderophores shows saturatable kinetics with a dissociation constant for iron in the micromolar range. The siderophore enterobactin is shown in Figure 1.1.

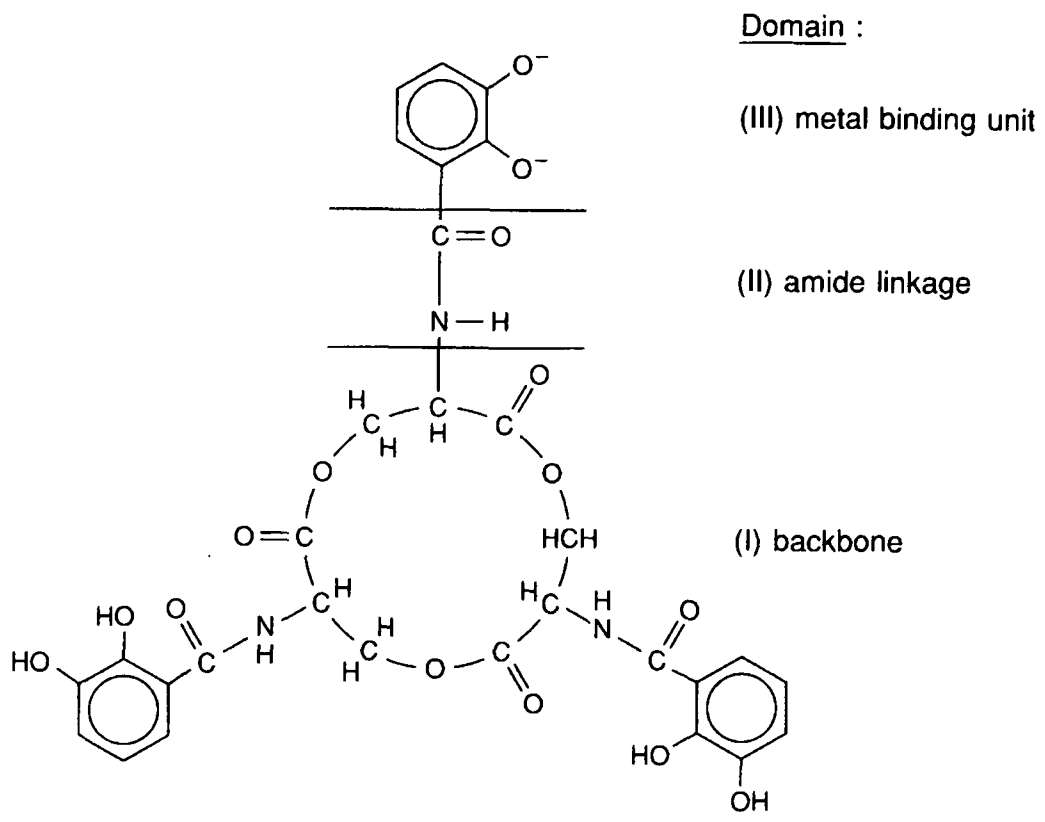

Figure 1.1 Enterobactin.

Some micro-organisms and some higher organisms have developed specialised iron storage proteins called ferritins. The concentration of Fe(III) in ferritins has been shown to be 10^{14} times greater than the concentration in solution at physiological pH[9]. The transport of iron from storage sites (in cellular ferritins) is tightly controlled and occurs *via* the serum transport protein transferrin[6].

Metal ions are required for critical functions in many cellular processes in higher organisms. In humans a deficiency of iron in the diet is known to cause pernicious anaemia[10,11]. The amount of iron within a healthy human individual is around 4-5 g per 75 kg which is complexed to many different proteins within the cells. Most of the iron is present in haemoglobin, the plasma oxygen transport protein (Table 1.1).

Table 1.1 Average iron distribution in humans (adapted from Theil and Raymond, 1994[8]).

Protein	Function	Oxidation state of Fe	Amount of Fe (g)	Percent of total
Haemoglobin	Plasma, O_2 transport	2	2.6	65
Myoglobin	Muscle, O_2 transport	2	0.13	6
Transferrin	Plasma Fe transport	3	0.007	0.2
Ferritin	Cell Fe storage	3	0.52	13
Hemosiderin	Cell Fe storage	3	0.48	12
Catalase	H_2O_2 metabolism	2	0.004	0.1
Cytochrome *c*	Electron transport	2	0.004	0.1
Other	Oxidases, other enzymes	2/3	0.14	3.6

1.2 Metallo-proteins

The polypeptide backbone of all proteins is made up of 20 common *L*-amino acids folded into compact three dimensional structures. The transition metal ions are commonly found at the active sites of the metallo-proteins where their role may be either: (a) to act as a collecting point for the reactants, (b) catalytic (to enhance the acidity of the co-ordinated ligand), (c) to serve as redox centres for the manipulations of electron transfer in redox reactions, or (d) structural.

1.2.1 Role of metals

Biological systems rarely have extremes of pH corresponding to conditions under which the catalysis, *e.g.* amide hydrolysis, by H^+ or OH^- can occur at reasonable rates. One mechanism harnessed by nature is to use the acidity of certain metal ions, particularly zinc, and build them into the protein structures in order to accomplish the catalysis of specific reactions. Zinc is used in a number of enzymes as a Lewis acid to co-ordinate carbonyl groups present in the substrate and hence activate them towards nucleophilic attack. Examples include carboxypeptidase A, a Zn dependent peptidase[12] and carbonic anhydrase, a Zn dependent enzyme found in the red blood cells. The crystal structure of carbonic anhydrase revealed a Zn ion in the active site with a distorted tetrahedral geometry[13]. Carbonic anhydrase catalyses the hydration of carbon dioxide at a rate of 10^6 s^{-1} (*ca.* 10^9 times the rate of uncatalysed turnover). Zinc ions are also used structurally to maintain tertiary structure, *e.g.* in the zinc finger DNA binding proteins by co-ordination with the thiolate side chains of four cysteine residues[14].

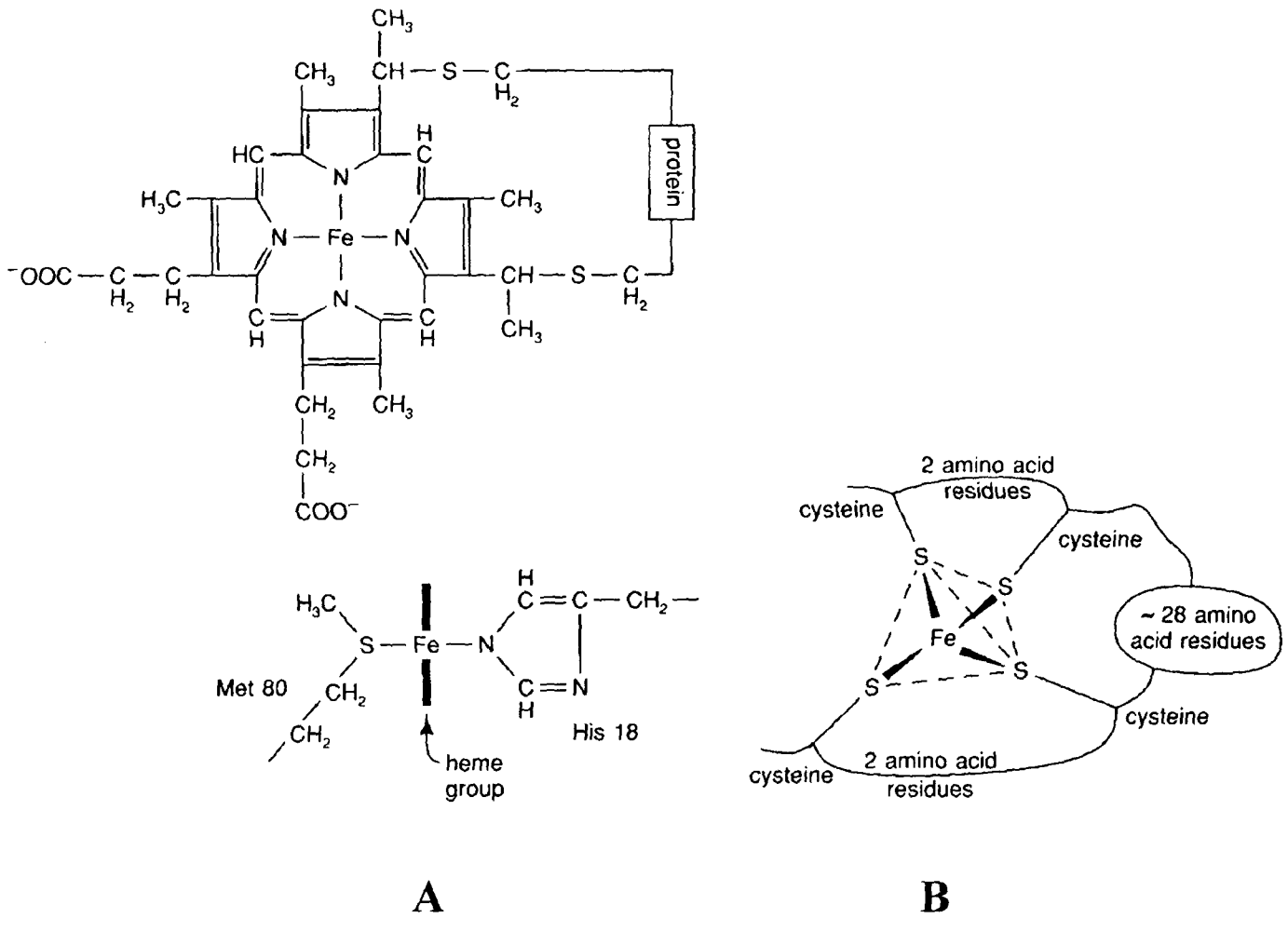

Figure 1.2 Electron transfer metallo-proteins. Haem type cytochrome *c* (A); FeS type rubredoxin (B) (adapted from Theil and Raymond, 1994[8]).

The other common role of metal ions are as redox reagents. Since a majority of the 20 common amino acids alone are not able to perform any useful catalytic redox chemistry, it is not surprising that redox enzymes employ metal ions. One class of redox proteins are the cytochromes which are a large group of proteins containing an iron prosthetic group[15]. In cytochrome *c* the iron atom is bound to a porphyrin prosthetic group *via* four planar nitrogen atoms (Figure 1.2). It is the high degree of mesomerism inherent within the porphyrin structure which allows a particular substituent on the porphyrin ring to relay its electron donating or attracting tendency to all four co-ordinating atoms. A wide range of reduction potentials for iron is achieved in biology by subtle variations in differences in the protein structure, as listed in Table 1.2. The

standard reduction potential for hydrated iron is 0.77 volts compared with that observed for cytochrome *c* of 0.39 volts[8]. It is thought that the highly resonant porphyrin ring system leads to the increased stability seen in cytochromes.

Table 1.2 Redox potentials of some iron complexes (adapted from Theil and Raymond, 1994[8]).

Complex	Co-ordination number	Fe(III)/Fe(II) E^o (mV)
$Fe(OH_2)_6^{3+}$	6 aquo complex	770
Cytochrome a_3	6, haem	390
Cytochrome *c*	6, haem	250
Rubredoxin	4, $Fe(SR)_4$	-60
Ferridoxin	4, Fe_4 S4 $(SR)_4^{2-}$	-400

Most higher organisms use iron co-ordinated prosthetic groups in their redox enzymes but some lower organisms use copper instead of iron[16]. The light harvesting complex of plants contains a chlorophyll prosthetic group which is quite similar to the porphyrin of haem except that normally a co-ordinated magnesium atom is substituted for the iron atom[17].

Table 1.3 summarises the role of some metal ions observed in metal-binding proteins. Metallo-enzymes represent 40 % of all enzymes found in nature and range in sizes from small proteins (*e.g.* 80 amino acids cytochrome c_{551}) to very large multi-domain entities (*e.g.* glutamine synthetase, MW 619 kDa). The transition metals show a variation in their oxidation states and preferences for the donor atom. Manganese and calcium (s-block)

show a preference for oxygen donors. Iron, copper and cobalt (d-block) show a preference for nitrogen, oxygen and sulphur donors.

Table 1.3 Examples of metal ligands in biology.

Metal	Donors	Examples
Ca^{2+}	Only O donors known (Glu, Asp, Ser)	Calmodulin, hydroxyapatite (bone and teeth)
Mg^{2+}	O preferred (phosphate)	Kinases, phosphatases, DNA, RNA
Zn^{2+}	N, O, and S (His, Glu, Asp, Cys)	Carboxypeptidase A Carbonic anhydrase
Fe^{2+}	N, O, and S (His, Asp, Glu, Cys)	IPNS/DAOCS Haemoglobin Transferrin
Cu^{2+}	N, O, and S (His, Asp, Glu, Cys)	Plastocyanin
Mn^{2+}	O preferred over N, S	Hydratases
Co^{2+}	N, O, and S	Vitamin B_{12} coenzyme
Hg^{2+}	Favours S donors	Mercuric reductase

X-ray crystal structures have revealed various geometric arrangements of the metal binding ligands in metallo-enzymes. In some cases the crystalline form is not the one pertaining to physiological environments *in vivo* and therefore it is questionable whether the structures in solution and in crystal are really comparable. The possibility exists that the conformations are different, and so attempts to interpret the crystal structure in detail and relate this directly to the function may be misleading. High resolution NMR techniques are available for determining the structures of some proteins, but at present this technique is limited to proteins < 30 kDa.

1.2.2 Geometry of metal ligands

Some co-ordination environments observed for metallo-proteins are shown in Figure 1.3a. Tetrahedral geometries are found in iron and copper electron transfer proteins, rubredoxin[18], plastocyanin[19].

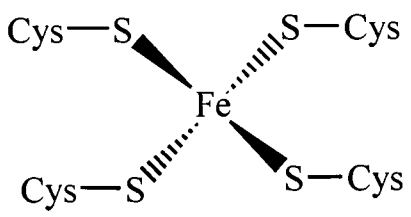

Rubredoxin

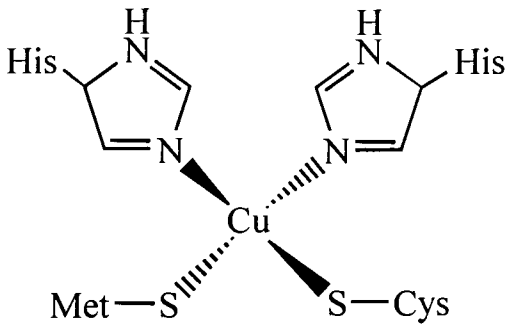

Plastocyanin

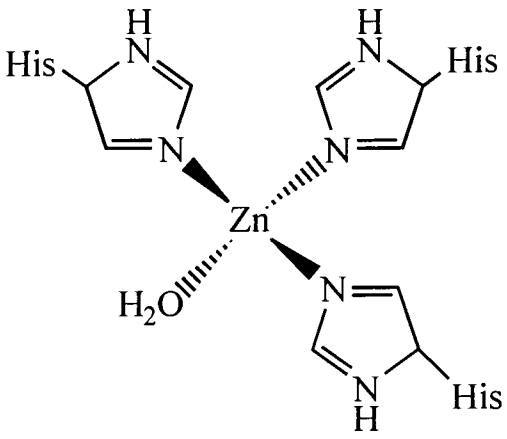

Carbonic anhydrase

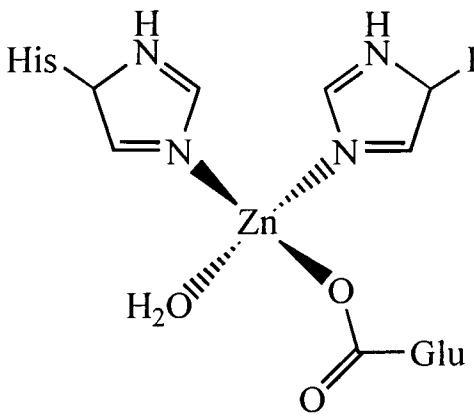

β-lactamase

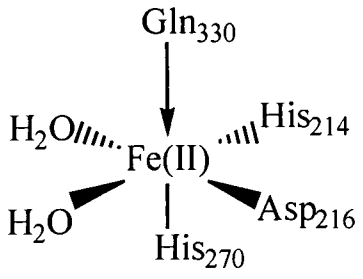

IPNS

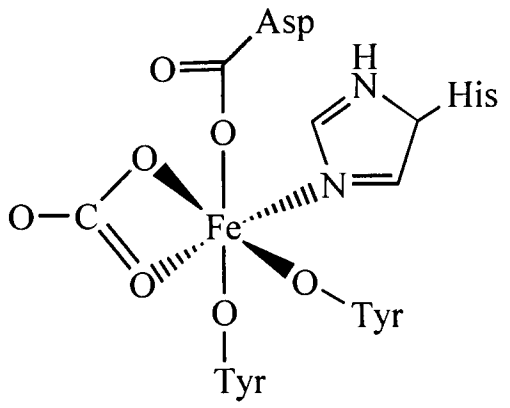

Transferrin

Figure 1.3a Structurally defined metal binding ligands in mononuclear metallo-enzymes. The protonation states of histidine and water molecules are shown arbitrarily.

A tetrahedral geometry is also observed for zinc enzymes, carbonic anhydrase[13] and metallo β-lactamases[20], with the unsymmetrical tetrahedral geometry being a unique feature of the zinc sites. Octahedral geometries have been found in both haem proteins, *e.g.* cytochrome *c* and haemoglobin[21,22], and non-haem proteins, *e.g.* transferrin[23] and IPNS[24].

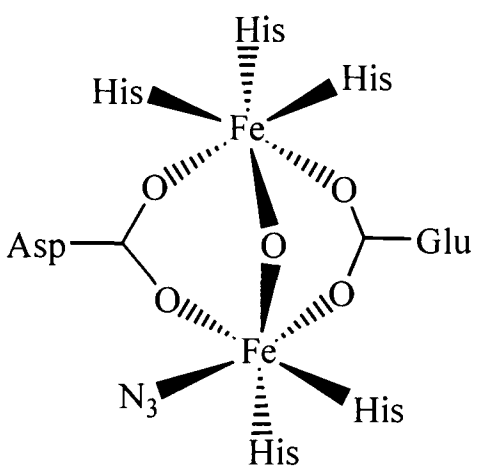

Haemerythrin

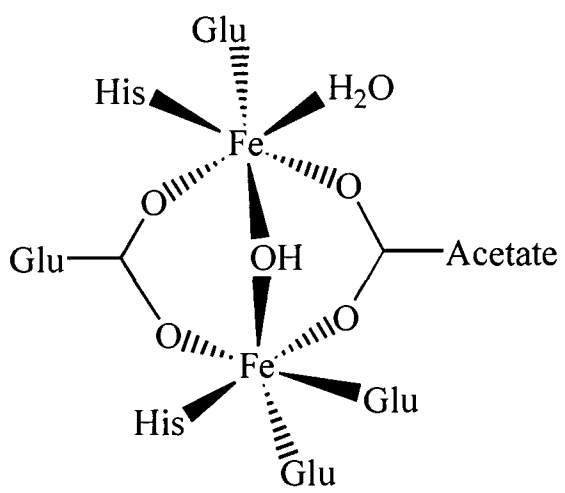

Methane monoxygenase

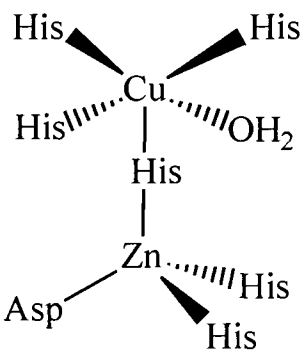

Superoxide dismutase

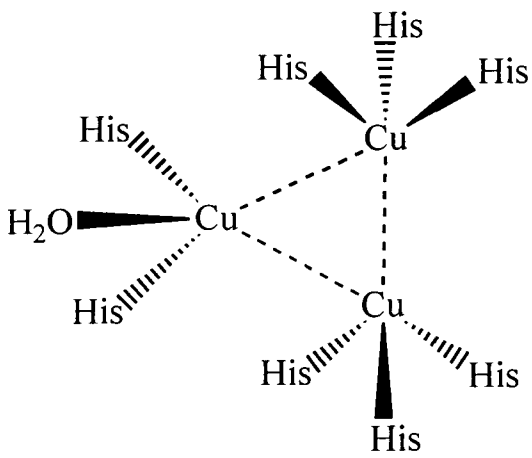

Ascorbate oxidase

Figure 1.3b Structurally defined metal binding ligands in dinuclear metallo-enzymes. In the haemeryhthrin structure shown the normal oxygen binding ligand is replaced by N_3.

Figure 1.3b shows the various geometries of the metal ligands, observed from crystallography, in four binuclear metallo-proteins. Haemerythrin[25] and methane monooxygenase[26] use a di-iron site based on a confacial bi-octahedron, that is two octahedra joined along one face which is composed of three oxygen donor atoms. The

heteronuclear site in bovine erythrocyte superoxide dismutase is composed of a tetrahedral zinc atom linked to a square pyramidal copper atom by a shared imidazole anion[27]. An unusual non-symmetric triangular cluster of three copper atoms occurs in the active site of ascorbate oxidase[28]. In many cases model compounds have made useful contributions to understand the protein-metal chemistry, *e.g.* by simulating the absorption, and electron paramagnetic resonance (EPR) spectra of the ligand environment of proteins[29,30].

1.3 Non-haem iron dioxygenases and oxidases

Dioxygenases which use mononuclear metal iron participate in many metabolically important reactions that have significant applications in the pharmaceutical, environmental and medical fields. Dioxygenases incorporate both atoms of dioxygen into the product(s) of their enzyme reactions and commonly require an Fe(II)/Fe(III) cofactor for activity [Mn(II) is used as a cofactor in a few cases[31]].

The comparison of the amino acid sequences of dioxygenases from a number of sources, or of different dioxygenases with a common function, can allow a reasonable guess as to which amino acids are essential for catalytic activity. These will include residues that bind the metal ion and other invariant amino acids. In light of the isopenicillin N synthase (IPNS) crystal structure[24], sequence comparisons of known members of the iron dependent oxygenase family suggest that many have a similar three dimensional structure to IPNS. Thus, three residues, His214, Asp216 and His270 (using the *A. nidulans* IPNS numbering) appear to be totally conserved in the case of those members of the dioxygenase family which are related to IPNS by overall sequence identities [including 1-aminocyclopropane-1-carboxylate oxidase (ACCO) and α-KG

dependent dioxygenases]. These three conserved residues are also known as the '2-His-1-carboxylate' motif (see Chapter 3). It is remarkable that, deactoxycephalosporin C synthase, deacetylcephalosporin C synthase (α-KG dependent dioxygenases) and ACCO (ascorbate dependent) have similar sequence similarities to IPNS (including the '2-His-1-carboxylate' and 'Arg-X-Ser' motifs) despite their different substrate specificities. In the case of other oxygenases which belong to this family of enzymes by virtue of their iron and α-KG dependence, *e.g.* proline 3-hydroxylase (P 3-H), no convincing overall sequence alignments with IPNS related dioxygenases can be made (see also introduction to Chapter 3).

The alignment of the primary sequence of the R2 subunit of ribonucleotide reductase and the α-subunit of the soluble methane monooxygenase, using the amino acids known to be the metal ligands in R2, led to the prediction of the active site of the latter[32]. The prediction was later confirmed by X-ray crystallography[26].

In the next section of this introduction crystallographic and spectroscopic information on selected dioxygenases will be reviewed. During the course of this work the crystal structures of two α-KG dependent non-haem iron oxygenases were determined (P 3-H[33] and DAOCS[34]) and some relevent observations arising from their structure will be presented.

1.3.1 Catechols

The catechol dioxygenases and the aromatic dihydroxylating dioxygenases occur in species of soil bacteria where they are able to degrade aromatic molecules in their environment into aliphatic products. The intradiol-cleaving enzymes utilise an iron(III) cofactor whilst the extradiol-cleaving utilise an iron(II) [and in a few cases

manganese(II)] cofactor. The intradiol-cleaving enzymes are represented by catechol 1,2-dioxygenase (1,2-CTD) and protocatechuate 3,4-dioxygenase (3,4-PCD). The 3,4 PCD is the best characterised of the two catechols and converts 3,4- dihydroxybenzoate (or protocatechuate) to β-carboxy-*cis-cis* muconate (Scheme 1.1).

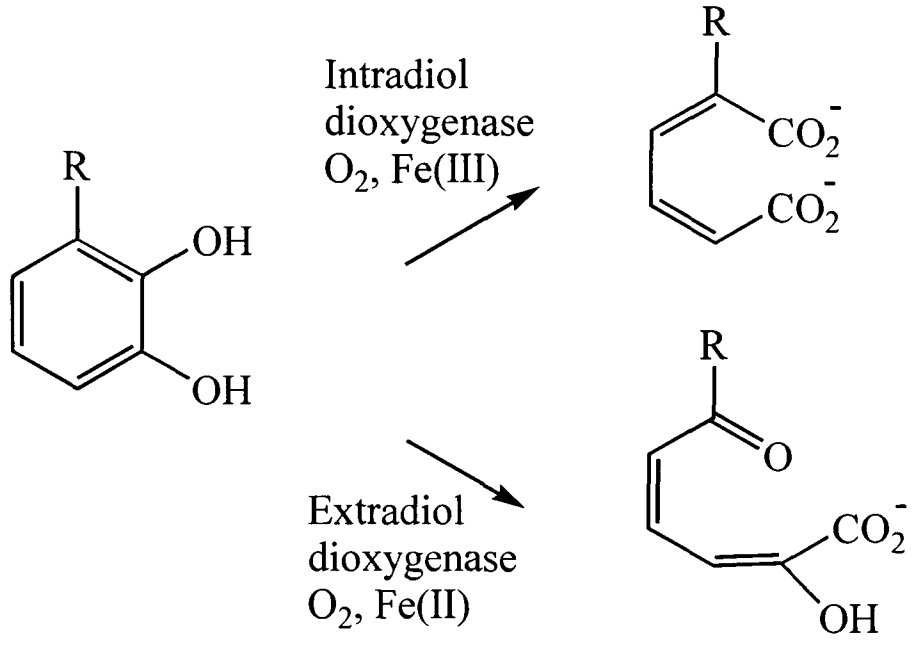

Scheme 1.1 Modes of catechol cleavage by catechol dioxygenases.

The crystal structure of the 3,4-PCD (*Pseudomonas putida*) reveals that the iron (III) centre lies in a trigonal bipyramidal environment co-ordinated by two tyrosines, two histidines and a solvent molecule (Figure 1.4)[35]. The burgundy red colour of this enzyme is a consequence of ligand to metal charge transfer (LCMT) from tyrosinate ligands to the iron. The optical spectrum is relatively broad because Tyr408 and Tyr447 contribute to discrete LMCT bands at 435 nm and 525 nm respectively[36].

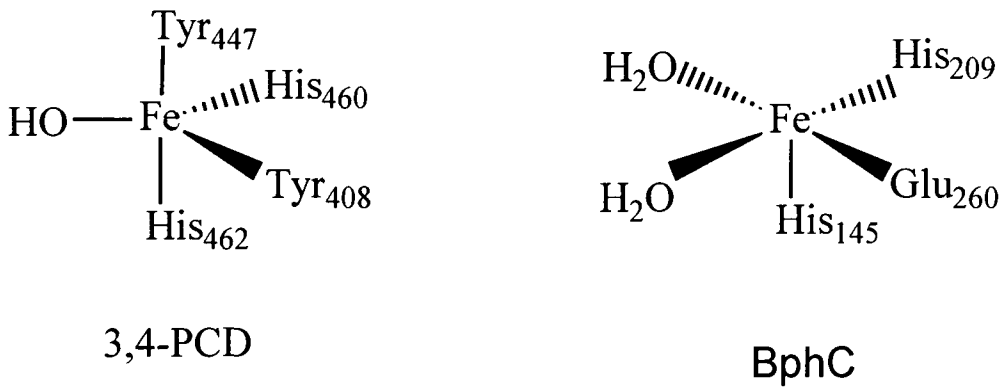

Figure 1.4 The metal co-ordination in crystallographically characterised protocatechuate 3.4-dioxygenase (3,4-PCD) and 2,3-dihydroxybiphenyl 1,2-dioxygenase (BphC).

Polychlorinated biphenyls (PCBs) are toxic and carcinogenic pollutants which are widely distributed in the biosphere. A number of micro-organisms have been found that degrade PCBs[37]. The major biodegradation pathway of PCBs involves the sequential involvement of four different enzymes: biphenyl dioxygenase (BphA), dihydrodiol dehydrogenase (BphB), 2,3-dihydroxybiphenyl dioxygenase (BphC) and 2-hydroxy-6-oxo-phenylhexa-2,4-dienoic acid hydrolase (BphD). The crystal structure of the extradiol cleaving 2,3-dihydroxybiphenyl 1,2-dioxygenase (BphC) from *Pseudomonas* sp. strain reveals a square pyramidal geometry around the Fe(II) metal centre with two histidines, one glutamate and two water molecules acting as ligands (Figure 1.4)[38].

1.3.2 Lipoxygenases

Lipoxygenases catalyse the oxidation of unsaturated fatty acids containing the *cis,cis*-1,4-pentadiene moiety to the corresponding 1-hydroperoxy-*trans*, *cis*-2,4-diene product. The mammalian enzymes act on arachidonic acid to produce hydroperoxides that are precursors to leukotrienes and lipoxins, compounds that have been implicated as potential mediators of inflammation[39]. Linoleic acid is the substrate of the plant

lipoxygenases to give a hydroperoxide products (Scheme 1.2). The function of hydroperoxide products in plants is unknown[39].

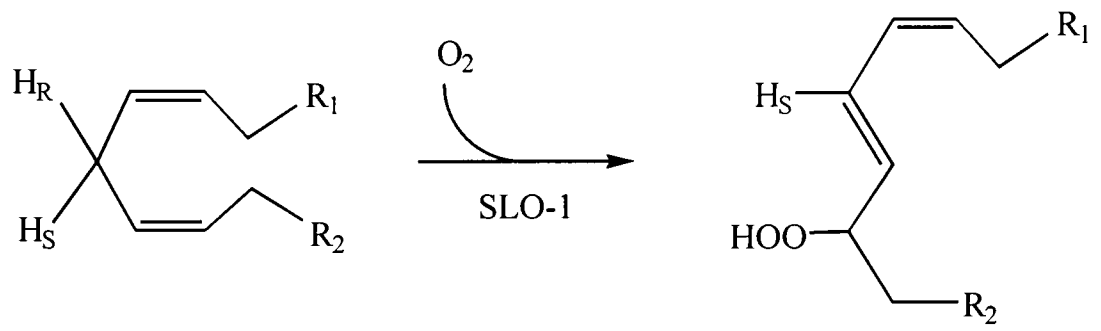

Scheme 1.2 Reaction catalysed by soybean lipoxygenase-1.

Purified soybean lipoxygenase-1 (SLO-1) is colourless and when treated with the product hydroperoxide, the Fe(II)-SLO-1 undergoes a spectral change to give a yellow complex (λ_{max} = 350 nm) and is associated with an axial EPR spectrum[40]. Sequence comparisons of 14 lipoxygenases from both plant and animal sources reveals significant sequence homology; in particular six conserved histidine residues are apparent[41]. Site directed mutagenesis on SLO-1 indicates that only three of these six histidines are iron ligands[41]. The proposed ligand set of three histidines and one carboxylate was confirmed by two crystal structures of Fe(II)-SLO-1[42,43]. In both structures the carboxylate ligand derives from the C-terminal Ile839 residue (Figure 1.5). A fifth endogenous ligand Asn694 was also identified in one of the crystal structures[43]. A mutagenesis study of the corresponding asparagine ligand in SLO-3 suggests that it is not required for iron binding, but is important for catalysis[44].

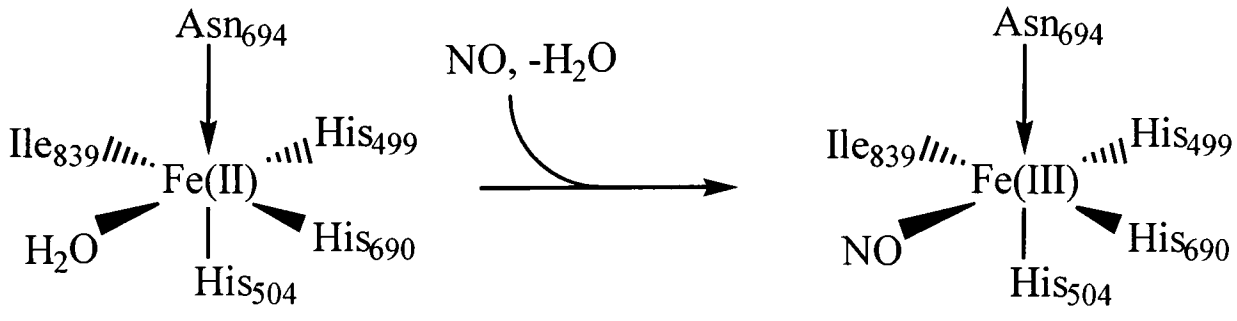

Figure 1.5 Metal co-ordination in soybean lipoxygenase-1. (A) the crystal structure of Fe(II)-SLO-1 and (B) the NO adduct. Note that Ile839 co-ordinates to the iron *via* it's C-terminal carboxylate rather than it's side chain.

1.3.3 Penicillin and cephalosporin biosynthesis

Since the initial discovery of the penicillin and cephalosporin antibiotics around 60 years ago[45], their biosynthesis has been studied in detail. Much effort has been put into understanding the mechanisms of these enzymes since the organic synthesis of antibiotics cannot compete with fermentation production. Presently, the annual antibiotic sales is greater than $22 billion world-wide[46]. However, not all antibiotics are derived directly from fermentation and 'semi'-synthesis from a fermented product has been successfully used to produce variants of naturally occurring β-lactams with altered sidechains.

The biosynthetic pathways leading to penicillins and cephalosporin share a common origin in their tripeptide progenitor δ-(*L*-α-aminoadipoyl)-*L*-cysteinyl-*D*-valine (ACV) as shown in Figure 1.6[47]. This ACV tripeptide is 'non-ribosomally' condensed from the three amino acids (*L*-α-aminoadipic acid, *L*-cysteine and *L*-valine) by a large multi-domain ACV synthetase[48]. The second enzyme, IPNS, a non-haem iron dioxygenase catalyses the cyclisation of ACV to give a fused ring system of IPN.

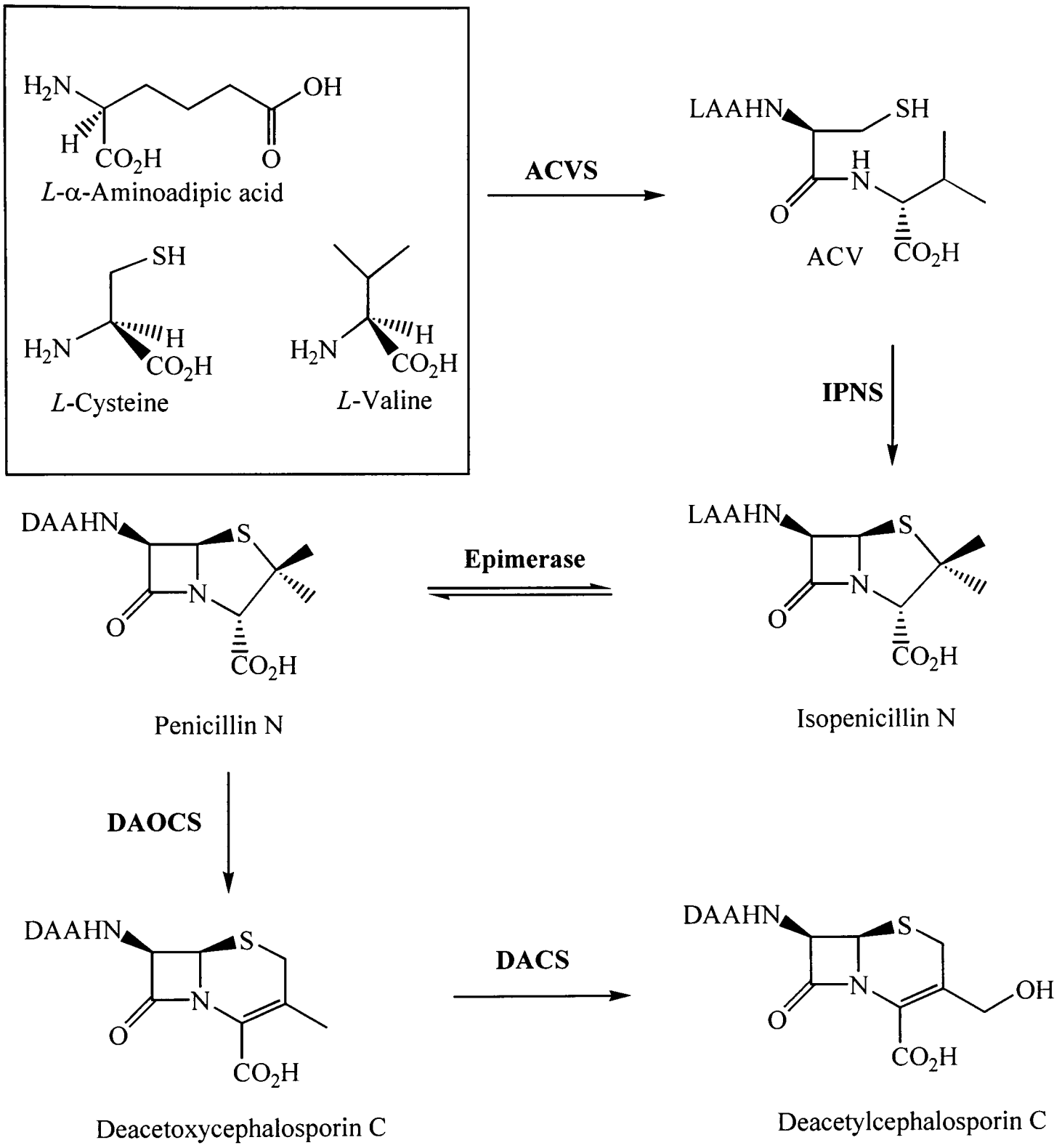

Figure 1.6 Biosynthesis of Penicillins and Cephalosporins.

The next enzyme in the pathway is an epimerase, which converts the *L*-α-aminoadipic side chain to the *D*-isomer. Penicillin N is the substrate for deactoxycephalosporin C synthase (DAOCS, also known as ring expandase) which modifies the five membered ring of the penicillin N to a six-membered ring system of the deactoxycephalosporin C (DAOC). A subsequent second step is performed by a deacetylcephalosporin C synthase

(DACS, also known as hydroxylase) which hydroxylates the DAOC to give deacetylcephalosporin C (DAC).

1.3.3.1 Isopenicillin N synthase

Isopenicillin N synthase (IPNS) is a non-haem iron dependent oxidase which catalyses the biosynthesis of isopenicillin *N*[49]. Sequence alignments of IPNS isozymes showed the conservation of '2-His-1-carboxylate' and Arg-X-Ser motifs[50]. Mutational analysis of IPNS from *S. jumonjinensis* and *C. acremonium* showed that the 2-His-1-carboxylate metal binding motifs are essential for activity[50,51]. The first reported crystal structure of IPNS showed a six co-ordinate Mn(II)-IPNS with an octahedral geometry[24]. The structure revealed that the Mn(II) atom was co-ordinated to four protein ligands (two histidines, one aspartate and one glutamine) and two water molecules in active site and lies unusually buried within a 'jelly-roll' core lined by hydrophobic residues.

The crystal structure of the ferrous iron complexed to ACV has been determined to 1.35 Å resolution[52]. The ACV appears to be anchored within the active site *via* ligation of its thiolate to the iron centre and by interactions with its two carboxylate groups: *via* salt bridges between the ACV aminoadipoyl carboxylate with the side chain of Arg87 and between the ACV valine carboxylate with side chains of Tyr189, Ser281 and Arg279. One of the two water molecules ligating the metal ion in the Mn(II)-IPNS complex is displaced upon ACV binding concomitant with the change in the metal co-ordination from an octahedral to a square pyramidal geometry. The penta-coordinated Fe(II)-ACV-IPNS with a displaced water molecule supported the previous spectroscopic results[53,54]. The resultant ternary complex (with a square pyramidal geometry) suggested that the Gln330 might not be an essential metal binding ligand and is displaced by the

binding of ACV. The structure of the quaternary IPNS-Fe(II)-ACV-NO was also determined by the same authors which showed that NO (and presumably oxygen) binds in the vacant position and *trans* to Asp216[52]. The crystallographic studies revealed a rotation of 30 degrees had occurred between the valine Cα-Cβ (and an increase in the distance from 3.90 to 4.81 Å between the valine methyl carbon and iron atom) to accommodate the NO. The NO was bound in a non-linear orientation (Fe-N-O angle of *ca.* 120 degrees). The movement of Phe211 opens the channel to the protein surface that is bordered by the side chains of Thr331, Val100 and Tyr189 and contains three water molecules. The arrangement of ligands around the iron metal centre in the ternary and the quaternary complex of IPNS-ACV-Fe-NO can be summarised by the complex C in Figure 1.7.

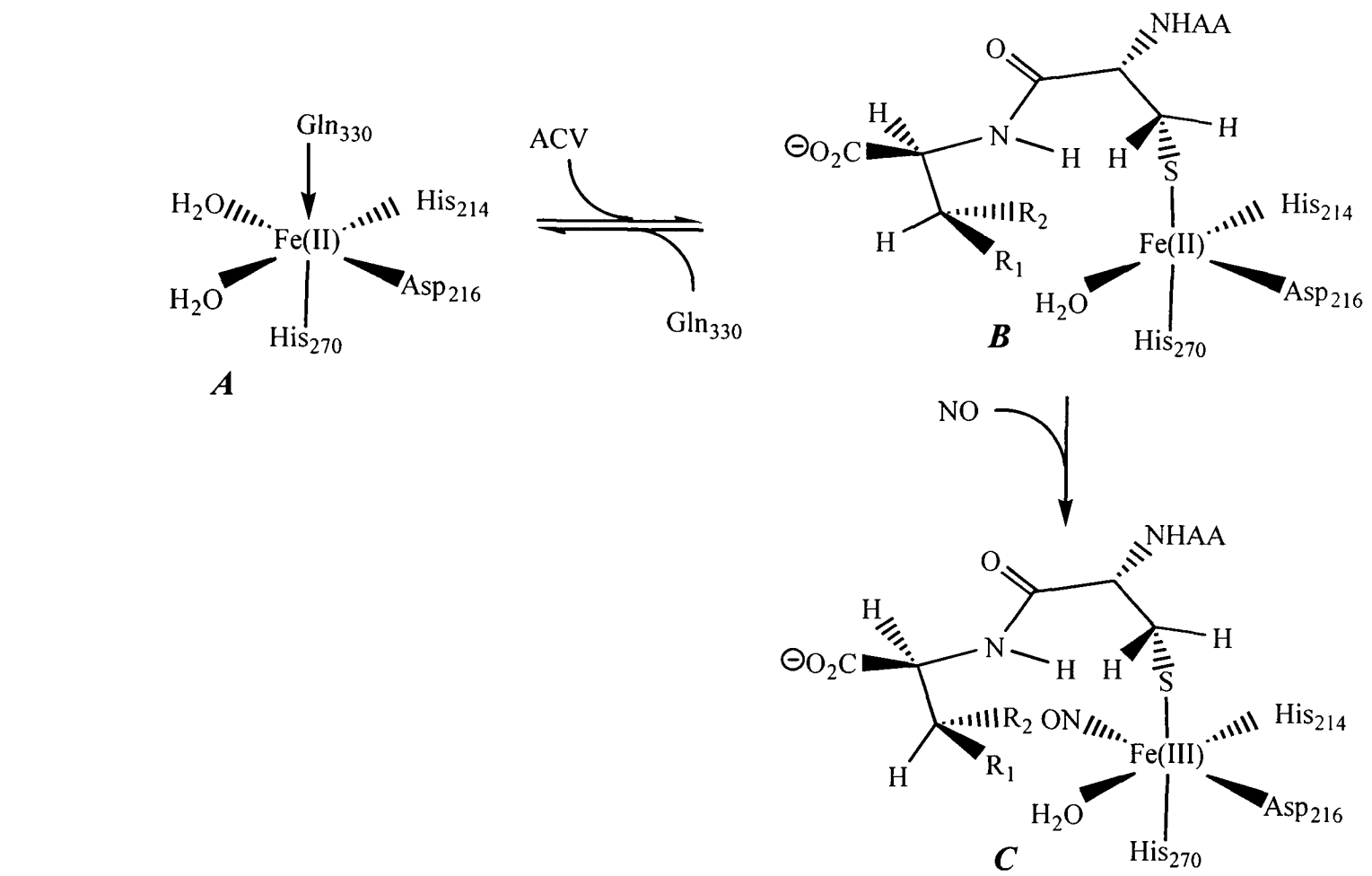

Figure 1.7 Proposed mode of binding of NO, ACV and ACV analogues in the active site of IPNS as determined from crystal structures[52,55]. Mode of ACV (R_1 = R_2 = Me) and ACAB (R_1 = Me, R_2 = H) binding is shown by complexes B and C. ACG and ACA are shown by D and E respectively. Note that the second water molecule observed in the crystal structure of D is not shown (see text).

It has been demonstrated that ACV analogues, including δ-(*L*-α-aminoadipoyl)-*L*-cysteinyl-*D*-*α*-aminobutyrate (ACAB), can be converted using crude IPNS extracts to give an α-methyl and β-methyl penams and a cepham product[56]. The analogues δ-(*L*-α-aminoadipoyl)-*L*-cysteinyl-glycine (ACG) and δ-(*L*-α-aminoadipoyl)-*L*-cysteinyl-*D*-alanine (ACA) were not converted into β-lactams by IPNS, but instead gave shunt products, resulting from two electron oxidation of the tripeptide (Scheme 1.3).

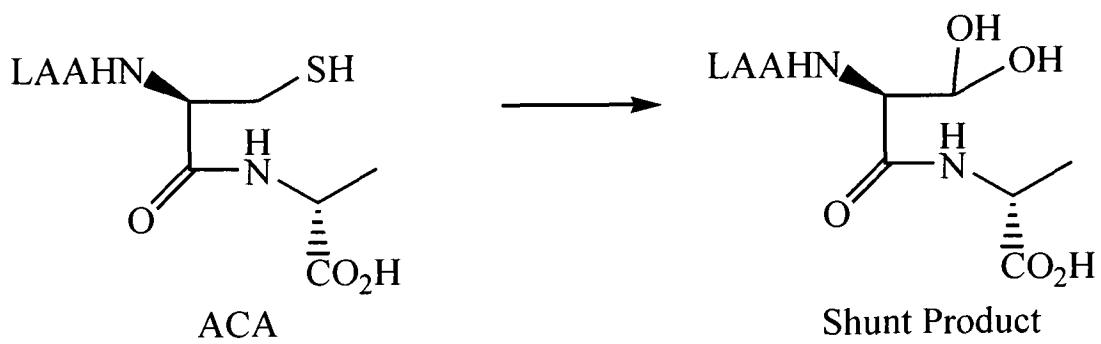

Scheme 1.3 Formation of shunt product from ACA.

The crystal structures of ternary complexes of Fe-ACAB-IPNS Fe-ACG-IPNS and Fe-ACA-IPNS have been recently obtained by Ms Alexandra Long (O.C.M.S.). These crystal structures revealed that all these ACV analogues (except ACG) bound IPNS *via* a thiolate bond to the iron atom and salt bridge from the carboxylate of the amino adipoyl of the substrates to the Arg87 side chain[55]. The binding of ACG, ACA or ACAB led to the displacement of a single water molecule from the iron centre and this vacant position in the active site was subsequently shown to be the binding site for NO, as observed with the IPNS-ACV complex (Figure 1.7 *cf* C, D and E). The crystal structure of the ternary Fe-ACG-IPNS complex showed the presence of an extra water molecule in the active site which appears to be held in place *via* a hydrogen bonding network from the glycine carboxylate of the ACG and a water molecule attached to the iron centre[55]. The quaternary Fe-ACG-IPNS-NO structure confirmed that NO does bind to the vacant

position on the iron centre and the glycine carboxylate was observed to move away from the iron centre and form a salt bridge with Arg279 and Ser281[55].

Nevertheless, the results of these combined crystallographic studies supported the previous spectroscopic studies of Orville *et al.*[57] which demonstrated that cysteinyl thiol group is essential for the generation of characteristic pink colour of the Fe-ACV-IPNS-NO complex.

EPR studies using NO have indicated that NO binds to the Fe(II)-ACV-IPNS complex to give an octahedral complex[53]. Evidence for the formation of a quaternary complex was also obtained from spectroscopic studies which showed that a pink complex was formed when NO is added to Fe(II)-ACV-IPNS resulting from a thiolate to Fe(III) charge transfer[53]. These spectroscopic results were essentially confirmed by the crystal structure of the Fe(II)-ACV-IPNS-NO[52].

The IPNS reaction mechanism for the formation of isopenicillin *N* as proposed by Roach *et al.*[52] is shown in Scheme 1.4. ACV is first bound to the octahedral holoenzyme complex A concomitant with the removal of one water molecule in the position *trans* to Asp216 to give a square pyramidal complex, B. The non-linear, haemoglobin-like, binding of oxygen (trans to the Asp216) produces a superoxide in the previously vacant position to give complex C. In the octahedral complex, C, the superoxide removes the *pro-3-S* hydrogen from the ACV cysteinyl residue to produce a hydroperoxide complex, D. The cleavage of the hydroperoxide with the concomitant deprotonation of the amide N-H allows simultaneous ring closure and ferryl formation (complex E→F).

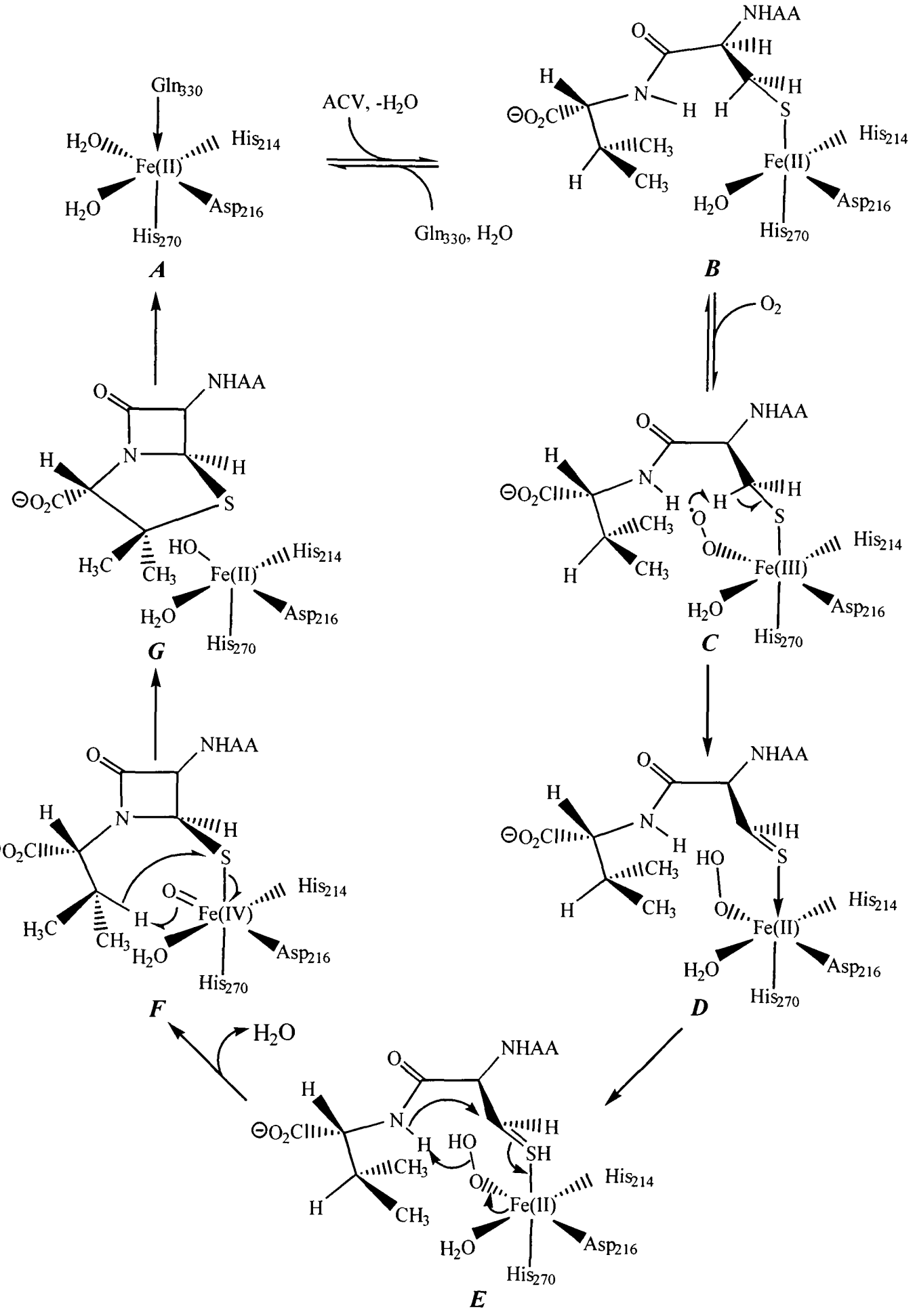

Scheme 1.4 Proposed reaction mechanism for isopenicillin *N* formation[52].

Rotation of the isopropyl group must occur before or at the same time as the β-lactam ring closure to relieve its steric hindrance with the sulphur ligand. This rotation also

directs the valine β-hydrogen towards the ferryl-oxene species with which it reacts (complex F→G) to give isopenicillin *N*.

1.3.3.2 **Deacetoxycephalosporin C synthase**

DAOCS and DACS are non-haem iron-dependent dioxygenases which catalyse the biosynthesis of cephalosphorin from its penicillin *N* precursor (see Figure 1.6). Whereas, in *Cephalosporium acremonium* one bifunctional enzyme (DAOCS/DACS) catalyses both the ring expansion and hydroxylation reactions, the same two steps are largely catalysed by two distinct and separate enzymes in *Streptomyces clavuligerus*[58]. DAOCS and DACS belong to a family of enzymes that use α-KG as a co-substrate, which is converted into succinate and carbon dioxide as shown in Scheme 1.5. In the currently proposed mechanism the iron(II) can donate one electron to the oxygen, forming iron(III)-superoxide which can react with the carbonyl group of the α-KG, forming a cyclic peroxy-intermediate. Decarboxylation of this intermediate releases succinate and produces a iron(IV) ferryl species which can carry out the hydroxylation reaction *via* a radical mechanism.

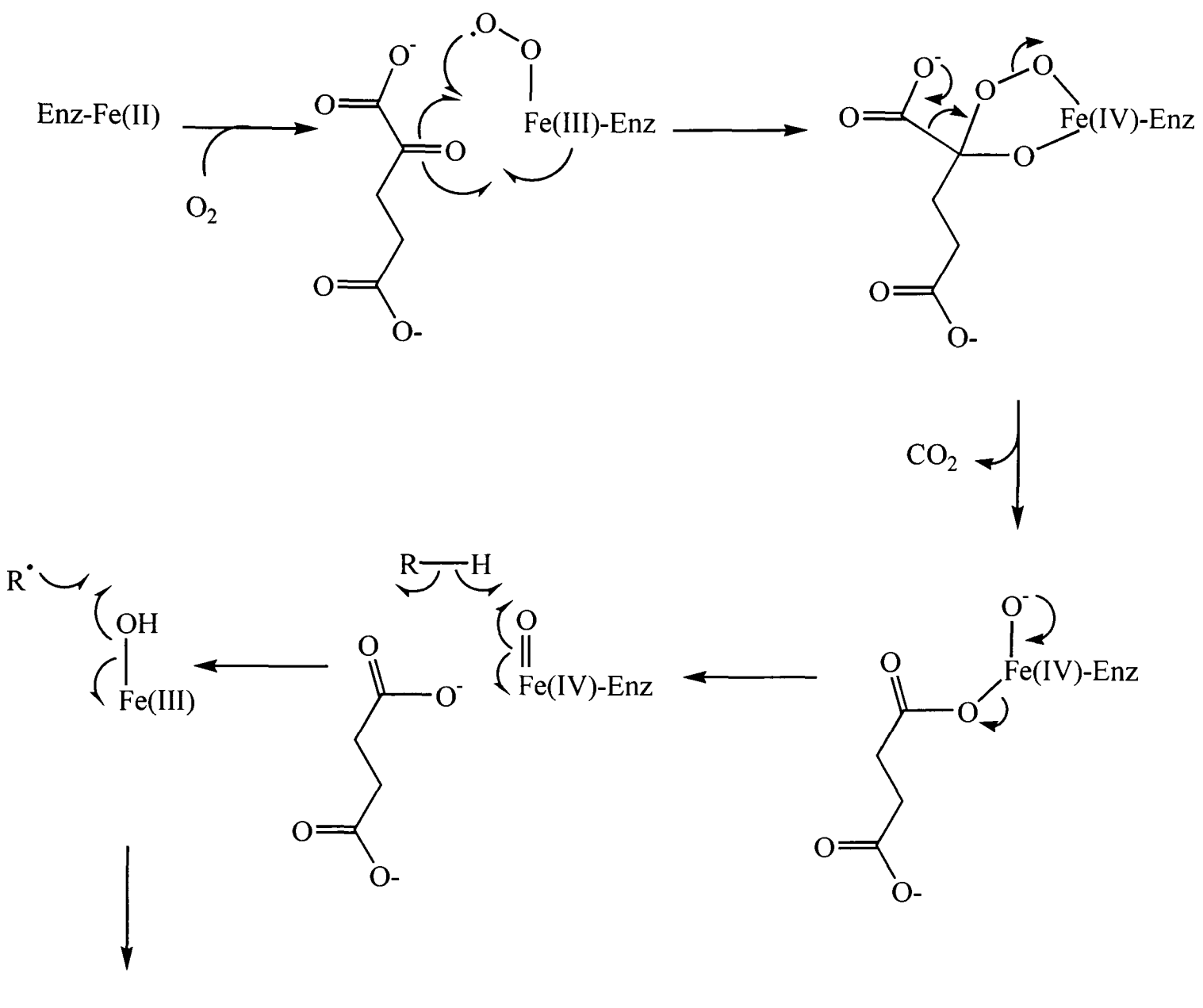

Scheme 1.5 Proposed outline mechanism for a hydroxylation reaction catalysed by an α-KG dependent dioxygenase[59].

The X-ray crystal structure of DAOCS has been determined recently by Valegård *et al.*[34], and reveals high structural similarity with IPNS. The three structures described by these researchers show Fe(II)-free DAOCS (apoenzyme at a 1.3 Å resolution), DAOCS-Fe(II) holoenzyme (at 1.5 Å resolution) and DAOCS-Fe(II)-α-ketoglutarate ternary complex (also at 1.5 Å resolution). This was an important breakthrough as it was the first reported crystal structure of an α-KG dependent dioxygenase.

Figure 1.7a and Figure 1.7b shows crystal structures of DAOCS[34] and IPNS[52] respectively. The overall structure of DAOCS shows a inner jelly-roll motif surrounded

by α-helices analogous to that observed in IPNS[52]. The jelly-roll motif is composed of two large β-sheet domains which form a hydrophobic pocket containing the iron binding ligands. The α-helices, in particular α-helix 6, are thought to aid in the stabilisation of the jelly-roll motif. In the absence of Fe(II) the enzyme forms a trimer where the C-terminus of one subunit penetrates the active site of the neighbouring subunit in a cyclical fashion[60].

The binary DAOCS-Fe(II) complex shows that the metal centre is co-ordinated to side chains of three protein ligands (His183, Asp185, and His243) and three water molecules within the hydrophobic pocket. Previous sequence comparisons between IPNS and DAOCS also predicted that this His-X-Asp-His motif served as metal binding site on the basis of sequence alignment and spectroscopic studies[52,61]. In the ternary DAOCS-Fe(II)-α-ketoglutarate structure, the co-substrate, α-ketoglutarate, binds in a bidentate manner with the displacement of two water molecules (Figure 1.7c). The 1-carboxylate of α-ketoglutarate binds *trans* to His243 and the 2-carbonyl group *trans* to Asp185. By analogy with the IPNS structure this position, *trans* to Asp185 in DAOCS, is the binding site for NO and oxygen[52]. The 5-carboxylate of the co-substrate forms a salt bridge with Arg258 and Ser260 of DAOCS (Figure 1.7c). These conserved residues are analogous with Arg279 and Ser281 which bind the valine carboxylate of ACV in IPNS. An oxygen binding site *trans* to His183 was proposed for DAOCS.

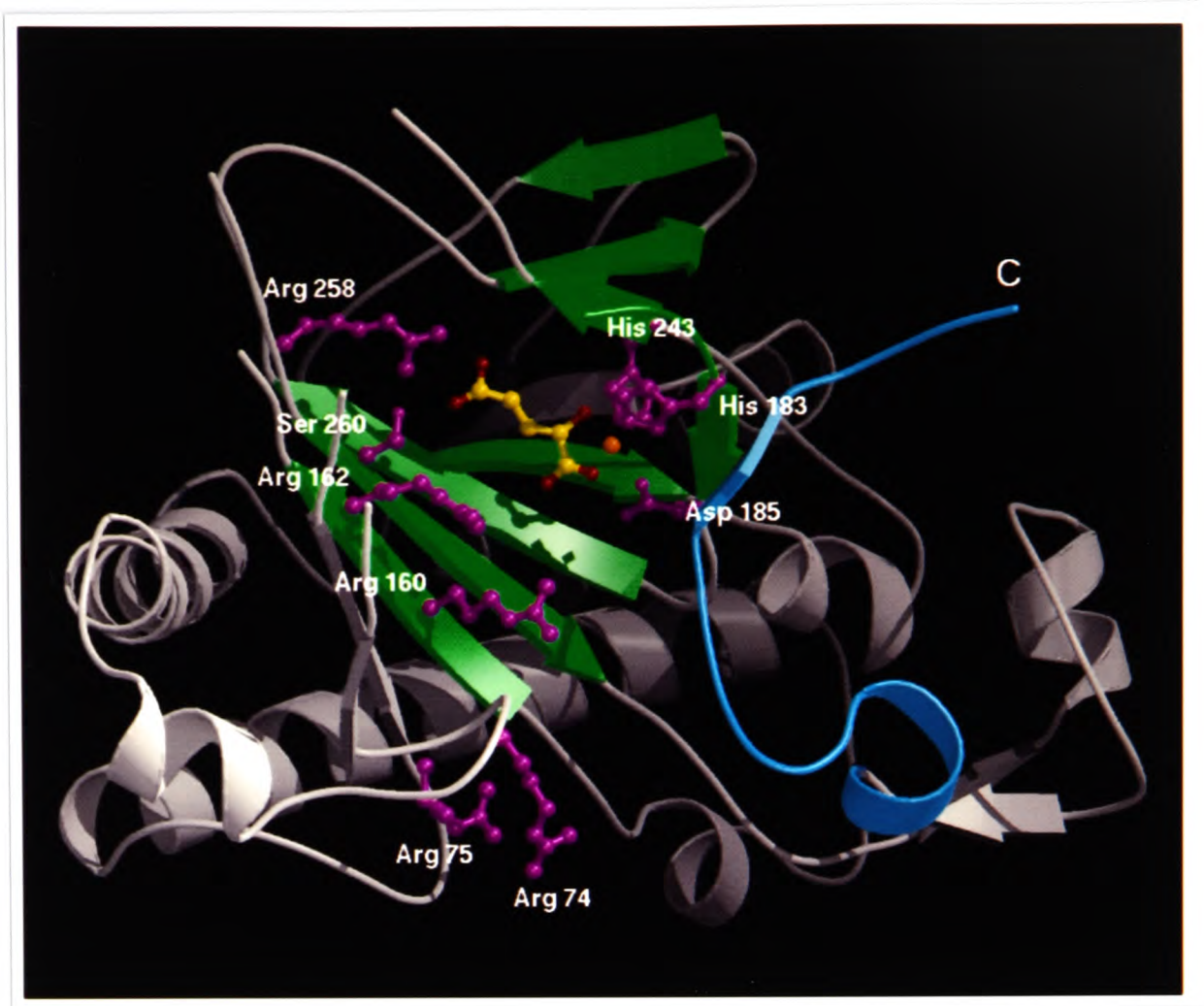

Figure 1.7a The crystal structure of DAOCS[34].

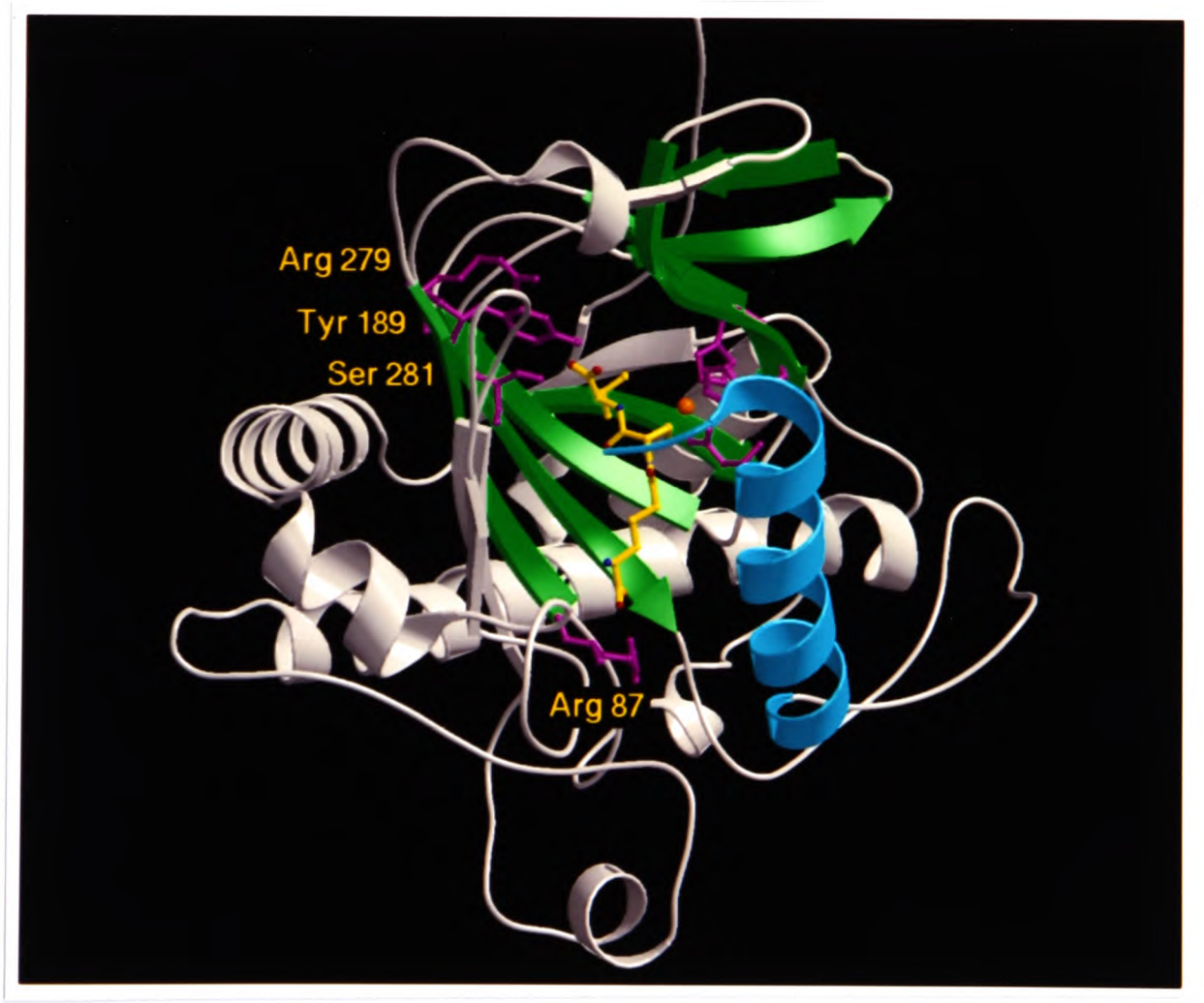

Figure 1.7b The crystal structure of IPNS[52].

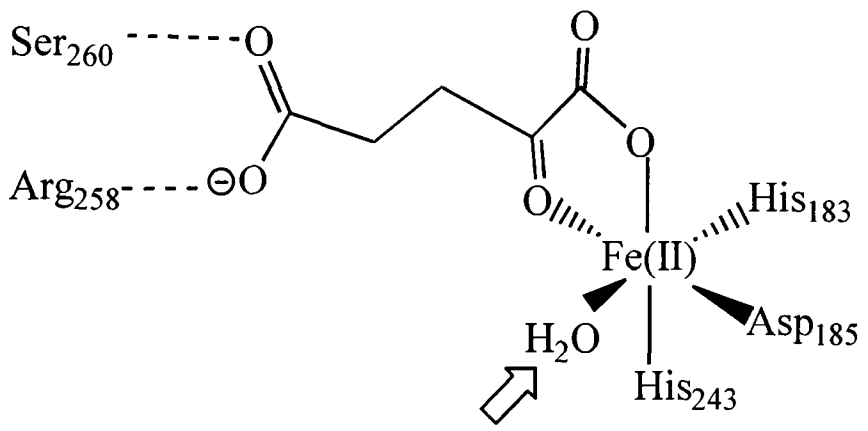

Figure 1.7c The binding of α-KG in DAOCS from the crystal structure[34]. The arrow shows the proposed oxygen binding site.

In view of the similarity between the structures of DAOCS and IPNS, and also in view of their close sequence homology (21 % homology, 19 % identity), it seems likely that these enzymes evolved from a common ancestral precursor to use the same basic reaction platform.

1.3.4 1-Aminocyclopropane-1-carboxylate oxidase

Ethylene is a potent plant signalling molecule (hormone) and a regulator of ripening, stem and root elongation, seed germination and many other developmental processes[62]. The ethylene biosynthetic pathway 'starts' with the synthesis of 1-aminocyclopropane-1-carboxylate (ACC) from S-adenosyl-*L*-methionine, which is part of the Yang cycle[63], followed by the conversion of ACC to ethylene. ACCO is an iron(II) dependent dioxygenase which catalyses the final step in the biosynthesis of ethylene in higher plants (Scheme 1.6).

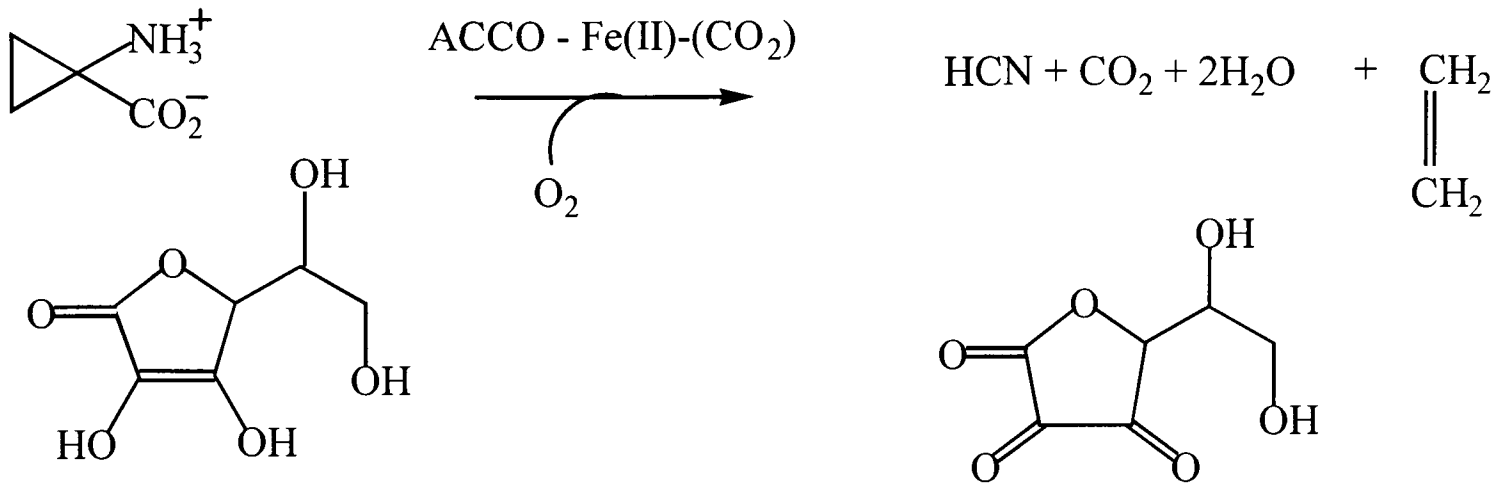

Scheme 1.6 Reaction catalysed by ACCO.

Although ACCO shows significant sequence similarities to the α-KG dependent dioxygenases and IPNS sub-family[61], it does not require the α-KG co-substrate for activity[64]. In ACCO the role of α-KG as a co-substrate is apparently filled by ascorbate which is presumably oxidised to dehydroascorbate[65]. Sequence comparisons of ACCO isozymes shows that certain residues are totally conserved, particularly the His177, Asp179, His234 (using the tomato fruit ACCO numbering sequence[66]). Mutagenesis studies reported that the substitution of either His177 or H234 of ACCO with Phe, Ala, Asn, or the substitution of Asp179 with His, Ala, resulted in the complete loss of activity[67,68]. Chemical modifications have implicated these two histidine residues for metal binding by ACCO and other members of this family[69].

In contrast with previous mutation studies on ACCO, the substitution of either Asp179 or His177 residues with glutamate resulted in modified ACCOs with activities of *ca.* < 1% of that observed for the wild-type[66]. These findings suggest that the mutant ACCOs (H177E or D179E) can bind iron, ACC and dioxygen. However, ACCO was shown to be particularly prone to inactivation and fragmentation [*via* a metal catalysed oxidation (MCO)] under the assay conditions[70]. H177D (inactive), H177E (low activity), D179E (low activity) and H234Q (inactive) modified ACCOs all underwent

fragmentation. Furthermore, these results suggested that whilst the ligation to H179, D177 and H234 was essential for activity, ligation to H234 was not essential for fragmentation.

CHAPTER 2

The Role of the Glutamine-330 Metal Binding Ligand in Isopenicillin N synthase Activity

2.1 Introduction

Spectroscopic studies have demonstrated the presence of an aspartyl and two or three histidyl residues ligating an iron atom at the active site of IPNS[57]. It has also been suggested that one of the histidyl ligands might be displaced upon binding of ACV[71]. The spectroscopic assignments of an aspartyl and two histidyl ligands were supported by mutagenesis studies which investigated the primary sequences of IPNS and related oxygenases from several different species[50,51]. The crystal structure of IPNS from *A. nidulans* complexed to manganese substituting for iron revealed a six co-ordinate metal atom with octahedral ligation by two water molecules and four protein ligands: His270, His214, Asp216 and an unexpected fourth ligand, Gln330, the penultimate residue on the C-terminus of IPNS[24]. The active site of IPNS was located within the jelly roll barrel core, rather than on an external site. The C-terminus which forms a 'lid' to the active site, is a relatively mobile structure compared with the rest of the molecule and appears to be stabilised in the active site of the resting enzyme. The possibility should also be considered that the ligation of Gln330 to the manganese atom seen in the Mn-IPNS crystal structure is a crystallographic 'artefact' which does not occur in solution.

Comparison of the last eight C-terminal residues of IPNS derived from different organisms reveals that all, except with the sole exception of IPNS from *Streptomyces*

cattleya, have a region of close similarity in which the penultimate glutaminyl residue is conserved (Figure 2.1, consensus sequence L I N K N G Q T). The DNA sequence of IPNS from *S. cattleya* encodes IPNS with an apparently truncated C-terminus[72]. If the *S. cattleya* sequence does indeed encode for a catalytically active IPNS, it would seem likely that ligation of the active site iron by Gln330 is not essential for catalytic activity of IPNS.

Comparisons of the sequences of IPNS, ACCO and related α-KG dependent oxygenases display a conservation of His-x-Asp-x-His (metal binding) and Arg-x-Ser motifs[24]. It is perhaps surprising that a low sequence identity is observed in the C-terminal regions throughout this subfamily of dioxygenases and in particular the loss of the conserved IPNS Gln330 ligand (Figure 2.2). It was considered possible that this difference in co-ordination chemistry between IPNS and other members of this family reflects differences in their mechanism and substrate specificity, and in particular the fact that IPNS does not use α-KG as a co-substrate.

Penicillium chrysogenum (P08703)	S Y G D Y L Q N G L V S L I N K N G **Q** T
Cephaloporium acremonium (P05189)	S Y G E Y L Q G G L R G L I N K N G **Q** T
Lysobacter lactamdurans (X56660)	S Y G D Y L Q H G L L D L I R A N G **Q** T
Flavobacterium sp. (P16020)	S Y G D Y L Q H G L L D L I R A N G **Q** T
Streptomyces jumonjinensis (P18386)	S Y G E Y L Q H G L R A L I V K N G **Q** T
Streptomyces clavuligerus (P10621)	S Y G D Y L Q H G L R A L I V K N G **Q** T
Norcardia lactamdurans (P27744)	R Y G D Y L N H G L H S L I V K N G **Q** T
Streptomyces griseus (X54609)	R Y G D Y L Q Q A S N A L I A K N G **Q** T
Streptomyces griseus lipmani (P12438)	T Y G E Y L Q E G F H A L I A K N V **Q** T
Streptomyces griseus cattleya (D78166)	S Y G E Y L Q E G F T R
Aspergillus nidulans (P05326)	S Y G D Y L Q N G L V S L I N K N G **Q** T
Q330A	S Y G D Y L Q N G L V S L I N K N G A T
Q330L	S Y G D Y L Q N G L V S L I N K N G L T
Q330D	S Y G D Y L Q N G L V S L I N K N G D T
G329	S Y G D Y L Q N G L V S L I N K N G
I325	S Y G D Y L Q N G L V S L I
Mcat	S Y G D Y L Q E G F T R
similarity/identity	S **Y** G D **Y L** Q n G l v s **L I** n K **N G Q T**

β-sheet (β-16) α-helix (α-10)

Figure 2.1 Sequence comparison of the C-terminal regions of IPNSs from sequence databases (with accession numbers in brackets) together with IPNS mutants. The last row shows identity/similarity of the C-terminus amino acids: totally conserved (bold capitals); significantly conserved (capitals); non-conserved residues (lower case). The Gln330 is shown in bold with numbering according to IPNS from *A. nidulans*[24]. The bar indicates the residues which form part of the C-terminal α-helix (α-10, shaded) and β–sheet (β-16, white) based on the Mn (II) IPNS structure.

ACCO (P05116)	K F Q A K E P R F **E** A M K A M E S D P I A S A
F3OH (U04434)	A **R** L K K Q A K A **D** K K Q Q Q Q S A N K E F A D S K P L D A I F A
H6H (P24397)	D S G V K P Y K I **N** V
FOLS (S67953)	L P Q
GC20 (X73314)	Y **R** P D C N T L E A F K T W V Q E G K A L D T G S T I T A P S A
DAOCS (P18548)	I **R** R T S K A
DACS	M **H** A K N E P Q A G
DAOCS/DACS (P11935)	M **R** R D K P A A A **E** A A V P A A A P V S T A A P I A T
IPNS (P05326)	L V S L I N K N G **Q** T

Figure 2.2 C-terminal sequence comparisons between ferrous dependent oxygenases (with accession numbers in brackets). Aminocyclopropane-1-carboxylic acid, ACCO (from tomato); flavanone 3-β-hydroxylase, F3OH (from *Zea Mays*); hyoscyamine 6-β-hydroxylase, H6H, (from henbane); flavanone synthase, FOLS (from *Pertunia hybdrida*); gibberellin C-20 oxidase, GC20, (from *Cucurbita maxima*); deactoxycephalosporin C synthase, DAOCS, (from *S. clavuligerus*); deacetylcephalosporin C synthase, DACS, (from *S. clavuligerus*); deactoxycephalosporin C synthase/ deacetylcephalosporin C synthase (DAOCS/DACS) (from *C. acremonium*); IPNS (*A. nidulans*). Bold letters show conservative substitutions.

The lack of sequence identity observed between the C-termini regions of the DAOCS and DACS isozymes is surprising. It is also noteworthy that there is no consensus of conserved amino acids in the C-termini of DAOCS isozymes. Biophysical studies of DAOCS (*S. clavuligerus*) have revealed some interesting findings which suggest the involvement of the C-terminus in oligomerisation. In the absence of ferrous iron, DAOCS adopts a trimeric form which has been proposed to represent the 'resting' state of the enzyme. In this resting form, the C-terminus of one subunit acts as 'lid' for the neighbouring subunit in a cyclical manner[34,60]. The addition of ferrous iron or ferrous iron/α-KG to DAOCS converts the enzyme into the monomeric (catalytic) form. A similar oligomerisation process may occur with other non-haem dioxygenases.

The crystal structure of soybean lipoxygenase also shows an octahedral geometry with four protein side chain ligands (2 histidines, one aspartate and one asparagine), the carboxylate of the C-terminal isoleucine and one water molecule[42]. Site directed mutagenesis of the corresponding asparaginyl ligand has suggested that it is not essential for iron binding but is important for catalysis[44].

An investigation into the role of the C-terminus of 4-hydroxyphenylpyruvate dioxygenase (4-HPPD) was made by site directed mutagenesis[73]. These studies suggest that Asn380 might be an important residue for substrate binding and its mutation to alanine weakened the affinity of the enzyme for its substrate, α-ketoisocaproate, by 10 fold.

2.1.1 Site directed mutagenesis

Studies on protein function have revealed that proteins can be quite tolerant to small mutational changes and can adapt their structures to accommodate many changes in large

regions of the sequence. Mutational studies on proteins suggest that only a fraction of the residues are important for stability and most proteins have the ability to adjust structures to compensate for changes in sequence, even in important sites[74]. This implies that a certain amount of conformational flexibility is needed; if proteins were completely rigid, small changes in sequence would have a large effect on stability.

The most common metal binding ligands in non-haem iron (II) dependent oxygenases are charged (histidine, aspartate, glutamate) rather than hydrophobic (tyrosine, tryptophan) amino acids (see Chapter 1). In the case of soybean lipoxygenase the terminal carboxyl group of isoleucine was reported to be a metal binding ligand. In the present study, the glutaminyl side chain (from residue 330) was substituted by side chains of aspartyl, alanyl and leucyl (Figure 2.3). The residues in Figure 2.3 have side chains with very different properties making them a good choice for mutagenesis. The alanyl and leucyl sidechains are both non-polar and hydrophobic which makes them extremely unlikely to ligate with the active site metal ion. The corresponding aspartyl or glutamyl sidechains are more polar, and better electron donors, which might make them good metal ligands (in the correct environment).

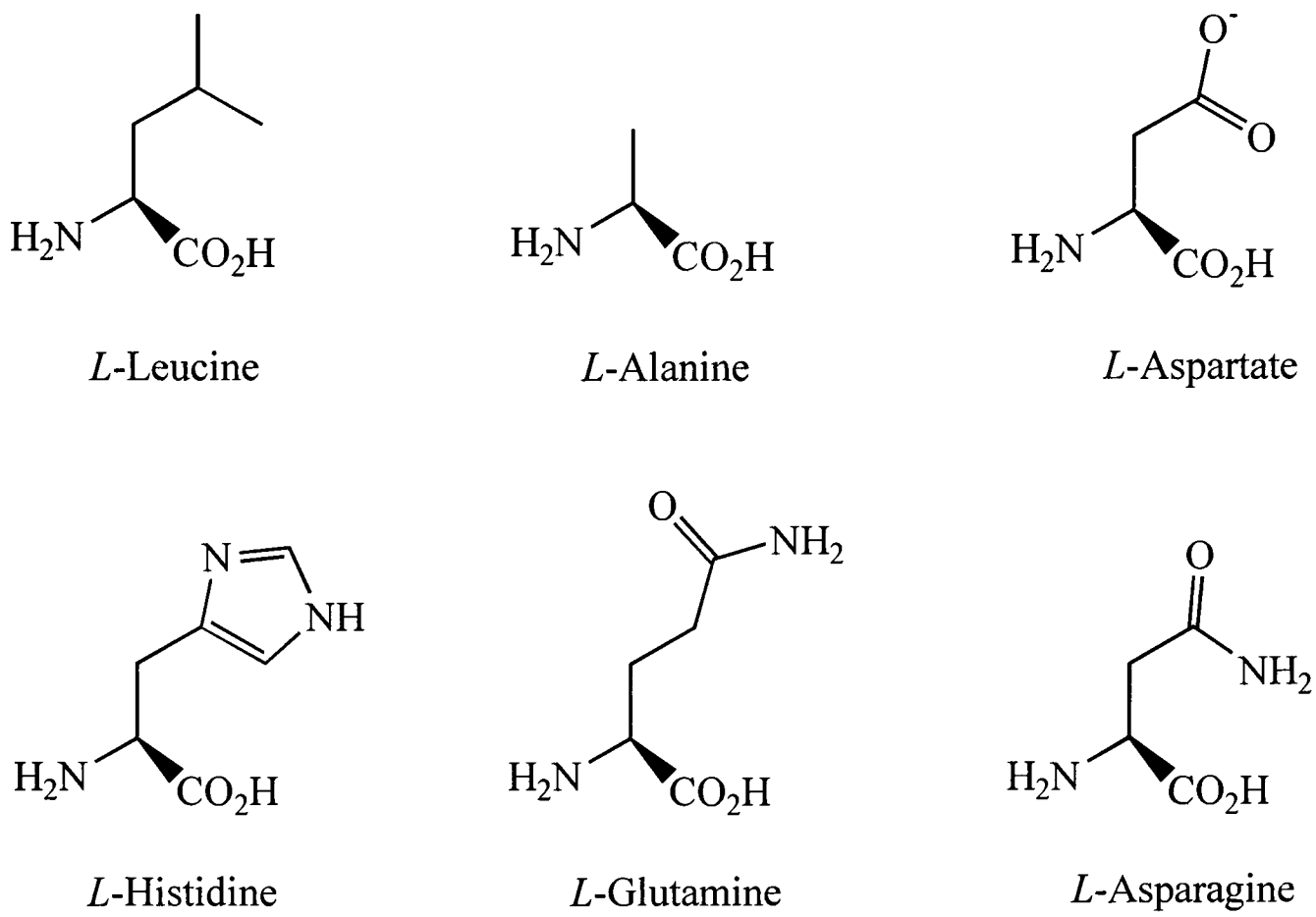

Figure 2.3 Amino acids which were used for site-directed mutagenesis study to replace the metal binding ligands of IPNS.

The two methods for site directed mutagenesis employed in this study used either ssDNA or dsDNA templates with the U.S.E. Mutagenesis Kit (Pharmacia). This kit is based on a site-directed mutagenesis procedure known as unique site elimination[75], or USE. It utilises two primers (selection and target primers) which introduce mutations into the plasmid. The selection primer contains a mutation in a unique, non-essential restriction site. Elimination of this mutated site renders plasmid DNA resistant to restriction digestion, providing the basis for selection. The desired target mutation is introduced into a defined sequence of the plasmid by the target mutagenic primer. By coupling a non-selectable mutation with a selectable mutation in a unique restriction site it is reported that mutagenesis frequencies of 85% can be obtained[75].

2.1.2 HPLC assays

An additional aim of this study was to develop a quantitative HPLC assay to characterise the IPNS mutants. Hole plate bioassays using indicator organisms provide an effective method for the detection of IPNS activity. However, large errors can be obtained in these assays because the size of the kill zone is dependent on a logarithmic scale (relatively small errors in the kill zones have significant impact on the specific activity calculation). Another drawback is that the bioassay plates have to be calibrated each time fresh plates are made. The overnight incubation needed to measure the kill zones makes this procedure slow. The bioassay is also restricted to the detection of antibiotic products, and cannot be used to distinguish any novel bioactive products which may be more or less bioactive than IPN. Therefore a change in the antibiotic potency may give misleading results as was reported in previous studies[76]. This HPLC study was done in collaboration with Mr Toby Brown (from the Dyson Perrins Laboratory).

An HPLC system was developed by Jensen *et al.*[77] which separated IPN from all other reaction components and permitted quantification of IPNS activity. This method employed a C_{18} reverse phase column with a mobile phase of sodium dihydrogen phosphate pH 4.0 and a linear methanol gradient. Complete separation was achieved in a little over 20 minutes.

The results of a study which explores the importance of Gln330 in the catalytic activity of IPNS (*A. nidulans*) are reported in this chapter. Single amino acid substitutions were made by replacement of Gln330 residue with amino acids having hydrophobic (alanine, leucine) or acidic sidechains (aspartate) (see Figure 2.1). Since Gln330 was the penultimate residue on the C-terminus, it is possible that in Q330A,

Q330L and Q330A the role of the metal ligation may be fulfilled by the C-terminal carboxylate of Thr331. To exclude this possibility further C-terminally truncated versions of IPNS were made (Figure 2.1, G329, I325). Mutant proteins were analysed by kinetic studies.

Both DAOCS and IPNS display similar overall folds and show high sequence similarities. In DAOCS (*S. clavuligerus*) the C5-carboxylate of α-KG molecule forms a salt bridge with Arg258 and Ser260[34,60]. This highly conserved Arg-x-Ser motif is characteristic of other α-KG binding enzymes. An identical Arg-x-Ser motif has also been identified in IPNS which binds the valine carboxylate of ACV. In view of active site similarities between DAOCS and IPNS, it was postulated that IPNS may bind α-KG as shown in Scheme 2.1 (overleaf). To test this hypothesis the uncoupled turnover of α-KG by wild-type IPNS and with C-temininally truncated IPNS mutants was measured.

Previous researchers have reported that glutathione (γ-glutaminylcysteinylglycine, GSH) acts as a strong competitive inhibitor of IPNS[78]. In light of this finding and the observation that GSH is ubiquitous in cells, the inhibition of IPNS activity by GSH was measured. Since the GSH molecule shows similar structural entities to ACV it was postulated that the mode of binding may be such that the cysteinyl thiol bonds with Fe(II) and the terminal carboxylate of glycine can form a salt bridge with the Arg-x-Ser motif (Scheme 2.1C). Binding of GSH was investigated by measuring the activity of the wild-type and C-terminus mutants in the presence of increasing concentrations of GSH.

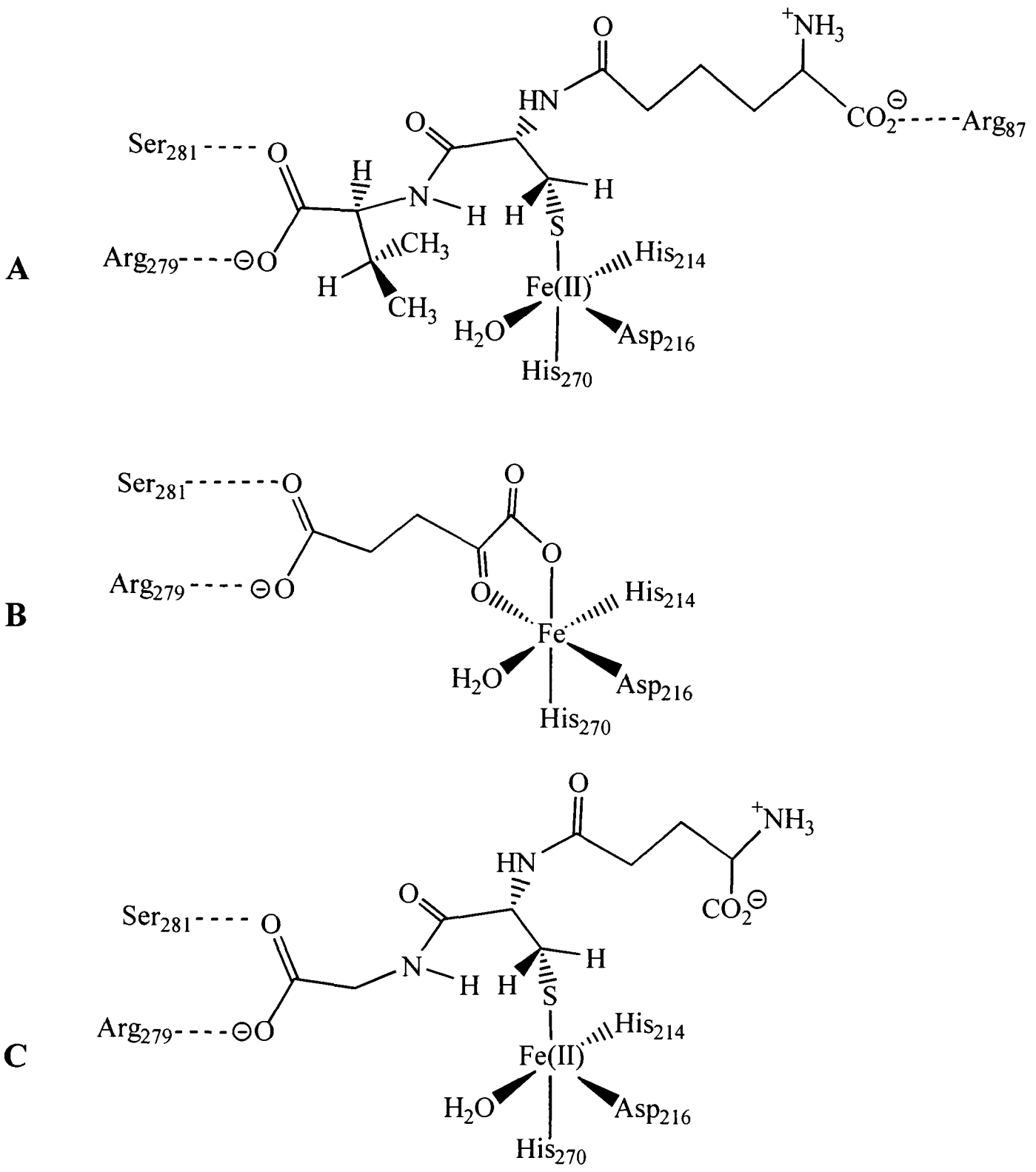

Scheme 2.1 Possible mode of binding in IPNS by ACV (A), α-KG (B) and GSH (C)

2.2 Results

Initial screening of plasmids was performed by restriction digestion selection followed by sequencing in both directions (see Chapter 6.2). Mutants having the correct

base changes were identified and stored at -80 °C for further characterisation (*vide infra*).

2.2.1 Purification

Cells transformed with mutant plasmids were grown overnight in shake flasks (2TY media) at 37 °C which resulted in the over expression of protein (*ca* 40%) which co-migrated with wild-type IPNS on SDS-PAGE. Some mutants always gave low protein expression levels and no improvements were seen in these by lowering the growth temperature to 27 °C. No variability was seen in the solubility of mutant proteins expressed. A five litre overnight growth typically gave 20-50 g of wet cell paste which yielded 200-300 mg (>95% purity by SDS-PAGE) IPNS after three column purification.

2.2.2 HPLC assays

The materials and methods for the HPLC assay are given in the experimental section (Chapter 6.2). The major components of the IPNS mixture showed distinct retention times when applied individually to the C_{18} column as previously described (Figure 2.4a). The resulting retention times are given in Table 2.1. Reproducible separations of the relevant compounds was achieved by maintaining the column at 30°C. Additionally, it was observed that the samples could be maintained at 4 °C for several hours without significant degradation of IPN.

In order to establish that IPN production could be detected by this method, an IPNS assay was performed using the concentrations of substrate and cofactors usually employed in the hole plate assay (Chapter 6.2). After approximately 5 minutes a new peak was observed which was absent in a control sample lacking enzyme (Figure 2.4b).

The new peak increased in size with incubation time and showed the same retention time as a synthetic IPN standard.

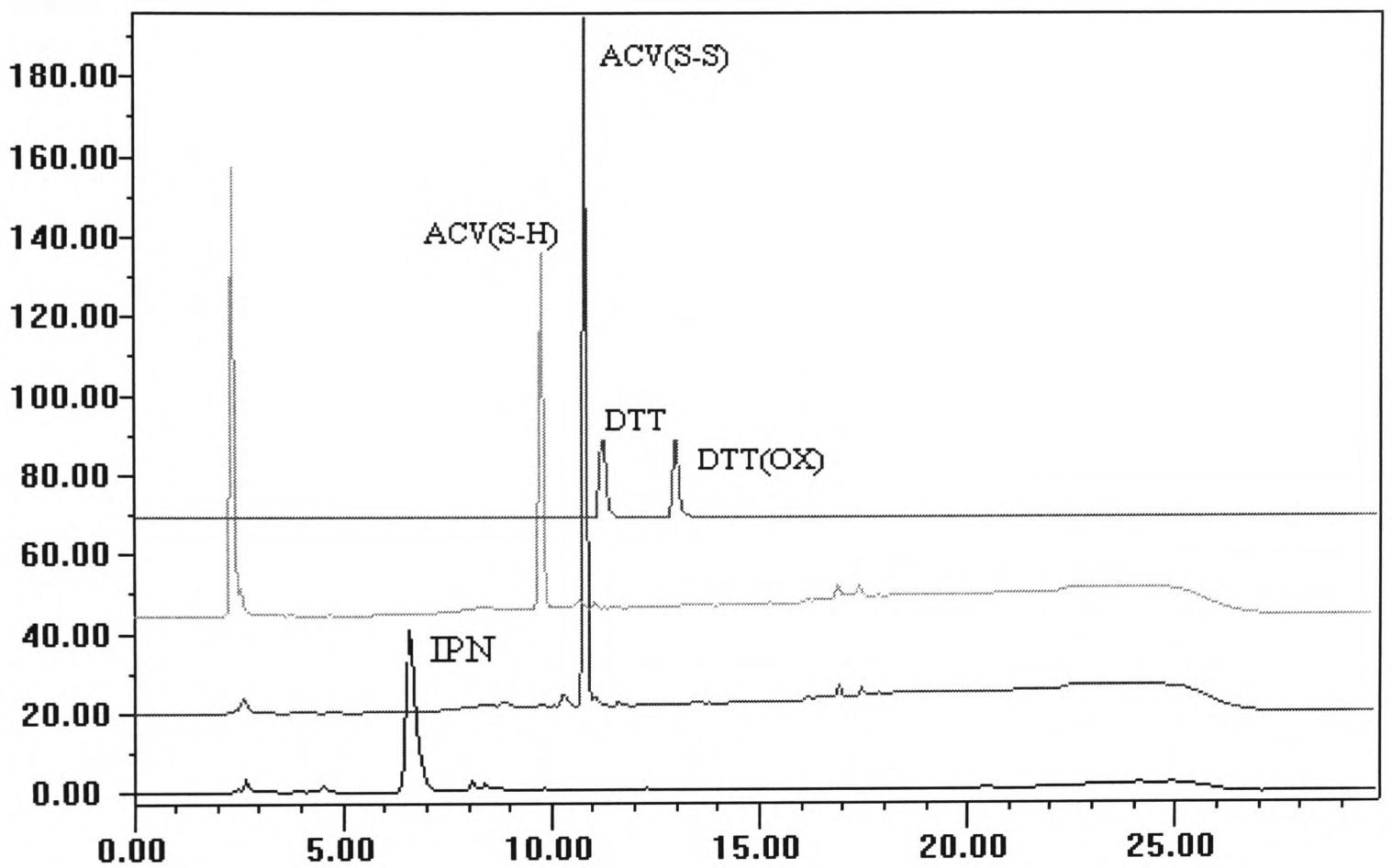

Figure 2.4a Resolution of the components of the assay mix by HPLC

Table 2.1 The retention times of components in the IPNS HPLC assay

Component	Retention Time (min)
Ascorbate	2.5
IPN	6.8
ACV-thiol	9.8
ACV-disulphide	10.8
DTT(oxidised)	14.0

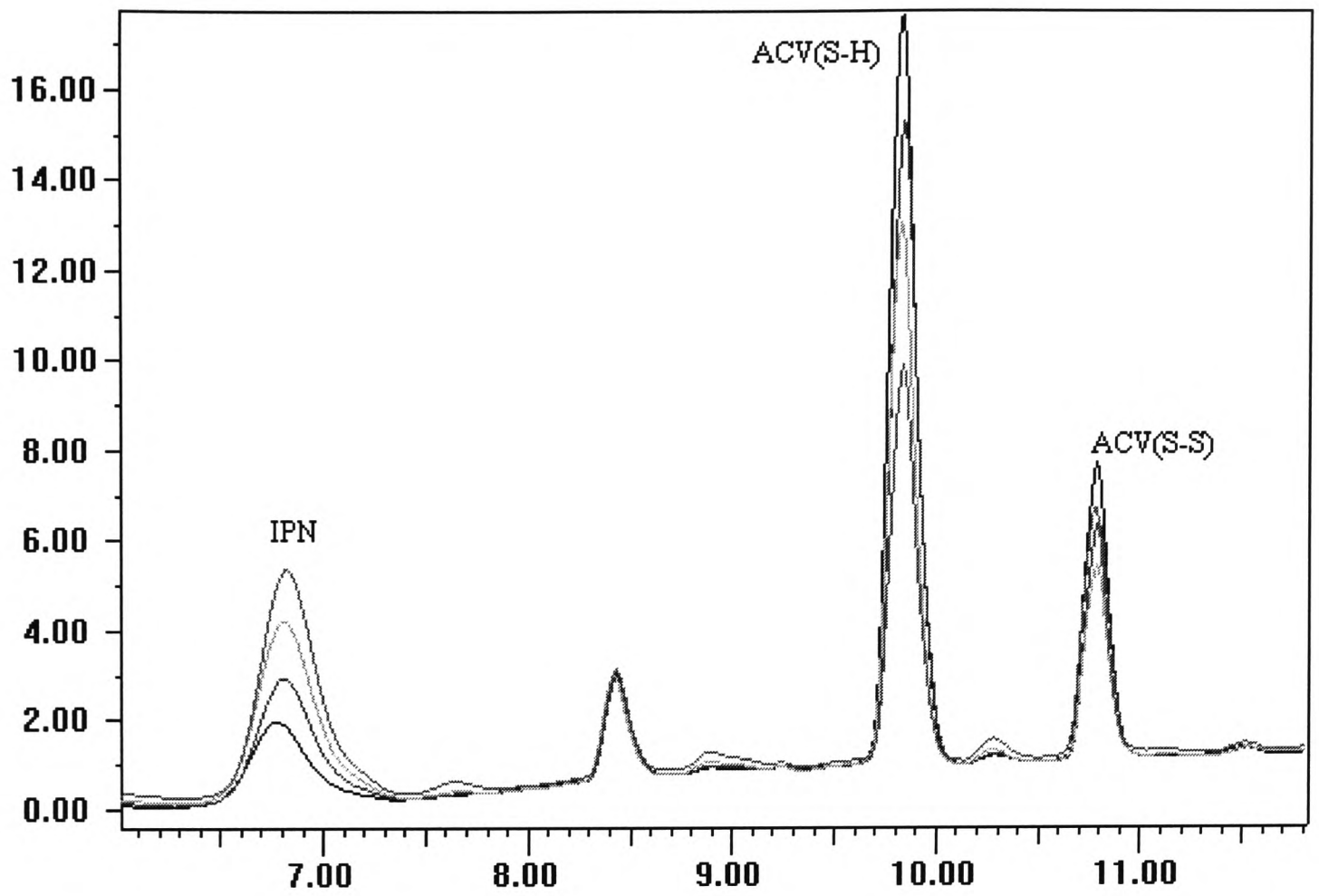

Figure 2.4b. Increase in IPN production and depletion of ACV with time. IPN peaks from bottom to top show an increase in time (5, 10, 15, 20 minutes).

Since both the ACV-thiol and ACV-disulphide appear to be present in the incubation mix it was clear that under these incubation conditions the effective concentration of ACV-thiol would be lower from the intended values. Therefore the ACV-thiol concentration was estimated from standard curve rather than the starting concentrations. The observation that no reduced DTT was present in the incubation mix at the end of the assay suggests that it had been completely oxidised.

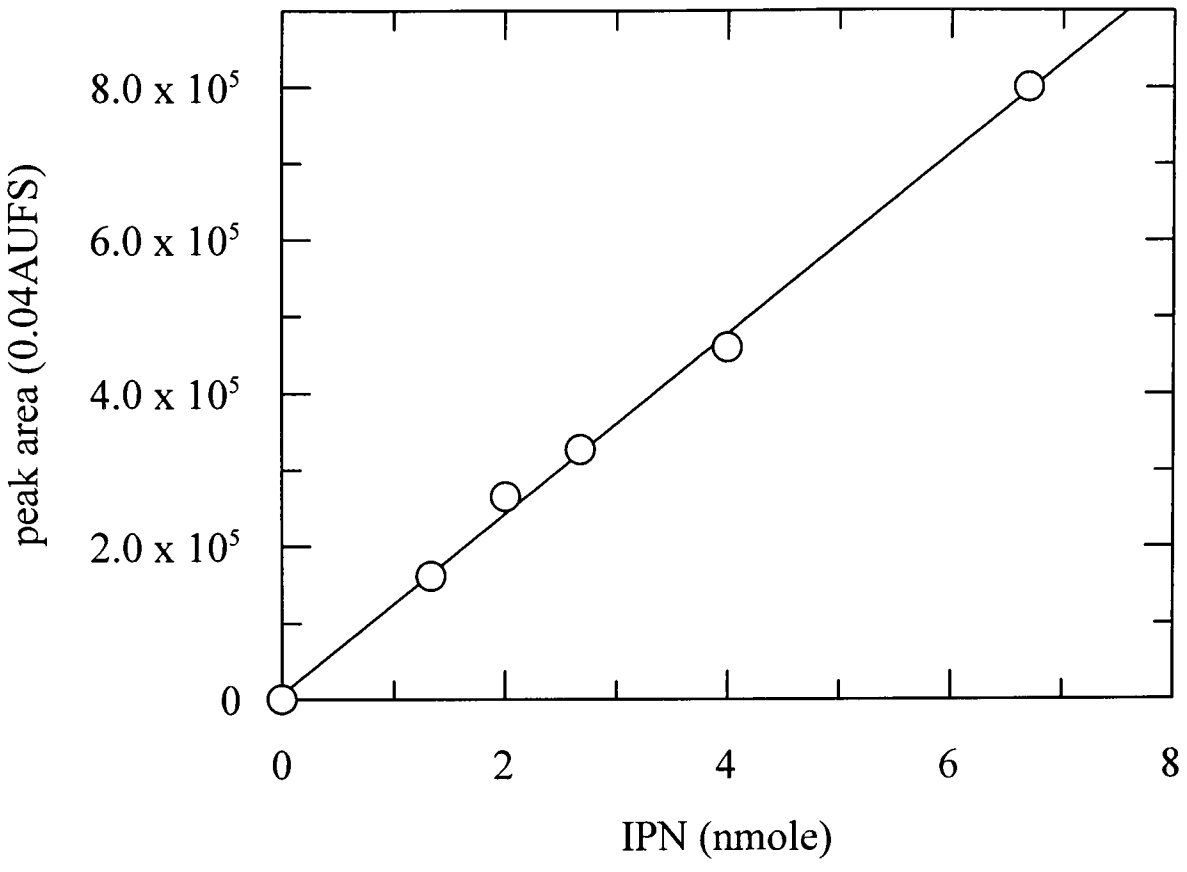

Figure 2.4c Calibration curve for IPN

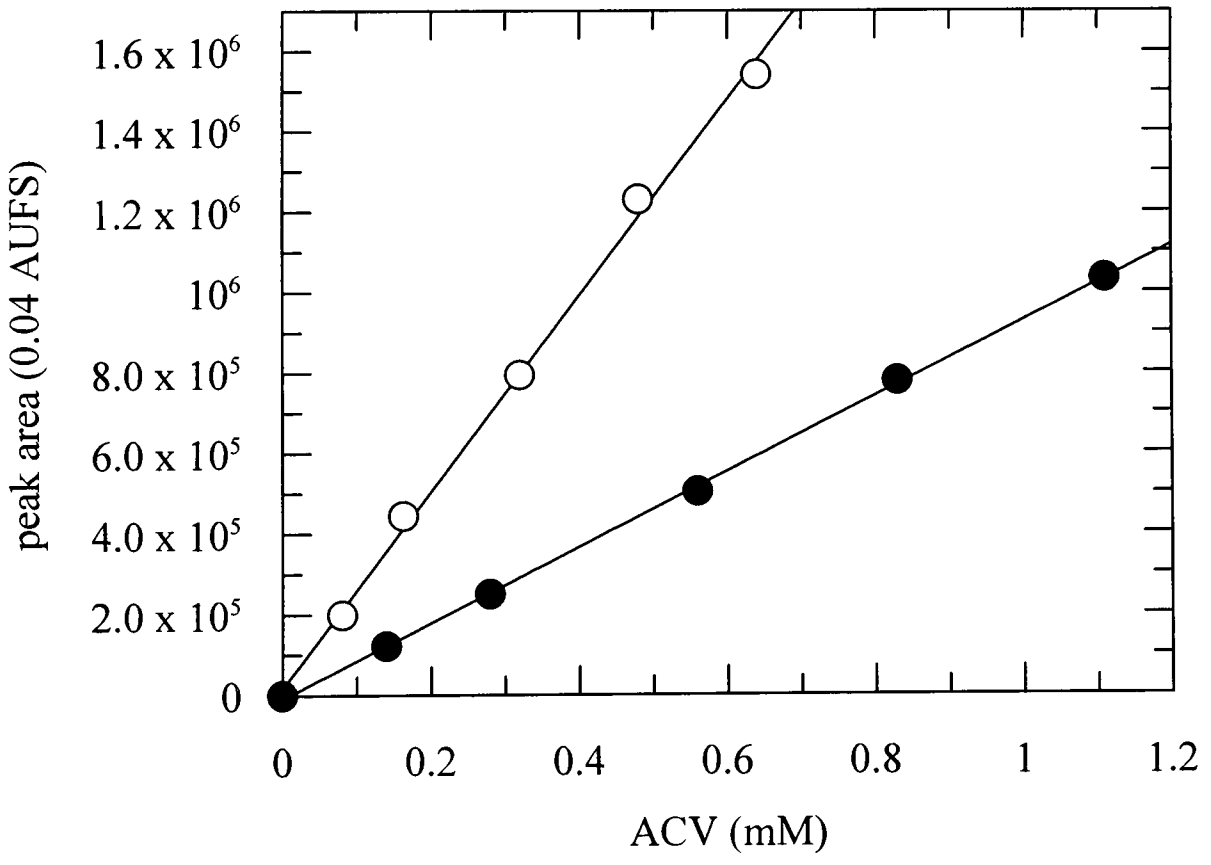

Figure 2.4d Calibration curve for ACV-thiol (closed circles) and ACV-disulphide (open circles).

Calibration curves (Figure 2.4c, Figure 2.4d), were generated by estimating the concentration of IPN, ACV-thiol or ACV-disulphide by ^{1}H-NMR. These calibrated standards were injected onto the HPLC column using the same elution conditions as before. The peak areas were plotted against the concentration of known standards to obtain standard curves. Hence the concentration of IPN or ACV in an unknown sample can be readily determined from a measurement of the peak area.

A large scale incubation of IPNS with cofactors was carried out and samples were removed after 5, 10, 20, 30 minutes. The production of IPN with time showed a linear range of activity over 20 minutes (Figure 2.4e). After 5 minutes < 20 % of the substrate has been converted. The kinetic parameters (Figure 2.4f) were derived by fitting the experimental data to Michaelis-Menton equation using the Leonora program[79].

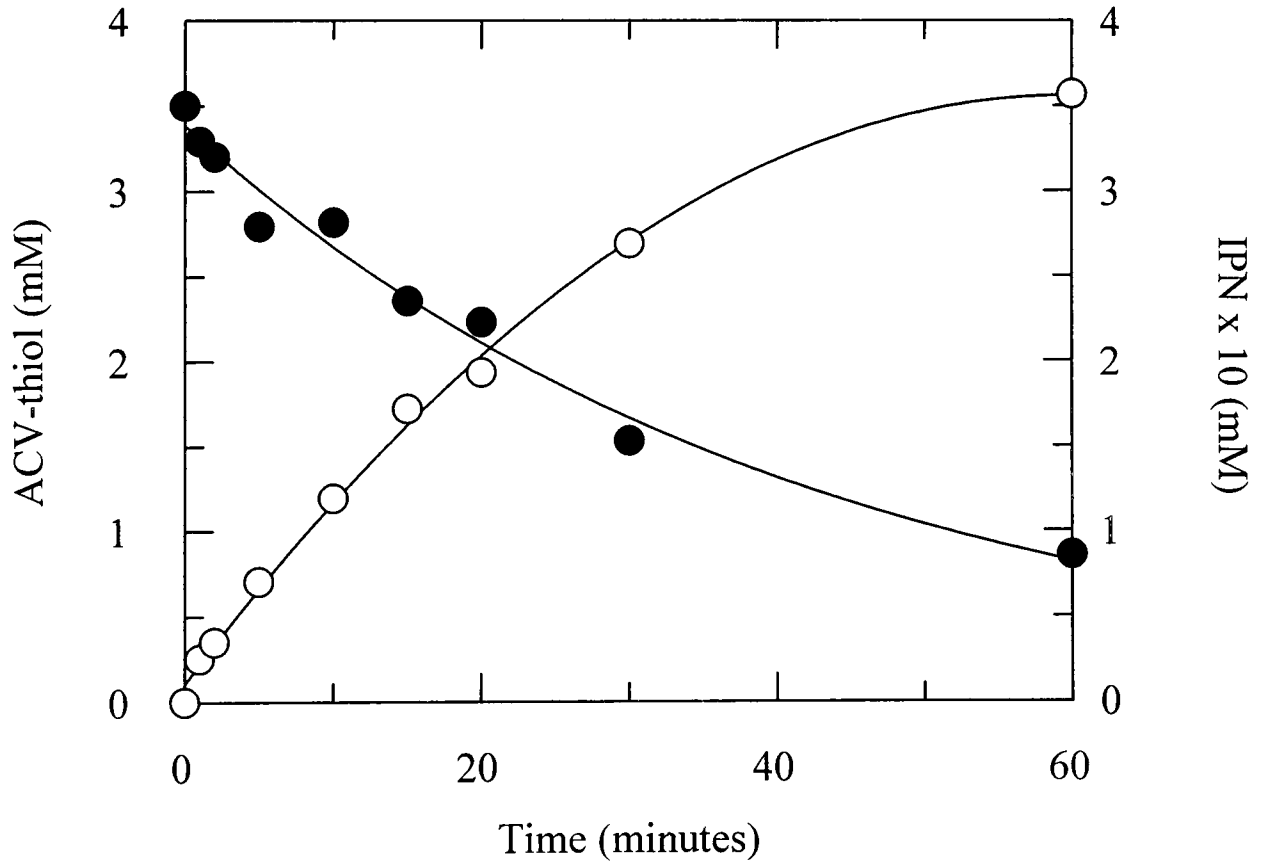

Figure 2.4e Time dependent IPN production (open circles) and ACV-thiol depletion (filled circles) under assay conditions.

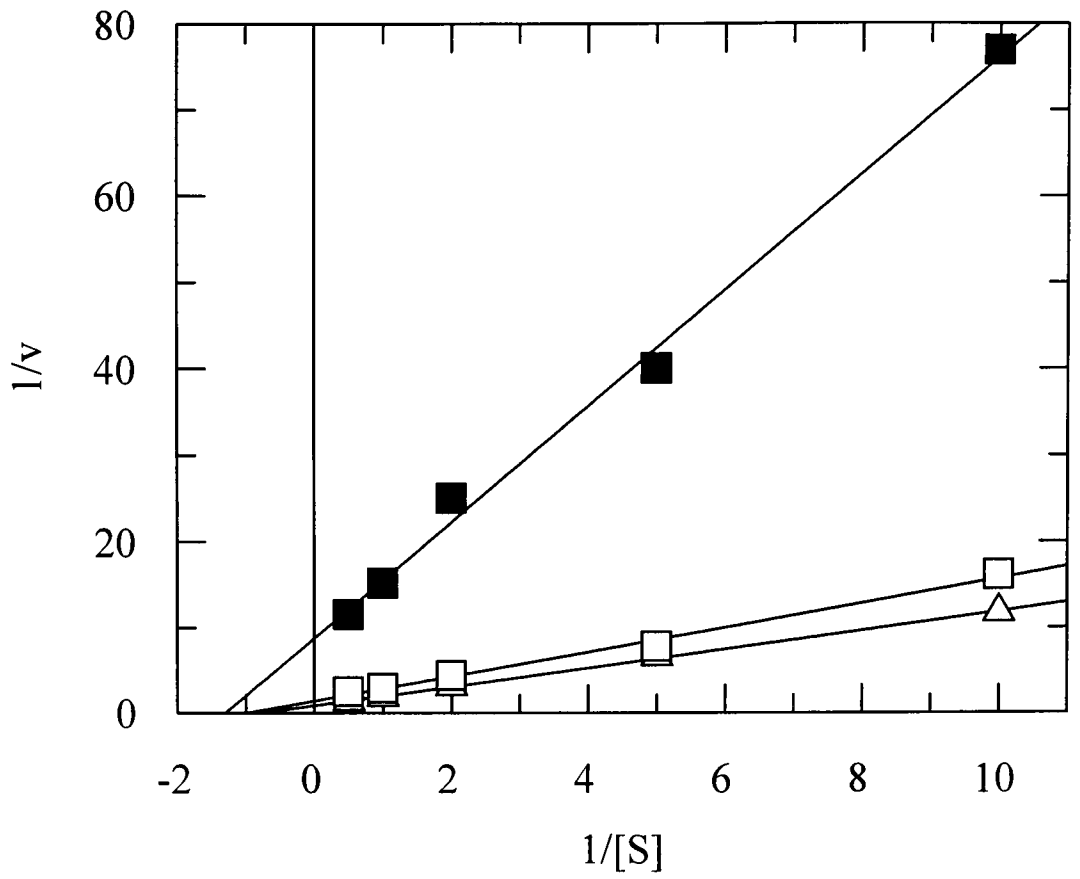

Figure 2.4f Lineweaver-Burk plot of kinetic data showing IPN production by wild-type IPNS (open triangles), G329 mutant (open squares) and I325 mutant (filled squares)

Table 2.2 Apparent kinetic parameters for wild type IPNS (*A. nidulans*) and mutants

Enzyme type	V_{max} (nmol/min/mg)	K_m (mM)	k_{cat} (min^{-1})	k_{cat}/K_m (mM^{-1} min^{-1})
wild-type	909 (±90)	1.22 (±0.23)	40	32.3
Q330A	475 (±66)	0.72 (±0.22)	20	27.4
G329	495 (±40)	0.70 (±0.11)	20	28.0
I325	106 (±3.3)	0.82 (±0.06)	3.3	4.3

2.2.3 Hole plate assays

Enzyme assays were carried out (at least) in duplicate using two different protein concentrations of each mutant enzyme with essentially the same results. IPNS mutants were tested for production of IPN using the hole plate bioassays. The results from hole plate assays are summarised in Table 2.3. The Mcat hybrid mutant (made by Mr Toby Brown, Dyson Perrins Laboratory) encodes a truncated *S. cattleya* IPNS C-terminus which is shorter by eight amino acids (see Figure 2.1 earlier). Apart from Mcat, the mutants Q330A, Q330L, Q330D, G329 and I325 were active. The Mcat showed no activity by hole plate assay method (Table 2.1) and further assays repeated with higher protein concentrations (up to 100 μM) also failed to show activity with this protein.

The trends in the observed specific activities for the other IPNS (*A. nidulans*) mutants from the hole plate assay correlated qualitatively with the HPLC assays (Table 2.2). The HPLC assays were carried out (at least) in duplicate on each mutant IPNS with essentially the same results and the measurements varied no more than 20% between two independently purified batches of the same protein. The specific activity for the recombinant wild type IPNS (*A. nidulans*) using the HPLC assay was somewhat lower than reported for IPNS (*C. acremonium*) enzyme using an oxygen electrode[80] assay or an ACV consumption assay[51].

Table 2.3 Hole plate assays and mass spectrometric analyses of IPNS (*A. nidulans*) and mutants. Results show the average of three separate determinations of specific activity.

Enzyme type	Calculated[a] MW (Da)	Observed MW (Da)	Relative specific activity (wild type=100%)
wild type	37391	37392 (±1)	100
Q330A	37334	37335 (±1)	63
Q330L	37376	37381 (±2)	100
Q330D	37378	37382 (±2)	64
G329	37161	37161 (±3)	40
I325	36748	36746 (±2)	10
Mcat	36652	36653 (±4)	<0.5

[a] Values calculated from translated amino acid sequences based on reported DNA sequences.

2.2.4 CD Spectra

Each mutant CD spectrum was compared with that of the wild-type to see if any significant changes in the secondary structures could be observed. If a protein displays incorrect folding, this may be one reason for low catalytic activity other than the introduced mutation itself. All of the CD spectra from mutant IPNS enzymes (either active or inactive) could be superimposed onto the wild-type indicating that no major change in the protein secondary structure took place after mutagenesis (results not shown).

The molecular masses from ESIMS analysis of the mutant IPNS enzymes (*A. nidulans*) correlated well with the values from the predicted amino acid sequences (Table 2.3).

2.2.5 Uncoupled turnover of α-KG

The uncoupled decarboxylation (*i.e.* without any 'prime' substrate) of α-KG in wild-type and mutant IPNS enzymes were measured (as described in Chapter 6.2) with the following cofactor mix: DTT (5 mM), ascorbate (5 mM), α-KG (2 mM), $FeSO_4$ (2 mM). All incubations were performed at 28 °C for 60 minutes and the results are summarised in Table 2.4a. The specific activity of uncoupled turnover by DAOCS was estimated to be 5 nmol/min/mg. This figure is low compared with the previously reported value of 30.5 nmol/min/mg for the uncoupled conversion[60]. There was no significant uncoupled turnover of α-KG in wild-type or mutant IPNS enzymes over the background level observed with buffer alone.

Table 2.4a Comparisons of uncoupled turnover of α-KG by DAOCS, wild-type and mutant IPNS enzymes. Results show incubations for 30 minutes from an average of two separate determinations.

Enzyme	μg	dpm[‡] (± 2 %)	specific activity (nmoles/min/mg)
DAOCS[†]	42	5264	4.9
IPNS	12	413	0
IPNS	68	369	0
G329	8	386	0
G329	49	454	0
I325	12	404	0
I325	72	419	0
buffer	-	444	0
BSA	100	456	0

[†] Uncoupled turnover.

[‡] Specific activity of [^{14}C] labelled α-KG of 178000 dpm/400 nmoles.

2.2.6 Effect of α-KG on IPNS activity

The activity of IPNS was measured using standard incubation conditions as described in Chapter 6.2 except that α-KG was added to the cofactor mix before initiating the reaction. Table 2.4b summarises the results from bioassay activity using an initial ACV concentration of 1 mM. The results show that up to 8 mM α-KG has no significant effect on the IPNS activity. No inhibition was shown by α-KG under all the incubation conditions; at 8 mM α-KG the concentration is roughly 8 times the apparent K_m value (around 1 mM) for the ACV.

Table 2.4b Effect of α-KG on the specific activity of wild-type IPNS. Activity measured by hole plate assay. Results show 20 minutes incubations from an average of three separate determinations with errors in parenthesis.

concentration of α-KG (mM)	specific activity (nmol PenN/min/mg)
0	3420 (± 500)
2	3280 (± 390)
4	4030 (± 450)
8	3660 (± 310)

2.2.7 Effect of GSH on IPNS activity

The hole plate IPNS assays were performed as described in Chapter 6.2 except that a higher iron concentration (up to 1 mM) was employed. Table 2.4c summarises the results from the effect of GSH on the IPNS activity. No effect on the activity of wild-type and mutant IPNS was seen with GSH concentrations of up to 10 mM. No kill zones were

seen in wild-type or mutant IPNSs with high (>10 mM) GSH concentrations. No kill zones were seen in buffer alone under all concentrations of GSH.

Table 2.4c The effect of GSH on the specific activity of wild-type and IPNS mutants. Specific activities (measured by hole plate assay) are given as a percentage of control with no GSH (top row). Results show 30 minutes incubations from an average of two separate determinations with errors in parenthesis.

GSH added (mM)	wild-type	G329	I325	buffer
0	100 (± 30 %)	100 (± 30 %)	100 (± 30 %)	0
5	100 (± 30 %)	100 (± 30 %)	100 (± 30 %)	0
10	100 (± 30 %)	100 (± 30 %)	70 (± 21 %)	0
50	<5	<5	<5	0
200	<5	<5	<5	0

2.3 Discussion

The results clearly demonstrate that neither Gln330 nor the C-terminal carboxylate of Thr331 are essential for catalytic activity. Further evidence in support of this finding was obtained from mutagenesis studies on IPNS, from *Streptomyces jumonjinensis,* which also showed that the C-terminus was not essential for activity[81]. Strong support for this proposal was obtained from the crystal structure of the Fe(II)-IPNS-ACV complex which shows the displacement of the C-terminus Gln330 metal ligand upon ACV binding[52].

The crystal structure of IPNS complexed to manganese shows the C-terminal α-helix projecting between two of the eight β-strands forming the 'jelly roll' β-barrel of IPNS[24]. The eight residues subsequent to the C-terminal helix form a loop terminating in the conserved (except apparently for the *S. cattleya* IPNS) Gln330-Thr331 dipeptide. Analysis of the IPNS-manganese structure suggests that this cannot occur without prior displacement of at least one of the four metal ligands (His214, Asp216, His270, Gln330). Since the two histidyl and aspartyl residues form a part of the jelly roll platform of IPNS and are conserved throughout other sequence related members of the family, we have proposed that the amide side chain of Gln330, which is only conserved through IPNS isozymes, is displaced from the iron during catalysis. Ligation of the cysteinyl thiol of ACV to the active site iron has been demonstrated by crystallographic[52] and spectroscopic[54,82] studies.

The modified IPNS enzymes in which Gln330 was substituted by alanyl (Q330A) or leucyl (Q330L) residues display reduced but substantial catalytic activities of greater than 50% of that of the wild type enzyme. Deletion of two C-terminal residues (G329) also led to a *ca.* 50% reduction in specific activity. Hence, ligation of the amide side chain of the histidyl residue to the active site metal is clearly not essential for catalysis (Tables 2.2 and 2.3). Since Gln330 is the penultimate residue on the C-terminus of IPNS it is possible that in the Q330A, Q330L and G329 mutants, the role of the amide side chain of Gln330 might be fulfilled by the C-terminal carboxylate. However, a further C-terminally truncated version of IPNS with six residues deleted (I325) was still active, albeit with a much reduced specific activity of only *ca.* 10% of that of the wild type enzyme.

In order for the C-terminus of the I325 mutant to reach to the active site metal (minimally) some unravelling of the C-terminal α-helix must occur. Since this is unlikely to occur without a distortion of the structure, the possibility of the C-terminal carboxylate substituting for the amide side chain of Gln330 in the modified IPNS is considered to be extremely unlikely. IPNS (*A. nidulans*) was also modified by the deletion of eight residues from its C-terminus and substitution of four other residues at the C-terminus (Figure 2.1) to give a protein with a similar truncated C-terminus to that reported for *S. cattleya*. However, the resultant hybrid IPNS (Mcat) was completely inactive with respect to isopenicillin N formation.

CD spectroscopic comparisons of the wild type, hybrid IPNS (Mcat) and other modified IPNS enzymes showed no differences in secondary structure. Precise reasons for the lack of activity of the hybrid IPNS (Mcat) are presently unclear. The possibility should be considered that the stop codon apparently truncating the *S. cattleya* IPNS sequence is either read through *in vivo* or is artefactual; a single base change to the published *S. cattleya* IPNS sequence restores a 'typical' C-terminus to the *S. cattleya* enzyme.

2.3.1 Kinetic results

Although we have determined the apparent K_m and k_{cat} values for the wild-type IPNS and three modified IPNSs, the interpretation (and accuracy) of the kinetic data is complicated by a number of factors: (1) the liability of the product with respect to hydrolysis; (2) conversion of the substrate thiol to its disulphide (a facile process under the incubation conditions); (3) non-enzymatic consumption of dioxygen (again significant under the incubation conditions); (4) inactivation of IPNS (either *via*

'incorrect' reaction of catalytic intermediates or by Fenton/Udenfriend type reactions); (5) production of 'shunt products'[49]. Nonetheless the preliminary results based on the analysis of IPN production are intriguing and merit brief discussion. During the course of the present kinetic studies, several modifications to the reported assays were made which resulted in much higher activities than those reported in the present studies[83].

The apparent K_m values for ACV for the Q330A, G329 and I325 modified IPNSs are all reduced by similar amounts (*ca.* 35-45%) relative to the wild type enzyme. We propose that the side chain of Gln330 is displaced from the active site iron by the thiol of ACV and the observed reductions in K_m for ACV are consistent with this proposal. Part of the role of the C-terminus may be to maintain ferrous iron at the active site under the relatively low iron concentrations (*c.f. in vitro* incubations) likely to be found *in vivo*. However, there is also a clear reduction in k_{cat} in the C-terminally modified IPNSs, by *ca.* 50% in the case of the G330A and G329 mutants and by >90% in the case of the I325 mutant. These observations imply a role for the C-terminus in steps subsequent to iron and ACV binding such as protection of the ferryl intermediate from quenching by water, or the loss of partial product.

2.3.2 Uncoupled turnover of α-KG

The uncoupled turnover of α-KG by DAOCS was approximately 3% of the total α-KG used in the incubation mix and in agreement with previous findings[60]. The results clearly demonstrate that under similar conditions neither the wild-type IPNS or IPNS mutants convert α-KG. One possible reason for this may be due to the differences in the C-terminal sequences between the two enzymes. However, a more obvious reason for this lack of activity may be due to the stereochemistry at the metal binding ligands. A

comparison of the crystal structures of DAOCS and IPNS show significant differences of the metal binding α-KG and dioxygen binding sites. In the DAOCS the 2-carbonyl of α-KG binds *trans* to Asp185 which allows (in the proposed mechanism) the oxygen binding *trans* to His183 (Scheme 2.2B). If a similar mode of α-KG binding occurs in IPNS this will give rise to a topology shown in Scheme 2.2A. If this complex is formed then oxygen binding is unlikely to occur in IPNS since the proposed dioxygen binding site is already occupied by 2-carbonyl group of α-KG.

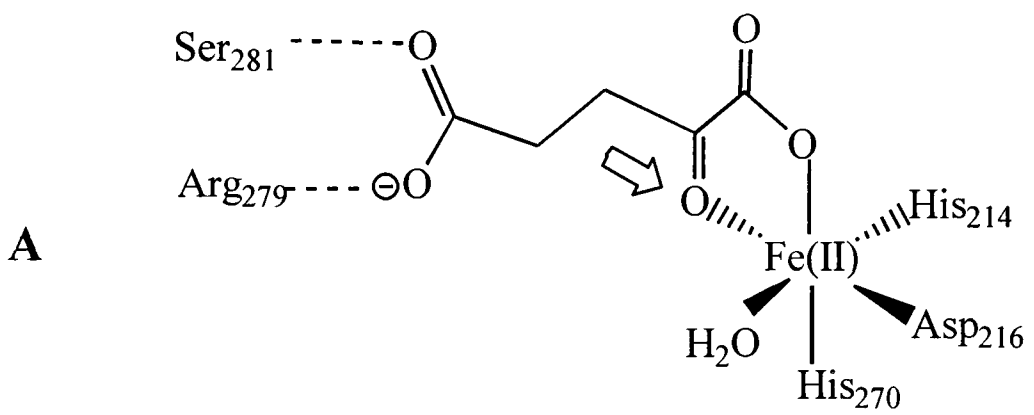

Scheme 2.2 Possible mode of binding of co-substrate, α-KG, in IPNS (A) and DAOCS (B). Arrows show proposed oxygen binding sites.

In contrast to the previous reported findings, the present results demonstrate that GSH was not an inhibitor of catalytic activity in either wild-type and mutant IPNS enzymes (at concentrations up to 50 mM). Previous substrate analogue studies on the α-aminoadipoyl side chain variants reported that linear side chains terminating in a carboxyl group were good substrates[49]. The crystal structure of the IPNS-Fe-ACV complex show that GSH

would have a poor binding affinity because the glutaminyl side chain is shorter by one methylene compared with an ACV aminoadipoyl side chain. Therefore the GSH molecule is not long enough to form a salt-bridge with Arg87. One possible reason for the loss of activity at increased GSH (>10 mM) concentrations in the present study may result from sequestration of the ferrous iron (~1 mM) by the GSH. The observed loss of activity by previous researchers may also be explained by the sequestration of the ferrous iron by GSH and possibly by the different incubation conditions employed[78].

2.3.3 Role of the C-terminus

The high sequence similarity and conservation of the C-terminus of the IPNSs and the reported C-terminal dependent oligomerisation of DAOCS suggests that that there must be some significant role for the C-terminus.

It is clear from the kinetic studies that the C-terminus is not essential for catalytic activity. Kinetic results imply a role for the C-terminus subsequent to iron and ACV binding. One possibility is that the C-terminus promotes release of the intact penicillin product from the active site; if the penicillin is allowed to remain at the active site the iron may promote Lewis acid catalysed fragmentation of the bicyclic penicillin *via* complexation to the sulphur of the thiazolidine ring. However sulphur in the penicillin ring product would be expected to bind the iron less well than the sulphur of the ACV substrate.

The inherent mobility seen in the C-terminal region seen with IPNS and DAOCS from crystal structures suggests a role for the C-terminus as a 'gate' controlling the access to the active site. In the open 'gate' form of enzyme the active site is exposed and is therefore more susceptibile to (1) proteases, (2) misfolding and (3) oxidative damage. The observation that both IPNS and DAOCS are unstable *in vitro*, particularly under

catalytic conditions (in the presence of ferrous iron, oxygen and ascorbate) which results in oxidative damage to the exposed active site, supports this suggestion. The *in vitro* inactivation rates of wild-type IPNS have been measured and results show that they arise principally from oxidative damage at the active site (*vide infra*). The failure to observe differences in the CD results between wild-type and C-terminus mutants precludes the second possibility. The measurement of oxidative inactivation rates of the wild-type and C-terminus truncated IPNS mutants would be one way to investigate the third possibility.

CHAPTER 3

Role of the 2-His-1-Carboxylate Motif of Isopenicillin N synthase

3.1 Introduction

The IPNS isozymes display significant sequence similarity with other members of an extended subfamily of mononuclear ferrous iron dependent oxygenases/oxidases[24,61]. Partial sequence comparisons of IPNS, ACCO and other oxygenases which utilise α-KG, show that His214, Asp216 and His270 (using the *Aspergillus nidulans* IPNS sequence numbering) are conserved throughout all members of the 'IPNS subfamily' of oxygenases (Figure 3.1). The prevalence of these two conserved histidines and a carboxylate, also known as the '2-His-1-carboxylate motif', also appears to be a common reaction platform amongst the family of wider mononuclear iron enzymes and suggests that they may have evolved *via* a convergent process[84].

Notably, a similar 2-His-1-carboxylate motif has also been observed in zinc hydrolases[85] which suggests that iron oxygenases/dioxygenases may have evolved from a common ancestral hydrolase gene. It has been suggested that many millions of years ago, in the anaerobic environment of the earth, micro-organisms evolved metal dependent hydrolases to regulate the control and metabolism of the precious amino acid source (and other metabolites). As the environment became aerobic (over millions of years) these hydrolases may have evolved into oxygenases/oxidases, including penicillin forming enzymes. The acquisition of this penicillin biosynthesis gene probably gave an

evolutionary advantage to early organisms which were now able to release penicillin into their environment and ultimately reduce competition for nutrients by other organisms.

	Block A (214-217)	Block B (270-289)
1 ACCO	HTDAGGILLFQDDK	HRVIA----QTDGT-RMSLASFYNPG
2 F3OH	HTDPGTITLLLQDL	HQAVV----NSECS-RLSIATFQNPA
3 H6H	HYDGNLITLLQQD	HRVVT----DPTRD-RVSIATLIGPD
4 FOLS	HTDMSYITILVPNE	HRTTV----NKDKT-RMSWPVFLEPP
5 GC20	HTDPTSVTILHQDP	HRAVV----NSMNA-RKSLAFFLCPS
6 DAOCS	HYDLSMVTLIQQTP	HHVAAPRRDQIAGSSRTSSVFFLRPN
7 DAOCS/DACS	HYDLSTITLVHQTA	HRVKSPGRDQRVGSSRTSSVFFLRPK
8 C. acremonium	HEDVSLITVLYQSD	HRVK------WVNEERQSLPFFVNGL
9 P. chysogenum	HEDVSLITVLYQSD	HRVK------WVNEERQSLPFFVNGL
10 N. lactamdurans	HFDVSMITVLYQTE	HRVK------FVNAERLSLPFFFHAG
11 S. jumonjinensis	HLDVSMITVLYQTE	HRVK------FINAERLSLPFFLNAG
12 A. nidulans	HEDVSLITVLYQSN	HRVK------WVNAERQSLPFFVNLG
	↑ ↑	↑ ⇧ ⇧
	He**D**VSLITVLYQSn	**H**RVK----------**R**q**S**LPFFVnLg

Figure 3.1 Partial sequence comparisons of the putative metal binding ligands of IPNS, ACCO (tomato) and α-KG dependent oxygenases. Arrows show absolutely conserved residues: filled arrows, show metal binding ligands; unfilled arrows, residues that bind IPNS valine carboxylate or C5 carboxylate of α-KG in α-KG dependent enzymes. Bottom row shows IPNS consensus sequence (from nine IPNS isoenzymes): totally conserved (bold), conserved (capitals) and non-conserved (lower case). (DAOCS (*S. clavuligerus*); DAOCS/DACS (*C. acremonium*); F3OH, flavanone 3-β-hydroxylase (*Zea mays*); H6H, hyoscyamine 6-β-hydroxylase (henbane); FOLS, flavanol synthase (*Pertunia hybrida*); GC20, gibberellin C-20 oxidase (*Cucurbita maxima*). IPNS isoenzymes from various organisms shown in rows 8-12. (Adapted from Roach *et al.*[52])

3.1.1 The 2-His-1-carboxylate motif

Several crystal structures and sequence alignment studies have reported that the 2-His-1-carboxylate motif provides a common iron binding platform in non-haem iron dependent dioxygenases[82,84]. This motif has been observed in crystal structures of a number of enzymes which were previously thought to be unrelated based on primary sequence alignments. A comparison of the common structural platform suggests that it is

composed of two histidines and a carboxylate surrounding the iron centre as shown in Figure 3.2. The active sites of these enzymes has revealed at least one co-ordination site that is vacant or occupied by solvent water and is thus available for the binding of exogenous ligands such as substrates, cofactors or dioxygen.

A 2-His-1-carboxylate motif was predicted to be present in DAOCS based on sequence alignment studies. This prediction was confirmed by crystallographic studies on this enzyme (see Chapter 1). However, in other cases the situation is unclear, for example, convincing overall sequence alignments cannot be made between IPNS and proline 3-hydroxylase (P3-H) an enzyme that catalyses the oxidation of proline to give 3-hydroxyproline. The crystal structure of P3-H (*Streptomyces* THI) has also been recently solved[33]. Structural similarities with IPNS and DAOCS were revealed when the crystal structure was determined. These include the presence of the 2-His-1-carboxylate iron binding motif and the presence of a 'jelly-roll' barrel core.

Prolyl 4-hydroxylase catalyses the hydroxylation of proline in -X-Pro-Gly- sequences in collagen and related proteins. The hydroxylation reaction requires Fe(II), α-ketoglutarate and O_2 and involves the oxidative decarboxylation of α-KG[86]. Mutagenesis studies indicated that a 2-His-1-carboxylate motif also exists in the α-subunit of this enzyme. The mutation of the conserved Asp414 to a glutamate gave an enzyme with 15% of the residual activity of the wild-type enzyme. Based on the results from the α-KG coupled turnover assay, the increase in the apparent K_m for Fe(II) of the D414E mutant was correlated with the proposed function of this metal binding ligand. The reported increase in the K_m of α-KG for the K493R mutant was surprising in view of the proposed binding of this cofactor in DAOCS (see Chapter 2).

2,3-Dihydroxybiphenyl-1,2-dioxygenase (BphC) is an extradiol-cleaving catechol catalysing the extradiol ring cleavage of the polychlorinated 2,3-dihydroxybiphenyl[38]. Sequence alignments of the extradiol cleaving dioxygenase showed that three histidines, one tyrosine and one glutamate were totally conserved throughout all known BphC sequences. The crystal structure revealed a square pyramidal geometry with two histidines and one glutamate forming the 2-His-1-carboxylate motif as shown in Figure 3.2 (see overleaf).

Tyrosine hydroxylase (TyrOH) catalyses the conversion of tyrosine to *L*-DOPA (3,4-dihydroxyphenylalanine), the first step in the biosynthesis of the catecholamine neurotransmitters dopamine, noradrenaline and adrenaline. Sequence homologies and partial proteolysis have demonstrated that it is composed of an N-terminal domain with regulatory function and a C-terminal domain with catalytic function. The crystal structure of C-terminal TyrOH (rat enzyme) revealed a square pyramidal geometry around the metal centre also with two histidines and a glutamate forming the 2-His-1-carboxylate motif[87].

The high sequence similarity and mutagenesis studies suggest that the 2-His-1-carboxylate motif also occurs in ACCO (Figure 3.2). Studies on ACCO have demonstrated that the replacement of His177 or Asp179 with glutamate resulted in active ACCO, albeit with much reduced activity (*ca.* < 0.2 %) compared to the wild-type enzyme. The modified and active ACCO enzymes all underwent MCO (metal catalysed oxidation) fragmentation, indicating that they can bind iron, dioxygen, ACC and ascorbate[66]. The D170E ACCO mutant displayed an increased apparent K_m for ACC and Fe(II).

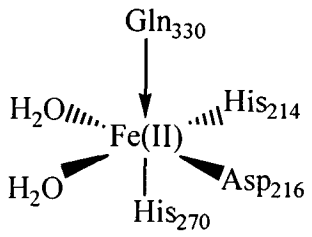

IPNS

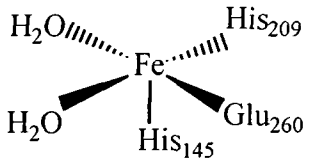

BphC

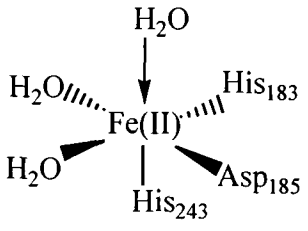

DAOCS

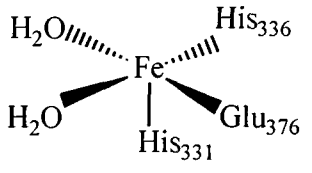

TyrOH

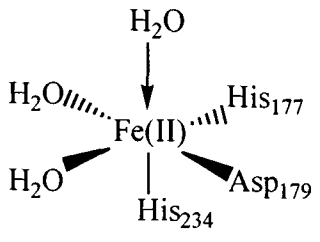

ACCO

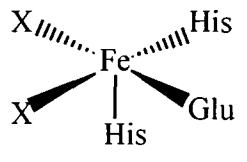

TfdA

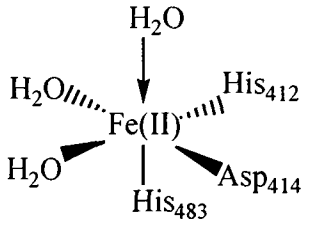

PH

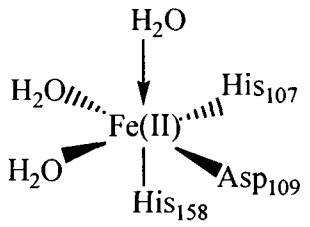

P3-H

Figure 3.2 The 2-His-1-carboxylate motif. Isopenicillin N synthase (crystal structure), IPNS[24]; deacetylcephalosporin C synthase (crystal structure), DAOCS[34]; 1-aminocyclopropane-1-carboxylate oxidase, ACCO[66]; prolyl 4-hydroxylase, PH[86]; proline 3-hydroxylase (crystal structure), P3-H[33]; 2,3-dihydroxybiphenyl-1,2-dioxygenase (crystal structure), BphC[38]; tyrosine hydroxylase (crystal structure), TyrOH[87]; 2,4-dichlorophenoxyacetate dioxygenase, TfdA[88].

Previous researchers have reported that the substitution of the His214, His270 or Asp216 with alanine in *Streptomyces jumonjinensis* IPNS, resulted in the complete loss of activity[50]. Similar results and conclusions were reported in studies on *C. acremonium*

IPNS substituting His214 or His270 with Leu[51]. Both these studies demonstrated the importance of the putative metal binding triad of amino acids around the reaction platform.

3.1.2 UV-Visible spectroscopy

The spectra of transition metal complexes can be interpreted in terms of d→d transitions. The intensities and band position depend on the metal, the ligand, and the arrangement (stereochemistry) of the ligands. In addition to the d→d transitions, many transition metal complexes exhibit very intense absorption peaks ($\varepsilon = 10^6$-10^7 M^{-1} cm^{-1}) that are often referred to as charge transfer spectra. In these, the electronic transition can be thought of as one in which an electron is moved from one atom and is 'transferred' to another. Charge transfer bands often appear in the UV region and tail into the visible region. However, one important exception is the Fe(III) porphyrin systems which have bands at ~1000 nm, well into the infra-red. The position of the charge transfer bands depends upon both the metal ion and ligand and on the relative ease of oxidation and reduction of these species. It is not surprising that many metal-containing oxidases and electron-transfer enzymes show strong charge-transfer bands. IPNS, in the presence of Fe, ACV and NO has been reported to give a charge transfer species with a pink colour which arises from the thiolate→Fe(III) charge-transfer[53]. The resulting spectrum is very similar in shape and position to that observed for an electron transfer protein, rubredoxin, which results from four tetrahedrally arranged cysteinyl thiols[89] and gives a peak at 497 nm ($\varepsilon = 8700$ M^{-1} cm^{-1}).

The studies described herein were aimed at investigating the roles of the IPNS iron ligands and determining the functional consequences of their modification for catalysis and oxidative modification. An important aspect of the experimental design was to use anaerobic UV-visible spectral studies to investigate metal binding of the modified IPNS enzymes. These studies demonstrate that the D216 ligand can be modified to a glutamate (D216E), with retention of catalytic activity, albeit with a specific activity of *ca.* 10% of that observed in wild-type enzyme. The remaining mutants (H214D, H214E, H214N, D216Q, D216H, H270D, H270E, H270N and H214D/D216H, D216H/H270D) were inactive with respect to catalytic turnover of ACV.

Previously it has been demonstrated that the ACV analogue, ACAB, is a substrate for IPNS giving a single cepham and two isomeric penam products[49]. The activity of the D216E and H270E was measured with ACAB since it was anticipated that the enhanced flexibility in the aminobutyrate moiety may affect the ratio of the three products. In collaboration with Dr Nicolai Burzlaff (Dyson Perrins Laboratory) the crystal structures of two mutant IPNS enzymes [D216E (active) and H270E (inactive)] in the presence Fe(II)-ACV were obtained.

3.2 Results

The IPNS mutants were made by using U.S.E. Mutagenesis kit ssDNA (Pharmacia) as described in Chapter 6.2. The primers designed for the mutagenesis reactions are given in Chapter 6.2. Positive mutants were identified by sequencing in both directions using an automated DNA sequencer operated by Mrs Amrit Bhomra (Dunn School of Pathology).

3.2.1 Purification and activity

Cells transformed with mutant plasmids were grown overnight in shaker flasks (2TY medium) at 37 °C which resulted in the over expression of protein, which co-migrated with wild-type IPNS on SDS-PAGE analysis. All mutants showed similar protein expression levels (*ca.* 40% of total cell protein). However, there was some variability observed in the solubility of mutant proteins. H214D, H270D, H270E mutants showed *ca.* 10 % of total soluble cell protein and no improvements in the yield of soluble protein was made by lowering the growth temperature to 27 °C or by supplementing the growth media with iron. All purifications were performed essentially as described for the wild-type enzyme (Chapter 6.2). A 5 litre overnight growth typically gave 20-50 g of wet cell paste which after a three column purification gave IPNS of >95% purity. For initial screening, by hole plate assays, IPNS mutants were purified using an ion-exchange resin [(Resource Q, 6 ml column (Pharmacia)].

The molecular masses from ESIMS analyses of the IPNS mutants correlated well with the values from the predicted amino acid sequences (Table 3.1).

Hole plate assays

IPNS mutants were tested for production of IPN from ACV using the hole plate assays as described in Chapter 6.2. The results from hole plate assays and mass spectrometric analyses are summarised in Table 3.1 (overleaf). Apart from the D216E mutant all the modified IPNS enzymes showed no activity or very low activity by hole plate assay (increasing the protein concentrations to 100 μM failed to give detectable activity with IPNS mutants). Identical samples from hole plate assays using mutant

enzymes were re-analysed using the HPLC assay which is more sensitive than the hole plate method for the detection of IPN.

Incubation of the wild-type IPNS with ACAB gave bioactive products which produced kill zones in the holed plate assay. In contrast, incubations using ACAB with D216E mutant did not give any kill zones therefore it seems unlikely that bioactive products were produced.

Table 3.1 Mass spectrometric analyses and measurements of the relative specific activity by hole plate assays of wild-type and mutant IPNS enzymes.

Enzyme	Calculated MW (Da)	Observed MW (Da)	Relative specific activity (wild-type = 100 %)
Wild-type	37391	37392 (±1)	100
D216E	37405	37409 (±1)	10
D216H	37413	37417 (±1)	<0.30
D216Q	37404	37408 (±2)	<0.40
H214D	37369	37368 (±1)	<0.40
H214E	37383	37384 (±2)	<0.30
H214N	37368	37370 (±1)	<0.50
H270D	37369	37370 (±2)	<0.70
H270E	37383	37384 (±2)	<0.70
H270N	37368	37369 (±2)	<0.60
D216H/H270D	37391	37393 (±1)	<1.0
H214D/D216H	37391	37392 (±1)	<2.0

HPLC assays

The apparent kinetic parameters of the D216E mutant were determined using the HPLC assay as described in the previous Chapter (*vide supra*) using a kinetic data analysis program (Grafit, Erithacus Software, 1995). The results indicated that the apparent K_m value for ACV (0.90 mM compared with 1.20 mM for the wild-type) does not appear to change significantly within experimental error. However the apparent k_{cat} value (1.3 min^{-1}) was reduced more than thirty fold compared with the wild-type enzyme (Figure 3.3a and Table 3.2).

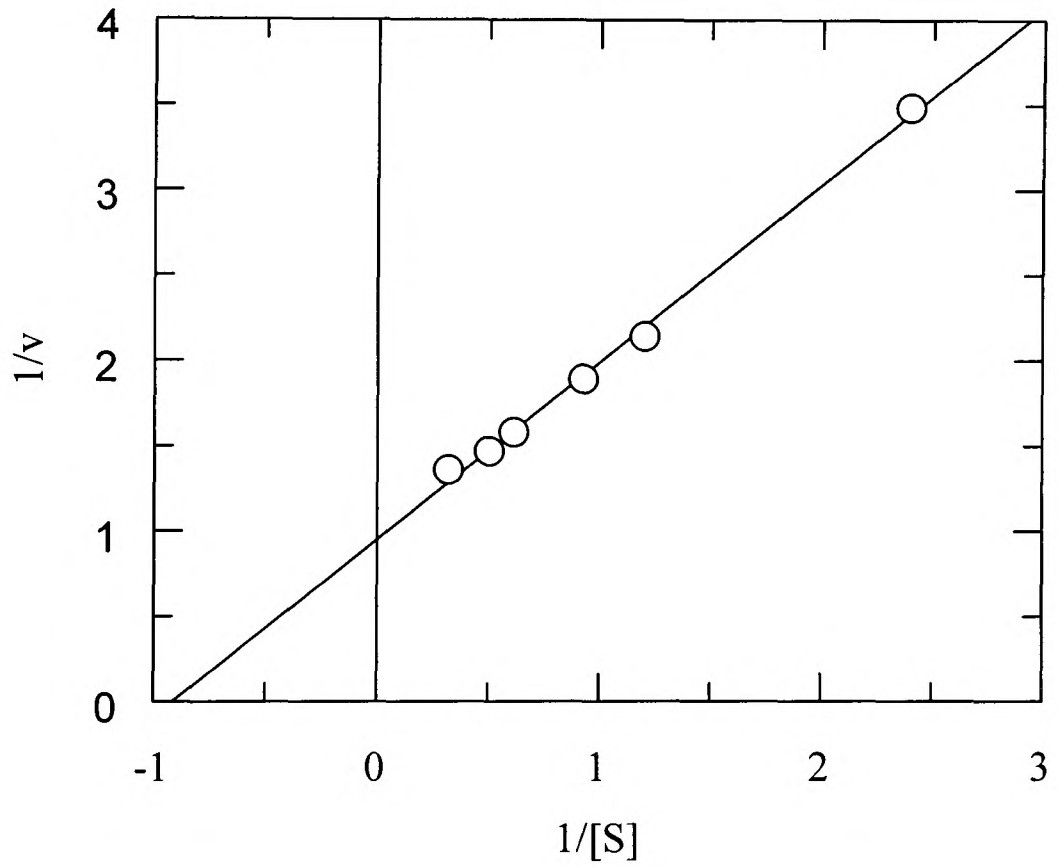

Figure 3.3a Lineweaver-Burk plot of kinetic data showing IPN production by the D216E mutant. Note that the kinetic data was calculated using Grafit program and not from this plot.

Table 3.2 Apparent kinetic parameters for the D216E IPNS mutant.

	V_{max} (nmol/min/mg)	K_m (mM)	k_{cat} (min^{-1})	k_{cat}/K_m (mM^{-1} min^{-1})
wild-type	909 (±90)	1.22 (±0.23)	40	32.3
D216E	33 (±2)	0.90 (±0.13)	1.3	1.4

CD spectra

Physical characterisation of the wild-type and mutant IPNS enzymes indicated only minor differences in their secondary structure by CD analysis, at least with the levels of α-helical content [mutants H214D, H214E, H214D/D216H and H214N (Figure 3.4a); mutants D216E, D216H, D216H/H270D, D216Q (Figure 3.4b); mutants H270D, H270E, H270N (Figure 3.4c)].

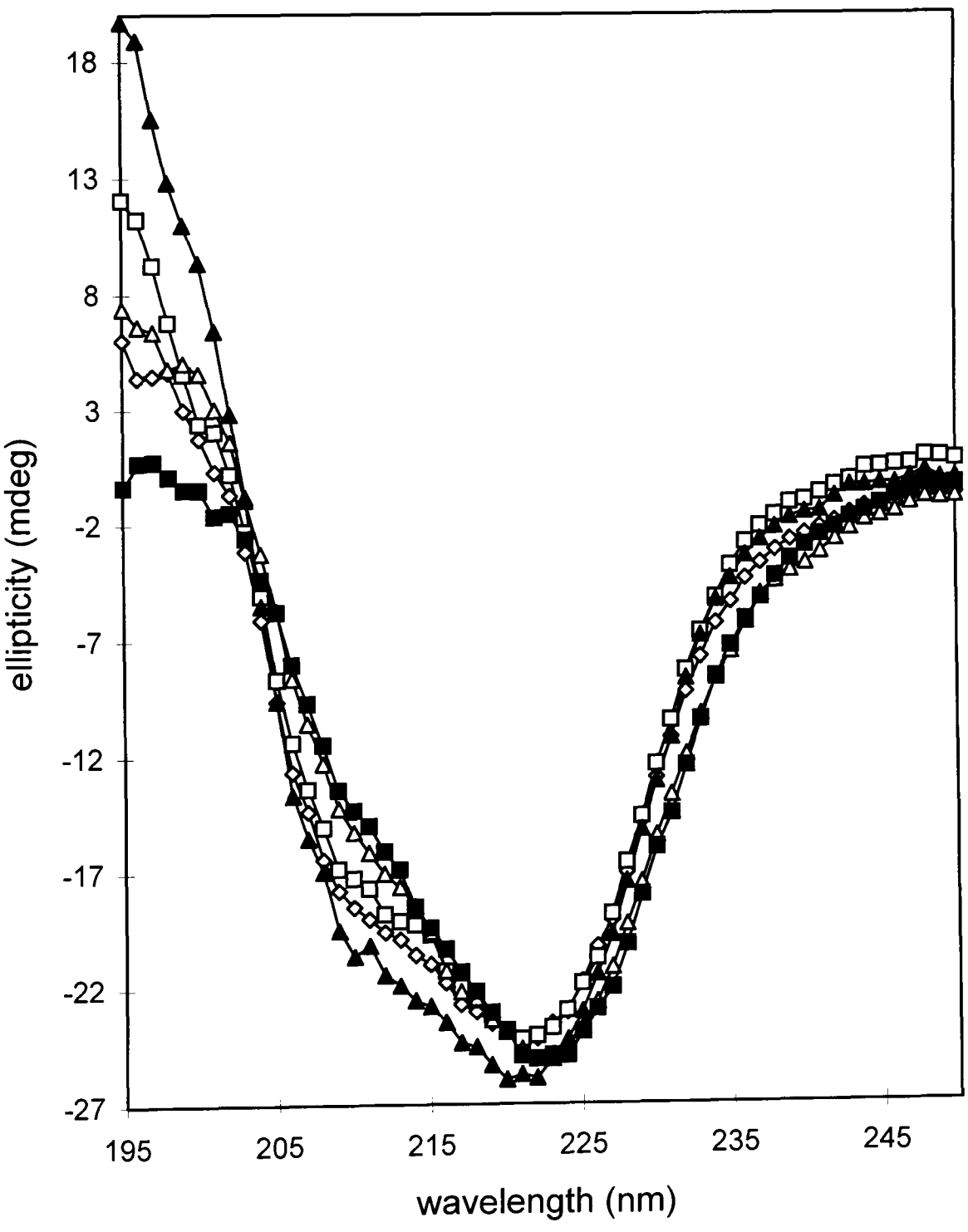

Figure 3.4a CD spectra of H214D (open diamonds), H214E (open squares), H214D/D216H (open triangles), H214N (filled squares) and wild-type IPNS (filled triangles).

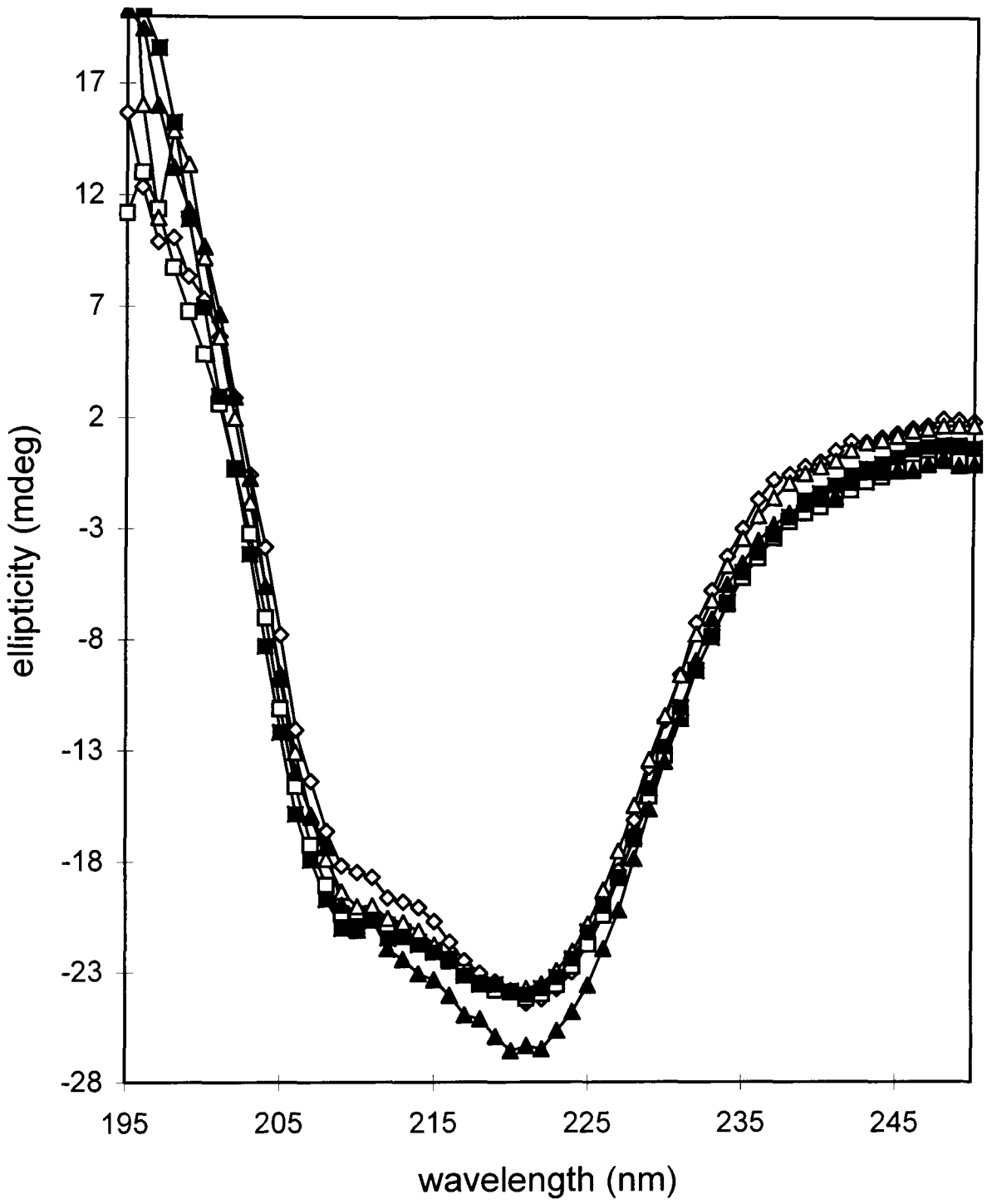

Figure 3.4b CD spectra of D216E (open diamonds), D216H (open squares), D216H/H270D (open triangles), D216Q (filled squares) and wild-type IPNS (filled triangles).

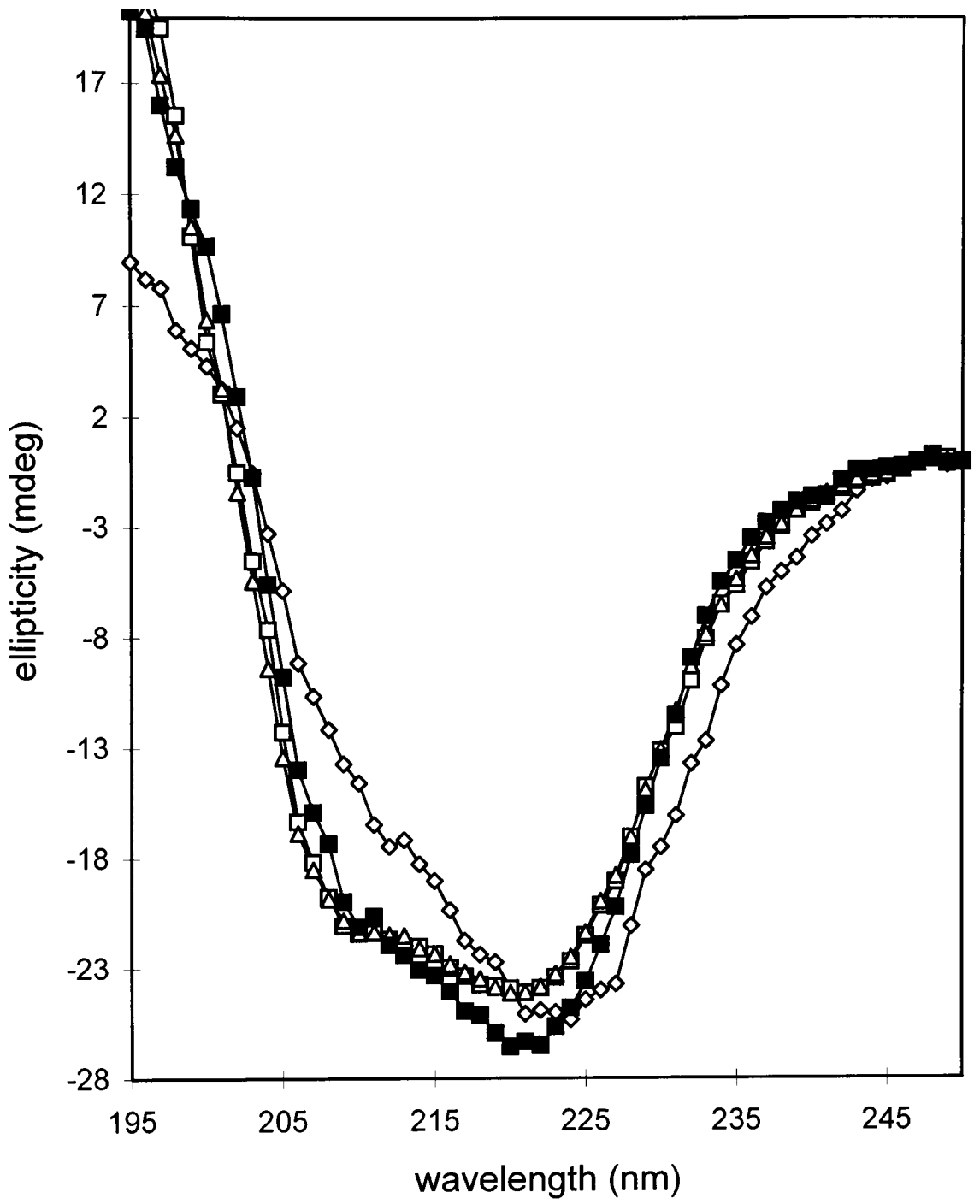

Figure 3.4c CD spectra of H270D (open diamonds), H270E (open squares), H270N (open triangles) and wild-type IPNS (filled squares).

3.2.2 ^{1}H NMR Studies

ACV turnover

The ACV and ACAB substrate turnovers by the D216E mutant were compared by ^{1}H NMR analysis as described in Chapter 6.3. The results of ACV incubations with D216E (Figure 3.3a) and wild-type IPNS showed that, in both cases, IPN was formed. Both wild-type and mutant enzyme products showed the characteristic spectral features also seen for the synthetic IPN including the characteristic doublets of the β-lactam protons (5-H and 6-H) observed between 5.48 ppm (J = 4 Hz) and 5.56 ppm (J = 4 Hz).

Estimations based upon the internal TSP standard suggested that *ca.* > 90% conversion of ACV to IPN took place in incubations with the wild-type enzyme and approximately 35% conversion was observed in an incubation using the D216E mutant under similar conditions.

ACAB turnover

ACAB (made by Ms Alexandra Long, Dyson Perrins Laboratory) was incubated with 26 μM of wild-type and mutant IPNS enzymes. The results showed that at least two different β-lactam products were formed with wild-type IPNS in agreement with previous reported studies[56]. The spectral features revealed the characteristic *cis*-β-lactam hydrogens of the β-methyl penam (5-H and 6-H) at 5.42 ppm (doublet, J = 4 Hz) and 5.47 ppm (doublet, J = 4 Hz) and those of the cepham product (6-H and 7-H) observed at 5.25 ppm (doublet, J = 4 Hz) and 5.38 ppm (doublet, J = 4 Hz). Based upon the starting concentrations of ACAB (~1.2 mM) < 25% of the ACAB was converted into penam and cepham products. There was no evidence for the α-methyl penam product, but it cannot be ruled out that it was formed in low yield.

Given the results obtained with ACV, it was somewhat surprising that ACAB was not apparently turned over (< 2.5%) by the D216E mutant but was converted by wild-type IPNS under similar incubation conditions. Incubations with the D216E enzyme showed a small amount of unidentified material, based on the appearance of a doublet at 5.25 ppm. The resultant unidentified material was not bioactive (no kill zones were detected on bioassay plates). However, the observed chemical shift and the coupling constants were similar to those reported for a synthetic 'shunt' product[90]. Assays repeated with higher enzyme concentrations (260 μM) also gave small amounts of another unidentified material, based on the appearance of an apparent quartet at 5.3 ppm (J = 1 Hz) and a doublet at 5.25 ppm (as seen previously with low concentrations of D216E). However, the failure to detect kill zones by hole plate assays suggested that neither of these unidentifiable material were bioactive. The possibility of *cis* or *trans* β-lactam products was considered, but appears to be unlikely due to the size of the J value for the quartet. It cannot be entirely ruled out that the apparent quartet reflects the presence of an enzyme produced product, but it seems to be unlikely and it is possible that it is 'simply' a contaminant in the enzyme, catalase or in the buffer. Studies are ongoing to identify this material and to verify the production of the shunt metabolite.

3.2.3 UV-Visible Spectroscopy

ACV-NO Spectra

Anaerobic IPNS or BSA with Fe(II) and ACV exhibited no absorption above 280 nm (results not shown). The addition of NO to an anaerobic complex of IPNS with Fe(II) resulted in a pale yellow coloured solution with a feature at 430 nm in agreement with previous studies of Orville *et al.*[57].

Figure 3.5a Colour changes observed with wild-type IPNS. Cuvettes (from left to right) show the following: IPNS-ACV-Fe-NO, IPNS-ACV-Fe(anaerobic).

Addition of NO to anaerobic IPNS-Fe(II)-ACV resulted in a species with a distinct pink colour (Figure 3.5a) with spectral features at 508 nm (ε = 1500 M^{-1} cm^{-1}) and 720 nm (Figure 3.5b). This observation agreed well with previous reported findings on IPNS from *C. acremonium*[53]. The anaerobic ACV-NO spectra of D216Q, D216H, D216E IPNS mutants were compared with wild-type IPNS (Figure 3.5b, spectrum D). The spectrum for the D216E mutant was very similar to that of the wild-type IPNS enzyme and showed a large increase in absorption at 508 nm (ε = 1300 M^{-1} cm^{-1}) and at 720 nm (Figure 3.5b, *cf* spectra C and D). The spectra for the remaining IPNS mutants [H214D, H214E, H214N (Figure 3.5c), H270D, H270E, H270N (Figure 3.4d) and H214D/D216H, D216H/H270D (Figure 3.5e)] showed no distinct features at 508 or 720 nm. Some mutants (H214D and H270D) became opaque after NO was added and the

resultant precipitate was later identified as protein. This observation may relect a conformational instability in the case of these mutants. Mutant H270E showed a weak broad feature at 600 nm after NO was added (Figure 3.5d, B).

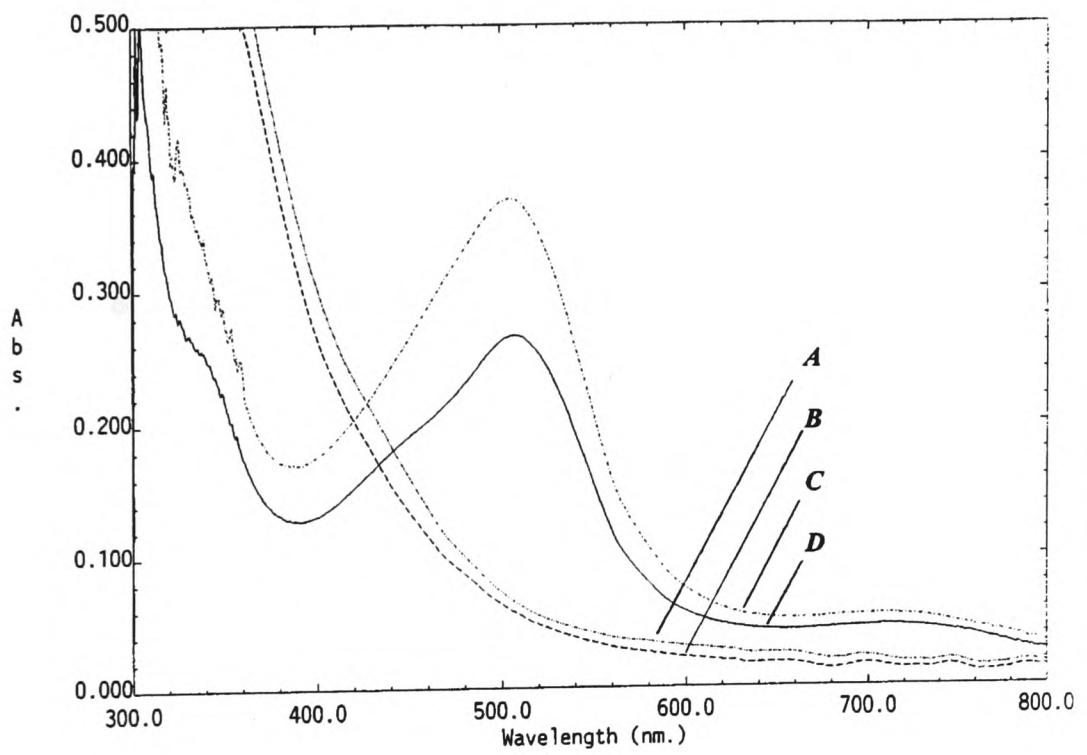

Figure 3.5b Anaerobic UV-visible spectra of wild-type and mutant IPNS enzymes (0.3 mM) in the presence of ACV (1.5 mM) and NO. Spectra of the following enzymes are shown: D216Q (A), D216H (B), D216E (C) and wild-type (D).

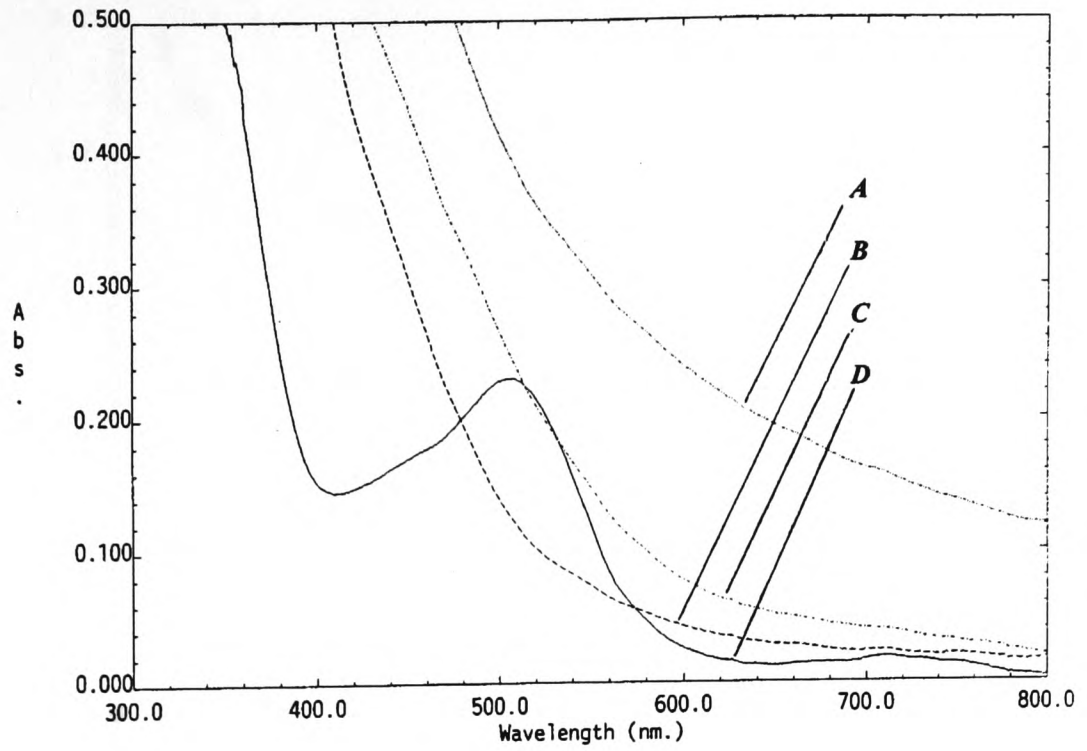

Figure 3.5c Anaerobic UV-visible spectra of wild-type and mutant IPNS enzymes (0.15 mM) in the presence of ACV (0.75 mM) of NO. Spectra of the following enzymes are shown: H214D (A), H214E (B), H214N (C) and wild-type (D).

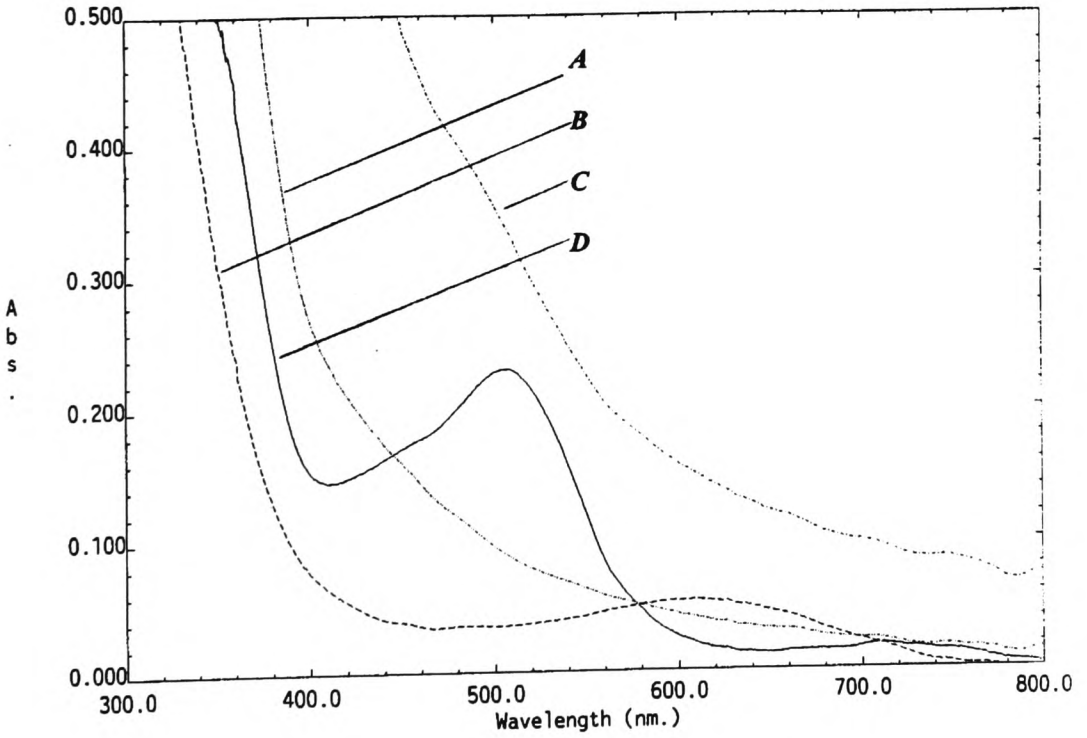

Figure 3.5d Anaerobic UV-visible spectra of wild-type and mutant IPNS enzymes (0.15 mM) in the presence of ACV (0.75 mM) and NO. Spectra of the following enzymes are shown: H270D (A), H270E (B), H270N (C) and wild-type (D).

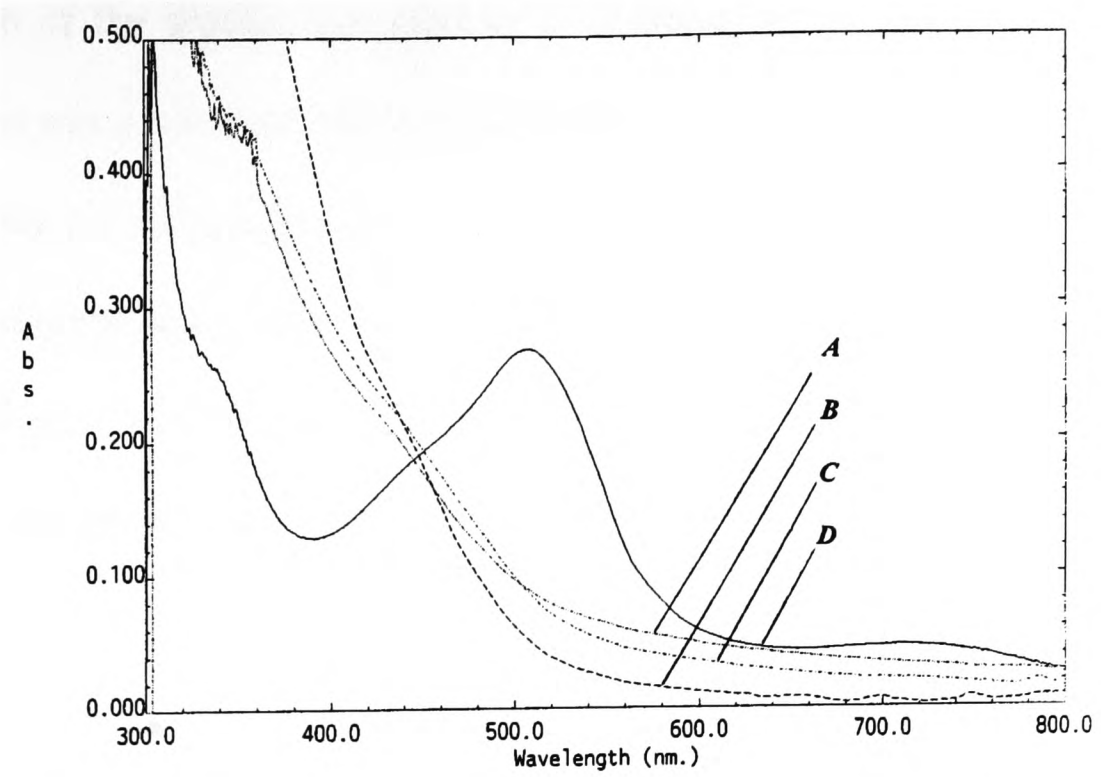

Figure 3.5e Anaerobic UV-visible spectra of wild-type and mutant IPNS enzymes (0.15 mM) in the presence of ACV (0.75 mM) and NO. Spectra of the following enzymes are shown: H214D/D216E (A), D216H/H270D (B), buffer alone (C) and wild-type (D).

ACAB-NO Spectra

Having demonstrated that the conversion of ACAB to the β-lactam product is not catalysed by the D216E mutant, further experiments were carried out to investigate why this substrate was not turned over. The H270E mutant also fails to convert ACAB into penam/cepham products (data not shown). To investigate whether ACAB binding was affected, the ACAB-NO spectra were measured for these two mutants and compared with the wild-type enzyme. The ACAB-NO spectra of the wild-type enzyme gave a distinct pink colour with features at 508 nm (ε = 1400 M^{-1} cm^{-1}) and 720 nm (Figure 3.5f, spectrum C). The D216E mutant gave an orange-pink colour with weak spectral features at 508 nm (ε = 700 M^{-1} cm^{-1}) (Figure 3.5f, spectrum A). In contrast, the H270E mutant gave a yellow colour with spectral feature at 600 nm (Figure 3.5f, spectrum B). Occasionally the mutant samples rapidly turned opaque after NO was added due to

precipitation of the protein indicative of conformational instability. Interestingly, this phenomenon was never observed with the wild-type IPNS enzyme which suggests that in these mutants an exaggerated or an aberrant conformational change occur upon NO binding. Although little conformational change occur upon NO binding to the wild-type IPNS-Fe(II)-ACV complex in the crystalline state[52], the lack of movement may reflect crystal packing interactions.

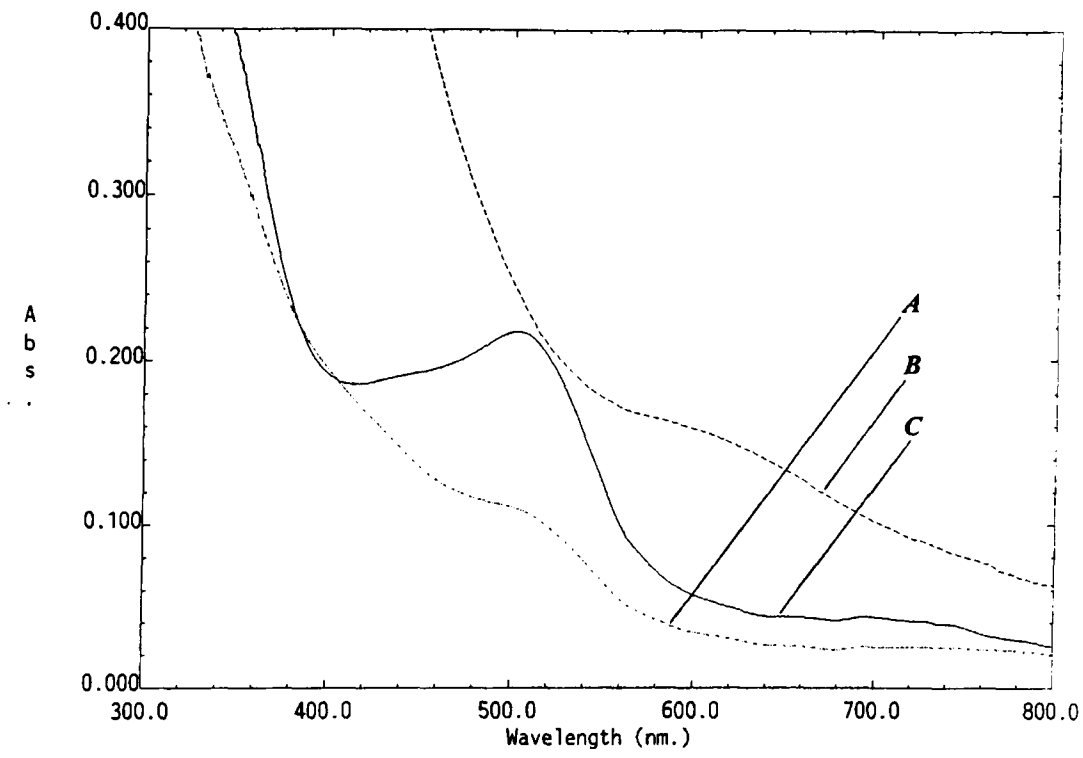

Figure 3.5f Anaerobic UV-visible spectra of wild-type and mutant IPNS enzymes (0.15 mM) in the presence of ACAB (0.75 mM) and NO. Spectra of the following enzymes are shown: D216E (A), H270E (B) and wild-type (C).

ACV-O_2-Spectra

The unusual feature at 600 nm observed for the H270E in the ACV-NO and ACAB-NO complexes was intriguing since both these samples appeared to be slightly blue before NO was added. Residual O_2 present in the samples may account for these

observations (see below). Therefore the ACV-O_2 spectra were measured for the H270E and wild-type IPNS.

Anaerobic H270E with Fe(II) gave no observable peak above 280 nm. The oxygenation of this sample gave only a pale yellow solution with no spectral features above 400 nm (results not shown). Similar studies with the mutant enzyme were repeated in the presence of ACV and showed a distinct blue coloration (Figure 3.5g). The resultant spectra showed a broad peak, λ_{max} 600 nm (ε = 700 M^{-1} cm^{-1}), which increased in intensity over 15 minutes (Figure 3.5h). In contrast, the wild-type IPNS appeared to be yellow colour and showed only a weak feature at 600 nm (Figure 3.5i).

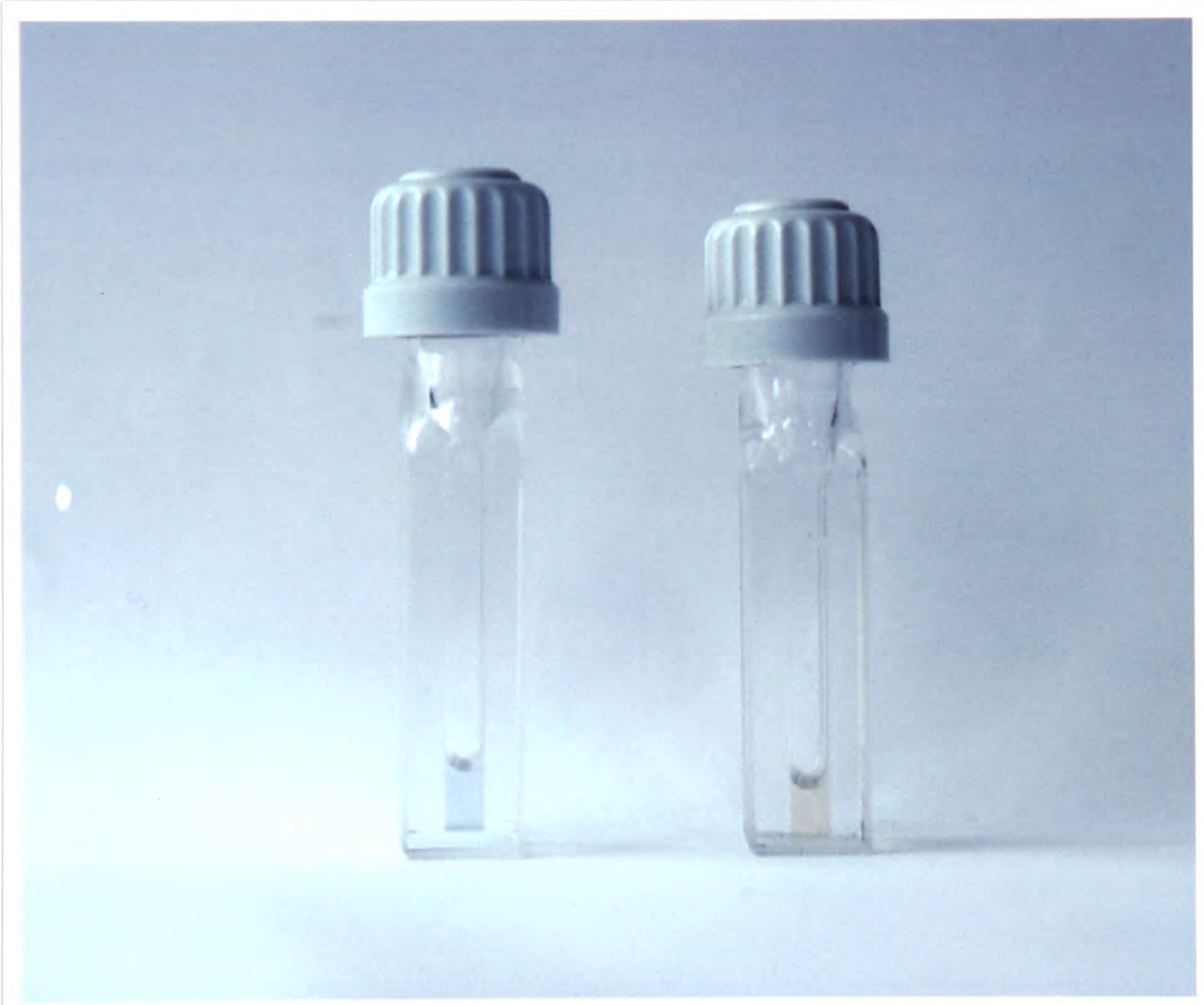

Figure 3.5g Colour changes observed with the H270E mutant. Cuvettes (from left to right) show the following: H270E-ACV-Fe-O_2 and H270E-ACV-Fe-NO.

The blue colour, and the feature at 600 nm, observed in H270E mutant was abolished after fresh ascorbate (10 mM) was added to the sample (Figure 3.4j, spectra C, D, E). The addition of O_2 to H270E in the presence of ascorbate did not give this blue feature (results not shown).

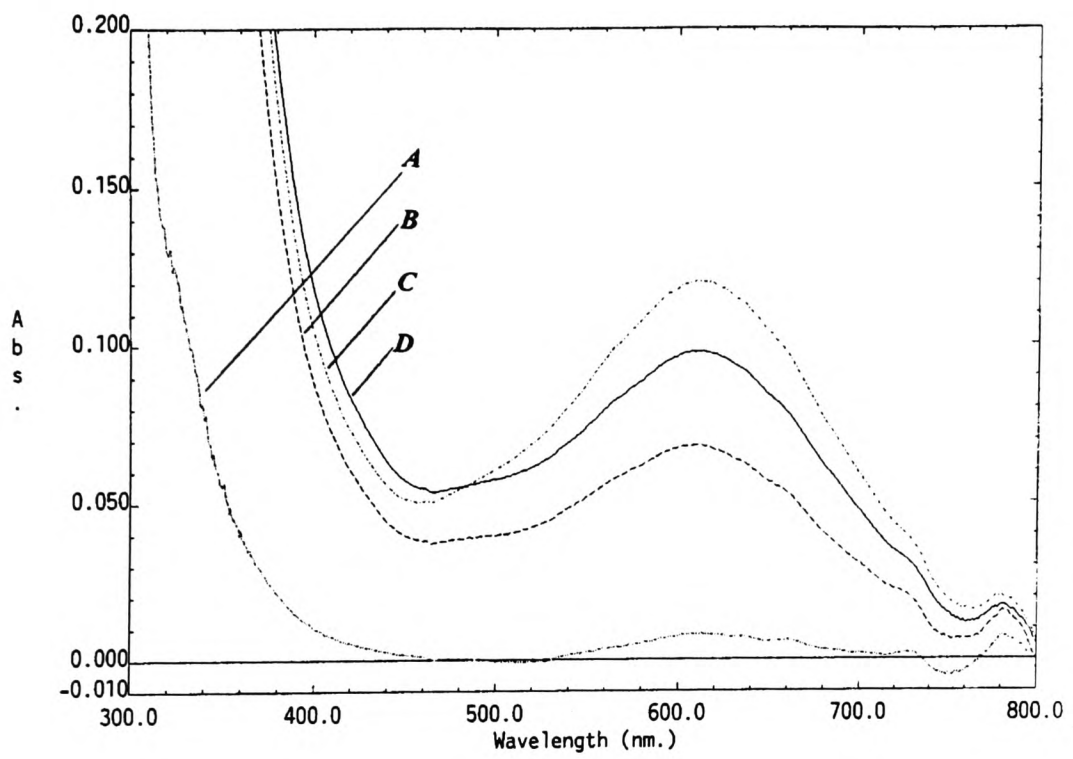

Figure 3.5h Effects of O_2 on the UV-visible spectrum of the H270E mutant enzyme (0.15 mM) in the presence of ACV (0.75). Spectra were measured after the addition of O_2 at various time points (minutes): 1 (B), 15 (C), 40 (D). Anaerobic spectrum of the H270E mutant with ACV is shown by the bottom curve (A).

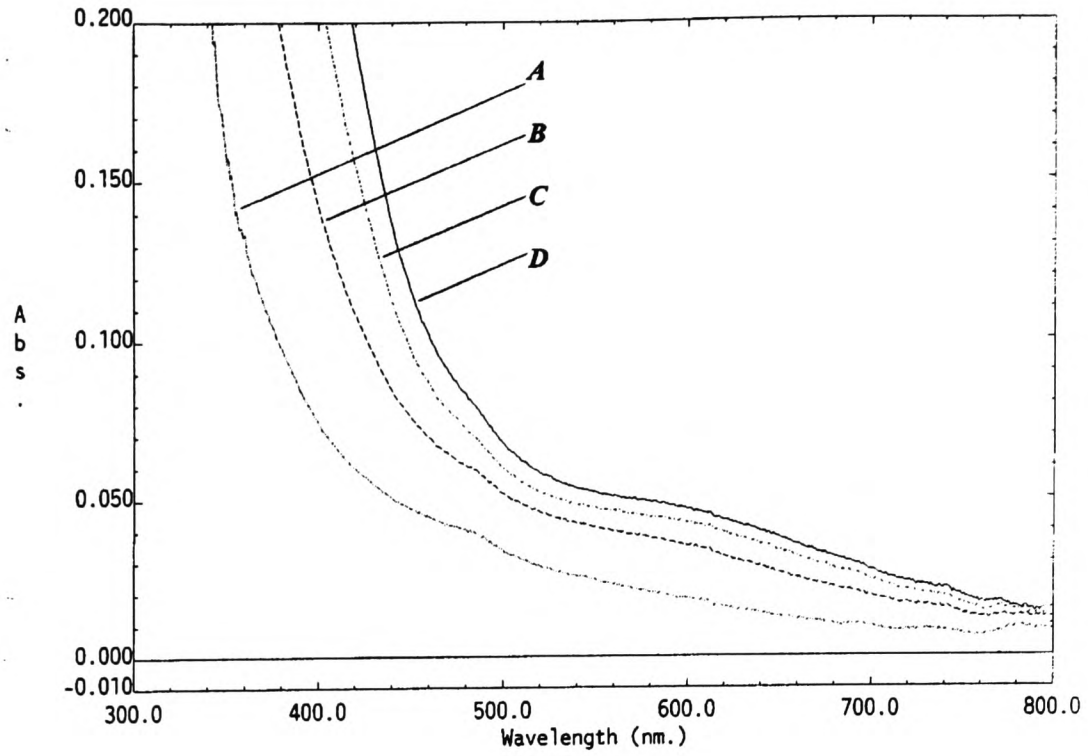

Figure 3.5i Effects of O_2 on the UV-visible spectrum of wild-type IPNS (0.15 mM) in the presence of ACV (0.75 mM). Spectra were measured after the addition of O_2 at various time points (minutes): 1 (B), 15 (C), 40 (D). The anaerobic spectrum of wild-type IPNS with ACV is shown by the bottom curve (A).

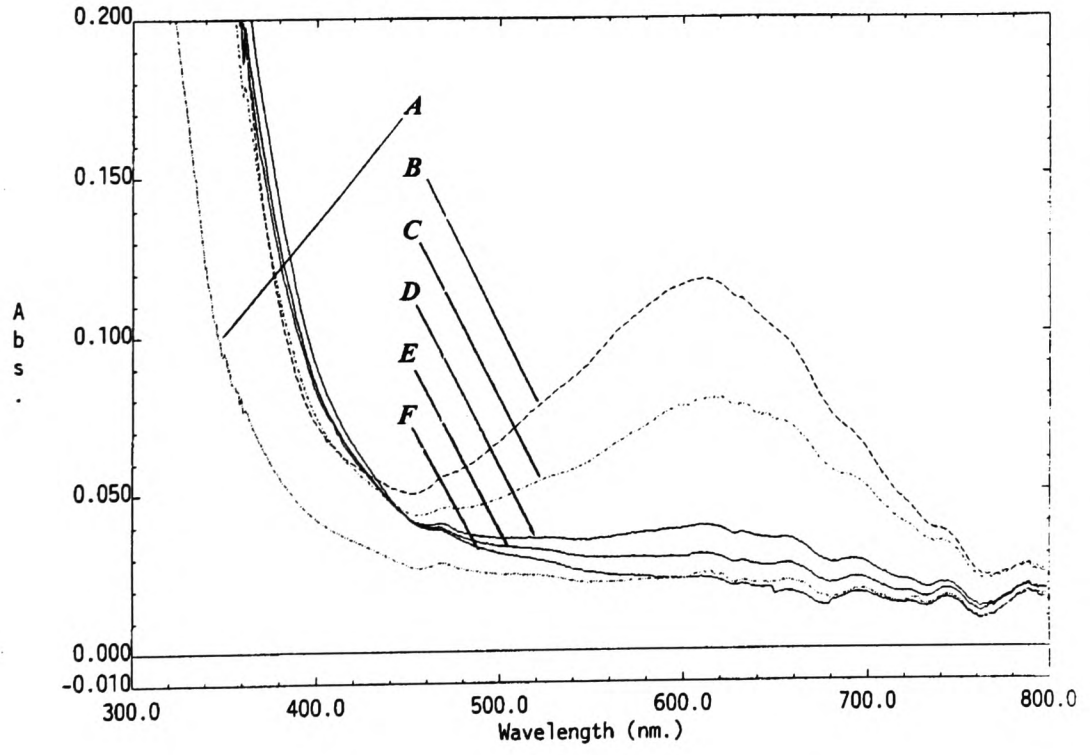

Figure 3.5j Effects of ascorbate on the UV-visible spectrum of the H270E IPNS mutant (0.15 mM) in the presence of ACV (0.75 mM) and O_2. Spectra were measured after the addition of ascorbate (10 mM) at various time points (minutes) as follows: 5 (C), 10 (D), 15 (E). Spectrum (F) was obtained after more O_2 was added to (E). Spectra of H270E with ACV in the absence of O_2 is shown by the bottom curve (A) and after addition of O_2 (B).

3.2.4 Crystal structures

Crystals of D216E and H270E IPNS mutants were grown anaerobically as described in Chapter 6.2. It was noted for the wild-type IPNS that three different crystal forms (plates, hexagons and needles) can be obtained under the crystallisation conditions but only the plate type crystals were shown to give good diffraction data[91]. Plate form crystals were grown with the mutant IPNS using a seeding stock made from a single crushed wild-type IPNS plate crystal. After initial crystallisation trials with the mutant enzymes it was observed that the rate of crystallisation was dependent upon the iron concentration used in the crystallisation buffer. Mutant D216E crystals only grew to a small size with iron concentrations of 12.5 mM (after a few days) and bigger plate type crystals were grown (by Dr Nicolai Burzlaff, Dyson Perrins Laboratory) after employing an elevated iron concentration of 125 mM (Figure 3.6a). Plate type crystal forms grew with H270E mutant using similar crystallisation conditions as for the wild-type enzyme but a longer period (1 week) was needed to grow suitably sized crystals. All data collection and refinements were performed by Dr Nicolai Burzlaff. The crystal structures of D216E (Figure 3.6b) and H270E (Figures 3.6d, 3.6e) further confirmed the sequencing and ESIMS studies that the desired mutations had been made.

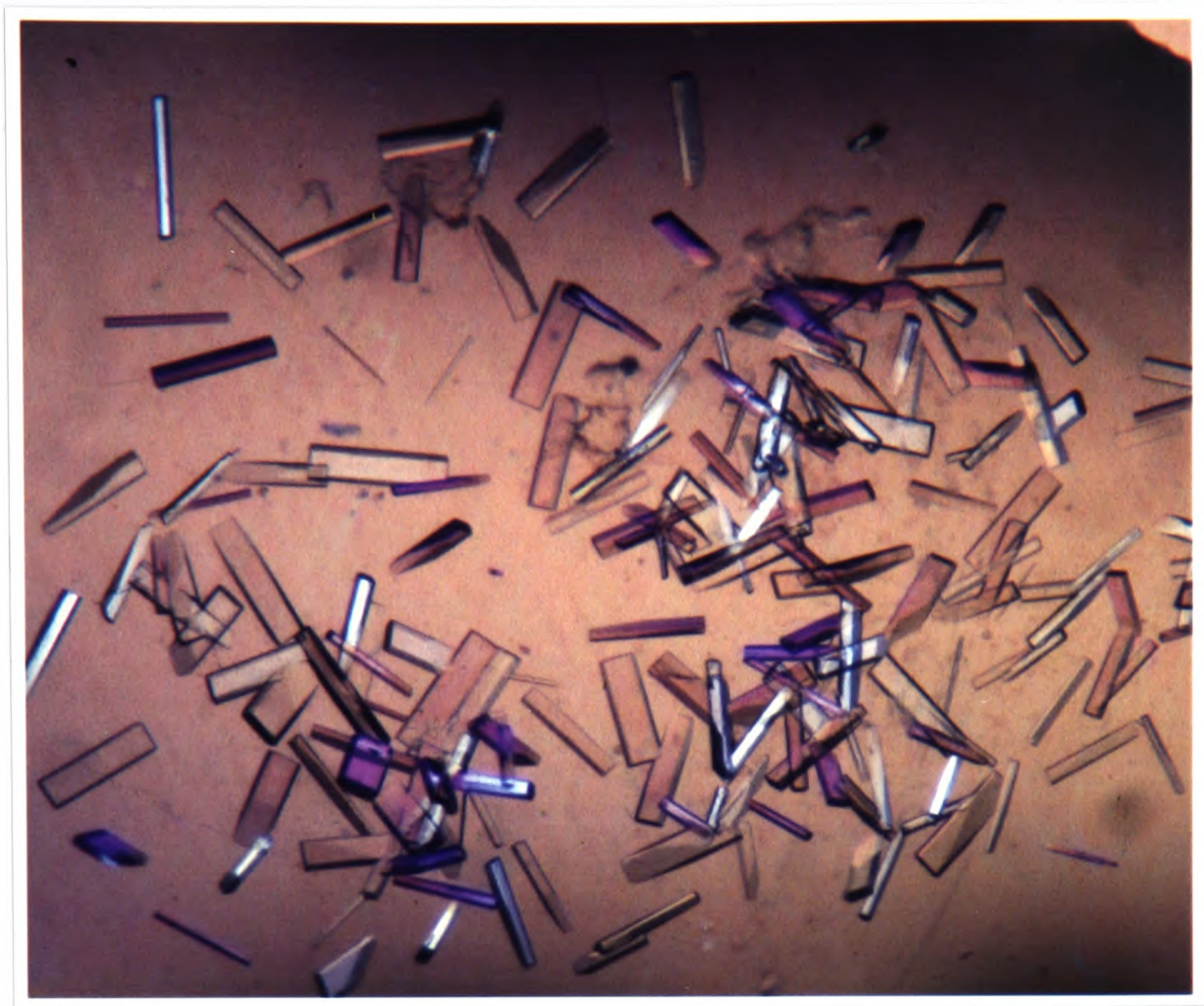

Figure 3.6a Crystals of D216E mutant grown anaerobically. Note that the picture was taken under a polarising microscope.

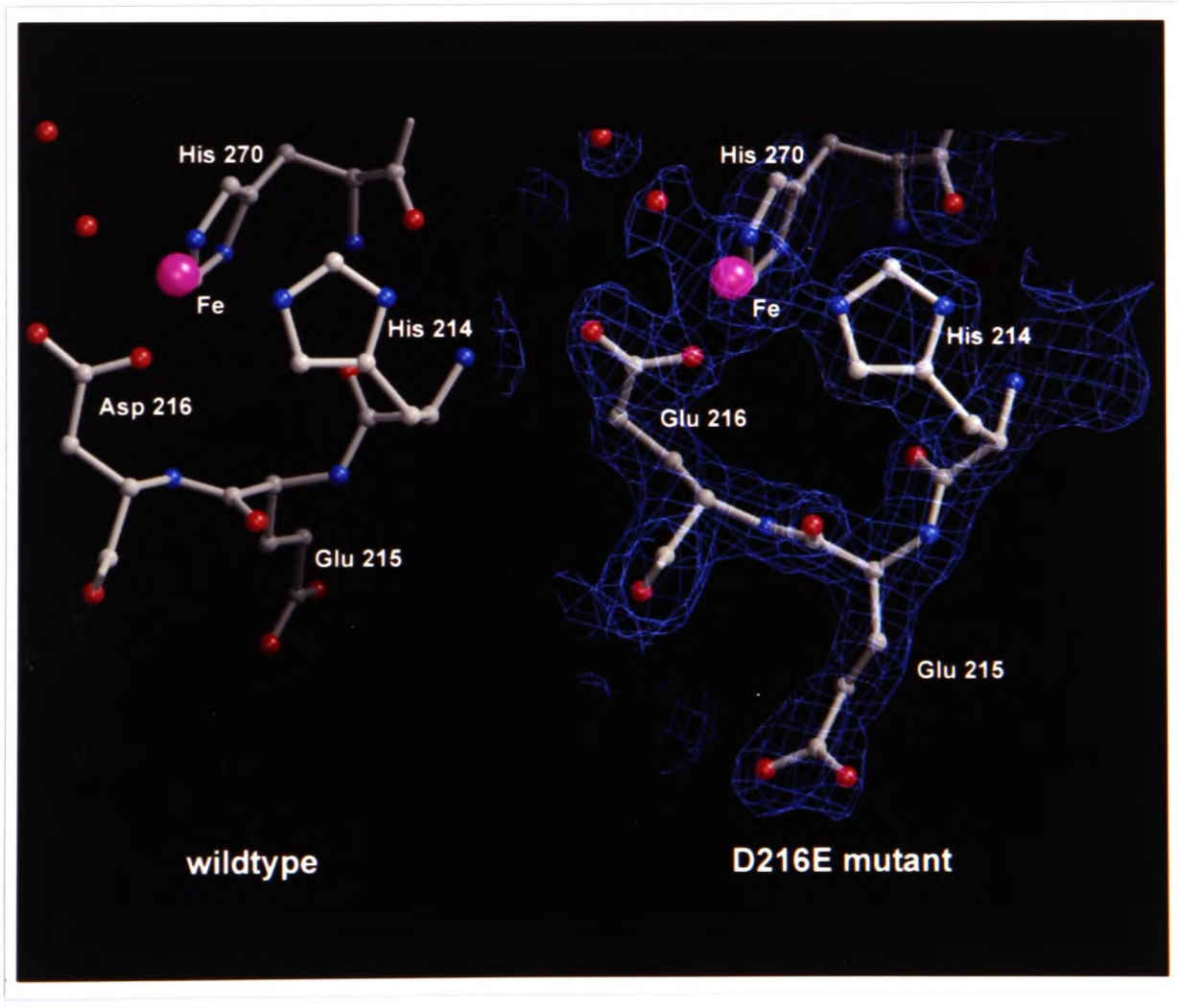

Figure 3.6b Crystal structure of the D216E mutant.

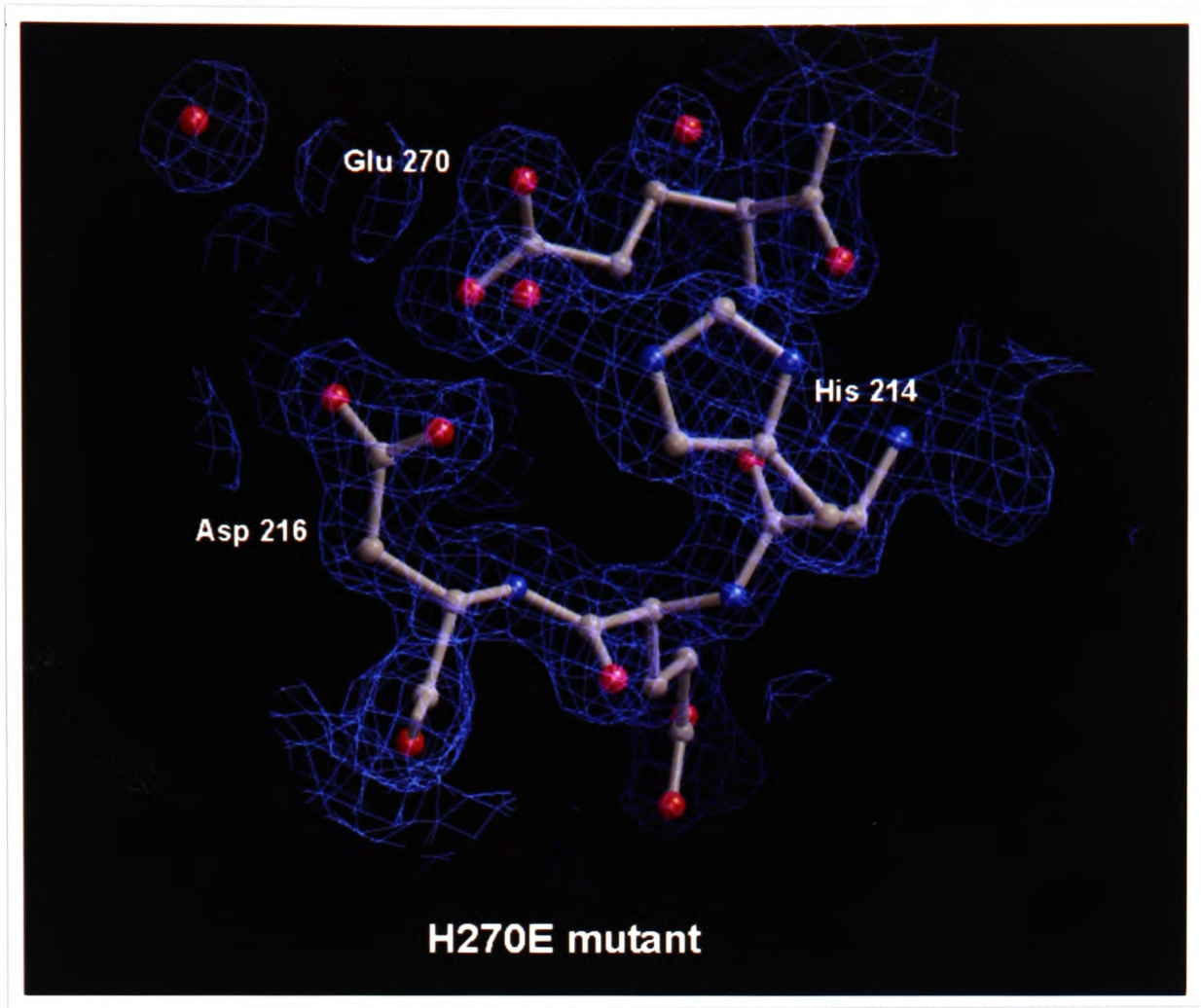

Figure 3.6c Crystal structure of the H270E mutant.

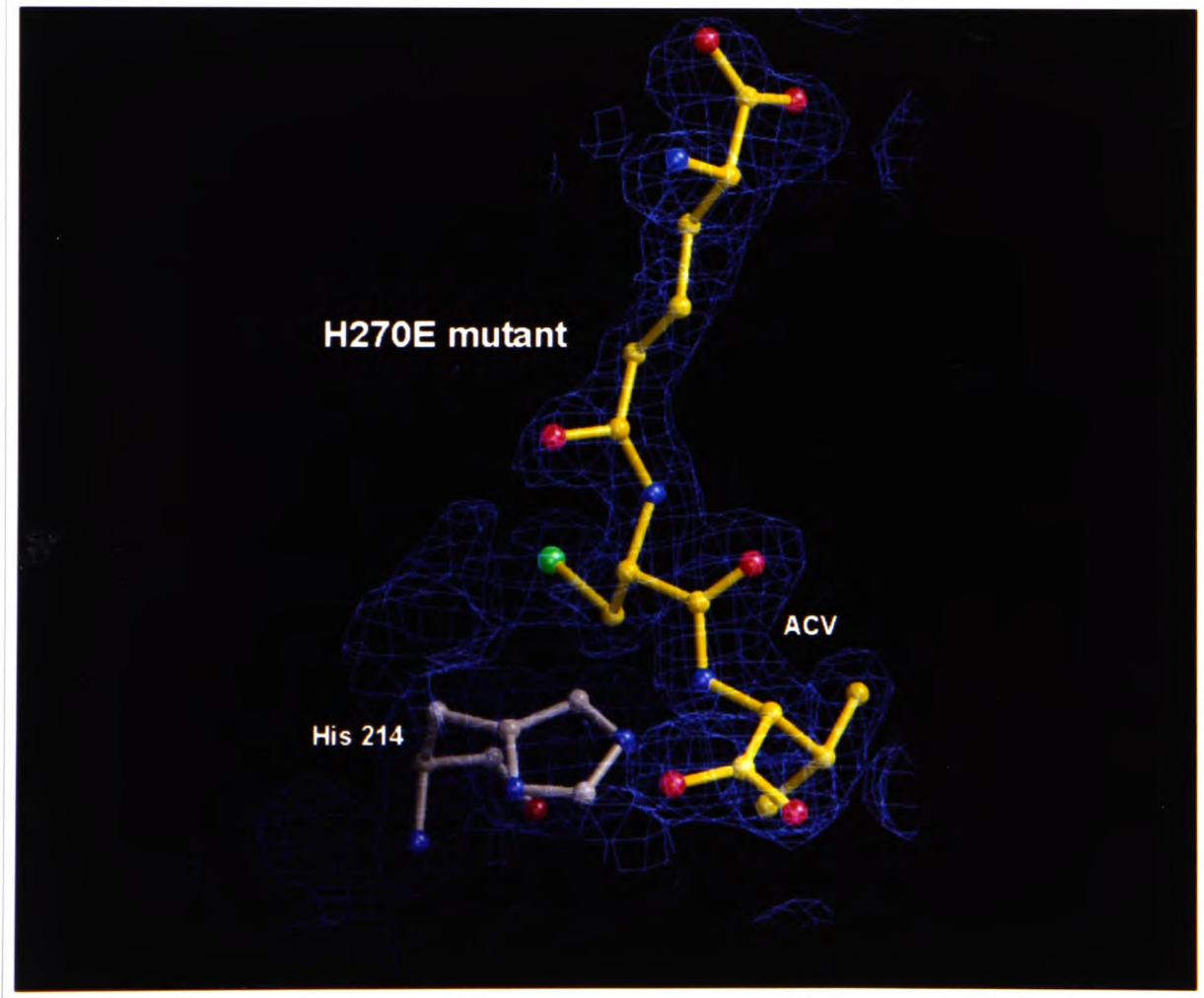

Figure 3.6d Crystal structure of the H270E mutant showing bound ACV.

3.3 Discussion

The results from the present study are consistent with the previous conclusions that H214, D216 and H270 act as iron binding ligands during IPNS catalysis. Complete loss of activity was observed after substitution of His214 or His270 with aspartate, glutamate or asparagine residues. However, the modification of Asp216 to a glutamate residue resulted in a mutant enzyme (D216E) with substantially reduced activity (*ca.* 10%) compared with the wild-type IPNS under standard assay conditions. The observation that the ACV-NO spectrum of the D216E mutant showed almost identical spectral features to wild-type IPNS suggested that the binding of iron, ACV and O_2 to this mutant was probably very similar to the wild-type enzyme. It is interesting to speculate why no activity was detected with the D216E mutant when using ACAB as a substrate. The UV-visible studies showed that a charge transfer complex was formed with ACAB-NO (similar to the wild-type enzyme) which suggests that binding of iron, ACAB and NO (or O_2) also occurs with this modified enzyme.

The H270E mutant was inactive with respect to ACV and ACAB turnover. The blue colour observed with the H270E (inactive) mutant is intriguing and the observations that blue charge transfer complexes were only formed in the presence of the protein + ACV + iron + oxygen suggests that it may result from an Fe(III) to thiolate charge transfer complex.

3.3.1 D216E with ACV

Given the difficulties in interpreting the kinetic results on IPNS (*e.g.* substrate oxidation, oxygen consumption and enzyme inactivation), only a brief discussion is merited. The results suggests that the affinity of the enzyme for the substrate appears to

be reduced, although not significantly and quite possibly within experimental error relative to the wild-type IPNS. It was not possible to use the present kinetic analysis to determine an apparent K_m for the Fe(II) in this mutant. However, there is a clear reduction (*ca.* 30 fold) in the apparent k_{cat} value for the D216E mutant. This observation implies a 'role' for the Asp216 ligand in catalytic steps subsequent to ACV binding.

Similar mutational analyses have been performed on ACCO and PH. The studies on the D179E ACCO mutant showed an increased K_m for Fe(II) without affecting the substrate binding substantially[66]. The apparent K_m for Fe by this mutant ACCO was increased by 10 fold which suggests that the D179E mutation affected iron binding. This D179E ACCO mutant also showed an apparent decrease in the k_{cat} of 700 fold with an apparent increase in the K_m for ACC of 1.5 fold. Myllyharju and Kivirikko[86] also reported an apparent increase in the K_m for α-KG. They observed that the coupled turnover in PH was increased by only 5 fold after the mutation of Asp414 (equivalent to Asp216 in the IPNS consensus sequence) to a glutamate. The apparent K_m for Fe(II) in their study was increased by 15 fold.

The combined results from the present study on IPNS and the previous studies (on ACCO and PH) suggests that glutamate can replace the Asp216 residue and still allow the binding and reaction of iron, substrate and oxygen. The observed drop in activity in these enzymes suggests that a 'rigid' metal ligand at the 216 position is better than a flexible one (*i.e.* the aspartate better than a glutamate as shown in Figure 3.7). A key factor in the loss of activity observed for the D216H and D216Q mutant IPNS enzymes probably results from the introduction of relatively poor donor ligands (reduced ability to polarise) from the side chains of histidine and glutamine (Figure 3.7, H and Q), compared with electron donating carboxylate of aspartate and glutamate.

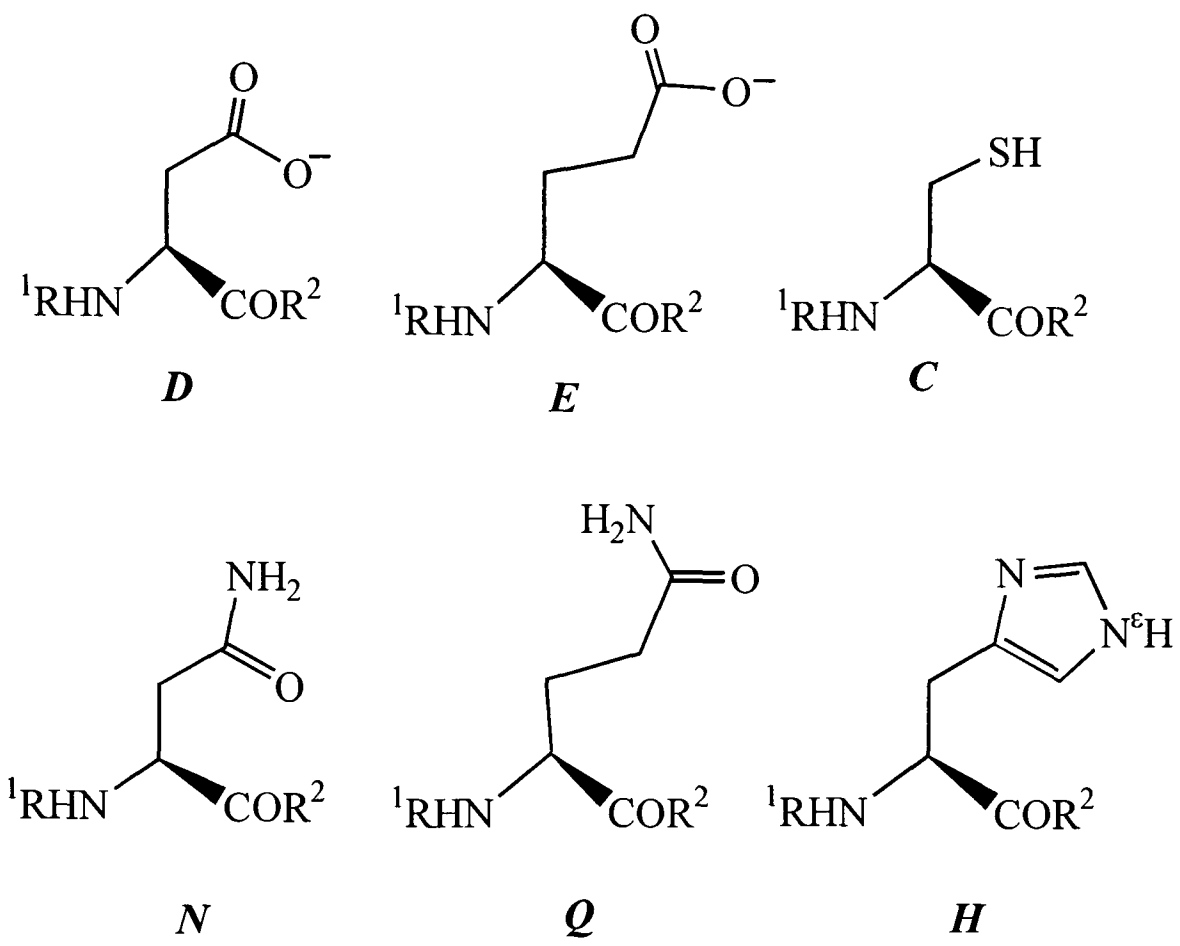

Figure 3.7 The amino acids used in the mutagenesis study. Aspartic acid (deprotonated): strong (electron) donor (D); glutamic acid (deprotonated): strong donor (E); cysteine: weak donor (C); asparagine: weak donor (N); glutamine: weak donor (Q); histidine (not protonated): weak donor (H).

The apparent ability of IPNS to bind ACV and NO simultaneously suggests that the active site complex involves separate binding sites for ACV and O_2[52]. The findings that the molar absorption coefficient of the 508 nm peak in wild-type IPNS (ε = 1300 M^{-1} cm^{-1}) was similar to that in the D216E mutant (ε = 1400 M^{-1} cm^{-1}) suggests that ACV and NO binding is very similar in both the wild-type and mutant enzymes. Other than thiolate, only tyrosinate ligation has been shown to produce spectra of similar band positions and intensities (ε = 2600 M^{-1} cm^{-1})[92]. This is unlikely to occur in the present study using ACV where a cysteine ligates to the iron. The four tetrahedrally arranged cysteinyl thiols of rubredoxin[89] give a peak at 497 nm (ε = 8700 M^{-1} cm^{-1}) resulting in a

spectrum that is very similar in shape and position to the ACV-NO IPNS spectrum. Thus, in the present study ACV contains no potential ligands other than thiolate which could account for the observed optical spectrum.

The crystal structure of the D216E mutant in the presence of ACV showed that the ferrous iron was ligated by two histidines and one glutamate confirming that the predicted mutation from an aspartate to a glutamate residue had indeed occurred. The ligation of the metal centre with these ligands was very similar to the reported ligation in the wild-type enzyme (Figure 3.6a). The ACV thiol ligation was *trans* to His270 as reported for the wild-type enzyme. The aminoadipoyl carboxylate and the valine carboxylate forms salt bridges with Arg87 and with Ser179 and Arg281 residues respectively.

The carbon backbone between His214 and Glu216 appears to have moved away from the ferrous iron centre by 1 to 2 Å to accommodate the extra methylene carbon in the glutamate mutant. The most significant change observed was the movement of the side chain of the Glu215 through a 60 degree rotation towards the surface of the enzyme. In effect these combined changes in the structure apparently make space for the extra methylene group and also allow the metal binding amino acids (H214, His270 and Glu216) to ligate with the iron in an almost identical fashion to that observed in the structure of wild-type IPNS.

3.3.2 D216E with ACAB

It is not clear why the D216E mutant does not convert ACAB into bicyclic β-lactams. The lack of activity to form a penicillin product for D216E with ACAB may reflect a

contribution of many factors including a reduced binding affinity for: (1) ACAB (compared with ACV), (2) Fe(II) and (3) dioxygen coupled with a lower k_{cat} value. The observed weak charge transfer complexes observed with D216E-ACAB-NO [*cf* wild-type IPNS (1400 M^{-1} cm^{-1}) and D216E mutant (700 M^{-1} cm^{-1})] may reflect the lower affinity of the ACAB for the ferrous metal. However the spectroscopic studies clearly demonstrate that the D216E IPNS can bind iron, ACV, and NO (and by implication O_2) but not necessarily as well. Furthermore, the reduction in k_{cat} without an increase in the K_m, observed for the conversion of ACV to IPN suggests that a major influence of the D216E substitution may be on a step subsequent to dioxygen binding. This suggestion receives tentative support from the preliminary identification of an alternative (shunt) product resulting from the turnover of ACAB by D216E mutant.

The identity of this product giving rise to a doublet at 5.25 ppm in the NMR spectrum of the D216E mutant incubation with ACAB is not absolutely clear from these studies. However, the observation that a similar chemical shift (at 5.25 ppm) was reported, for a synthetic 'shunt' product, suggests that the unidentified material may be a 'shunt' product from the ACAB conversion by D216E. It is possible that the modification in the iron binding site perturbs the conformational relationship between the thiolazetidinone intermediate (Scheme 3.1, B) and the reactive ferryl oxygen species. If the ring closure reaction at the thiazolidine ring is slowed down by this D216E mutation then oxidation at the cysteinyl thiolate will produce the shunt product (Scheme 3.1, D) rather than the closure of the thiazolidine ring (Scheme 3.1, C). The formation of atomic sulphur during the formation of the 'shunt' product follows the mechanistic proposals of Baldwin and Bradley[49]. The formation of the monocyclic β-lactam intermediate during the formation of the shunt product is uncertain[55]. An alternative mechanism for the formation of the

'shunt' product without the formation of the monocyclic β-lactam is also possible (Scheme 3.2), *e.g.* the oxidation of the cysteinyl residue rather than *via* the ring closed reaction intermediate (Scheme 3.1).

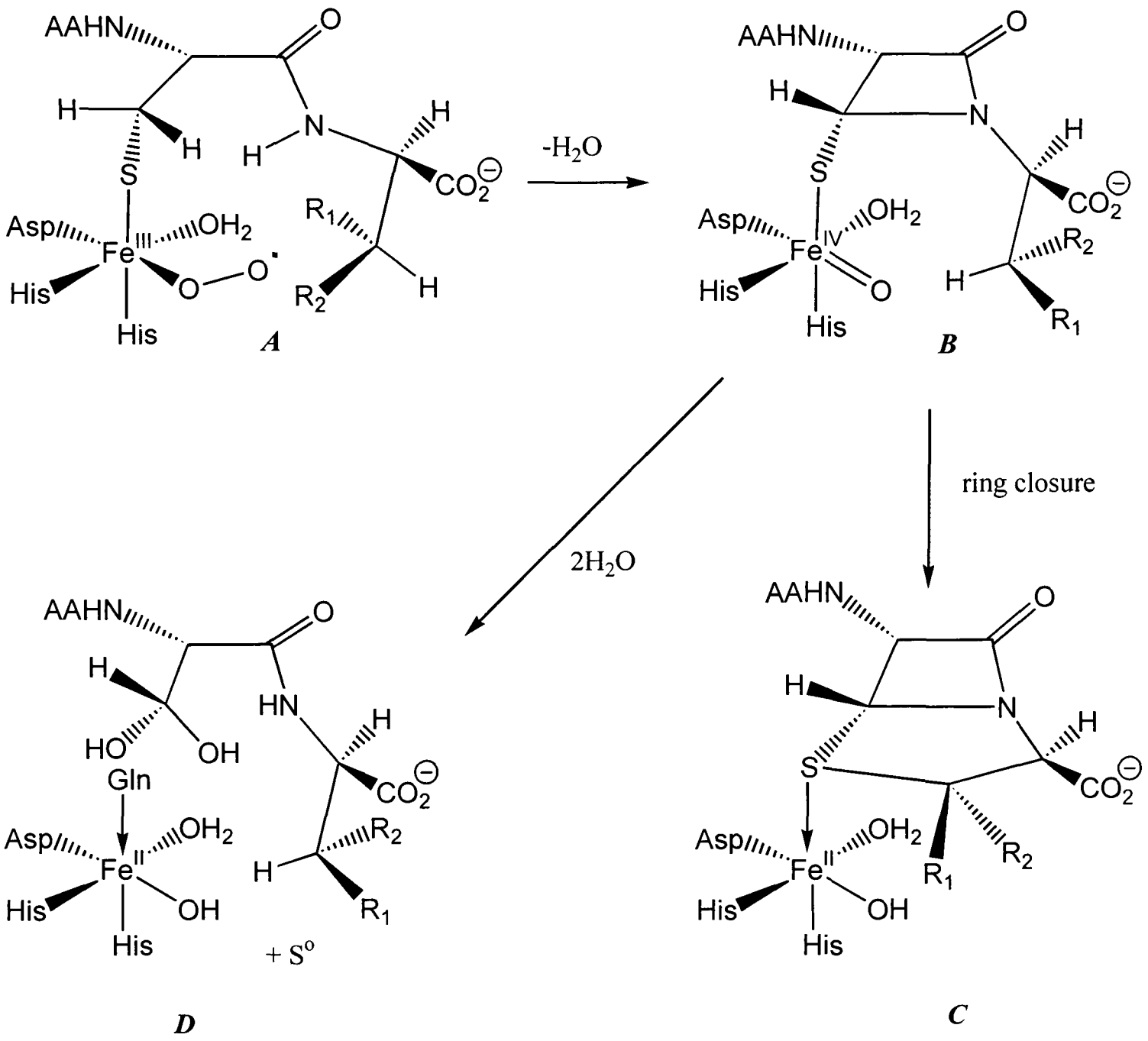

Scheme 3.1 Formation of IPN or a shunt product by IPNS. ACV R_1= R_2 = Me; ACAB R_1= Me, R_2 = H[49].

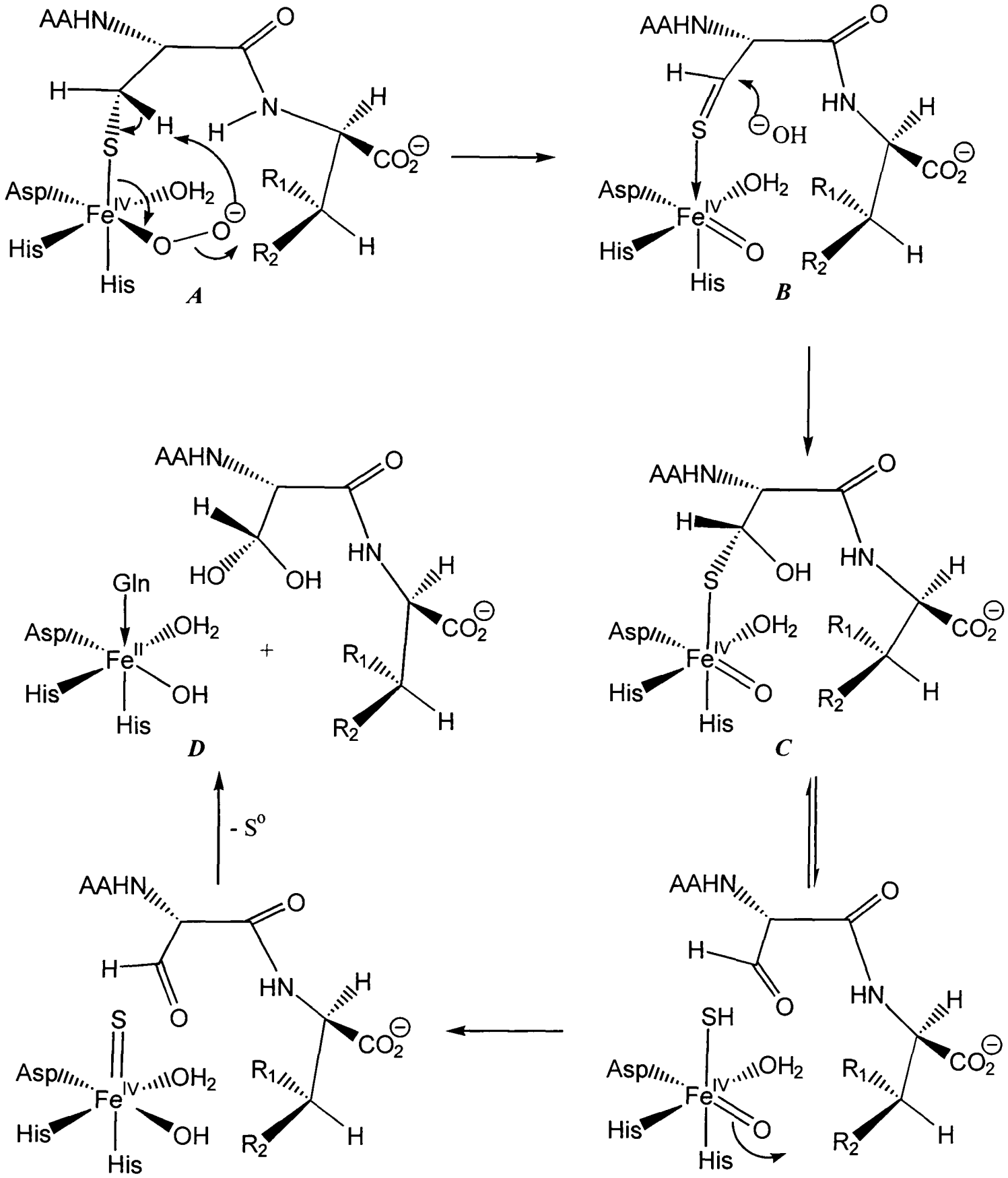

Scheme 3.2 Alternative possible mechanism for the formation of shunt product. Although shown as loss of atomic sulphur, the reduction of the Fe(IV)=S species may occur *via* a reaction with a reducing agent (DTT, ACV or ascorbate).

In the IPNS-Fe(II)-ACV complex the two methyl groups of the ACV valine isopropyl project towards the iron centre with the isopropyl C-H bond, which must be cleaved to form the new C-S bond, pointing away from the metal[52]. Reduction of the steric bulk of

the valine isopropyl group to glycine (ACG) or alanine (ACA) allows water molecules to enter the active site[55], which may be (partially) responsible in the case of ACA for directing the reaction away from the penam to the shunt product. Previously, it has been shown that neither ACG or ACA can form a penicillin product[55] and it is possible that other factors, *e.g.* bond strength may be important for this observation. However, no extra water molecules were observed in the IPNS-Fe(II)-ACAB crystal structure[55]. It may be that in the case of D216E mutant small changes in the active site allows extra water molecules to enter into the enzyme complex in the presence of ACAB, but not with ACV, resulting in the lack of β-lactam formation in the former case.

3.3.3 H270E IPNS mutant

Although it was anticipated that the substitution of a carboxylate for an imidazole of H270 may well lead to inactive IPNS the precise reasons for the lack of activity observed with the H270E mutant are presently unclear. The CD studies indicate that no major misfolding takes place in the mutant enzyme structure. Complete loss of iron binding to the active site may alone explain the inactivity with this mutant. If indeed no iron is bound in this mutant then it suggests that ACV can bind to the enzyme without the iron. However, this appears to be unlikely in view of the fact that this mutant forms metal-ligand charge transfer complexes with ACV. Therefore, it is likely that metal binding takes place in the active site in solution.

The present results suggest that a substrate (ACV or ACAB), and a ferrous metal ion is required for charge transfer complexes to occur with this mutant. This observation suggests that metal binding must take place in the active site or some other adventitous metal binding site of the enzyme in solution. The blue colour observed upon oxygenation

most probably arises from an Fe(III) to thiolate charge transfer complex. It is interesting to note that a blue coloured complex (λ_{max} 595 nm, ε = 2600 M^{-1} cm^{-1}) has been reported for 4HPPD from *Pseudomonad* P. J. 874[92] which was demonstrated to arise from a tyrosinate to ferric charge transfer. There was no evidence for such a tyrosinate charge transfer in the crystal structure of this mutant with ACV. However, the present crystal structure does not preclude the possibility that such charge transfers can take place in solution (see below).

The H270E mutant showed a remarkably different active site crystal structure compared with the wild-type and D216E mutant enzymes (Figure 3.6c). There appear to be regions of the H270E mutant protein structure which do not appear to be well defined compared with the wild-type IPNS structure (particularly the highly mobile region of the C-teminus). The observed electron density in the active site was too weak for a co-ordinated iron atom in the active site of this H270E mutant. The observation that this weak electron density was in contact with the side chains of His270 and Asp216 suggests that it may be a bound water molecule. These findings suggests that either the ferrous iron is absent (the ferrous metal ion being loosely bound at the active site in solution may become 'dislodged' during crystallisation) or that ferrous iron binding occurs at some other inadventitous metal binding site on the enzyme. It is unlikely that the absence of iron in the crystal structure was due to the low concentration used in the crystallisation conditions, since a saturating iron concentration (at least 25 times greater than the protein concentration used in solution studies of *ca.* one equivalent) was employed.

The overall position of ACV binding in the H270E mutant was similar to that observed in the wild-type IPNS. A major difference compared to wild-type IPNS was the

apparently disordered nature of the sulphur atom of ACV-thiol. In the mutant structure the disordered sulphur atom appears to occupy the former position of Phe211 of wild-type IPNS (Figure 3.6d). The new position of Phe211 also appears to be disordered and not well defined in this mutant. There also appears to be a region of diffused electron density in close proximity to the sulphur atom of the ACV which may be the new position of an iron atom in this mutant (Figure 3.6d).

Apart from the problems with the structural refinements, these studies demonstrate that it can be misleading to directly correlate the structure in the crystal form with that in solution. Further investigations using electron paramagnetic resonance are presently ongoing for the H270E mutant enzyme.

3.3.4 Model compounds

Intense efforts have been made to make mononuclear model iron complexes that mimic the spectroscopic and catalytic properties of IPNS[30]. Although there has been some success, the simple model compounds rarely replicate the functionality and specificity of the natural systems. Nevertheless, the results from these studies are intriguing and merit brief discussion.

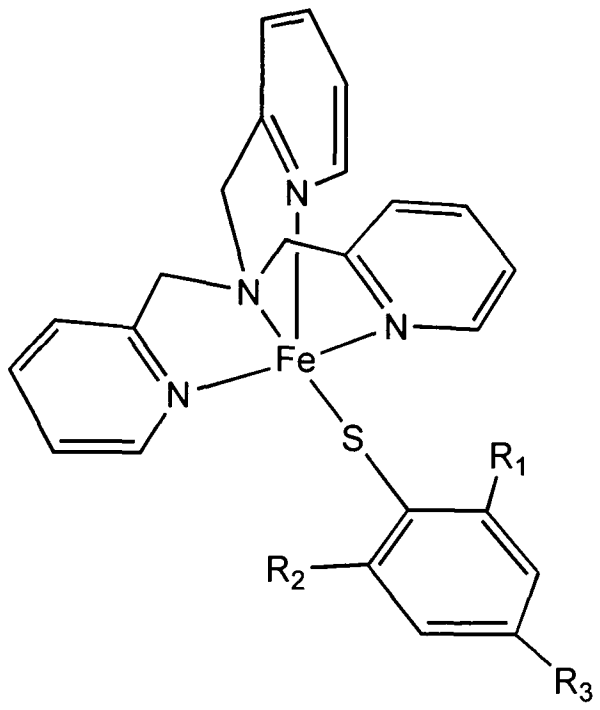

Figure 3.8 Thiophenolato iron(II) model complexes, $[Fe(TPA)(SAr)]^+$ (1, Ar = C_6H_2-2,4,6- Me_3; 2, Ar = C_6H_4-4-Me; 3, Ar = C_6H_5; 4, Ar = C_6H_4-4-Cl) where TPA is tris(2-pyridylmethyl)amine.

A series of thiophenolato iron(II) complexes were synthesised as model complexes (shown in Figure 3.8[30]). Complexes 1 to 4 react with NO at low temperatures to form NO adducts (Table 3.3). These NO complexes exhibited S to Fe charge transfer bands in the visible spectral region which are not present in the $[Fe(TPA)(O_2CCH_3)(NO)]^+$. Exposure of complexes 1 to 4 to air at low temperature generates metastable green species (1a-4a) corresponding to the one-electron-oxidised iron(III) derivatives (Table 3.3). Application of a vacuum or bubbling Ar through the solution does not affect the absorption band, indicating irreversible formation of the species. The absorption band near 600 nm shifts systematically from 624 nm (ε = 3000 M^{-1} cm^{-1}) for 1a, to 604 nm (ε = 2400 M^{-1} cm^{-1}) for 2a, to 584 nm (ε = 1900 M^{-1} cm^{-1}) for 3a, to 574 nm (ε = 1750 M^{-1} cm^{-1}) for 4a as the substitution on the thiophenol ring changes from electron donating CH_3 to electron withdrawing Cl.

Table 3.3 Comparisons of the visible absorption [$\lambda_{max,}$ nm (ε, M^{-1} cm^{-1})] of model compounds and tertiary complexes (Fe-ACV-IPNS) of mutant IPNS.

Complex	with NO	with O_2
1	450 (2700), 550(sh), 725 (~500)	624 (3000)
2	416 (3600), 555(sh), 710 (~500)	604 nm (2400)
3	404 (3700), 550(sh), 710 (~500)	584 nm (1900)
4	400 (2300), 560(sh), 715 (~400)	574 nm (1750)
wild-type	508 (1500), 720	none > 340
D216E	508 (1300), 720	none > 340
H270E	600	600 (700)

It is not possible to observe visible absorption spectra of the quaternary, wild-type IPNS-Fe(II)-ACV-O_2 since oxygen is a co-substrate for the reaction and gets consumed. Presently, the only way to observe a quaternary complex with wild-type IPNS is to substitute NO in place of O_2[53]. In the present study, a pink coloured complex was observed with the wild-type and D216E mutant which results from a thiolate to Fe(III) charge transfer. Unexpectedly, the inactive H270E mutant does not form a pink charge transfer complex with NO under similar conditions thus suggesting that the binding of iron, O_2 and ACV is affected. The blue coloured complex formed after the oxygenation of the H270E-Fe(II)-ACV which results from a Fe(III) to thiolate charge transfer was similar to that seen in model complexes. It is surprising, that the H270E mutant (with only one histidine and two carboxylate donors) displays a similar charge-transfer absorption spectra to that observed for the oxygenated model complexes (with three pyridine N donors in species 1a-4a).

CHAPTER 4

Kinetic Analyses of IPNS Inactivation

4.1 Introduction

4.1.1 Fenton chemistry

Oxygen reactivity

The toxic effects of dioxygen to aerobic organisms have been long known[93,94]. Increasing the dioxygen concentrations above normal atmospheric levels causes damage to plants, animals and aerobic bacteria[4]. The causes of the poisonous properties of dioxygen were obscure before the publication of Gershman and Gilbert's free radical theory of oxygen toxicity, which proposed that these toxic effects of dioxygen are due to partially reduced forms of oxygen[94]. The one electron reductions of dioxygen, by synthetic chemicals and/or enzymatic reactions, produces highly reactive semi-reduced states (Scheme 4.1).

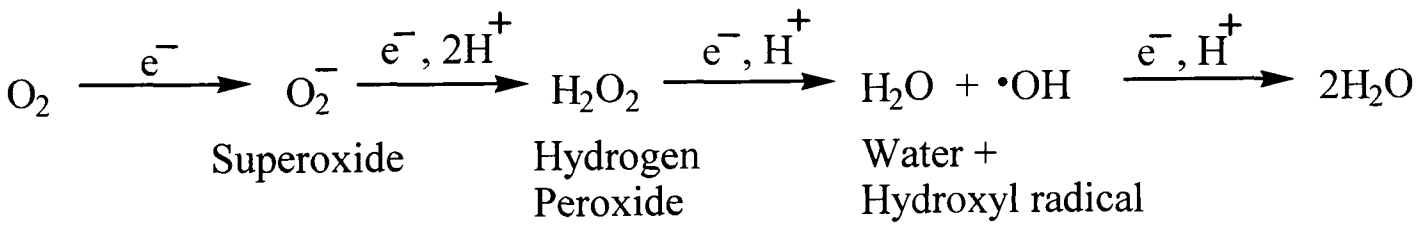

Scheme 4.1 The reduction products of dioxygen.

A free radical may be defined as any species that has one or more unpaired electrons. This broad definition includes the hydrogen atom (one unpaired electron), many transition metals and the dioxygen molecule itself. Dioxygen ordinarily exists as a diradical, since its two free electrons exist in two different orbitals and have parallel spins (the so called 'triplet state'). Dioxygen's reactivity is greatly lowered by spin

restriction (*i.e.* if oxygen is to oxidise another molecule by accepting a pair of electrons from it then both new electrons must have parallel spins, which cannot occur if both electrons occupy the same orbital). This imposes a restriction on the range of oxidations by O_2 since it tends to accept its electrons in a stepwise manner and therefore slows down its reaction with non-radical species. One way to remove this spin restriction in dioxygen is to move one of the unpaired electrons, *i.e.* to produce a singlet state molecule. More commonly in nature, the spin restriction can be removed by complexing dioxygen to a transition metal, which has the ability to donate and accept single electrons[95].

Oxygen free radicals

If a single electron is accepted by the ground state O_2 molecule, the product is a superoxide radical, O_2^- (Scheme 4.1). It has been proposed that free superoxide is the major species responsible for oxidative damage in the cell, but studies in neutral aqueous solutions have revealed that it rapidly disproportionates to give dioxygen and hydrogen peroxide (Scheme 4.2). The spontaneous rate for this (dismutation) reaction at physiological pH is 5×10^5 M^{-1} s^{-1} [96]. The enzyme that catalyses this reaction is superoxide dismutase (SOD) which increases this rate by a factor of 10^4.

$$2O_2^- + 2H^+ \rightleftharpoons H_2O_2 + O_2$$

Scheme 4.2 The dismutation reaction of superoxide radical.

Addition of a second electron to O_2^- reduces it to the peroxide ion, O_2^{2-}, which has no unpaired electrons and is not a radical. Any O_2^{2-} formed at physiological pH will be

immediately protonated to give hydrogen peroxide (H_2O_2) and hydroperoxide (HO_2^-) since the pK_a of O_2^{2-} is very high (>14).

Hydroxyl radicals can be produced by homolytic fission of the O-O bond by heat or ionising radiation. An alternative way to produce hydroxyl radicals is to use a mixture of H_2O_2 and iron (II) salts as was first observed by Fenton in 1894. Haber and Weiss (1934)[97] proposed a reaction pathway for Fenton's reaction in which the reactive species are $^{\bullet}OH$ radicals (Scheme 4.3):

$$Fe(II) + H_2O_2 \longrightarrow Fe(III) + {}^{-}OH + {}^{\bullet}OH$$

Scheme 4.3 The Haber-Weiss reaction showing the proposed products from the reaction of hydrogen peroxide with iron (II).

Traces of Fe(III) can react further with H_2O_2 as follows:

$$Fe(III) + H_2O_2 \longrightarrow Fe(II) + O_2^{-} + H^+$$

$$^{\bullet}OH + H_2O_2 \longrightarrow H_2O + O_2^{-} + H^+$$

$$Fe(III) + O_2^{-} \longrightarrow Fe(II) + O_2$$

$$Fe(II) + {}^{\bullet}OH \longrightarrow Fe(III) + {}^{-}OH$$

Thus the overall result of these reactions, unless some other reagent intercepts the $^{\bullet}OH$, is an iron catalysed decomposition of hydrogen peroxide:

$$H_2O_2 \xrightarrow{Fe(II)} 2H_2O + O_2$$

The $^{\bullet}OH$ radical reacts at extremely high rates with almost every type of molecule in the cell, *e.g.*, DNA[98,99], proteins[100] and small organic molecules[101]. Since some

researchers believe such reactions are a major cause of damage to proteins, the reaction of the $^{\bullet}OH$ with proteins will be discussed in Section 4.12 of this introduction. Whether or not free $^{\bullet}OH$ is a major cause of oxidative damage *in vivo* is unclear and it may be that metal complexes of reactive oxidising species are more important (*vide infra*).

The exact nature of the major reactive oxidative species produced by the Haber-Weiss reaction is still debated and some researchers have proposed that a high valent Fe(IV)=O species is formed instead of $^{\bullet}OH$[102-104] (Scheme 4.4). Fe(IV)=O has also been proposed to be the oxidant in the reaction of Fe(II) with ADP, orthosphosphate or EDTA[105].

$$Fe(II) + H_2O_2 \longrightarrow [Fe(IV)=O]^{2+} + H_2O$$

Scheme 4.4 Proposed products from the reaction of hydrogen peroxide with iron(II) to give an iron-oxene species.

Udenfriend's chemistry

Udenfriend's reagent is an aerobic aqueous solution of an EDTA-iron(II) complex in the presence of a reducing agent, such as ascorbic acid. It is a known oxidant of aromatic substrates. The oxidation of substrates by this reaction is inhibited by the presence of catalase[106], therefore hydrogen peroxide is thought to be one of the intermediates. Ascorbic acid is a strong electron donor and is thought to have a dual role in Udenfriend's chemistry: it reduces ferric iron to the ferrous state and serves as a source of hydrogen peroxide which, in turn reacts with the reduced ferrous complex and triggers the Fenton reaction to release $^{\bullet}OH$ radicals[107,108]. In this reaction, complexing with EDTA, or DTT may help to sequester the ferrous iron since ferric iron is less soluble at physiological pH. Aerobic solutions of EDTA-Fe(II) + ascorbate have been reported to

oxidise aromatic substrates[109], DNA[110] and amino acids[111,112]. Udenfriend's conditions have been used previously to inactivate a range of enzymes, often with the aim of identifying active site residues[70,113,114].

4.1.2 Metal catalysed oxidation of proteins

It is well known that the exposure of proteins to free radicals, produced by radiolysis, leads to modification of the amino acid residues. This leads to the formation of protein aggregates *via* protein-protein cross linking reactions and cleavage of some peptide bonds[112]. Nevertheless, it is unlikely that radiolysis is a major source of oxygen radicals *in vivo* except under extreme conditions of exposure to X-rays or to high levels of radioactivity.

The high capacity for free radical generation in cells by non-radiative processes is evident from the large increases in radical-mediated tissue damage that occurs following brief exposure to oxygen[94,115]. The site specific metal ion-catalysed oxidation reactions produce highly reactive species (probably $^{\bullet}OH$ and Fe(IV)=O) which can react non-specifically with various components of the cell. These reactive species have been implicated in various pathological processes, *e.g.* arthritis, pulmonary diseases, intracellular protein turnover and cellular ageing[100,116-118].

The control of protein degradation is thought to be as important as the control of protein synthesis but the mechanism by which cells identify damaged proteins is largely unknown. The half-lives of proteins in various mammalian tissues have been measured and range from a few minutes to many days[119]. Protein turnover has also been implicated in the maintenance of amino acid pools and the generation of peptide fragments which act as hormones and other effectors[120].

In vivo selective degradation of abnormal proteins, including oxidatively damaged proteins, is also thought to be important for regulatory protein turnover[121]. A well studied example of this process is the case of glutamine synthetase, which undergoes iron catalysed oxidation at two specific residues. This results in an inactive form of the enzyme which is specifically recognised and degraded by the cellular processes[122]. Some estimates, based on protein carbonyl group detection and quantification, suggest that around 10% of cellular proteins in a typical young human individual may be oxidatively modified, although not functionally damaged[116].

Many studies demonstrate that both metallo and non-metallo proteins undergo *in vitro* metal catalysed oxidative (MCO) inactivation mediated by transition metals, particularly iron[112]. However, enzymes that utilise metal/dioxygen chemistry (oxygenases; oxidases; oxygen transporters) are potentially exposed to much greater risks of oxidative damage than those that do not. Inactivation in these enzymes can result from several different processes: (1) enzymatic: an activated dioxygen species generated during the catalytic pathway of the enzyme may erroneously oxidise the protein itself; (2) alternatively, Fenton's/Udenfriend's or related chemistry may generate activated dioxygen species in solution, at the active site, or at an adventitious metal binding site on the protein. The two inactivation processes may be linked and the non-enzymatic metal/oxygen chemistry outside the enzyme may intercede the enzymatic inactivation. In either case, the presence of the metal centre in the protein may concentrate and direct oxidative damage into the active site area resulting in one or more of the following: (a) oxidation of the metal in the active site (*e.g.* in met-haemoglobin); (b) oxidation of amino acid side chains; (c) covalent adduct formation between the substrate/product at the active site; (d) fragmentation of the peptide backbone.

4.1.3 Inactivation of IPNS and other non-haem iron dioxygenases

All non-haem iron dependent dioxygenases utilise iron and dioxygen in order to catalyse the oxidation of a variety of substrates[82,111]. It has been reported that many members of this family of enzymes undergo inactivation during *in vitro* incubation[70,123].

The proposed reaction stoichiometry for α-ketoglutarate (α–KG) dependent and the sequence related non-α–KG dependent dioxygenases (IPNS and ACCO) is summarised in Scheme 4.5A-C. In Scheme 4.5A, one half of the oxidising potential of the dioxygen molecule is used to decarboxylate α–KG to give succinate; the other two electron equivalents required for the reduction of dioxygen are provided by the substrate, leading to hydroxylation, epoxidation or desaturation reactions[111,123]. ACCO and IPNS do not use α–KG as a co-substrate, but belong to the same family of non-haem iron oxygenases by virtue of their sequence similarity with a large sub-class of these enzymes and because of their requirement for an iron (II) co-factor (see Chapter 1).

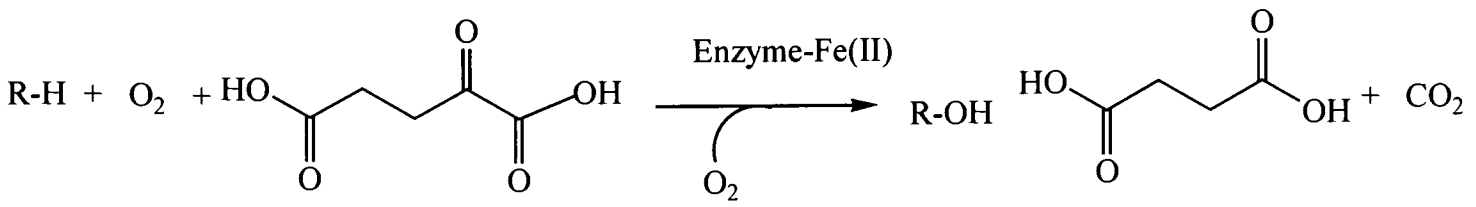

A

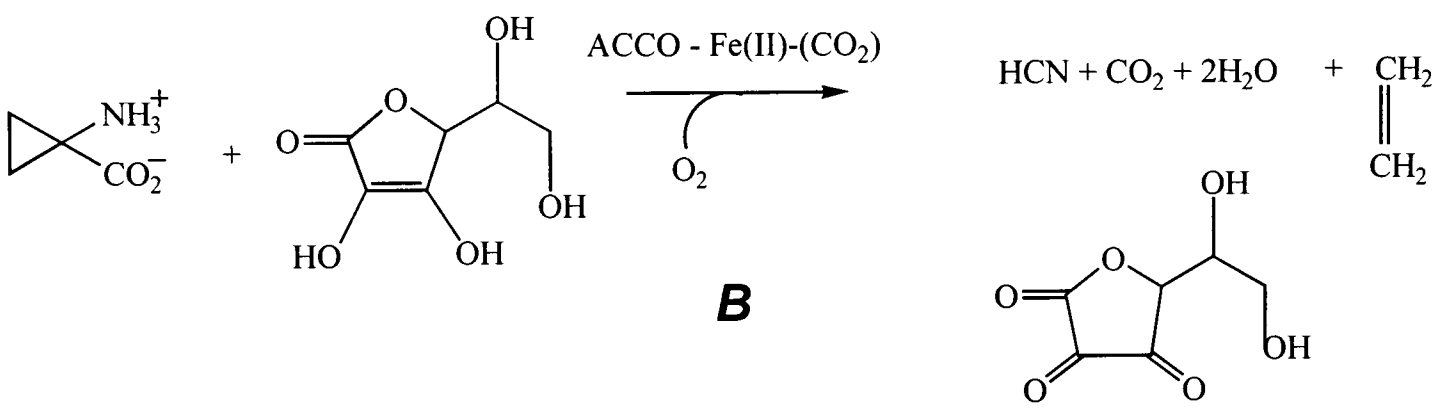

B

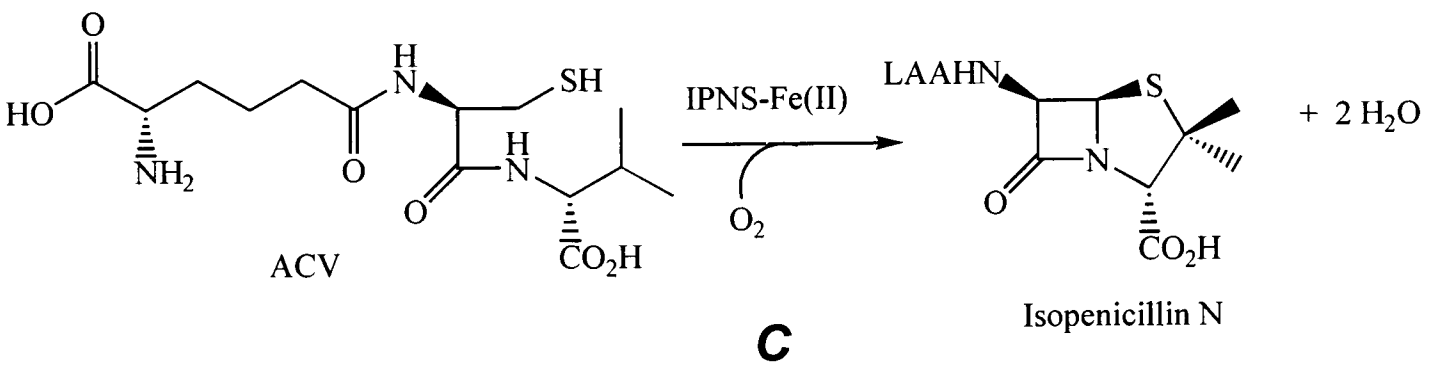

C Isopenicillin N

Scheme 4.5 Stoichiometry of: (A) 2-oxoglutarate dependent dioxygenase catalysed hydroxylation reaction; (B) ACCO catalysed biosynthesis of ethylene; (C) IPNS catalysed biosynthesis of isopenicillin N.

In ACCO the role of α-KG is fulfilled by ascorbate which is oxidised to dehydroascobate and the remaining two reducing equivalents are provided by ACC (Scheme 4.5B). IPNS does not use an α–KG co-substrate; all four reducing equivalents are provided by the substrate ACV to completely reduce the oxygen to water as shown in Scheme 4.5C[52,124].

In Scheme 4.5A one equivalent of succinate and carbon dioxide is produced per mole of substrate oxidation. In many instances though, this ratio is greater than unity and more succinate and carbon dioxide are enzymatically produced, in low amounts, even in the absence of substrate. This enzyme catalysed turnover of α-KG in the absence of substrate is termed the 'uncoupled decarboxylation reaction'. In the case of prolyl 4-hydroxylase it has been reported that the turnover of α-KG in the uncoupled reaction is stoichiometric with that of ascorbate[125]. Prolyl 4-hydroxylase has been shown to be especially susceptible to inactivation during uncoupled turnover of α–KG which has been proposed to be a consequence of side reactions of the putative Fe(IV)=O species[126]. The high reactivity of this species in the active site may well render amino acids in its vicinity susceptible to (irreversible) oxidation and inactivation. In the absence of substrate this probably represents the major reaction pathway and indeed pre-incubation of many of these dioxygenases with α–KG, ascorbate and dioxygen has been reported to give the rapid loss of enzyme activity[70,126]. It is thought that ACCO, IPNS and many members of the family of α-ketoglutarate dependent dioxygenases undergo inactivation during *in vitro* incubation for the same reasons. This may also explain the large variations in specific activities observed in previous studies on IPNS[127,128].

Ascorbate effects

IPNS does not require ascorbate for catalysis but previous studies have reported that its inclusion leads to a prolonged catalytic lifetime without affecting the initial rate[123]. Other studies have reported that ascorbate offers a protective effect[129] and a stimulatory effect[130] on IPNS activity.

ACCO uses ascorbate as a co-substrate and has been reported to be very susceptible to inactivation *via* Udenfriend's chemistry under *in vitro* assay conditions[64]. Inactivation was not reversible (implying a covalent modification) and was not due to product inhibition. Further studies, using Udenfriend's chemistry, showed that the rate of iron/ascorbate inactivation was increased when substrate (ACC) was added to the assay mix but decreased by the inclusion of catalase or ACC with CO_2 in the incubation mix[70]. The Fe(II)/ascorbate inactivation of ACCO was accompanied by partial proteolysis as observed by SDS-PAGE. The fragmentation pattern was altered when ACC was included in the assay mix[70].

Protective effects of ascorbate in the assay mixture have been reported with other α-KG dependent oxygenases including: gibberellin 20-oxidase[131]; flavanone 3β-hydroxylase[132]; prolyl 4-hydroxylase[125,126,133]. In all of these studies, it has been proposed that the active-site-generated reactive intermediate is also responsible for substrate oxidation. However, an inhibitory effect of ascorbate has been reported for clavaminate synthase[134] and proline 4-hydroxylase[123]. Thus, the role of ascorbate as an universal reductant in the uncoupled turnover of α-KG dependent enzymes is unclear. Indeed such a universal role is unlikely due to the limited bioavailability of ascorbate.

Substrate effects

The effects of including substrate on the inactivation rates of other enzymes varied from: increased inactivation (ACCO[70]; glutamine synthetase[114]), or total protection (pyruvate kinase[121]), to no effect at all (malic enzyme with *L*-malate and NADP[113]).

In this Chapter, a kinetic analysis of IPNS inactivation was carried out under *in vitro* assay conditions. The aim of this study was to investigate IPNS inactivation under various assay conditions and to examine whether the observed inactivation resulted from reactive species generated in solution or at the enzyme active site. In view of the fact that IPNS, DAOCS/DACS and ACCO show high sequence similarities, and they are also postulated to use similar mechanisms, IPNS was tested for ethylene production. Some preliminary data which compare the ethylene production in the presence of IPNS or DAOCS/DACS (*Cehaloporium acremonium*) and in different buffers is presented in this chapter. The structural changes accompanying inactivation will then be presented in the subsequent chapter.

4.2 Results

4.2.1 Inactivation studies

The measurement of inactivation rates for IPNS were performed as described in the experimental section (section 6.3, Chapter 6). IPNS was pre-incubated at a protein concentration of 1 mg/ml (26 μM) in buffer E (50 mM Tris-HCl pH 8.0) with various combinations of substrates and cofactors, and aliquots were withdrawn at regular time intervals to assay for IPN production. All cofactors were present at effectively saturating concentrations: iron(II) sulphate heptahydrate (0.5 mM), sodium *L*-ascorbate (25 mM) Catalase (0.5 mg/ml) and BSA (5 mg/ml) were added as required. Each time point was measured in duplicate and exponential decay curves were used to fit the inactivation data ($A=A_0e^{-kt}$; A = activity at time t, A_o = activity at time t = 0, k = exponential decay constant). Therefore the half-lives of the inactivation ($t_{1/2}$) could be calculated as (ln 2)/k. To simplify the interpretation of the data, DTT and ACV were not included in the assays; inclusion of ACV would produce IPN in the pre-incubation experiments and thus give misleading levels of activity in the HPLC assay. The pre-incubation conditions and the corresponding half-lives are summarised in Table 4.1 [the corresponding plots of first order exponential decay ($\ln A/A_o = -kt$), and second order, ($1/A-1/A_o = kt$), from pre-incubation data are shown in Appendix C].

The slowest rate of inactivation was observed in the absence of all cofactors (Figure 4.1, condition M, $k = 1.9 \times 10^{-3}$ min^{-1}) with a $t_{1/2}$ of approximately 6.5 hours. Complete inactivation was not observed even after 3 days at room temperature. This slow inactivation was not prevented by the inclusion of catalase or by the incubation of IPNS under anaerobic conditions and therefore is probably not due to a metal catalysed oxidation process.

Table 4.1 Effects of pre-incubation conditions on the IPNS inactivation

	ACV	Fe(II)	DTT	ASC	EDTA	H_2O_2	catalase	$t_{1/2}$ (min)[a]	Fragmentation
A	+	+	+	+	-	-	-	-	observed
B	-	+	+	+	-	-	-	-	observed
C	+	+	-	-	-	-	-	-	not observed
D	-	+	+	-	-	-	-	-	observed
E	-	-	+	-	-	-	-	-	not observed
F	-	+	-	+	-	-	-	48	observed
G	-	+	-	+	-	-	+	277	much reduced
H	-	+	-	-	-	-	-	-	not observed
I	+	+	-	+	-	-	-	-	observed
J	-	+	-	-	-	+	-	<5	observed
K	-	-	-	-	+	+	-	-	not observed[c]
L	+	+	+	+	-	-	+	-	much reduced
M[b]	-	-	-	-	-	-	-	385	not observed

[a] Values given to the nearest minute for the first order reaction ln $(A/A_o) = -kt$; [b] Buffer alone; [c] High molecular weight aggregate.

In the presence of ferrous iron (0.4 mM) and ascorbate (25 mM) the rate of inactivation was increased (Figure 4.1 condition F, $k = 14.2 \times 10^{-3}$ min^{-1}) when compared with buffer alone. Catalase (0.5 mg/ml) was found to offer total protection against this inactivation (Figure 4.2, condition G, $k = 2.5 \times 10^{-3}$ min^{-1}) whereas BSA, at 1 mg/ml, offered no protection (Figure 4.3, $k = 14.1 \times 10^{-3}$ min^{-1}).

This suggested the involvement of hydrogen peroxide in the iron/ascorbate inactivation process of IPNS. The inclusion of catalase at a concentration of 0.5 mg/ml significantly decreased the rate of inactivation compared with the iron(II)/ascorbate mediated inactivation process. Attempts at increasing the protective effects of catalase by increasing its concentration to 5 mg/ml made little difference to the protective effect.

To test the involvement of H_2O_2 in the inactivation process, the preincubation experiments were repeated using H_2O_2 (0.025% v/v) and iron (II) solution (0.01 mM) (Table 4.1, condition J). IPNS was rapidly inactivated in the presence of ferrous iron and H_2O_2 (Figure 4.4). The inactivation was dramatically reduced upon the inclusion of catalase (0.5 mg/ml), but BSA (up to 5 mg/ml) offered no protection against this inactivation. The data was not good enough to obtain an accurate value for the half-life for the inactivation under condition J, but a value of $t_{1/2} < 5$ minutes could be estimated.

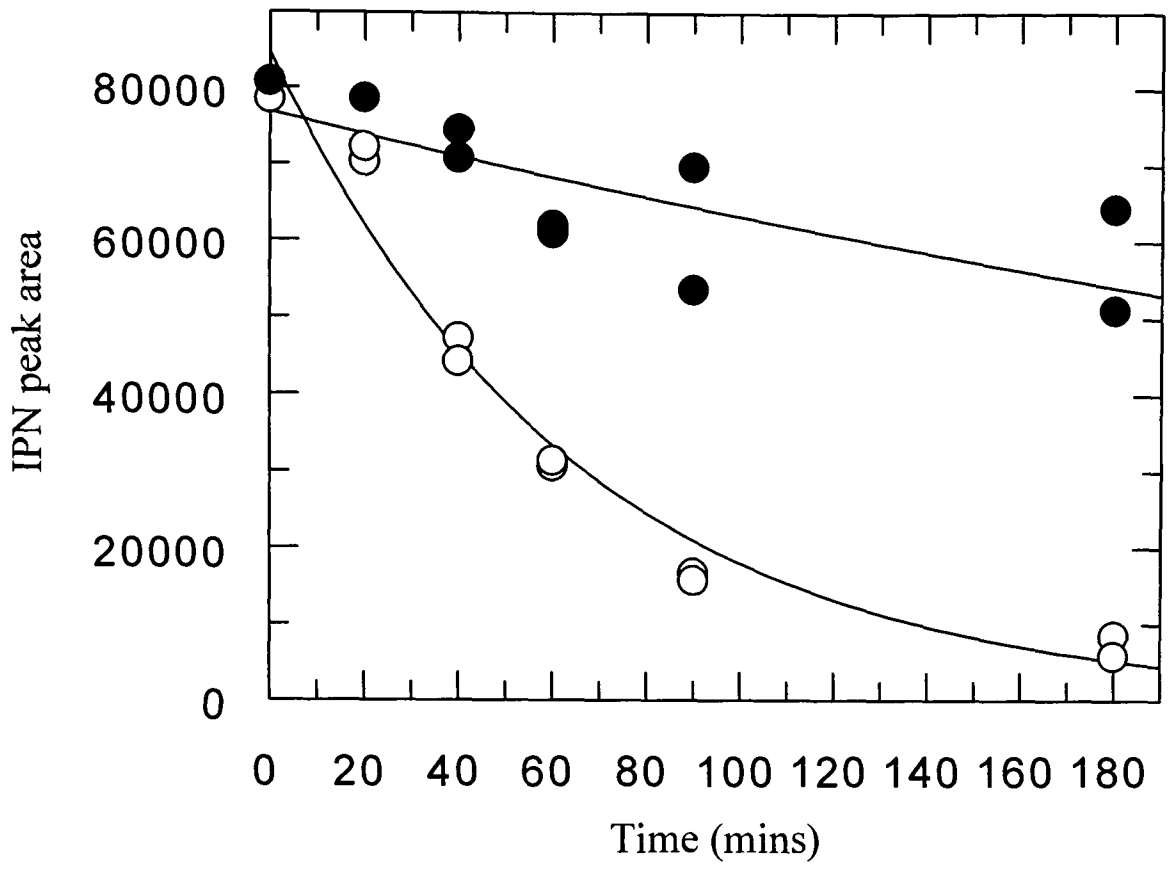

Figure 4.1 Inactivation of IPNS in the presence of: iron(II) and ascorbate (open circles); buffer only (filled circles).

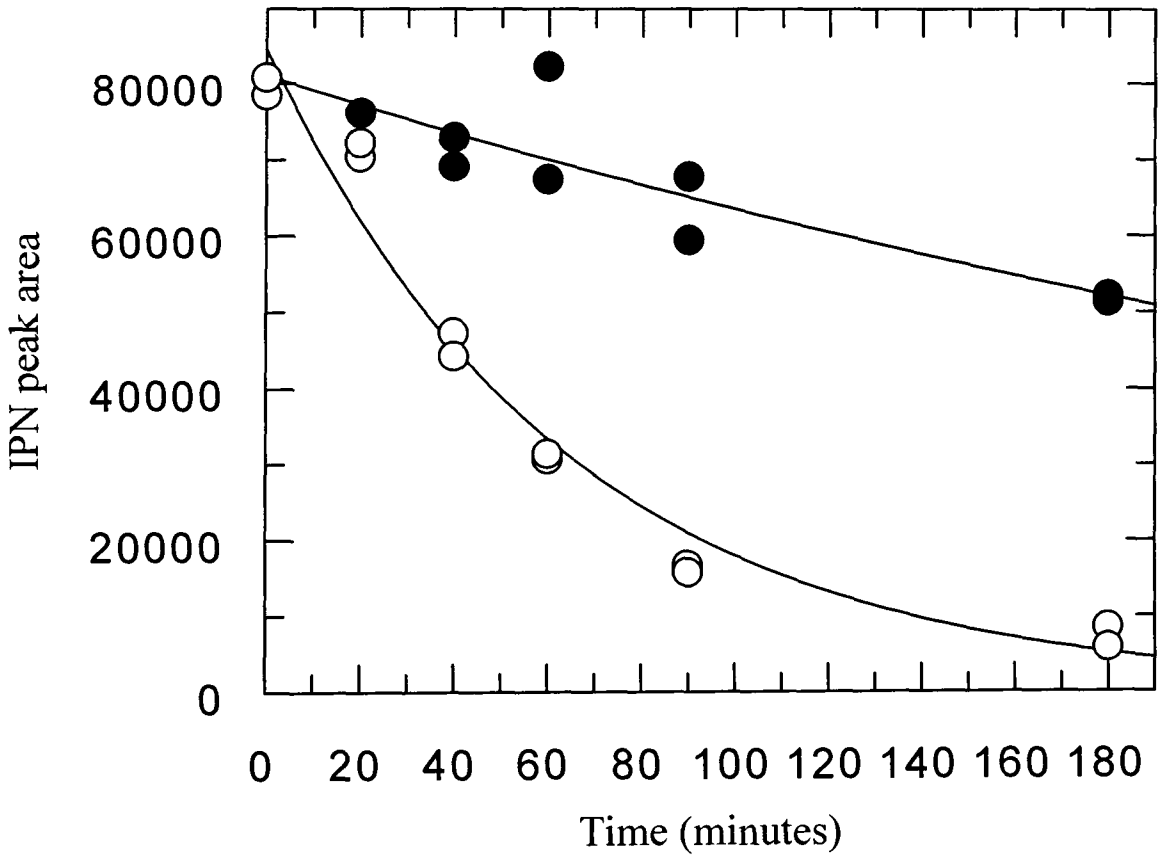

Figure 4.2 Inactivation of IPNS with iron(II) and ascorbate: without catalase (open circles); with catalase (filled circles).

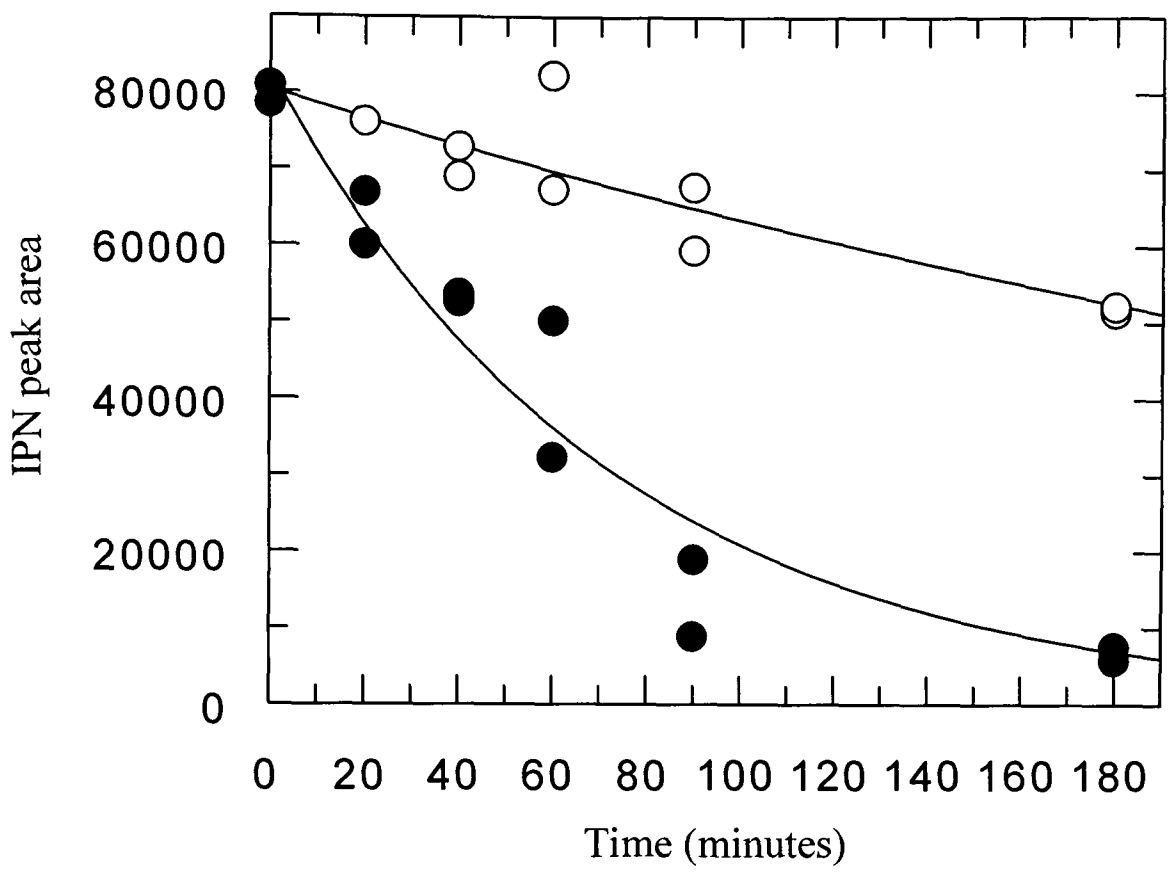

Figure 4.3 Inactivation of IPNS in the presence of iron(II) and ascorbate with: BSA (filled circles); catalase (open circles).

The iron/ascorbate mediated inactivation was shown to require oxygen by performing the pre-incubation studies anaerobically (inside a glovebox). The rates of inactivations with iron(II)/ascorbate (condition F) in the absence of oxygen (<0.4 ppm) were found to be identical, within experimental error, to those obtained in buffer alone (condition M).

IPNS samples from the pre-incubation experiments were also analysed by SDS-PAGE to look for protein modification and fragmentation. The results showed that IPNS incubated with iron(II)/ascorbate undergoes fragmentation (Fig 4.5, condition F). The fragmentation was cumulative over a period of 90 minutes (Fig 4.5 lanes 1-5, condition F).

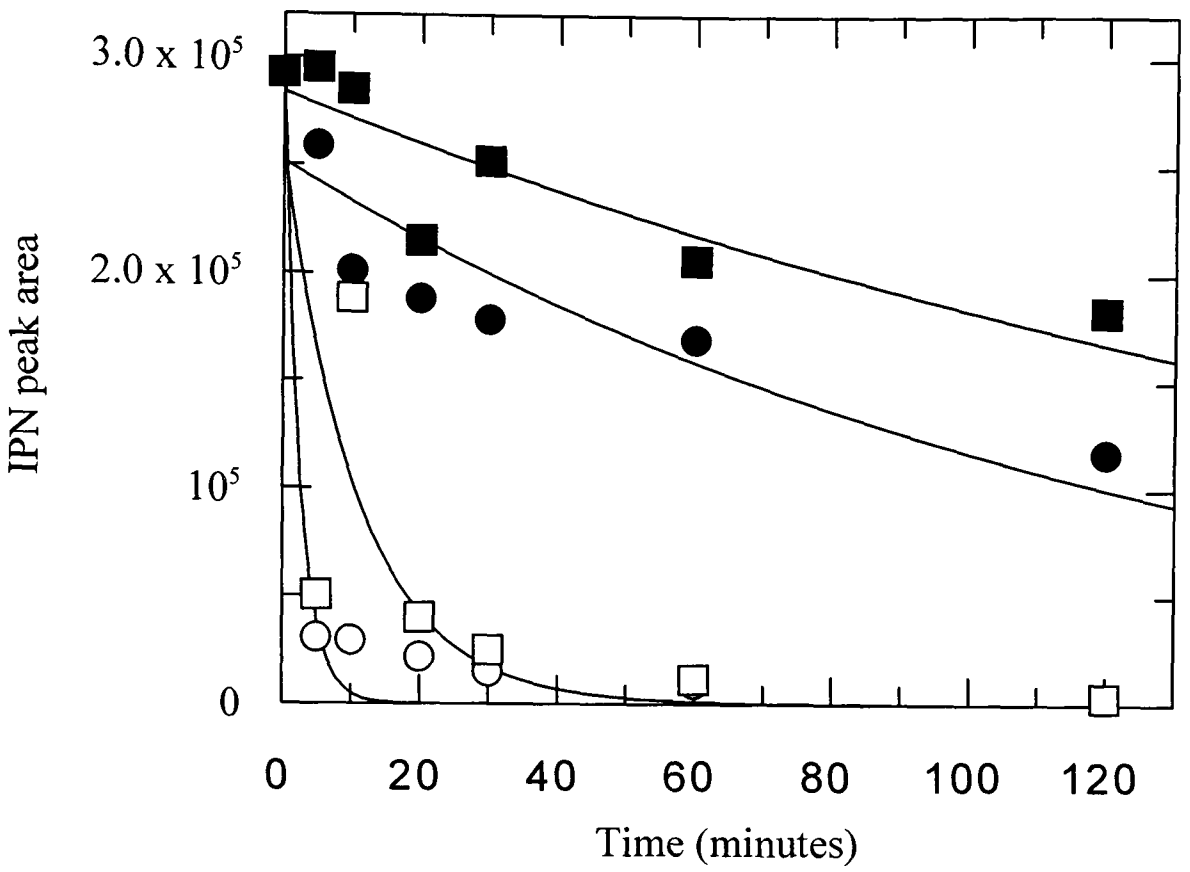

Figure 4.4 Effect of hydrogen peroxide and iron(II) on the inactivation of IPNS in the presence of: catalase (0.5 mg/ml) filled circles; BSA (0.5 mg/ml) open squares; without catalase or BSA, open circles. The inactivation rate in buffer alone is shown as filled squares.

Addition of catalase to IPNS under condition F significantly reduced fragmentation (Figure 4.5, lanes 6-7, condition G), but if BSA was added instead of catalase the fragmentation was not prevented (Figure 4.5, lanes 11-15). In the presence of iron (II) and H_2O_2 the fragmentation was similar to that observed with condition F, but intense smearing made it difficult to estimate the extent of fragmentation (Figure 4.5, lanes 16-20, condition J). No IPNS fragmentation occurred either in the presence of 1 mM Fe(II) sulphate alone (Figure 4.5, lanes 21-25, condition H) or with buffer alone (Figure 4.5, lanes 26-30, condition M). A more complete analysis of IPNS fragments, including the positions of cleavage, will be described later (Chapter 5).

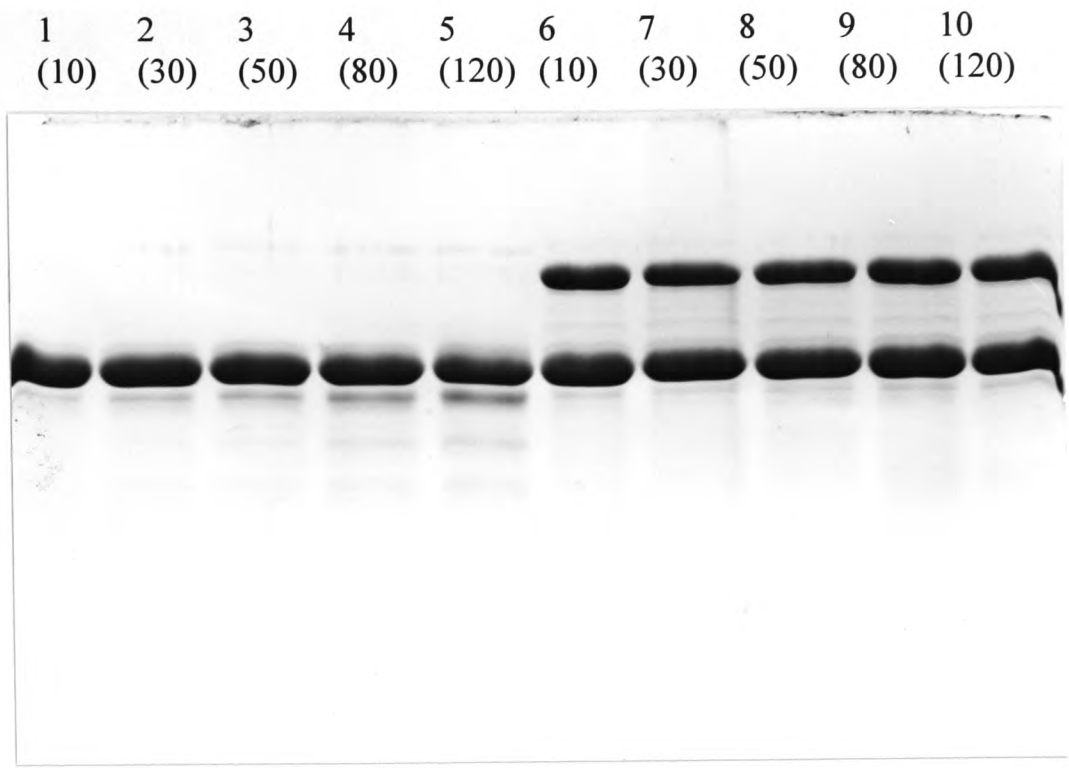

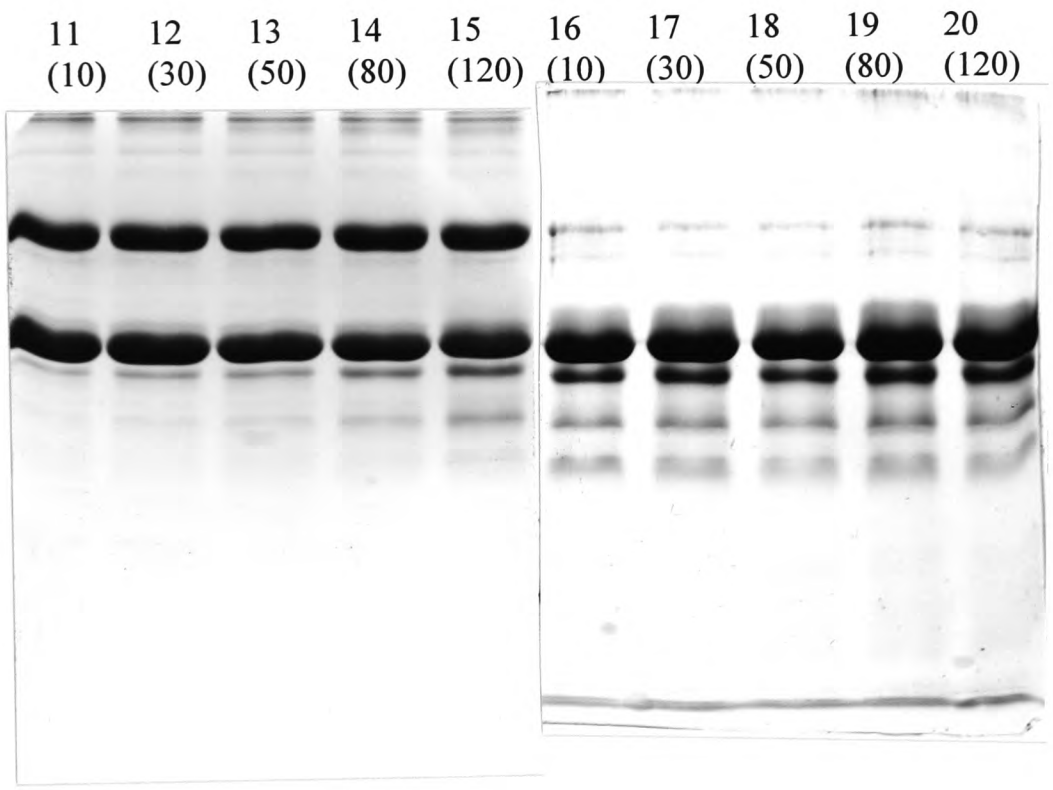

Figure 4.5 SDS-PAGE analysis of IPNS from pre-incubation studies. Lanes from left to right show length of incubation in minutes (given in parentheses) under the following conditions: (1) to (5) condition F (0.4 mM ferrous sulphate with 2.5 mM ascorbate); (6) to (10) condition F with catalase; (11) to (15) condition F with BSA; (16) to (20) condition J [0.4 mM ferrous sulphate with H_2O_2 0.025% (v/v)]; (continued overleaf).

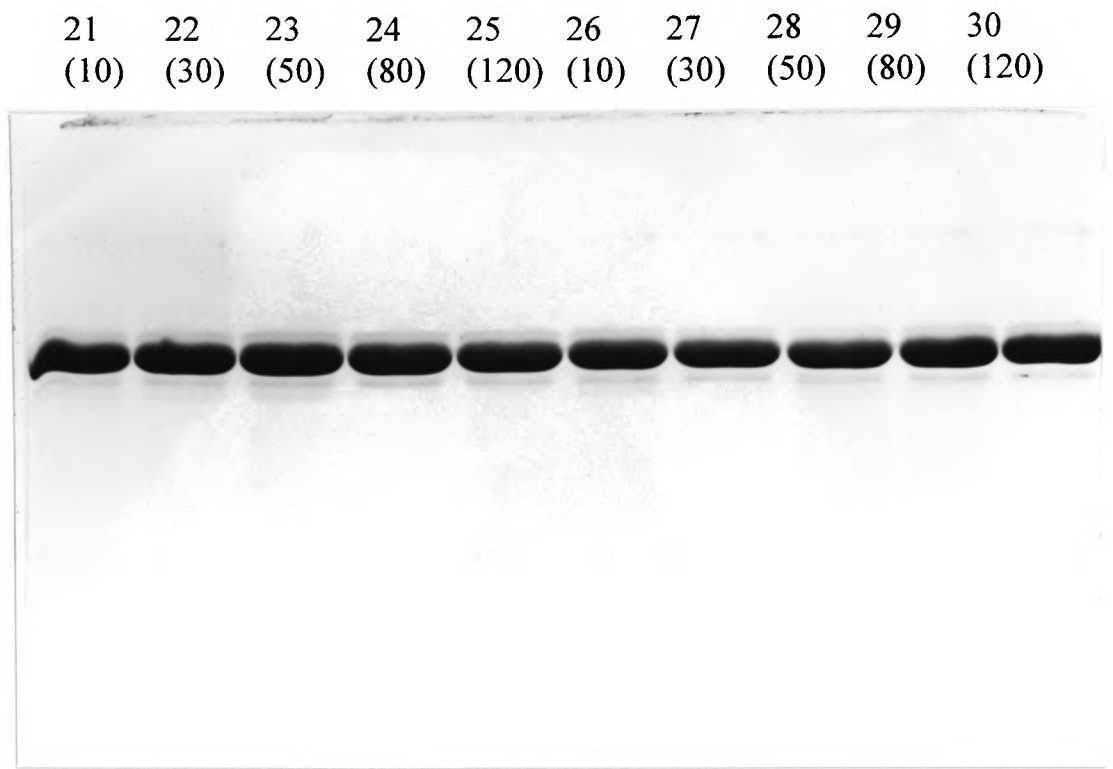

Figure 4.5 continued (21) to (25) condition M (buffer alone); (26) to (30) condition M with ferrous sulphate (0.4 mM).

4.2.2 ACV turnover experiments

The effect of ACV on the inactivation rate could not be readily determined by the pre-incubation experiments because the IPN produced during pre-incubation would give rise to misleading activity measurements. Thus, IPNS activity was measured in the presence and absence of catalase under saturating conditions of substrate and cofactors to see whether the protective effects of catalase could be observed under the *in vitro* assay conditions (Figure 4.6).

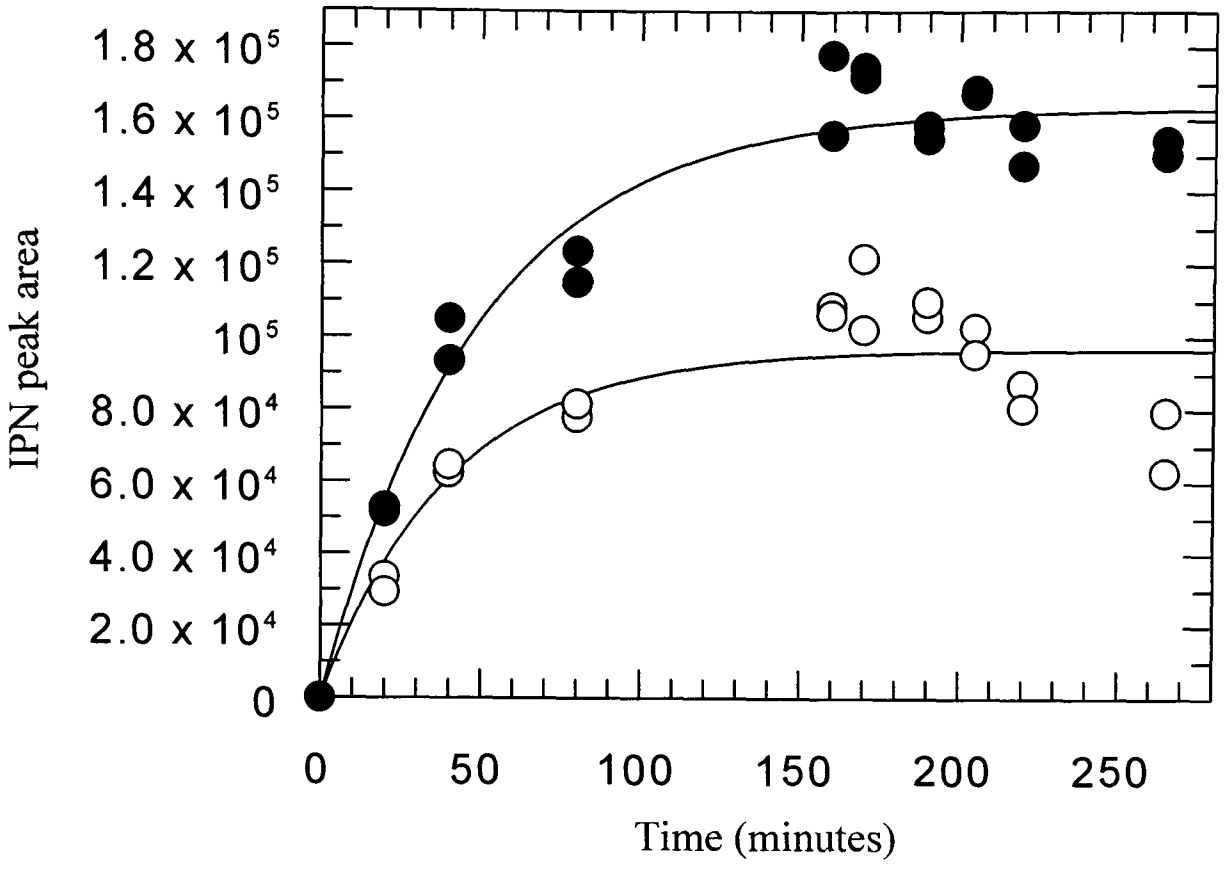

Figure 4.6 Effect of catalase on the activity of IPNS: with catalase 0.5 mg/ml (filled circles); without catalase (open circles).

Enhanced rates of IPNS activity were seen in the presence of catalase when compared with control samples (without catalase) under the *in vitro* assay conditions. This finding suggests that catalase stimulates *in vitro* IPNS activity. It was thought that the enhanced oxidation of ACV-thiol into ACV-disulphide occurs in the absence of catalase which reduces the concentration of the former to a sub-saturating level. Therefore the concentration of ACV-thiol under incubation conditions was estimated by HPLC in the presence and absence of catalase. The results from these determinations showed that indeed there was an enhanced rate of oxidation of the ACV-thiol to disulphide in the absence of catalase. The ACV-thiol concentration was found to be 1 mM in the absence and 3 mM in the presence of catalase after 4 hours incubation. Additionally, it was noted that the addition of fresh DTT, ascorbate and iron had no effect on the IPN production of either the catalase protected or the control sample after 150 minutes.

After approximately 3 hours there was an apparent decrease in the rate of IPN production in both samples and this anomaly produced large deviations between the fitted and the predicted data points. A reasonable explanation for this is the appearance of a second peak on the HPLC traces after approximately 3 hour incubation; this unidentified peak increased in area until it was 5-10 % of the total area of the main IPN peak (results not shown). This unidentified second peak with a slightly longer retention time is probably a breakdown product of IPN. A hydrolysed penicillin, to give a penicilloic acid, would be expected to give shorter retention times on reverse phase columns (so the peak probably represents a different decomposition product).

The samples from the ACV turnover experiments were analysed by SDS-PAGE to check for IPNS modification or fragmentation. In the absence of catalase a fragmentation pattern similar to that observed under condition F was observed but in the presence of catalase the fragmentation was much reduced (results not shown). These results suggest that the presence of ACV makes very little difference to the fragmentation pattern of IPNS or the rate of fragmentation.

4.2.3 Ethylene production

Table 4.2 summaries the results of the studies to determine the ability of IPNS, DAOCS/DACS from *C. acremonium* (purified by Dr Charles Hensgens, O.C.M.S.) to convert ACC to ethylene. All measurements were performed in duplicate or triplicate and the differences obtained were less than ± 10%. The wild type recombinant ACCO from tomato fruit (cloned by Dr Z. Zhang, O.C.M.S.) was used as a positive control in the ethylene assays and gave an activity of 62,886 nl/mg enzyme in 2 hours under the optimised conditions (Table 4.2, condition 1). Initially, the relative rates of ethylene

production in wild-type IPNS, wild-type DAOCS/DACS and buffer (non-enzymatic) were compared under the assay condition 1. Small increases in the ethylene production were seen when using DAOCS/DACS (23 nl/mg) or IPNS (9 nl/mg) over background level with buffer alone (3.3 nl) under condition 1.

The omission of bicarbonate lowered the activity of ACCO by > 90% (condition 2, Table 4.2) in agreement with previous findings[69]. Under similar conditions the ethylene production of IPNS fell by only 50%.

The omission of ascorbate in the assay mix lowered ACCO activity > 90% (condition 3, Table 4.2) but under the same conditions (with the omission of ascorbate) the ethylene production of IPNS was not significantly affected. In contrast, the ethylene production of DAOCS/DACS appears to increase upon the omission of ascorbate. The replacement of ascorbate with α-KG (condition 4, Table 4.2) lowers the ethylene activity of DAOCS/DACS but does not affect the ethylene activity of IPNS.

The most significant drop in the activity for ACCO was observed by the omission of catalase in the assay buffer (condition 5, Table 4.2) in agreement with previous findings[69]. However the omission of catalase in the assay mix also led to significant production of non-enzymatic ethylene (buffer alone 16 nl) the level of which was higher than that detected under analysis conditions using IPNS or DAOCS/DACS.

Table 4.2 Comparison of different assay conditions on ethylene production in ACCO, IPNS and DAOCS/DACS. All assays were incubated at a temperature of 28 °C for 2 hours. Key: (+) addition, (-) no addition

[1] Asc: sodium ascorbate; Bic: ammonium bicarbonate; Cat: catalase; α-KG: α-ketoglutarate.

[2] values are means of *n* determinations, with *n* given in parentheses; *nd* not determined.

Assay Condition	Asc[1]	ACC	Fe(II)	Bic[1]	BSA	DTT	Cat[1]	α–KG[1]	WT IPNS (nl/mg)	DAOCS /DACS (nl/mg)	ACCO (nl/mg)	No enzyme (nl)
1	+	+	+	+	+	+	+	-	12 (5)[2]	26 (5)[2]	62686 (3)[2]	3 (3)[2]
2	+	+	+	-	+	+	+	-	7 (3)[2]	nd	4286 (2)[2]	5 (3)[2]
3	-	+	+	+	+	+	+	-	15 (4)[2]	76 (3)[2]	4416 (2)[2]	9 (4)[2]
4	-	+	+	+	+	+	+	+	10 (3)[2]	20, 28	nd	5 (4)[2]
5	+	+	+	+	+	+	-	-	12 (3)[2]	28 (3)[2]	323, 1600	16 (3)[2]
6	+	+	+	+	+	-	+	-	13 (3)[2]	nd	14900 (2)[2]	6 (3)[2]

Further ethylene assays were performed on IPNS mutants [C-terminus deletion mutants (G329, I325) that were active for IPN production and a double mutant (D216H/H214D) that was not active for IPN production]. Under conditions 1 and 2 small amounts of ethylene could be detected (4-9 nl/mg above that observed for buffer alone) in all three mutants tested, *i.e.* these mutants did not stimulate ethylene production any more than the wild-type IPNS (results not shown). Further assays for the non-enzymatic production of ethylene are given in Appendix D.

4.3 Discussion

4.3.1 Pre-incubation studies

All IPNS inactivation time courses could be fitted assuming first order or pseudo first order kinetic analysis, suggesting that concurrent first order pathways lead to inactive or low activity enzyme. The observed rates of inactivation of IPNS are dependent on the presence of particular combinations of cofactors (ferrous iron, oxygen), co-substrates (ascorbic acid, DTT) and catalase.

The results from the present study suggest that inactivation of IPNS, under the *in vitro* assay conditions, takes place *via* relatively slow non-oxidative and fast oxidative pathways. One oxidative inactivation pathway which occurs under Udenfriend's conditions (iron(II)/ascorbate/oxygen) results in the generation of hydrogen peroxide in solution and is (almost) totally prevented by the presence of catalase. A second oxidative inactivation pathway, the evidence for which is the least clearest of all three possibilities, probably results from an active site generated reactive species during catalysis and is not catalase protectable.

4.3.2 Non-oxidative inactivation

The operation of the slowest form of inactivation occurs in the absence of all cofactors and co-substrates. This slow form of inactivation was not prevented by the inclusion of BSA or catalase at 5 mg/ml or under aerobic or anaerobic conditions. Therefore this mode of inactivation probably does not involve oxidation. The failure to find a chemical agent that caused slow inactivation led to the proposal that the slow inactivation was caused by a conformational change. Hence at room temperature in assay buffer, purified active IPNS (conformer A) may undergo a conformational change leading to a partially active enzyme (conformer B). Similar findings and conclusions have been obtained with ACCO but the reported first order inactivation rates were *ca.* 6.5 times faster ($t_{1/2}$ = 1 hour[70]) when compared with IPNS ($t_{1/2}$ = 6.4 hour).

4.3.3 Oxidative inactivation

Catalase protectable

The observed rates of aerobic inactivation of IPNS and the observation that catalase offered total protection to iron/ascorbate mediated pre-incubation suggests the operation of a major inactivation process which occurs *via* the generation of peroxide in the pre-incubation mixture. Reaction of dioxygen, iron and ascorbate (Udenfriend's reagent) is known to generate reactive oxygen species, including hydrogen peroxide and hydroxyl radicals[109,112] which may produce non-specific damage to proteins. Since IPNS contains a metal binding site it seems likely that hydrogen peroxide is generated in solution and can preferentially bind to the IPNS active site and effect oxidative damage. The observation that full protection was obtained in the presence of catalase against

iron/ascorbate mediated inactivation and fragmentation also supports this proposal (see Chapter 5).

Unlike ACCO, IPNS does not require ascorbate as a co-substrate for catalysis. It is probable that the protective effects of ascorbate on IPNS activity as observed by several authors arises from its reducing property[129,130]. The primary role of ascorbate is apparently outside the active site, probably as an iron reductant (from ferric to ferrous) or as an iron(III) 'solubiliser'. It may also be involved in reducing inadvertently produced iron(III) or iron(IV) active site species. The use of a reducing agent which will fulfil the role of ascorbate, but which does not generate oxidising species in solution or complexed to iron, may be one way of increasing the *in vitro* half life of IPNS.

The iron/ascorbate mediated inactivation of IPNS was totally prevented by the inclusion of 8 μM catalase thus confirming that inactivation of IPNS under these conditions results from peroxide in solution. Total protection against iron/ascorbate mediated inactivation was also observed by the inclusion of at least 0.1 mM catalase, for example glutamine synthetase[135] propanediol oxidoreductase[136], pyruvate kinase[121], phosphoglycerate kinase and γ-butyrobetaine hydroxylase[137]. In contrast, catalase did not afford total protection against Udenfriend's mediated inactivation in the case of ACCO[70] or in the case of a non-redox enzyme creatine kinase[121]. Hence, *in vitro* IPNS assays employing incubation mixtures of iron(II)/ascorbate generates hydrogen peroxide in solution which causes inactivation of the enzyme. The use of catalase in the assay may be one way of reducing damage from peroxide and increasing *in vitro* activity.

The results from SDS-PAGE analysis show that no change in the fragmentation pattern of IPNS occurred in the presence of ACV, and therefore suggests that no major structural changes take place in the active site after substrate binding (see Chapter 5).

Summary

To summarise, the inactivation of IPNS results from a combination of at least two types of inactivation processes as shown in Figure 4.7. The inactivation processes are: (1) a non-oxidative (probably due to a conformational change) and (2) an oxidative reaction mediated *via* hydrogen peroxide (generated from Fenton's/Udenfriend's chemistry). The slowest type of inactivation may arise from correctly folded and a fully active IPNS (Figure 4.7, species A) undergoing partial unfolding/misfolding to give a less active form(s) (non-oxidative process). The catalase protectable hydrogen peroxide mediated oxidative inactivation is relatively a faster process. Hydrogen peroxide generated in solution may bind to the IPNS-Fe(II) complex (Figure 4.7, species B) at the active site leading to damage and fragmentation.

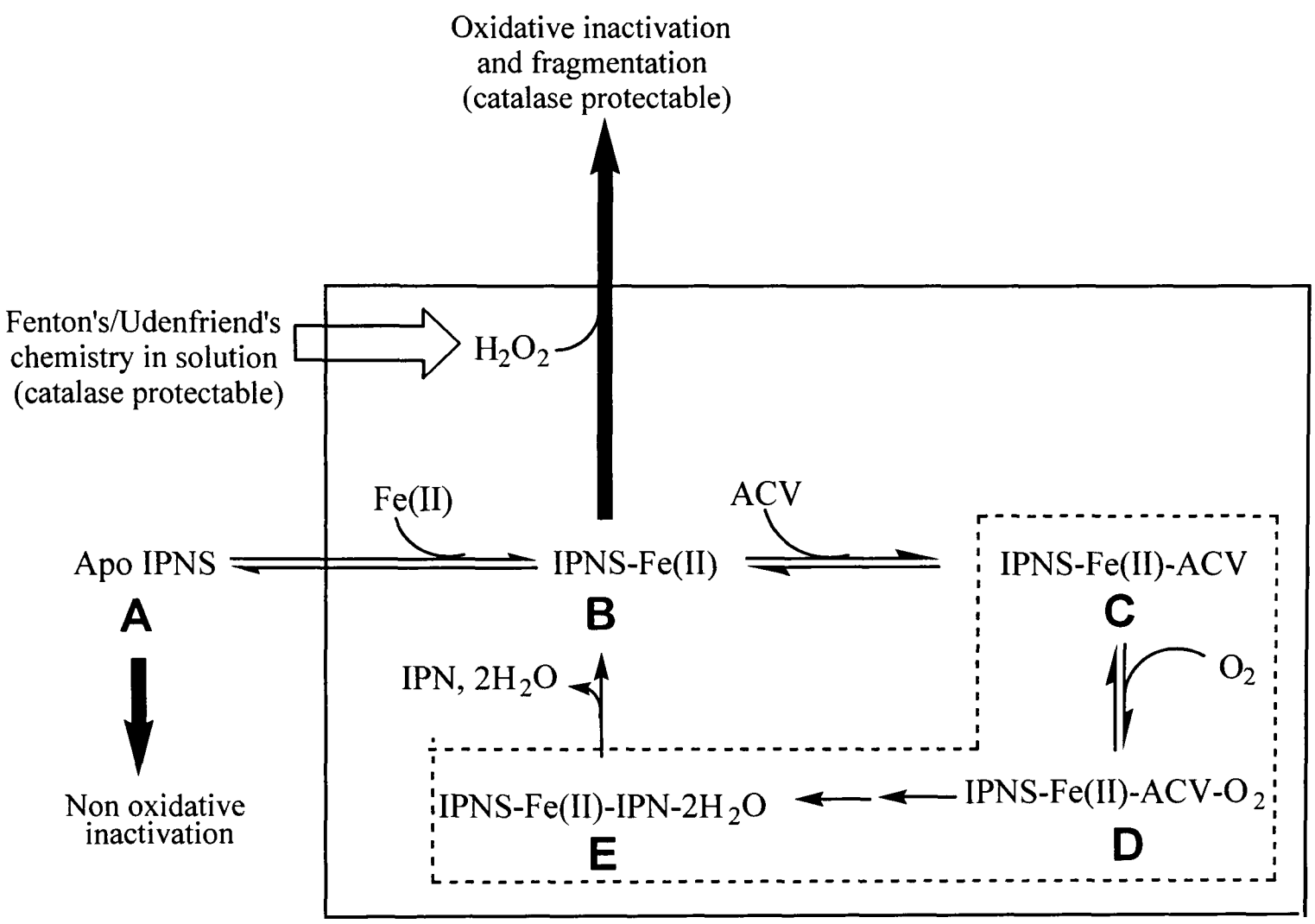

Figure 4.7 Summary of the catalytic cycle and inactivation of IPNS. Area enclosed by dashed line shows the 'catalytic' cycle after ACV is bound.

The evidence for ACV dependent IPNS inactivation is the least clear of all the processes. In the current IPNS mechanism[52] the dioxygen binds to the ternary IPNS-Fe(II)-ACV complex which leads to several intermediates in the catalytic cycle (Figure 4.7 species C, D and E). One or more of these may react inadvertently leading to inactivation which is not catalase protectable.

4.3.4 Ethylene production assays

The observed rates of ethylene production from ACC for IPNS and DAOCS/DACS were 3 to 4 orders of magnitude lower than those observed for the reference enzyme, ACCO. The observed stoichiometry of substrate turnover for ACCO of 1.0 x 10^2 mol ethylene/ mol enzyme in 2 hours was in agreement with previously reported values[69]. The results show small levels of stimulated ethylene production in the presence of IPNS (stoichiometry of substrate turnover of *ca.*1.9 x 10^{-2} mol ethylene/ mol enzyme in 2 hours) and DAOCS/DACS (stoichiometry of substrate turnover of *ca.* 4.1 x 10^{-2} mol ethylene/ mol enzyme in 2 hours) under appropriate conditions. It is difficult to say whether this arises from (a) enzymatic binding and turnover of ACC, or (b) non-enzymatic production *via* reactive intermediates (*e.g.* hydrogen peroxide) generated in the solution or at the enzyme's active site. The observation that the production of ethylene in buffer alone was significantly increased in the absence of catalase suggests that significant hydrogen peroxide can be generated in solution which converts ACC into ethylene[138]. If hydrogen peroxide was generated in solution in incubations with IPNS or DAOCS/DACS (*via* Udenfriend's/Fenton's chemistry) then it would be quickly removed by the presence of catalase. However, if a reactive intermediate (*e.g.* ferryl oxene) is generated in the active sites of either IPNS or DAOCS/DACS in the presence of ACC then ethylene may be produced enzymatically. Based on the observation that catalase did not affect the level of ethylene production by DAOCS/DACS or IPNS in the present study, it is proposed that the production of ethylene in these enzymes arises from reactive species generated at the active site. In ACCO, which was used as a control in the present study, the enzymatic ACC turnover was increased in the presence of catalase in agreement with previous studies[69]; the lower activity reported in the absence of catalase

was proposed to arise from oxidative damage. The interpretation (and accuracy) of this data is complicated by a number of factors: (1) significant levels of ethylene were detected under the modified assay conditions in buffer alone suggesting the operation of significant non-enzymatic catalysis; (2) inactivation of IPNS and DAOCS/DACS *via* Fenton's/Udenfriend's type reaction; (3) the non-enzymatic consumption of oxygen; (4) the low levels of ethylene production. However the preliminary results are intriguing and merit brief discussion.

Effects of ascorbate

It has been claimed that the conversion of ACC to ethylene is stoichiometric with the conversion of ascorbate to dehydroascorbate[65]. The proposed reaction mechanism for ACCO suggests that both ascorbate and oxygen bind and react to give a ternary ACCO-Fe(IV)=O-dehydroascorbate complex[66]. Whether or not this mechanism is correct (see below) ascorbate has been found to greatly stimulate ACCO turnover of ACC. The findings that the omission of ascorbate in the incubation mix did not affect ethylene production in IPNS suggests that this mechanism does not operate in the case of IPNS stimulated conversion of ACC to ethylene.

Surprisingly, the omission of ascorbate in the incubation mix increased the ethylene production of DAOCS/DACS to 0.12 mol ethylene /mol enzyme in 2 hours. Furthermore, the addition of α-KG inhibited the apparent DAOCS/DACS production of ethylene from ACC. One possibility is that ascorbate and α-KG may compete with ACC for the DAOCS/DACS active site. These results suggest that the DAOCS/DACS catalysed stimulation of ethylene is likely to be active site mediated. If this is true then it implies that neither ascorbate nor α-KG is required for ethylene production by

DAOCS/DACS. The findings that the catalytic turnover for ACCO was decreased but substantially above background levels of 6.4 mol ethylene/ mol enzyme in 2 hours, by the omission of ascorbate from the incubation mix, suggests the possibility of another or more than one mechanism. This observation combined with the evidence from IPNS and DAOCS/DACS ethylene assays suggests that ascorbate is not involved in the catalytic turnover. This raises the possibility for the following sequence of events as shown in Scheme 4.6.

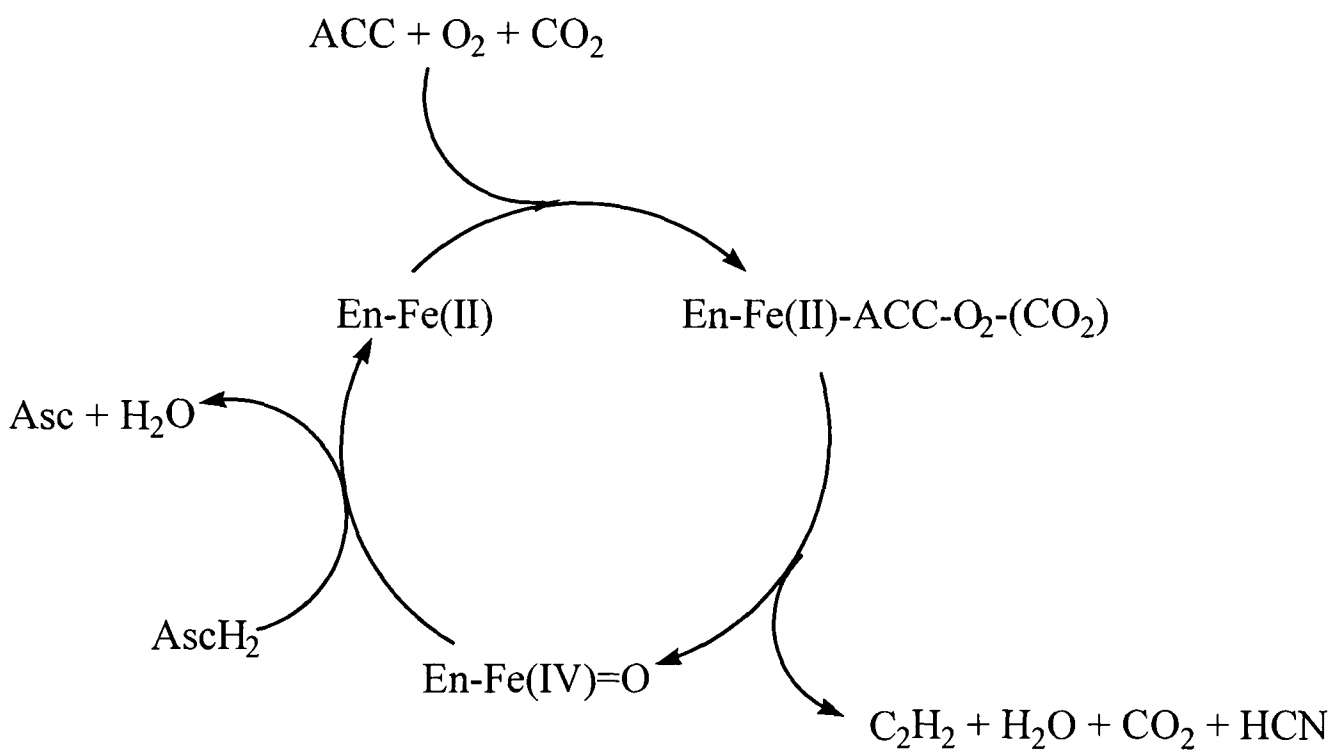

Scheme 4.6 Possible role of ascorbate in the catalytic cycle of ACC turnover by ACCO. Although ascorbate is shown as the reducing agent, this is unlikely for DAOCS/DACS since ascorbate inhibits ACC turnover. Note also the level of ACC turnover with respect to DAOCS/DACS was less than stoichiometric.

In Scheme 4.6, which may apply to ACCO as well as DAOCS/DACS, the ACC is oxidised before binding of the reducing agent, *i.e.* it implies that α-KG is replaced by ACC rather than ascorbate in the case of ACCO catalysis. Although contrary to previous

proposals there is little direct evidence to rule out this possibility [however, kinetic analysis indicate that the predominant kinetic mechanism for tomato ACCO, proceeds *via* the sequential formation of Fe(II)-ACC-ascorbate complex to which dioxygen binds[139]]. This proposal is also attractive in that the role of ascorbate in reducing an Fe(IV) species in the oxidation of ACC to ethylene by ACCO is analogous to that of its proposed role in the uncoupled turnover of α-KG. It is well known that ACCO cannot use α-KG in place of *L*-ascorbic acid and in fact studies have shown that competitive inhibition of ethylene production by ACCO occurs with α-KG[140].

In the case of DAOCS/DACS catalysed conversion of ACC to ethylene, the nature of the reducing agent (if any) returning the putative Fe(IV) species back to the Fe(II) level is unclear. The present results show that less than a stoichiometric level of ethylene is produced with respect to enzyme (0.12 mol /mol enzyme). Thus DAOC/DAC stimulated conversion of ACC to ethylene therefore arises from a single turnover event.

Based upon the sequence similarity and the conservation of metal binding ligands (His-X-Asp-X-His) and the carboxylate binding motif (Arg-X-Ser) a binding site for ACC in the IPNS, DAOCS/DACS and ACCO active sites can be proposed (Scheme 4.7, A-C). The Arg-X-Ser motif forms part of the conserved residues in IPNS (also conserved in DAOCS/DACS and ACCO) and binds the valine carboxylate of the ACV during catalysis[52]. The CO_2 activator is shown as a bicarbonate ion ligating to the iron opposite His270 in a position analogous to the ACV-SH.

It is interesting to note that *D*-valine, rather than *L*-valine, was oxidised (albeit very inefficiently) into *iso*-butanal by ACCO[139]. By analogy with IPNS the replacement of the *D*-valine of ACV with the *L*-valine, to give the tripeptide *L,L,L*-ACV, failed to give

enzymatic turnover[141]. These results seem to indicate the conservation of the *D*-valine binding pocket in the active sites of IPNS and ACCO.

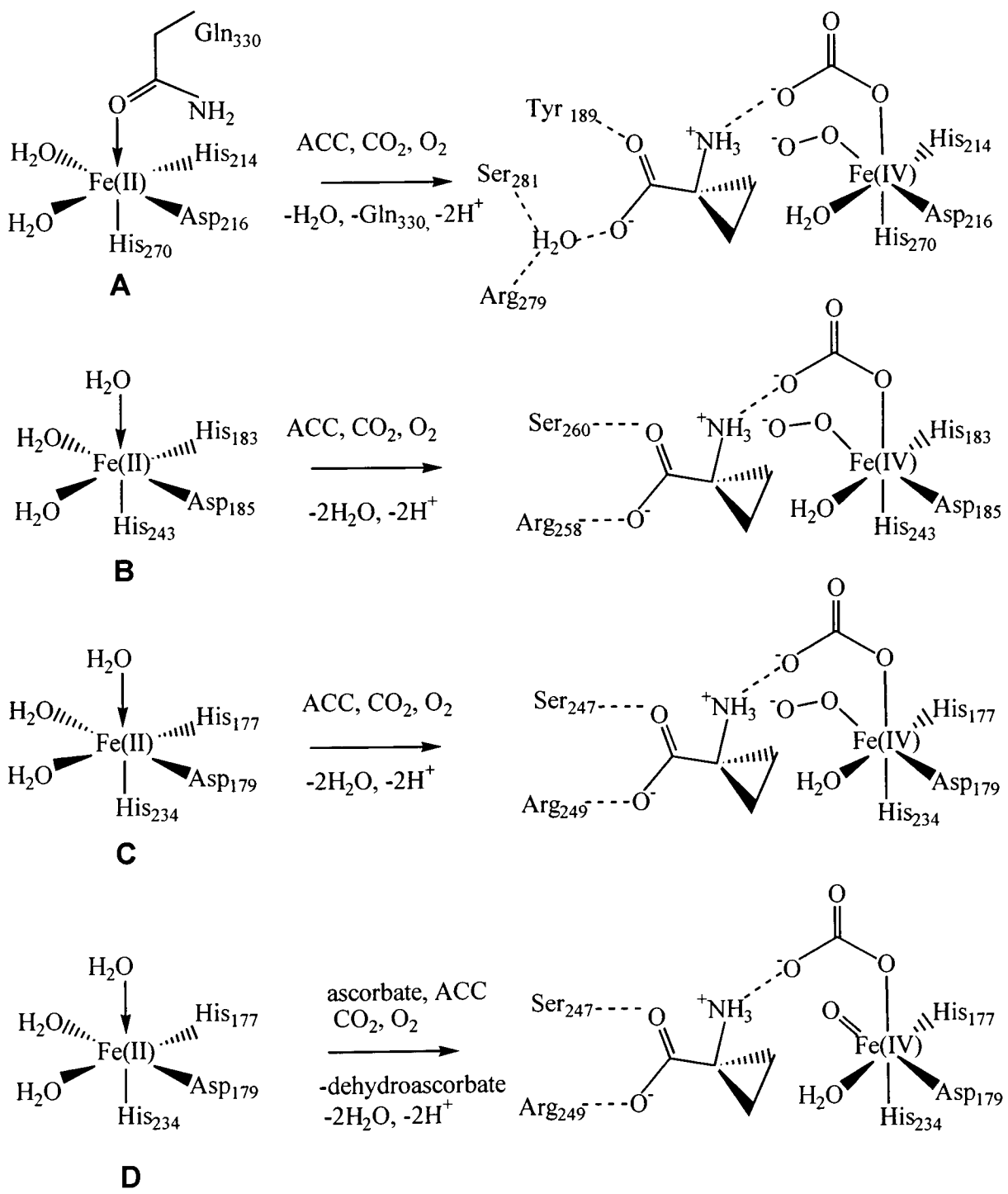

Scheme 4.7 Possible modes of ACC binding in IPNS (A), DAOCS/DACS (B) and ACCO (C). The intermediate for the previously proposed mechanism for ACCO[66] is given in (D). Note in (C) and (D) the ascorbate may be ligated to the iron instead of the water molecule. The possibility that ascorbate or another reducing agent (particularly in the case of ACCO) which binds to the RXS motif cannot be excluded.

Three postulated mechanisms of ethylene formation by ACCO are shown in Scheme 4.8. Ethylene formation *via* a radical type mechanism is shown by pathway a[66].

Alternatively, carbon dioxide and dioxygen can bind to the iron and form a superoxide intermediate (species II). Deprotonation of the amine nitrogen of ACC then forms a hydroperoxide intermediate on the iron atom (species III or V). In pathway b, species III breaks down to a give a hydroxyl radical which can deprotonate a second amine nitrogen of ACC to give a nitrene product (species IV). Alternatively, the radical intermediate (species V) rearranges *via* pathway c to give a second radical intermediate (species VI). The hydroxyl radical can deprotonate the amine nitrogen (in species VI) to give the nitrene intermediate (species IV) which leads to the products (species VII). In pathways b and c the dehydroascorbate is used to reduce the ferryl iron back down to the ferrous state.

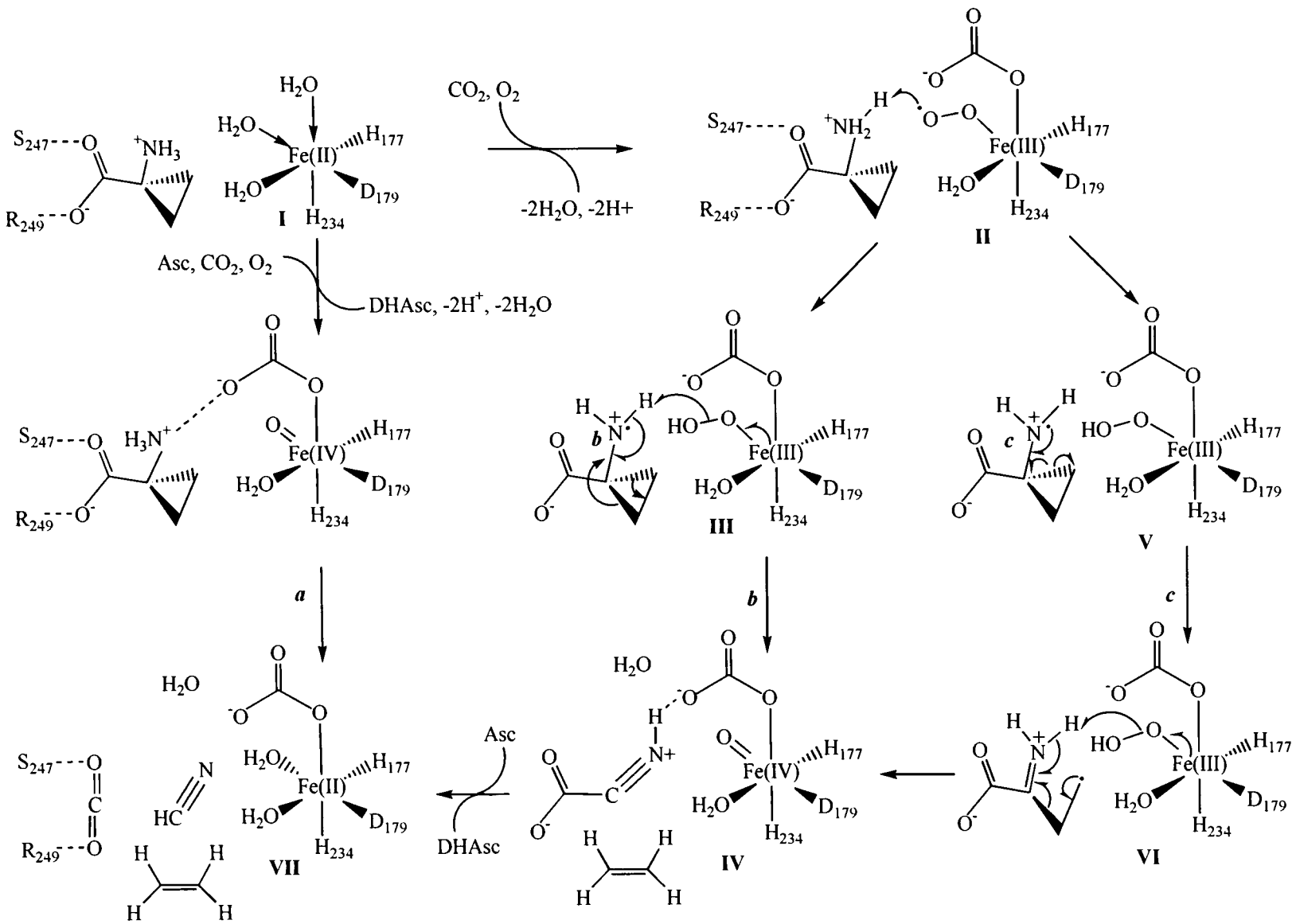

Scheme 4.8. Three different pathways for the conversion of ACC to ethylene by ACCO. Pathway *a* has been previously proposed[66]. [1] Asc = ascorbate; DHAsc = dehydroascorbate. Note although ACC binding is shown as the first step in this scheme, the order of substrate and cofactor binding is unknown[139].

[1] Labelling experiments indicate a radical type mechanism

CHAPTER 5

Structural Analysis of Inactivated IPNS

5.1 Introduction

The results from Chapter 4 suggested, although did not unequivocally demonstrate, that oxidative inactivation takes place at the active site of IPNS. In this Chapter the structural changes, rather than catalytic activity, under different incubation conditions are compared with respect to time. It was anticipated that the type of structural change occurring may depend upon the components present in the incubation mix.

The most striking observation from the SDS-PAGE analysis in Chapter 4 was that oxidative damage of IPNS was accompanied by a cumulative fragmentation. One aim of the present study was to identify the site of oxidative damage in IPNS. This information could be useful in determining which active site residues are most susceptible to oxidative damage. Another aim of this study was to correlate the information obtained from mapping with that from the recently obtained crystal structure[52].

Various combinations of Fe/ascorbate or Fe/EDTA incubation mixtures have previously been used to map active sites residues of metal binding proteins for which no crystal structures exist[113,142,143]. In most of these studies the active site residues were identified after N-terminal sequencing and sometimes in combination with information from mass spectra of the resulting peptides. In the case of ACCO, the identified oxidative modifications were restricted to the vicinity of the putative metal binding ligands[66].

In the case of glutamine, synthetase the Fe/ascorbate system involved the selective conversion of the metal binding His269 to an asparagine and Arg344 to a glutamic

semialdeyde derivative[144,145]; both these residues are situated at one of the two manganese binding sites on the enzyme. Fragmentation studies showed that protein cleavage was not the major cause of inactivation and the slow fragmentation of the enzyme (incomplete after *ca.* 14 hours) was preceded by a faster inactivation process (activity lost after 1 hour)[135,146].

5.1.1 Strategy for analysis

Preliminary structural characterisation of inactivated IPNS was performed by SDS-PAGE analysis using Tris-glycine gels[147]. This technique involves the migration of charged proteins through a matrix of acrylamide under the influence of an electric field. As SDS complexes with proteins in a fixed ratio of approximately 1.4:1, SDS-PAGE separation is based predominantly on differences in size. The separation of proteins with masses lower than 10 kDa cannot be achieved with Tris-glycine gels because small proteins do not stack in the separating gel. This causes streaking of small proteins if increased acrylamide concentrations are used in the separating gel. The use of tricine as the tracking ion improves the resolution of smaller proteins between 5-20 kDa without resorting to the use of urea[148]. Using this technique it is possible to obtain the approximate size (and molecular weight) of any small oligopeptides that might arise from fragmentation of IPNS. This simple technique can also be used to compare the fragmentation patterns of recombinant wild-type IPNS, IPNS mutants (D216E, I325, H270E), DAOCS (*Streptomyces clavuligerus*) and CAS (*Streptomyces clavuligerus*).

It was hoped that the N-terminal sequences of SDS-PAGE separated fragments would provide information on the location of the cleavage sites in IPNS. For this the proteins from the SDS-PAGE gels had to be blotted onto a polyvinylidene difluoride (PVDF)

membrane (Immobilon). The oligopeptides were submitted for either N-Terminal sequencing or complete amino acid analysis. It was anticipated that a direct comparison of the amino acid analyses of oxidatively modified IPNS and unmodified IPNS would reveal amino acids that were preferentially degraded.

Electrospray ionisation mass spectrometric (ESIMS) analysis of IPNS was attempted to measure the changes in the mass before and after oxidative modification. Purification of the IPNS polypeptide fragments was attempted in order to obtain accurate masses by ESIMS. These masses would provide useful verification of the sequencing results.

5.2 Results

5.2.1 SDS-PAGE analysis of IPNS

IPNS purified by a three column purification procedure as described in the experimental section (Chapter 6.2) was homogeneous (> 95% pure by SDS-PAGE analysis). At least four bands of lower molecular weight were observed by SDS-PAGE, with masses of 30 kDa (a), 24 kDa (b), 20 kDa (c), 17 kDa (d), (Figure 5.1a, lane 2) from a typical incubation under condition A [1 mM ACV, 2 mM DTT, 1 mM sodium ascorbate, 0.1 mM Fe(II)]. Proteolytic cleavage by a contaminating protease was excluded by the observation that no fragmentation appeared in buffer alone (Figure 5.1a, lane 1).

Anaerobic incubations (inside a glove box with < 0.4 ppm oxygen) of IPNS under condition M (Figure 5.1a, lanes 3-4) or condition A (lanes 5-6) produced very little fragmentation demonstrating that IPNS fragmentation involved an oxidative process.

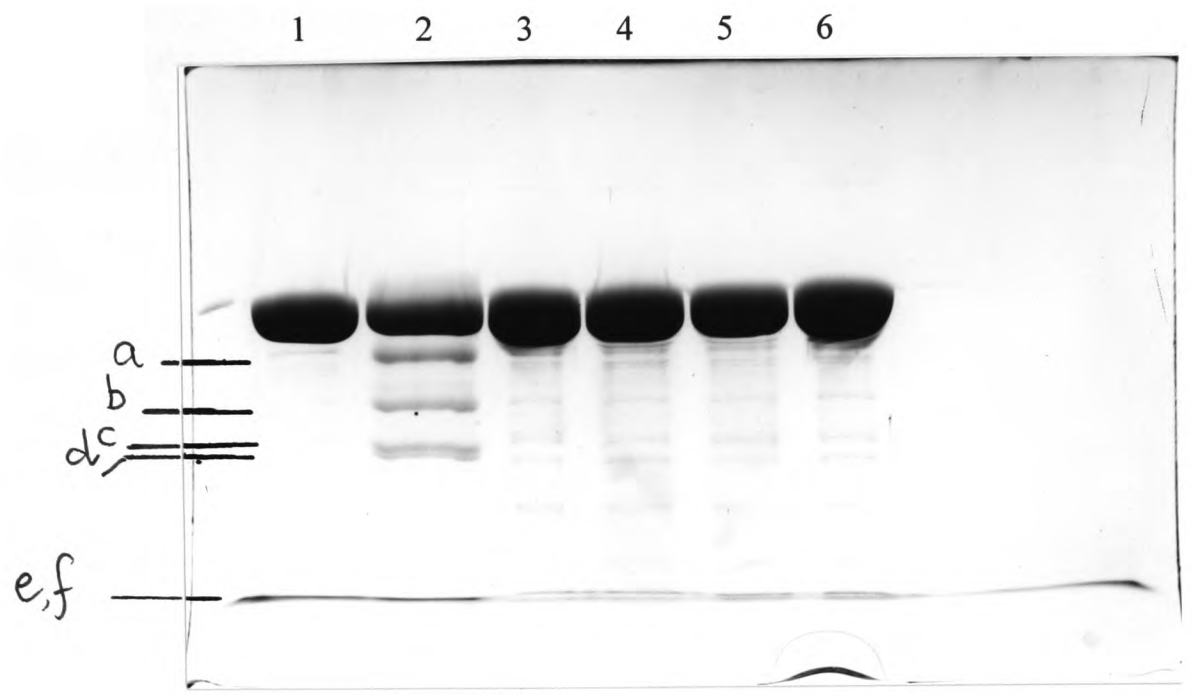

Figure 5.1a SDS-PAGE analysis of aerobic and anaerobic incubations under bioassay conditions. Lanes from left to right show: (1) condition M aerobic 90 minutes; (2) condition A, aerobic 90 minutes; (3) condition M, anaerobic 3 hours; (4) as (3), 72 hours; (5) condition A, anaerobic 3 hours; (6) as (5) 72 hours. All incubations were performed at 28 °C.

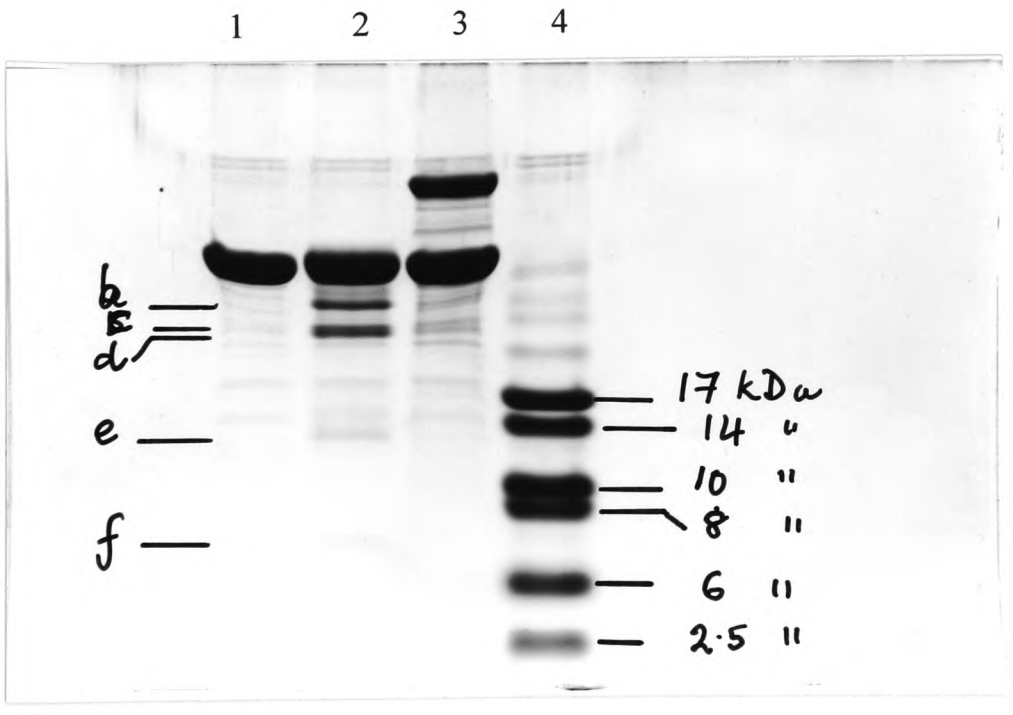

Figure 5.1b Analysis of IPNS fragmentation by Tris-tricine SDS-PAGE. Lanes show: (1) condition M; (2) condition A; (3) condition L; (4) molecular weight markers. All incubations were performed at 28 °C for 90 minutes.

IPNS samples incubated under condition A were reanalysed on Tris-tricine gels to resolve low molecular weight components which migrated very close to the tracking dye (see Appendix B). Two additional oligopeptides, of masses 13 kDa (e) and 7 kDa (f), were observed under condition A in addition to the previous four noted above (Figure 5.1b, lane 2). Therefore a total of six oligopeptides were present, indicating that cleavage had occurred minimally at three sites. The estimated extent of fragmentation was less than 10% of the intact protein. The inclusion of catalase in the incubation (condition L) significantly slowed the rate of fragmentation and only minor contamination with lower molecular weight components was visible (Figure 5.1b, lane 3). Since the degree of fragmentation was found to be cumulative with respect to time and also dependent upon the components of the incubation mix, modifications were made to the previous incubation conditions to enhance the fragmentation rate.

Effects of hydrogen peroxide

In order to see whether a particular component in condition A (all substrates and cofactors) was required for fragmentation to occur, incubations were performed with a single component absent. The samples were analysed by Tris-glycine SDS-PAGE (Figure 5.2a) and the results are summarised in Table 5.1. The use of DTT alone, ascorbate alone, or DTT in combination with ascorbate produced no fragmentation (lanes 4-6). $FeSO_4$ with either DTT, or ascorbate, or ascorbate and DTT produced fragmentation (lanes 7-9). The fragmentation was only observed when $FeSO_4$ was used in combination with a reducing agent, and was partially catalase protectable.

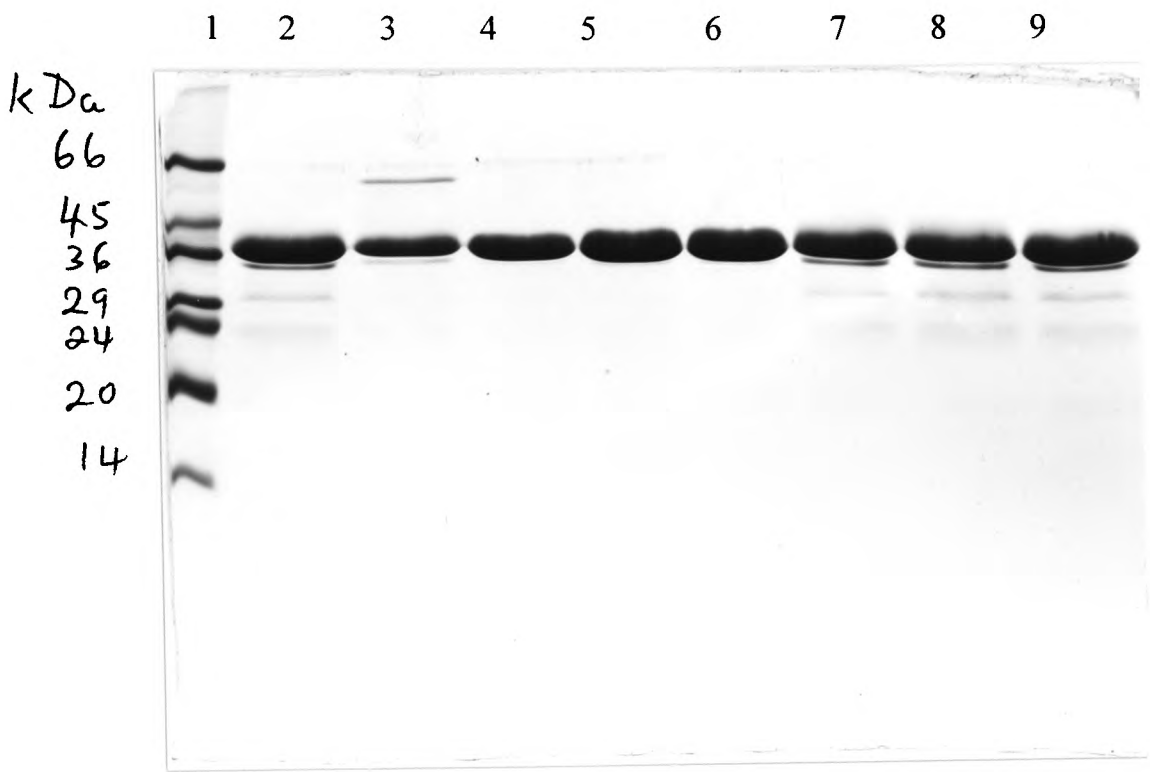

Figure 5.2a SDS-PAGE analysis of inactivated IPNS. Lanes from left to right show: (1) molecular weight markers; IPNS from: (2) condition A, no catalase; (3) condition A, with catalase; (4) DTT (4mM); (5) ascorbate (1.3 mM), DTT (4mM); (6) ascorbate (0.13 mM), DTT (4mM); (7) Fe(II)SO_4 (0.1mM), DTT (4mM); (8) Fe(II)SO_4 (0.1mM), ascorbate (1.3 mM), DTT (4mM); (9) Fe(II)SO_4 (0.1mM), ascorbate (0.13 mM), DTT (4mM). All incubations were performed at 28 °C for 90 min.

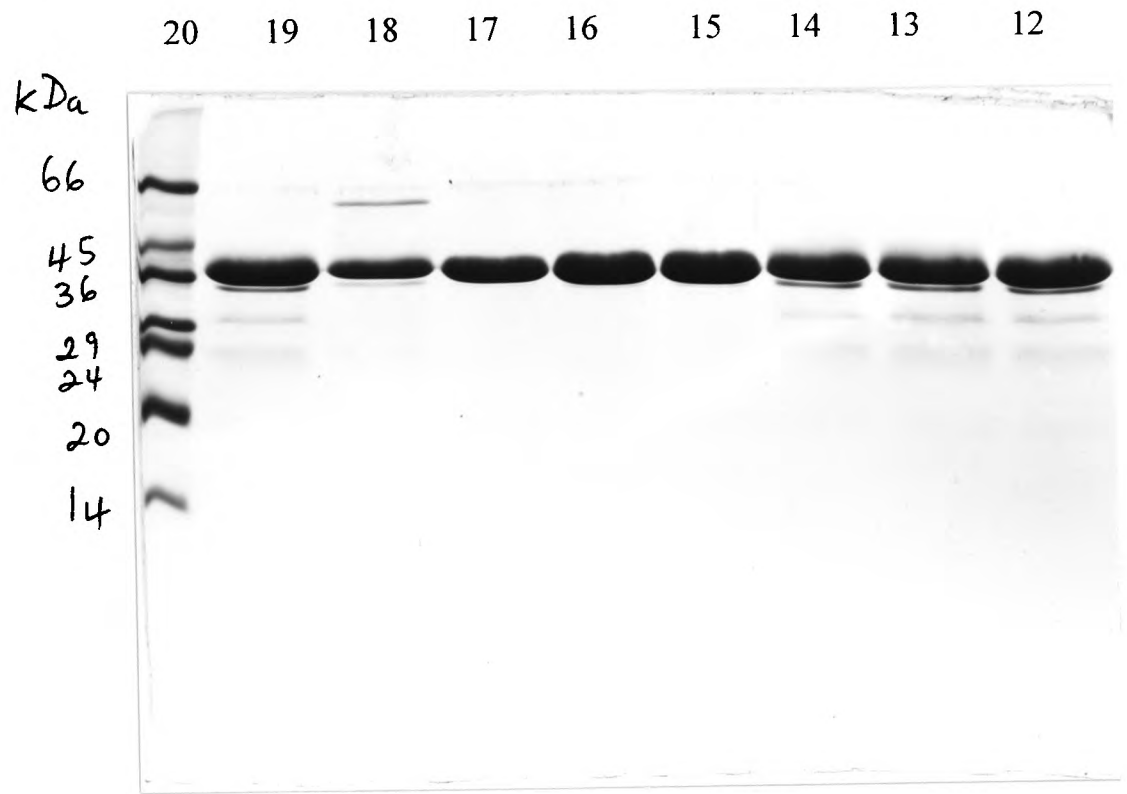

Figure 5.2b SDS-PAGE analysis of the effects of hydrogen peroxide on the fragmentation of IPNS. Lanes (12) and (13) as lanes (2) and (3). The incubation conditions for lanes (14)-(19) are identical to those for lanes (4)-(9) in Figure 5.1a except that hydrogen peroxide (0.5 % v/v) was added to the cofactors before incubation; (20) molecular weight markers.

To demonstrate that H_2O_2 was the reactive species involved in the present studies, fragmentation studies were repeated in the presence of H_2O_2 and the appropriate cofactor solution, prior to the addition of protein. H_2O_2 in the absence of iron (II), in combination with DTT, or ascorbate, or DTT and ascorbate, produced no fragmentation but gave rise to a high molecular weight component (Figure 5.2b, lanes 14-16). The identity of this high molecular weight component was not investigated further. Sometimes faint low molecular weight components were observed, particularly with impure batches of ascorbate. Enhanced levels of fragmentation were observed in the presence of H_2O_2 and $FeSO_4$ with all cofactor variations (Figure 5.2b, lanes 17-19). Hence these studies imply that Fe(II) in combination with a reducing equivalent (such as DTT or ascorbate) are required for fragmentation to occur [the role of the reducing agent may be simply to maintain a sufficiently high concentration of a particular form of iron].

Table 5.1 Effects of hydrogen peroxide on the fragmentation of wild-type IPNS.

	Fragmentation	
Incubation condition	without H_2O_2	with 0.5 % (v/v) H_2O_2
condition E	*no*	*no* [*#]
condition E + Asc (1.3 mM)	*no*	*no* [*#]
condition E + Asc (0.13 mM)	*no*	*no* [*#]
condition D	*yes*	*yes* [*‡]
condition B	*yes*	*yes* [*‡]
condition D + Asc (0.13 mM)	*yes*	*yes* [*‡]
condition A	*yes*	*yes*[‡]
condition L	*no*[#]	nd

[*]High molecular weight components observed.

[#]Only minor fragments visible.

[‡] Smearing.

nd = not determined.

Fragmentation rates

Figure 5.3 shows the fragmentation rates under aerobic conditions employing Fe(II), ascorbate and H_2O_2[149], Fe(II) and ascorbate[109], and Fe(II) and H_2O_2 (Fenton). Under Ettener's and Fenton's conditions the fragmentation was observable after a very short period (< 30s) compared with Udenfriend's conditions when fragmentation was only observed after 10 minutes (results not shown).

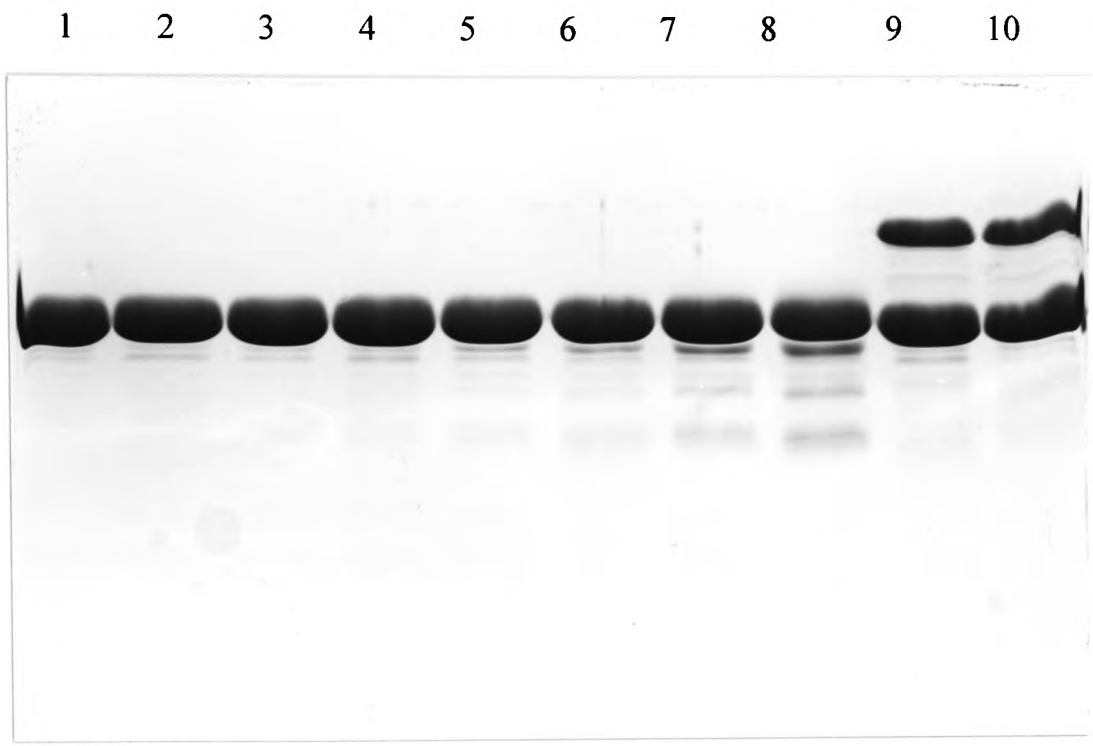

Figure 5.3 SDS-PAGE analysis of time dependent fragmentation of IPNS under Udenfriend's conditions (Fe(II)/ascorbate). Lanes (from left to right) show: (1) conditions M, 10 min; (2) as (1) after 90 min; (3) SDS sample buffer added before incubation under condition F, 10 min; (4) as (3) after 90 min; (5) condition F, 12 min; (6) as (5) after 24 min; (7) as (5) after 48 min; (8) as (5) after 90 min; (9) condition G, 10 min; (10) as (9) after 90 min. All incubations were performed at 28 °C.

No fragmentation was observed when SDS-PAGE sample buffer was added immediately prior to addition of cofactors in condition F (Figure 5.3 lanes 3 and 4). This suggests that correctly folded enzyme is required for fragmentation. Under condition F, the fragmentation rate was slow and varied from no fragmentation at 12 minutes (lane 5) to intense fragmentation after 90 minutes (lane 8). In contrast, the fragmentation of ACCO appeared to be complete after 5 minutes incubation under similar conditions.

Variation in the concentrations of Fe(II) and ascorbate in the incubation mix showed that the intensity of fragmentation was affected by the concentrations of both Fe(II) and ascorbate. Most fragmentation was observed with conditions employing 0.4 mM Fe(II) and 2.5 mM ascorbate (results not shown). It is interesting that the intensities of

fragmentation observed after 90 minutes under condition F [0.4 mM Fe(II), 2.5 mM ascorbate] and under condition A [1 mM ACV, 2 mM DTT, 1 mM Asc, 0.1 mM Fe(II)] were identical within experimental error.

5.2.2 SDS-PAGE analysis of IPNS and related enzymes

DAOCS from *S. clavuligerus* was purified (following the protocol given in reference[60]) and tested for fragmentation. Under condition F, or condition B, fragmentation of DAOCS gave at least four oligopeptides with the following molecular masses: *a* (~29 kDa), *b* (~27kDa), *c* (~22kDa), *d* (~12 kDa) (Figure 5.4 lane 3). Two additional fragments *e* (~7kDa) and *f* (~5kDa) were visible on a Tris-tricine gel giving six oligopeptides altogether (not shown). Under Fenton's conditions [Fe(II) + H_2O_2] the DAOCS appeared to form a higher molecular weight component and very little unmodified protein remained (lane 5). The fragmentation pattern for DAOCS under condition F was different to that observed for IPNS. Table 5.2 summaries the results from fragmentation the present studies on DAOCS, and IPNS and from previous studies on CAS[150] and ACCO[70].

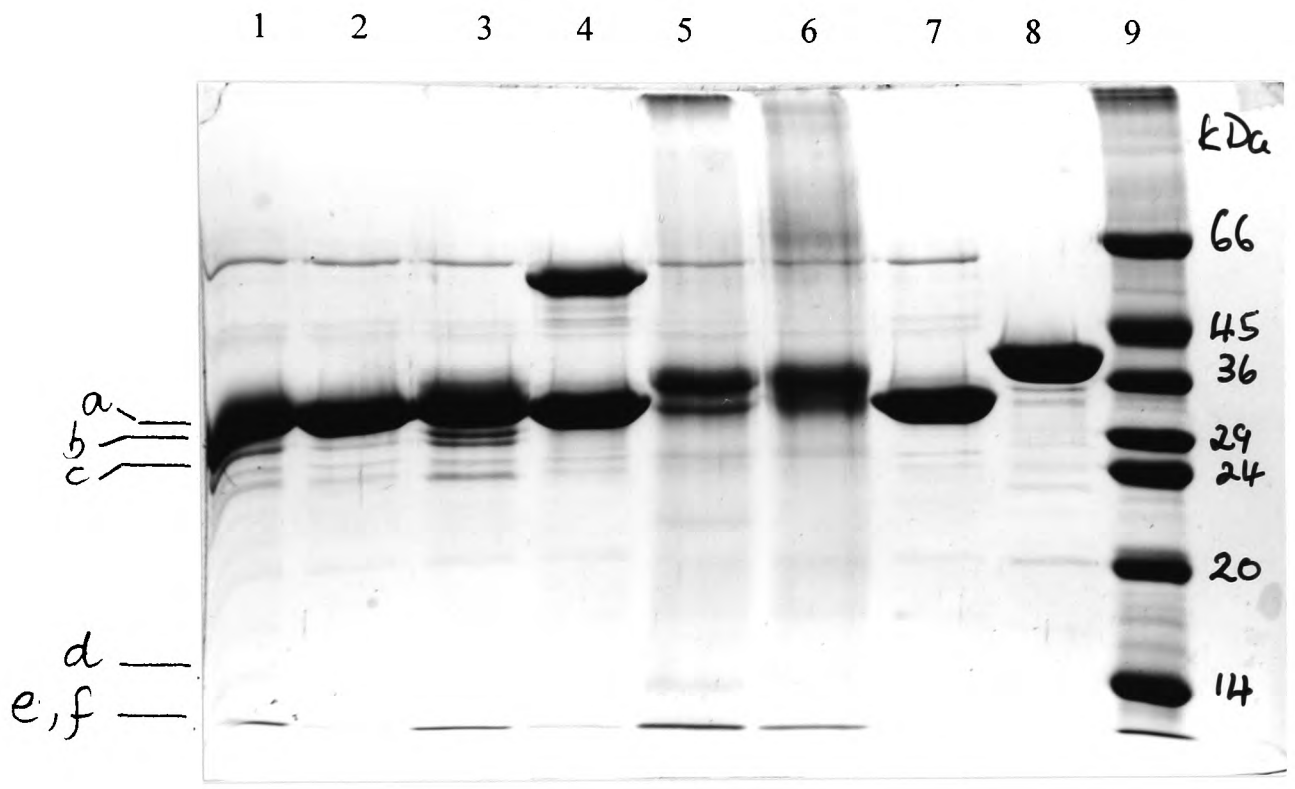

Figure 5.4 Analysis of fragmentation of DAOCS by SDS-PAGE. Lanes from left to right show: (1) $Fe(II)SO_4$ (2 mM), ascorbate (5 mM), DTT (2 mM); (2) $Fe(II)SO_4$ (2 mM), α-KG (2 mM); (3) $Fe(II)SO_4$ (2 mM), ascorbate (5 mM); (4) as (3) with catalase (0.5 mg/ml); (5) $Fe(II)SO_4$ (2 mM), H_2O_2 (0.06% v/v); (6) as (5) with EDTA (5 mM); (7) condition M; (8) wild-type IPNS under condition M; (9) molecular weight markers.

Table 5.2 Comparison of fragmentation results using IPNS, DAOCS, CAS and ACCO.

Incubation condition	wild-type IPNS	DAOCS	CAS	ACCO
Assay*	yes	yes	yes	yes
Assay*+	partial	nd	nd	yes
B	yes	yes	nd	nd
C	no	nd	nd	nd
D	yes	nd	nd	nd
E	no	nd	nd	nd
F	yes	yes	yes	yes
G	no	no	no	yes
H	no	no	no	yes
I	yes	nd	nd	nd
J	yes	yes	yes	yes
K	no	partial	nd	nd
M	no	no	no	no
N#	nd	yes	partial	nd

* Incubation conditions used for substrate turnover are described for measuring activity in the appropriate references: IPNS (condition A), DAOCS[60], CAS[150], ACCO[70].

+ Condition A with catalase (0.5 mg/ml).

Incubation conditions for uncoupled turnover: DAOCS , $FeSO_4$ (2 mM), α-KG (2 mM); CAS, Fe(II)SO_4 (0.4 mM), α-KG (2 mM).

nd: Not determined.

5.2.3 N-Terminal sequencing

Fragments of wild-type IPNS (generated using condition A) and DAOCS (generated using condition F) were separated by Tris-glycine or Tris-tricine SDS-PAGE, transferred to a PVDF membrane by electrophoretic transfer and analysed by Edman degradation (by Mr A. C. Willis of O.C.M.S.). Table 5.3 lists the N-terminal sequences obtained from wild-type IPNS and DAOCS.

Table 5.3 N-terminal sequencing of IPNS and DAOCS fragments.

Fragment	*ca* Mass (kDa)	N-terminal sequence
IPNS *a*	30	GSVSKANV
IPNS *b*	24	GSVSKANV
IPNS *c*	20	GSVSKANV
IPNS *d*	17	nd
IPNS *e*	13	VSLITVLY; *VSLITV*[a]
IPNS *f*	7	KWVNAERQ
DAOCS *a*	29	nd
DAOCS *b*	27	nd
DAOCS *c*	22	nd
DAOCS *d*	12	nd
DAOCS *e*	7	AAPRRDQIAG
DAOCS *f*	5	FFLRPN

[a]Sequence obtained by Barlow, 1996[151]; nd not determined.

For IPNS, fragments *a, b, c, d* gave sequences which corresponded to the N-terminus of intact IPNS. Fragments *d* and *e* possessed an N-terminus which corresponded to an internal sequence of the intact IPNS. Thus fragment *d* corresponded to a cleavage between Asp216 and Val217 and fragment *e* corresponded to a cleavage between Val272

and Lys273. These results support previous observations of Barlow[151], who observed a cleavage between Asp216 and Val217 for a 13 kDa fragment in IPNS.

In the analysis of DAOCS fragments only fragments *e* and *f* were sequenced since it was postulated (based on the IPNS sequences) that they would yield the most useful information. Thus fragment *e* corresponded to a cleavage point between Val245 and Ala246 and fragment *f* corresponded to a cleavage point between Val262 and Phe263. The remaining peptides were submitted for N-terminal sequencing but no data has been obtained to date.

Analysis of IPNS mutants

The fragmentation pattern of IPNS appears to be identical under inactivation condition F (iron/ascorbate) and assay condition A (iron/ascorbate/ACV/DTT). Mutation studies were made in the earlier part of this study to determine which iron binding ligands were important for IPNS activity [*vide supra* (Chapters 2 and 3)]. It was decided to use these IPNS mutants for fragmentation studies since the variation in the sequence may also produce differences in fragmentation. SDS-PAGE studies of wild-type and mutant IPNS enzymes (I325, D216E, H270E) were carried out to compare their fragmentation patterns (Figure 5.5, Table 5.4).

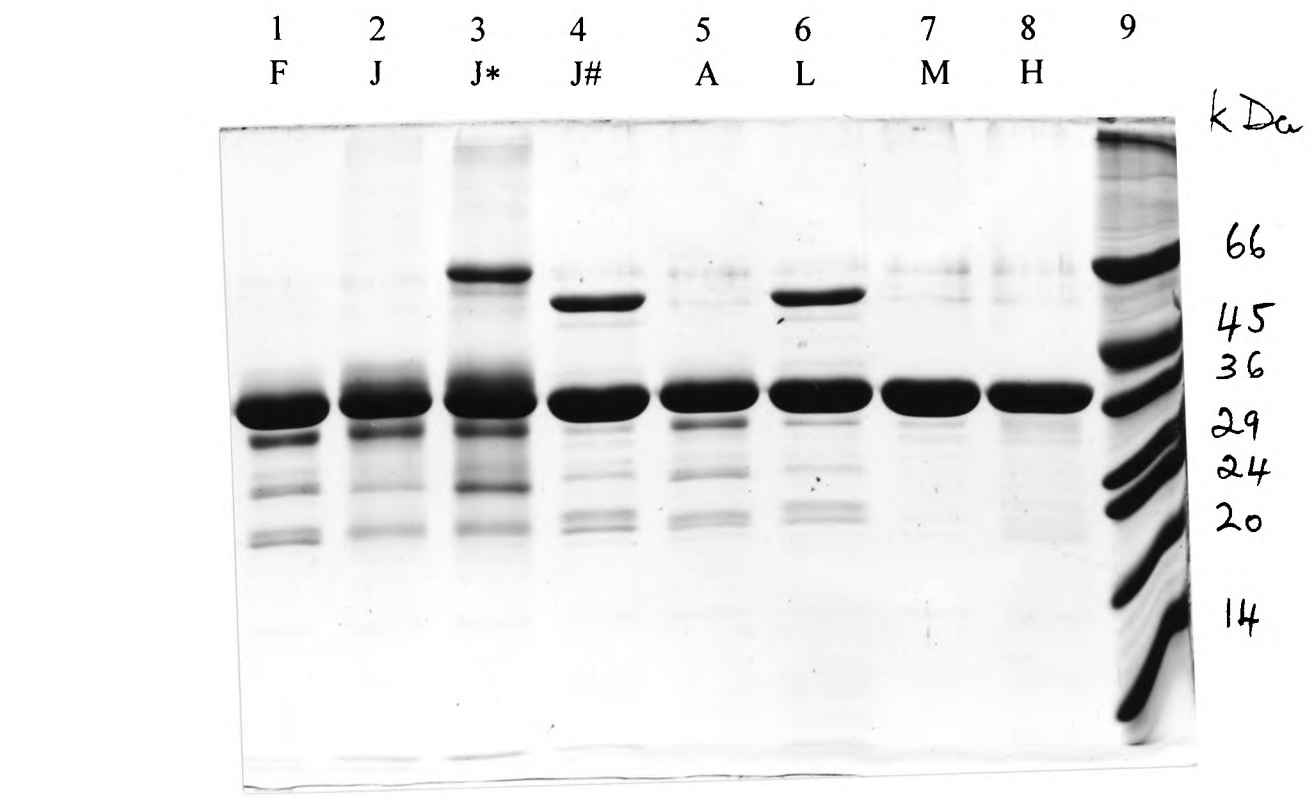

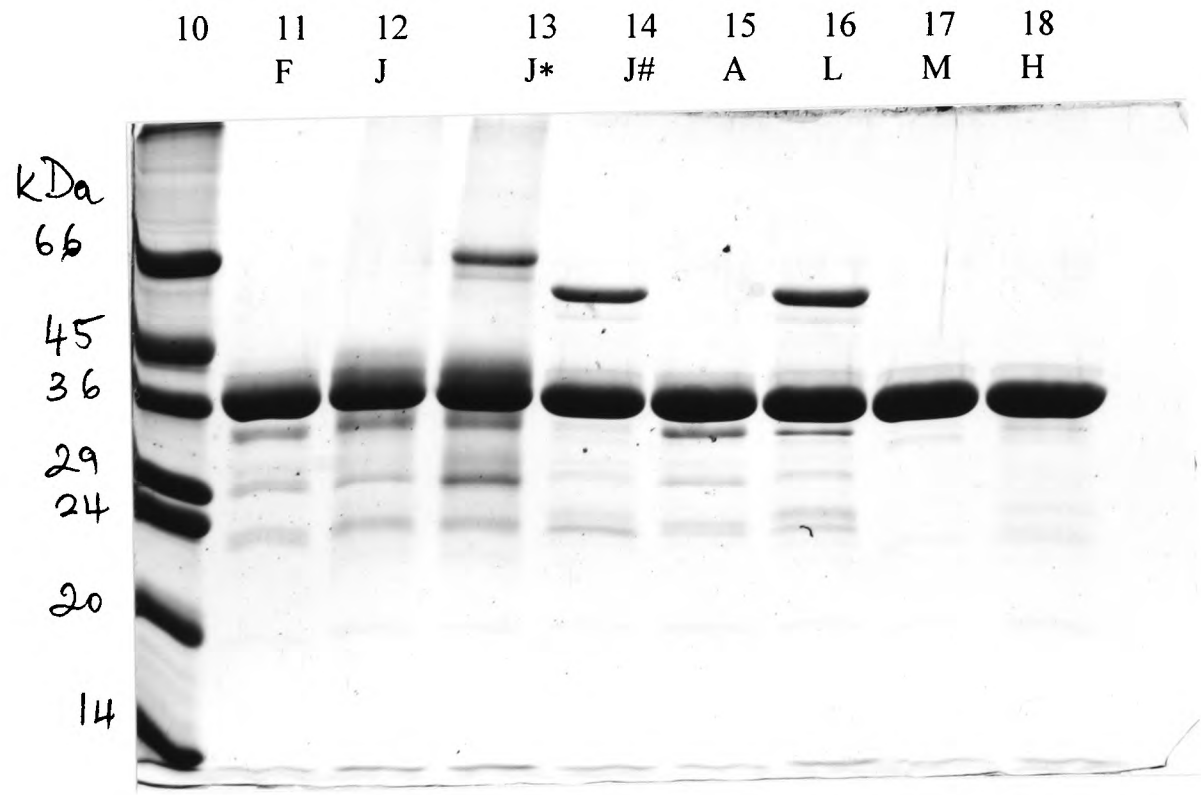

Figure 5.5 Comparison of fragmentation of wild-type and mutant IPNS. Lanes from left to right show: (1)-(8) wild-type; (11)-(18) I325. Incubation conditions, denoted by capital letters, show: (F) condition F; (J) condition J; (J*) as (J) with BSA (0.5 mg/ml); (J#) as (J) with catalase (0.4 mg/ml); (A) condition A; (L) condition L; (M) condition M; condition H. Molecular weight markers shown in lanes (9) and (10).

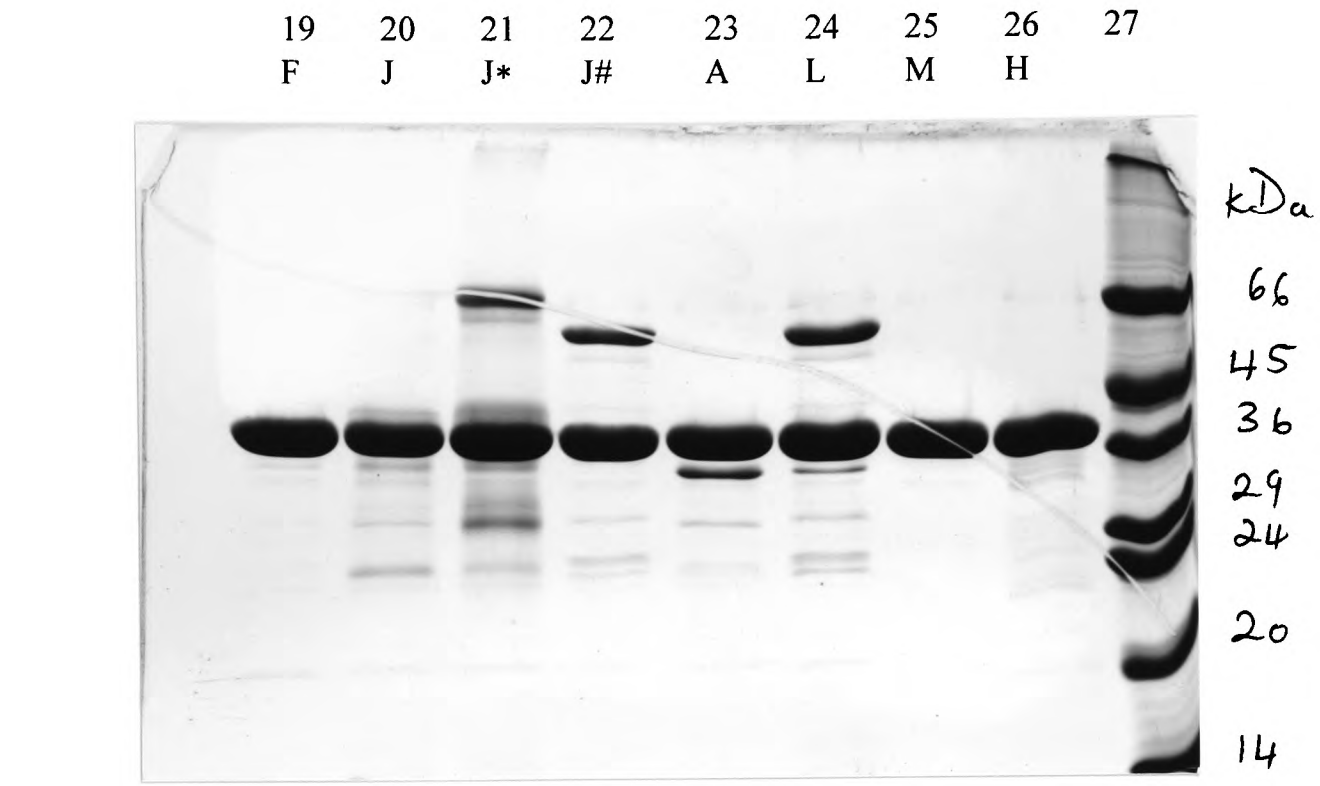

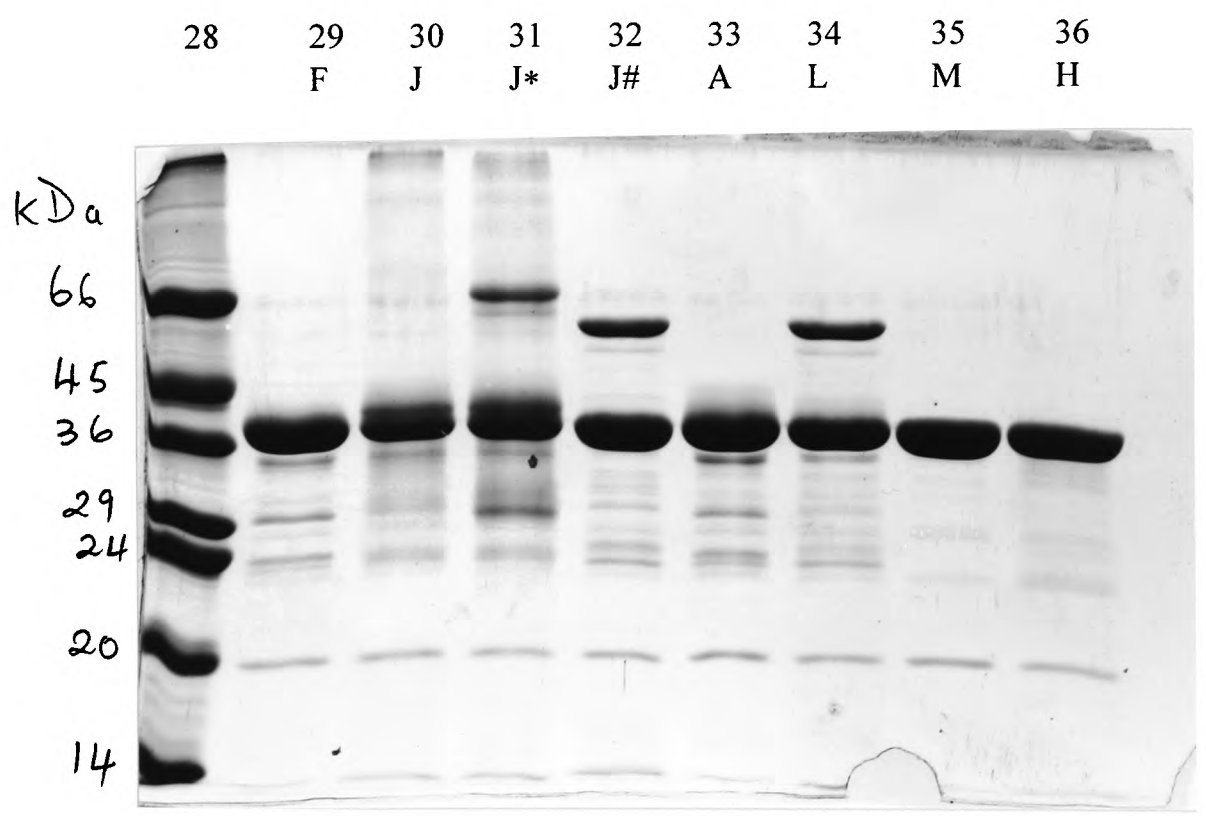

Figure 5.5 continued. Lanes from left to right show: (19)-(26) D216E; (29)-(36) H270E. All incubations were performed at 28° C for 90 min. Molecular weight markers shown in lanes (27) and (28).

Table 5.4 Comparison of the fragmentation between wild-type and mutant IPNSs. Incubation conditions were as follows: F, $Fe(II)SO_4$ (0.4 mM) + ascorbate (2.5mM); J [$Fe(II)SO_4$ + H_2O_2 (0.025 % v/v)]; J*, as J but with BSA (0.5 mg/ml); $J^{\#}$, as J but with catalase (0.5 mg/ml); L, [$Fe(II)SO_4$ (0.1 mM), ACV (1 mM), DTT (2 mM), ascorbate (1 mM)]; M, buffer alone; H, $Fe(II)SO_4$ (0.4 mM).

incubation	wild-type	I325	D216E	H270E
condition F	***a, b, c, d***	***a, b, c, d***	-	***a, b, c, d***
condition J	***a, b, c,*** *d*	***a, b, c,*** *d*	*a, b,* ***d***	*a, b, c, d*
condition J*	***a, b,*** *c, d*	***a, b, c,*** *d*	***b,*** *d*	*a,* ***b,*** *c, d*
condition $J^{\#}$	*a, b,* ***c, d***	*b,* ***c, d***	*b,* ***c, d***	*b,* ***c, d***
condition A	***a, b, c, d***	***a, b, c, d***	***a,*** *b,*	***a, b, c, d***
condition L	*a, b, c, d*	***a, b, c, d***	***a,*** *b, c, d*	*a, b, c, d*
condition M	‡	‡	‡	‡
condition H	†	†	†	†

Fragments *e* and *f* not resolved. Bold letters denotes normal intensity; non-bold represents weak intensity fragmentation.

‡ No fragmentation detected.

† Small amount of fragmentation detected.

Since it has been reported that Cu(II) can cause greater amounts of oxidative damage to (some) proteins than Fe(II)[113], the fragmentation of mutant D216E was carried out by substituting Fe(II) for Cu(II). No clear increases in the extent of fragmentation, or changes in its pattern, were made after substitution of Fe(II) with Cu(II) (Figure 5.6 lanes 1 and 5) but the intensity of smearing was enhanced. Fragments produced from this sample did co-migrate with those obtained with Fe(II)/ascorbate/ H_2O_2 (*cf* lanes 1 and 2).

Increasing incubation temperature from 27 °C to 37 °C produced only a small increase in the amount of fragmentation in the presence of either Cu(II) or Fe(II) in the incubation mix.

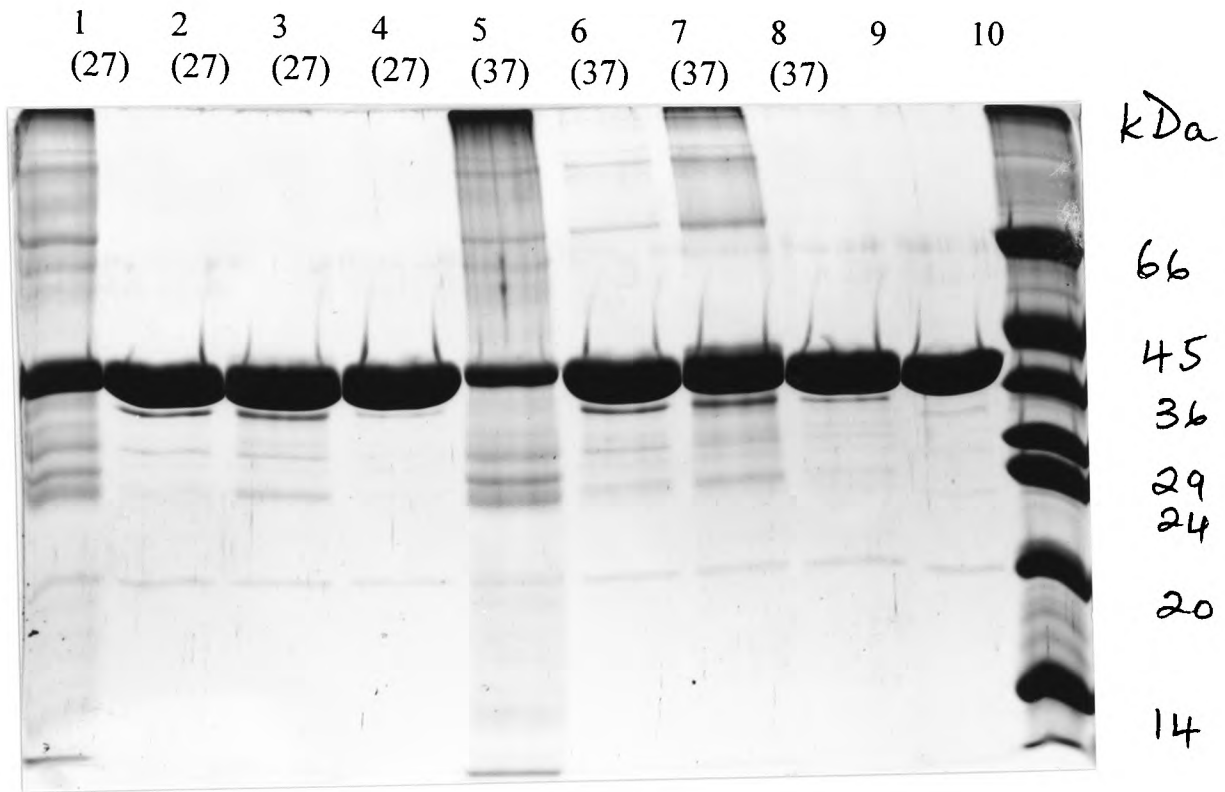

Figure 5.6 Effects of temperature on the fragmentation of D216E. Incubations were performed for 90 minutes (temperatures given in parentheses). Lanes show: (1) and (5) $Cu(II)SO_4$ (0.6 mM), ascorbate (2.5 mM); (2) and (6) condition B; (3) and (7) $Fe(II)SO_4$ (0.1 mM), ascorbate (2.5 mM), H_2O_2 (0.06% v/v); (4) and (8) condition F; (9) no incubation; (10) molecular weight markers.

5.2.4 ESIMS analysis of wild-type IPNS

ESIMS was performed to measure the mass of intact IPNS produced during non-oxidative incubation. Masses of 37391.3 ± 0.9 Da and 37292.7 ±1.0 Da were obtained before and after 24 hours incubation in buffer only (condition M). Thus, non-oxidative inactivation does not apparently involve covalent modification (although it is not possible to distinguish between thiol or disulphide crosslinking at this resolution).

Mass ranges between 37422.4 (± 5.4) Da and 37424.4 (± 4.8) Da were obtained for IPNS under condition F after 90 minutes and therefore an approximate mass increase between 24 and 30 Da relative to calculated mass for wild-type IPNS, can be estimated. Accurate masses for samples incubated under condition F were not obtained because of extensive peak broadening in the mass spectra (Figure 5.7). Salt contamination was thought to be unlikely because all samples were desalted twice using desalting columns. This mass increase probably represents a complex mixture of closely related species resulting from several modifications (*e.g.* methionine oxidations). The observed peak broadening data supports this explanation.

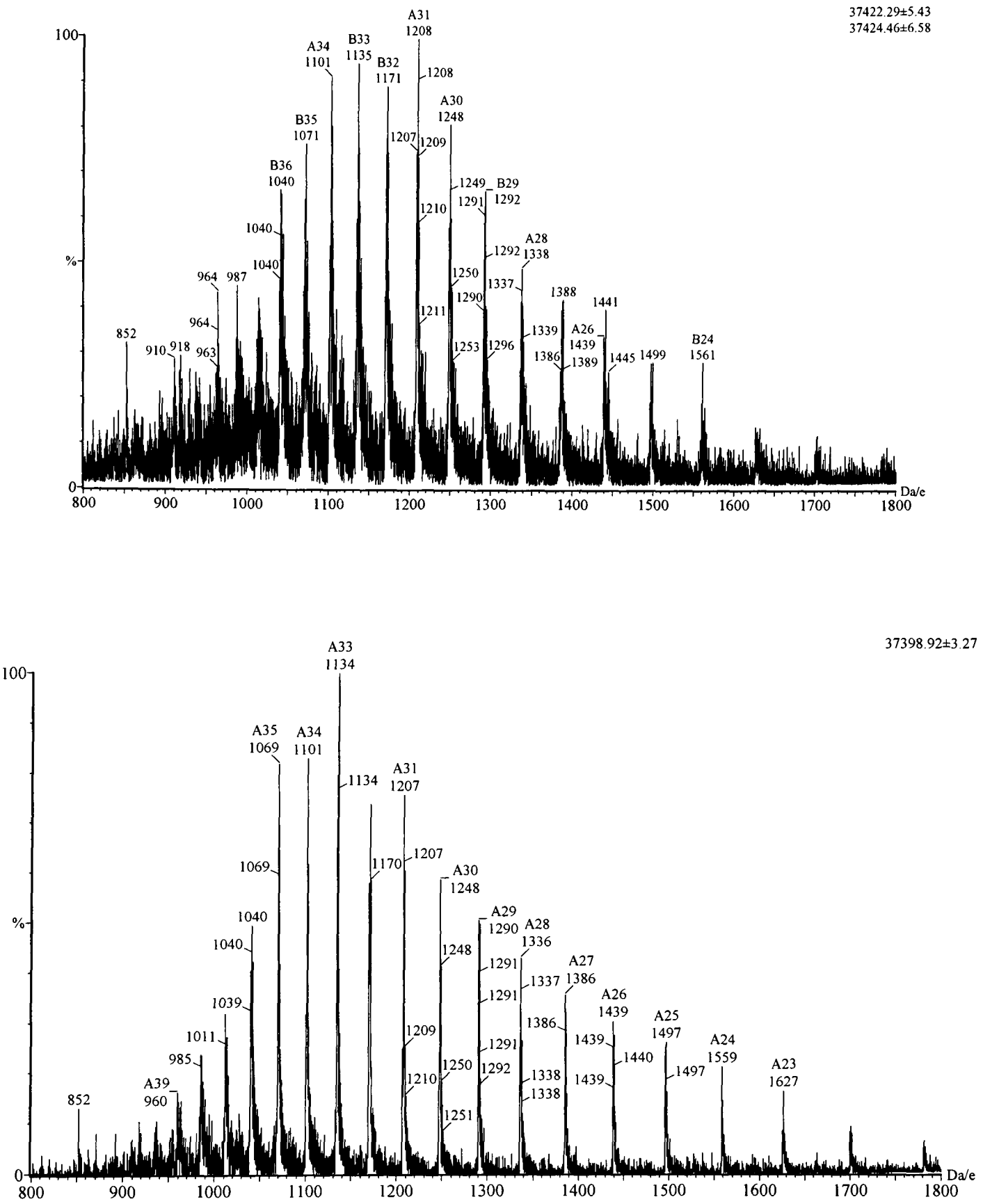

Figure 5.7 ESIMS analyses of desalted IPNS after incubation for 60 minutes under condition F (top) and no incubation (bottom).

5.2.5 Amino acid analysis

Bands on PVDF blots were excised to separate intact IPNS from its lower molecular weight fragments. Initially, intact IPNS bands from condition A and condition M were submitted for amino acid analysis (performed by Mr Bart Samyn, University of Ghent). The present study shows the results from a single amino acid analysis and therefore should be treated with caution (Figure 5.8). The experimentally determined values for glutamate and glutamine residues were higher than the calculated values for the control sample. Possible contamination by other proteins may account for this difference. Unexpectedly, the calculated values for histidine were higher than the experimentally determined values for the control sample.

The results from the amino acid analysis of intact IPNS displayed small differences when condition A was compared with condition M (Figure 5.8). Most notably, four amino acids were predominantly lost under condition A. The number of residues lost per subunit (calculated as a decrease in percentage of total number of residues per subunit in parentheses), were as follows: 2.6 aspartates (6 %), 0.6 histidines (9 %), 1.2 alanines (4.3 %) and 1.5 phenylalanines (10 %). In contrast the two amino acids that were apparently increased per subunit (and as a percentage of total) under condition A were: 1 arginine (9 %) and 1 threonine (7 %). Due to time constraints it was not possible to repeat these analyses.

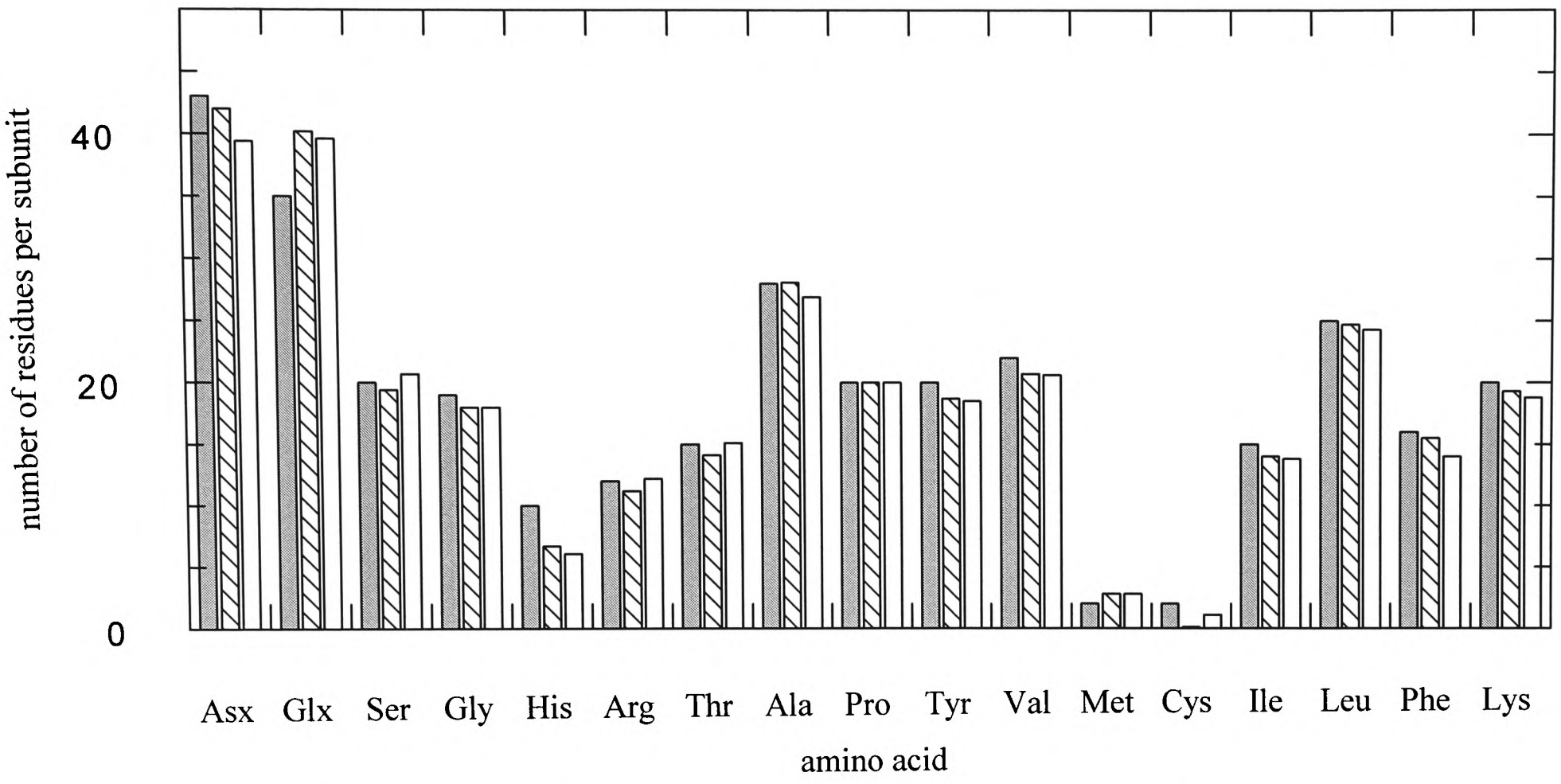

Figure 5.8 Amino acid analysis comparison of IPNS after pre-incubation conditions. Bars show the number of residues observed in: condition M (hatched) and condition A (blank). Amino acids theoretically expected per subunit of IPNS shown as grey bars.

5.3 Discussion

In Chapter 4, the slow inactivation mechanism occurring with IPNS was shown to be a non-oxidative process. It was suggested that this maybe the result of an equilibrium between high and low activity IPNS conformers. The failure to detect changes by CD, SDS-PAGE and ESIMS supports this hypothesis. However, the fact that IPNS does not fully lose activity suggests that a large conformational change is unlikely.

The results from Chapter 4 suggest that the predominant inactivation process results from the generation of a reactive oxygen species, such as a superoxide radical anion, hydrogen peroxide or hydroxyl radical. The generation of these reactive oxygen species is promoted by the presence of transition metals such as Fe(II) and Cu(I) in the presence of reducing agents such as ascorbate and DTT. The results presented here demonstrate that reactive oxygen species produce fragmentation of IPNS. The findings that fragmentation was very significantly reduced, but not totally prevented by catalase, suggests that fragmentation is primarily mediated by the generation of hydrogen peroxide in solution or reactive species from it. Fragmentation was shown to increase with time, but it is difficult to estimate the rate of fragmentation and therefore it is not possible to predict whether fragmentation was the sole cause of inactivation (*cf* Figures 4.1- 4.4 and Figure 4.5). Other covalent modifications, particularly at the IPNS active site, could also account for the observed inactivation. Some evidence for covalent modification of IPNS was obtained from peak broadening and the increase in the mass of intact IPNS by ESIMS.

5.3.1 Fragmentation of wild-type IPNS and wild-type DAOCS

The observation that the disruption of the metal binding site of IPNS by the addition of SDS sample buffer prevented fragmentation suggests that the integrity of the metal binding site is essential for fragmentation to occur. The present studies demonstrate that *in vitro* assay conditions of wild-type IPNS produces fragmentation to give (at least) six oligopeptides (*a, b, c, d, e* and *f*). The findings that the addition of either catalase, a catalyst for the removal of hydrogen peroxide from solution, the omission of ferrous iron or the addition of an excess of EDTA (a strong iron chelator) abolished fragmentation, suggests that the most likely cause of fragmentation results from hydrogen peroxide generated in solution (*via* Udenfriend's reaction). The observations that a similar fragmentation pattern for IPNS was observed after incubations in complete assay conditions (Figure 5.2a condition A) or in the presence/absence of ACV (Figure 5.2a condition F, condition D or condition B) suggests that the fragmentation is not related to catalytic turnover but is mediated *via* the generation of H_2O_2 in solution. The observation that fragmentation studies employing Fenton's conditions (H_2O_2 with ferrous iron) showed an identical fragmentation pattern to those under the assay conditions supports this proposal. The observation that faster rates of fragmentation under conditions of Ettener *et al.* [H_2O_2, Fe(II) and ascorbate] or Fenton [H_2O_2 and Fe(II)] compared with Udenfriend [Fe(II)/ascorbate] suggests that the rate of fragmentation in IPNS depends upon the rate of generation of H_2O_2 in solution.

ACCO fragmentation occurs in a burst (less than 5 minutes duration) under Udenfriend's condition. However IPNS fragmentation under similar conditions is slower and proceeds over 90 minutes. The fragmentation of ACCO was proposed to arise from incorrectly folded or 'primed' enzyme[70]. No evidence was observed for extensive

misfolding or other secondary structural changes in IPNS (no changes were observed by CD or fragmentation studies even after mutating the putative metal binding ligands). In the case of ACCO CD analysis also showed no major change in the overall secondary structure, but MCO studies did suggest that the ferrous iron can bind in more than one site[66].

Extensive IPNS inactivation gave six oligopeptides suggesting that there were minimally three cutting points. Results presented above suggest two cutting points specifically occur in the active site to give four fragments *a, b, e* and *f*. The N-terminal sequencing of fragments *e* showed that one cleavage point (Figure 5.9a, X_1) lies one residue away from the Asp216 metal binding ligand. The second cutting point (Figure 5.9a, X_2) produces fragment *f* which lies two residues away from the His270 metal binding ligand. The N-terminal sequences of fragment *a* and *b* were identical to those of intact IPNS, thus they result from cleavages at X_1 and X_2.

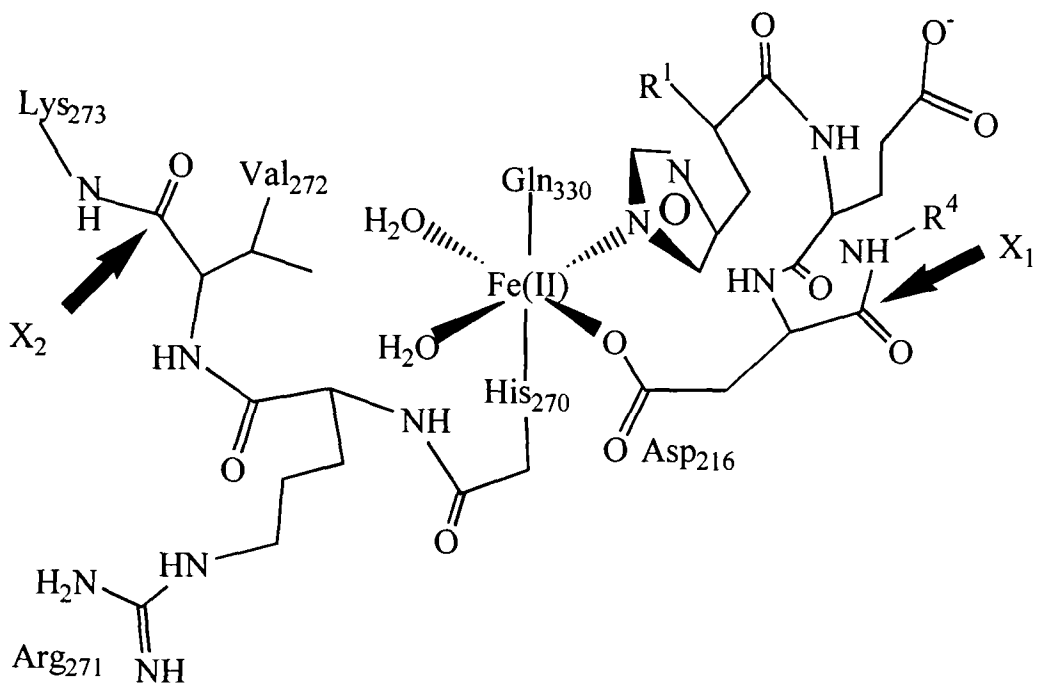

Figure 5.9a Location of cleavage sites in the active site of IPNS as visualised from the IPNS-Mn(II) structure[24]. The two cutting points are shown by X_1 and X_2 (note the position of cutting points X_2 and X_1 in this figure is drawn for clarity and therefore do not represent the true distances of the cutting points from the ferrous centre).

A third cutting point, the position of which is unclear, gives fragments *c* and *d*. Fragment *c* and *d* had a molecular mass of ~20 kDa and ~17 kDa by SDS-PAGE respectively. The N-terminal sequence of fragment *c* was identical to intact IPNS (it is not possible to get an N-terminal sequence for fragment *d*). It is proposed that the third cutting point lies on the loop region between α7 and β5. One possiblity is that this cutting point lies on a region of charged residues corresponding to the sequence FKPDDT. Alternatively, it is possible that the third cutting point arises from a cleavage from the Glu81 and His82, the second putative metal binding site reported by Roach *et al.*[24]. However, a cutting point in the vicinity of this second metal binding site would produce an N-teminus fragment with a mass of ~10 kDa and a C-terminus of 27 kDa which seems unlikely.

	Block A (214-217)	Block B (270-289)
C. acremonium	HEDVSLITVLYQSD	HRVK------WVNEERQSLPFFVNGL
P. chysogenum	HEDVSLITVLYQSD	HRVK------WVNEERQSLPFFVNGL
A. nidulans	HED***VSLITVLY***QSN	HRV***K------WVNAERQ***SLPFFVNLG
N. lactamdurans	HFDVSMITVLYQTQ	HRVK------FVNAERLSLPFFFHAG
ACCO	HTDAGGILL***FQDDK***	HRVIA----QTDGT-RMSLASFYNPG
F3OH	HTDPGTITLLLQDL	HQAVV----NSECS-RLSIATFQNPA
H6H	HYDGNLITLLQQD	HRVVT----DPTRD-RVSIATLIGPD
FOLS	HTDMSYITILVPNE	HRTTV----NKDKT-RMSWPVFLEPP
GC20	HTDPTSVTILHQDP	HRAVV----NSMNA-RKSLAFFLCPS
DAOCS	HYDLSMVTLIQQTP	HHV***AAPRRDQIAG***SSRTSSV***FFLRPN***
DAOCS/DACS	HYDLSTITLVHQTA	HRVKSPGRDQRVGSSRTSSVFFLRPK
	↑ ↑	↑ ⇧ ⇧

Figure 5.9b Comparisons of the putative metal binding ligands of IPNS, ACCO and other α-KG dependent oxygenases. Bold italics show N-terminal sequences of fragments resulting from an internal cleavage in the IPNS and DAOCS (from the present study) and ACCO (from the previous studies). Arrows show absolutely conserved residues: filled arrows, show metal binding ligands; unfilled arrows, residues that bind IPNS valine carboxylate or C5 carboxylate of α-KG in α-KG dependent enzymes. (F3OH, flavanone 3-β-hydroxylase; H6H, hyoscyamine 6-β-hydroxylase; FOLS, flavanol synthase; GC20, gibberellin C-20 oxidase).

Fragmentation of DAOCS occurred under Udenfriend's conditions results from H_2O_2 generated in solution and was catalase protectable. Incubations with ferrous iron/ascorbate produced 6 oligopeptides which again suggested that fragmentation results from at least three cutting points. N-terminal sequencing confirmed that at least two of the cutting points results from fragmentation in the active site. Cleavage between Val245 and Ala246 gave oligopeptide *e* which appears to be two residues away from His243 metal binding ligand. Oligopeptide *f* which resulted from a cleavage between Val262 and Phe263 and appears to be two residues away from the Ser260 and Arg258 α-KG binding residue. Figure 5.9b compares the sites of cleavage in DAOCS, IPNS and

ACCO[70] and sequence alignments with other oxygenases. Due to time constraints it was not possible to perform N-terminal sequencing of the remaining peptides.

5.3.2 Amino acid analysis

The preliminary results from amino acid analysis show the apparent losses of aspartate/aspargine, alanine, histidine and phenylalanine. However these results and suggestions should be regarded as preliminary and treated with caution. It is noteworthy that, apart from alanine, these residues lie close to, or form a part of, the active site pocket in the IPNS structure (*vide supra*). The losses in these amino acids were not balanced by the increases in other amino acids, suggesting that oxidative modification elicited the eventual loss of the primary amino group of these amino acids. It is surprising that there was an apparent loss of alanine residues- if this observation truly reflects a chemical event in IPNS inactivation, then it implys that some conformational change in the enzyme's active site must occur which makes the alanine more susceptible.

5.3.3 IPNS mutants

The observation that all mutant IPNS enzymes, apart from the D216E, showed a similar fragmentation pattern to the wild-type enzyme suggests that no or little conformational changes take place in the active sites of these enzymes after ACV and Fe(II) binding. D216E fragments least extensively than all the other mutants.

It is interesting that the inactive H270E mutant, which does not catalyse the turnover of ACV, fragmented identically to the wild-type IPNS. The X-ray structure of this mutant suggested that the metal binding site was too small to accommodate a ferrous ion, at least in the crystalline state. If no metal is bound in the active site then the

formation of a reactive intermediate (*e.g.* ferryl oxene) is unlikely to account for the fragmentation of this mutant (see Scheme 5.2). However, the observed spectroscopic charge transfer complexes seen with this mutant suggests that metal binding does occur, most likely at the active site, rather than at an adventitious metal binding site (note that ACV binding also occurs in H270E cystal structure, see Chapter 3). It is possible that a conformational change takes place in the enzyme's active site in the crystalline form which allows ACV binding but does not allow metal binding. Thus it seems that iron ligation by H270E is probably required for both activity and fragmentation. By comparison, the inactive ACCO mutants (H177Q and D179N) displayed reduced fragmentation[66]; however inactive H234Q displayed identical fragmentation pattern as wild-type.

In all mutants examined, it is unclear why this active D216E mutant was most resistant to fragmentation with iron(II) and ascorbate. Interestingly oligopeptide *a* was the most intense under incubation condition A, which suggest that this site (Figure 5.9b, X_2) is preferentially targeted. Poor staining by the other oligopeptides may be an alternative explanation for this observation. The crystal structure of this mutant in the presence of ACV and Fe(II) shows no overall conformational changes when compared with the wild-type IPNS, but does suggest a reason for its resistance to fragmentation (*vide infra*).

5.3.4 Mechanisms of fragmentation

It was proposed in Chapter 4 that the likely oxidant generated under Fenton's or Udenfriend's condition is either the hydroxyl radical or an iron oxene. Possible

mechanisms for the fragmentation of IPNS and DAOCS, *via* a hydroxyl radical, an iron oxene, a superoxide and a hydrogen peroxide will be presented (*vide infra*).

Hydroxyl radical-mediated

Scheme 5.1 shows the postulated mechanism of Stadtman[112] based upon the radiolytically-generated hydroxyl radical fragmentation of proteins. In this mechanism hydrogen atom abstraction is mediated by a hydroxyl radical to form a carbon centred radical species (1). Addition of dioxygen to form (2) is then followed by elimination of the protonated superoxide to give the imine (3) (pathway A). Alternatively, species (2) could abstract a hydrogen atom from a neighbouring group to form a peroxide (4) which undergoes elimination of the hydrogen peroxide to form (3) (pathway B).

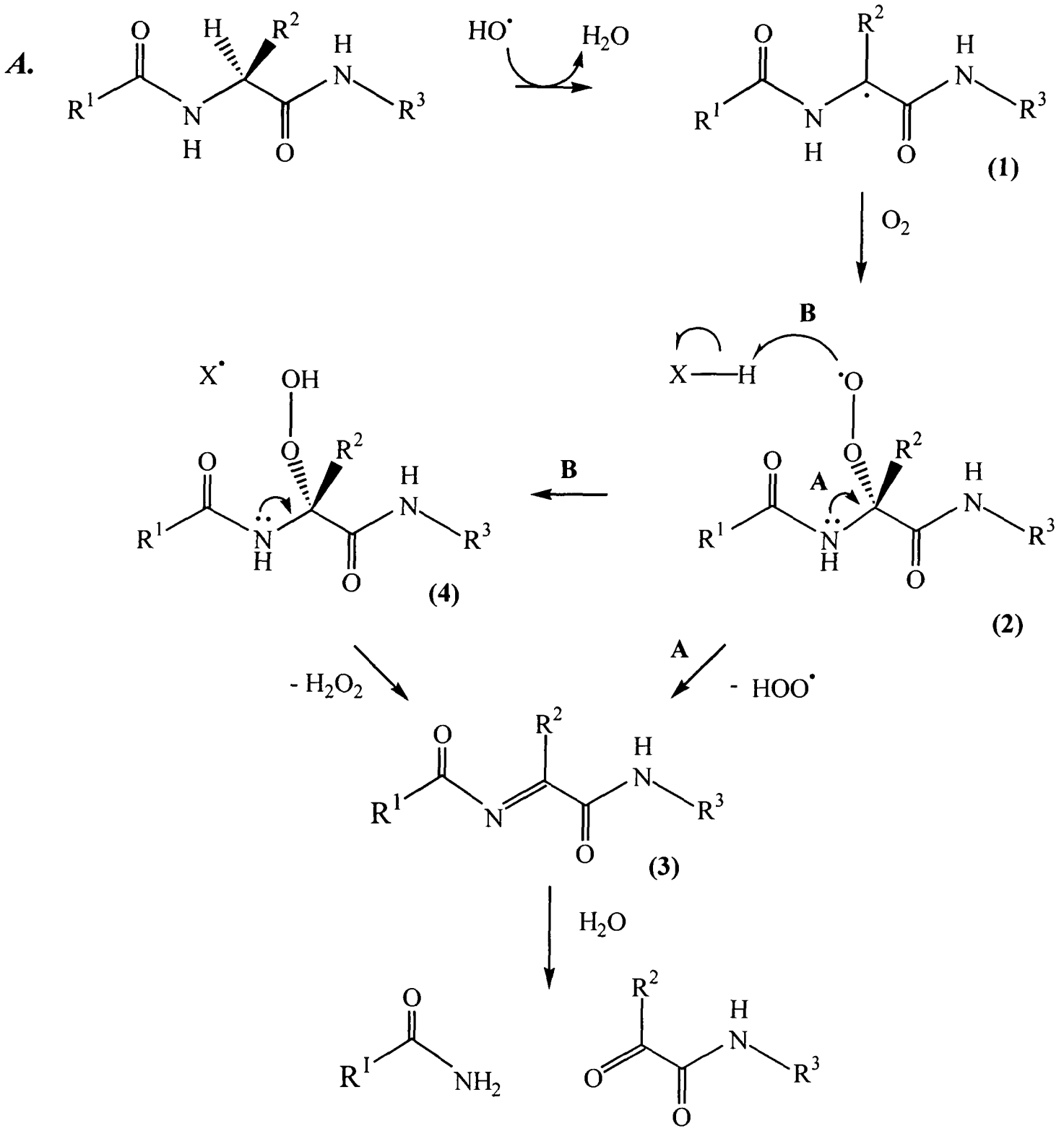

Scheme 5.1 Hydroxyl radical mediated fragmentation[112].

Iron oxene-mediated

Iron oxene-mediated mechanism for protein fragmentation is shown in Scheme 5.2. Thus the first step involves hydrogen atom abstraction from the α-carbon to produce a carbon-centred radical species (1) and the Fe(III)-OH species (5), which may be viewed as an Fe(II) bound hydroxyl radical. (1) may react by addition of the hydroxyl radical to form the C_α-hydroxide (6) or by further substrate oxidation at the amide nitrogen to form

the imine (3). Both (3) and (6) may fragment to give an amide functionality on the N-terminal fragment and a carbonyl functionality on the C-terminal fragment. Thus one of the two fragments is N-terminally blocked and is inaccessible to N-terminal sequencing.

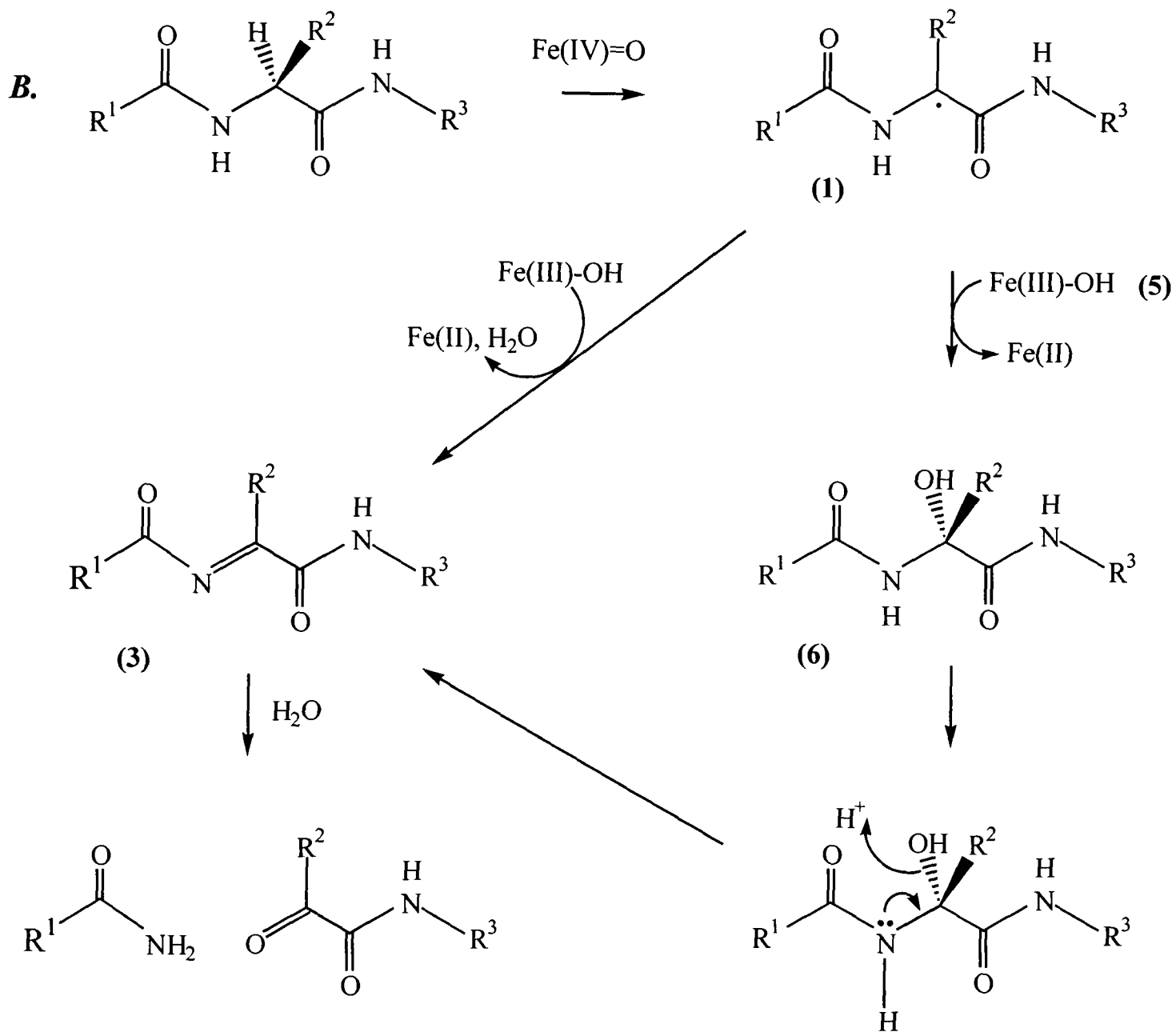

Scheme 5.2 Iron oxene mediated protein fragmentation[151].

A radical mediated fragmentation does not necessarily result in deamination at the α-carbon. A cleavage between an α-carbon and an adjacent amide carbon can occur (Scheme 5.3).

C.

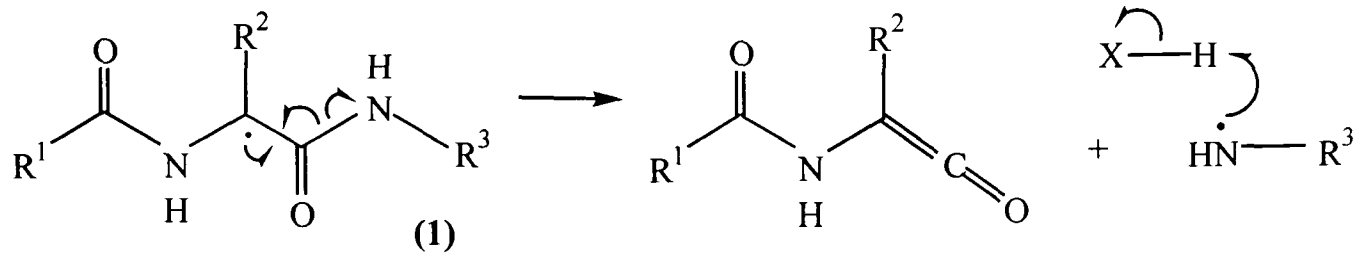

Scheme 5.3 Radical mediated protein cleavage between the α-carbon and the adjacent amide carbon[112].

Superoxide or peroxide-mediated

Superoxide radicals or peroxide anions, generated from the iron catalysed auto-oxidation of ascorbate, may cause nucleophilic attack at the amide carbonyl carbon (Scheme 5.4). In both mechanisms (D and E) the bond between the α-nitrogen and the α-carbon is left intact and therefore N-terminal analysis of both resulting fragments is possible. Release of the peroxide anion or superoxide radical from the iron and subsequent nucleophilic attack elsewhere in the protein is possible.

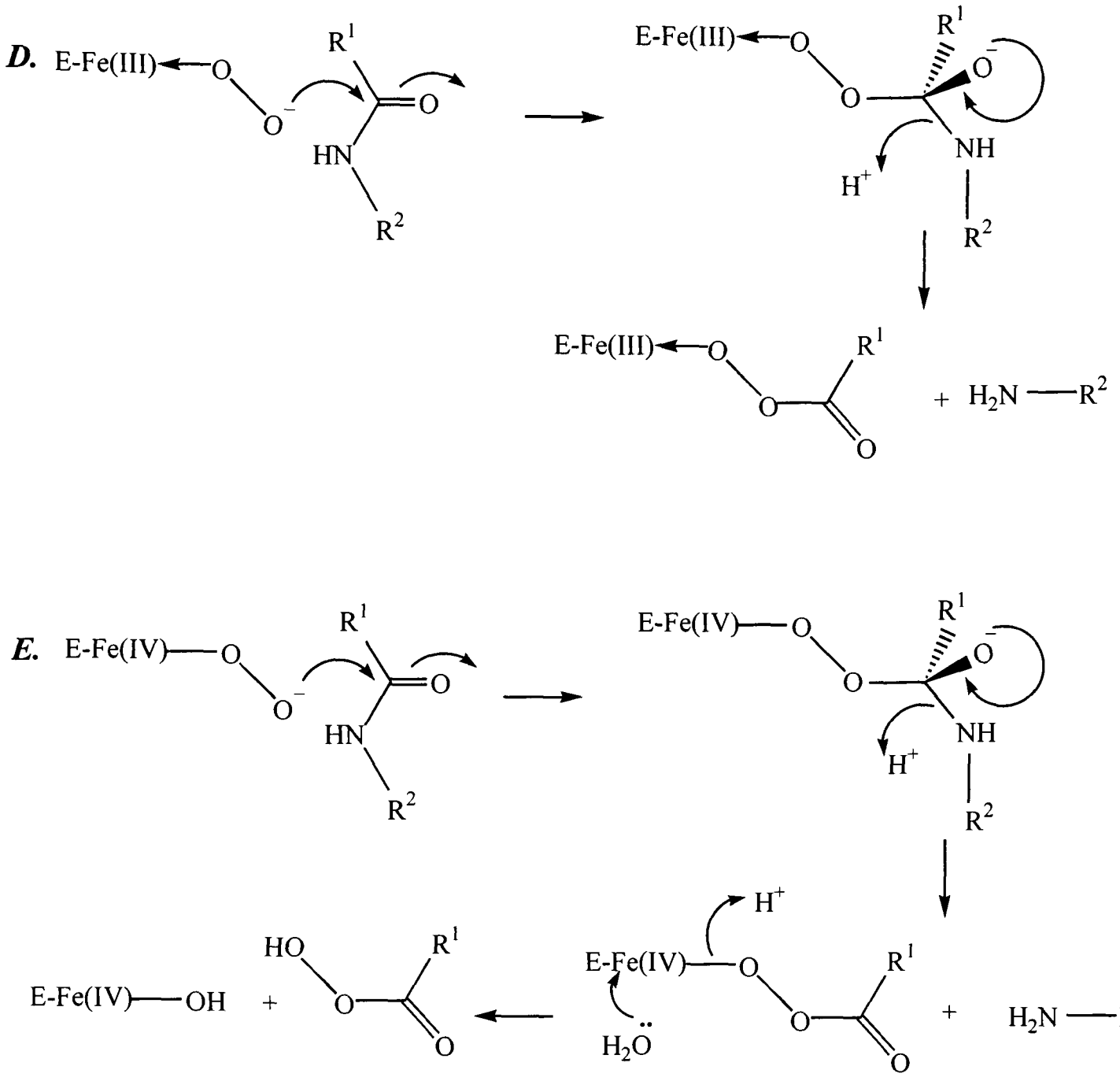

Scheme 5.4 Proposed ionic fragmentation mechanisms for IPNS mediated by superoxide radicals (D) and peroxide anions (E).

5.35 Conclusions

The present results suggest that fragmentation is probably mediated by an ionic mechanism, *via* H_2O_2, rather than a radical mediated cleavage process. In one possible ionic mechanism the peroxide binds on the active site iron *trans* to His270, *i.e.* in a position analogous to the thiol of the ACV in the crystal structure (Scheme 5.5). The amide carbonyls of the Asp216 or Val272 are too far away for direct attack by the lone

pair on the peroxide oxygen (a distance of 6 Å for the Asp216 or a distance of 8.8 Å for the Val 262). As shown in Scheme 5.5 a movement of at least several Angstroms by the amide carbonyl atom of Asp216 or Val272 towards the lone pair of the oxygen on the peroxide would be required for nucleophilic attack.

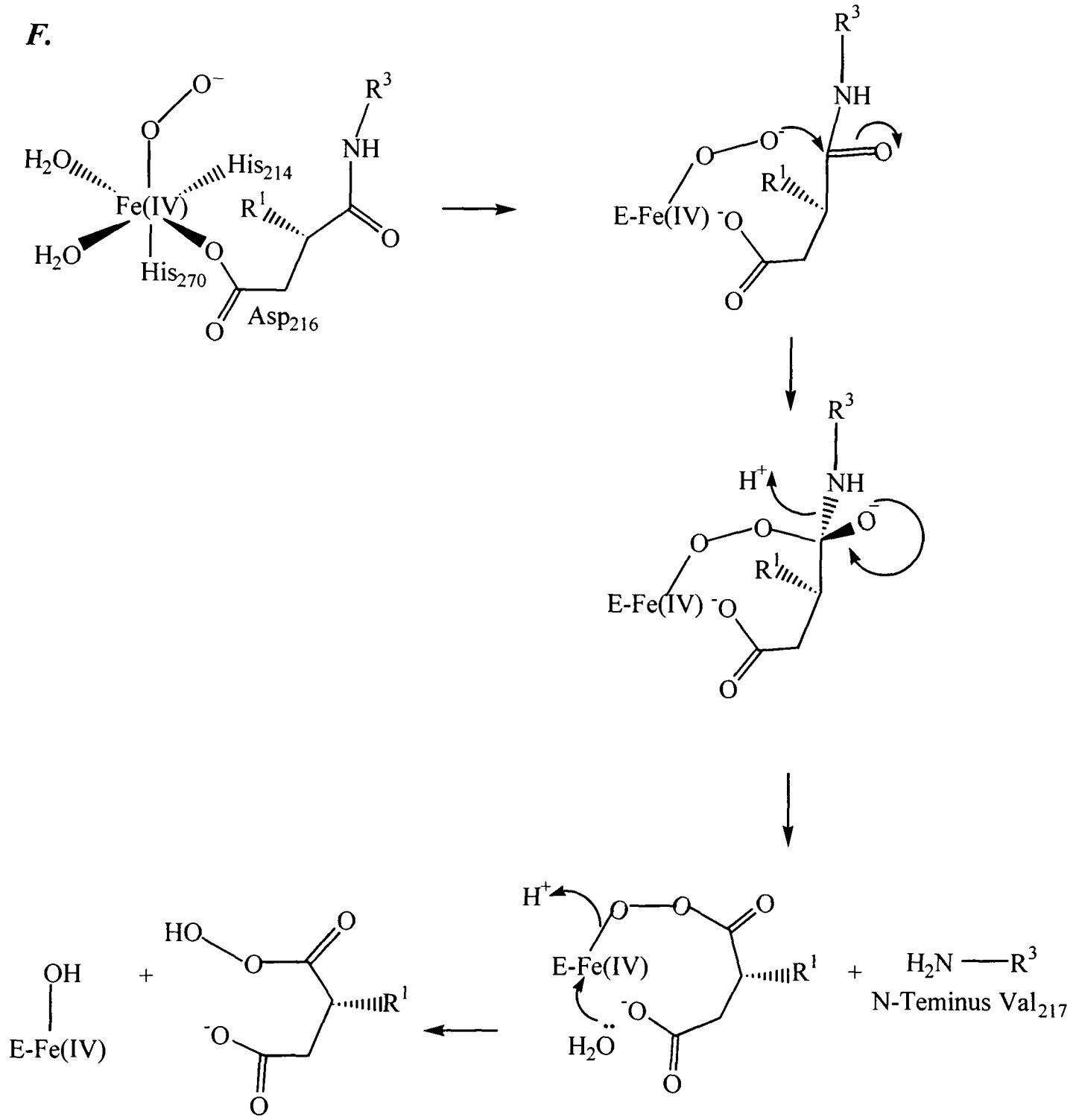

Scheme 5.5 Direct fragmentation mechanism of IPNS between Asp216 and Val217 mediated by a direct nucleophilic attack from a peroxide anion.

A second possibility is that the peroxide deprotonates one of the water molecules in the active site which indirectly attacks the amide carbonyl atom of Asp216 to release the N-terminal Val217 (Scheme 5.6). The latter mechanism seems more plausible in view of the long distances between the iron and the amide carbonyl atoms of the Asp216 and Val272 residues. It should be noted that the amide carbonyl of Asp216 is correctly positioned for nucleophilic attack as proposed. The carbonyl of Val272 seems to be less ideally positioned for nucleophilic attack. However, the flexibility within the active site may allow enough movement for cleavage at Val272.

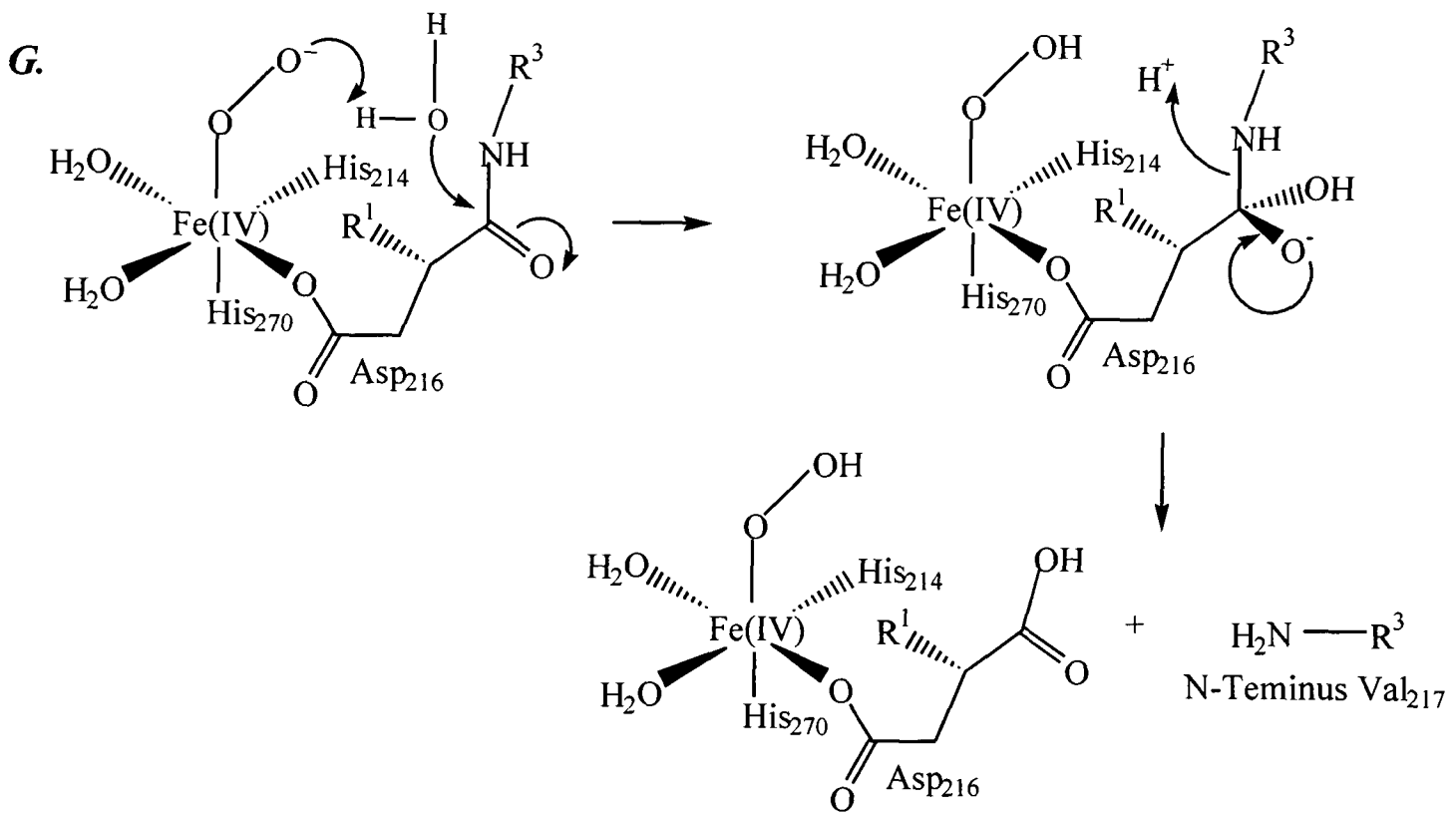

Scheme 5.6 Indirect fragmentation mechanism of IPNS between Asp216 and Val217 mediated by a hydrolytic water molecule in the active site.

One site (X_1, after Glu216) in mutant D216E appears to be more resistant to fragmentation compared with the wild-type. The crystal structure of D216E mutant

shows a significant movement of the peptide backbone occurs in the loop region (between His214-Glu216) which allows this Glu216 side chain to ligate with the ferrous metal. This repositioned Glu216 carbonyl in D216E mutant appears to be less well positioned for a direct attack from a peroxide. In this mutant the other site (X_2, after Val272) is preferentially targeted by the reactive species.

The cleavage pattern for H270E mutant is very similar to the wild-type enzyme. The orientation of the amide carbonyl of Val272 in the crystal structure of this mutant does not change significantly compared with wild-type IPNS.

The two cutting positions observed in DAOCS also lie in the vicinity of the active site but at a distance of ~8-10 Å away from the active site iron. Thus, the fragmentation in DAOCS probably also results from an indirect nucleophilic attack mechanism as proposed for IPNS and shown in Scheme 5.6.

It has been speculated that some iron dependent oxygenases may have evolved from hydrolytic enzymes employing transition metal cofactors[85] (see introduction to Chapter 3). The present studies on the inactivation of IPNS clearly demonstrate that these oxygenases can catalyse the hydrolysis reaction (resulting in fragmentation). It maybe that these hydrolysis reactions observed in oxygenases are involved in their inactivation process.

CHAPTER 6

Experimental Section

6.1 Materials and General Methods

Equipment

Water purification system:	Millipore, Milli-RO and Milli-Q Plus system.
Spectrophotometer:	Shimadzu, UV-1601
Shaking Incubator:	New Brunswick Scientific, G24 Environmental incubator shaker
Centrifuge:	Beckman JA-21, JA-10
pH meter:	Mettler Delta 340
Balance:	Salter FA-2000, Sartorius Research A200S
Electrophoresis	Bio-Rad Mini Protean II system
Sonicator:	Soniprep 150
Microcentrifuge:	Jouan A-14,
Scintillation Counter:	LKB Rack beta 1215
Glove Box:	Belle Technology Model CV3 (Unit 1 Walnut Orchard, Portesham, Dorset) internal oxygen concentration <0.4 ppm
HPLC:	Gilson/Anachem HPLC system equipped with: Auto sample injection model 231 Dynamic mixer 811B Manometric pressure module 806 UV detector 116 Temperature regulator 832 Gilson pumps 305/306 Gilson 715 HPLC System Controller Software

Chemicals

General cell culture media was obtained from Difco or Oxoid. Salts for the media and buffers were obtained from BDH, Fisons, Fluka or Sigma-Aldrich. Chemicals for SDS-PAGE and Tris-Tricine gels were obtained from Bio-rad, Sigma-Aldrich, Serva or Scotlab. Bromophenol blue and Coomassie Brilliant Blue (G250, R250) were obtained from Sigma-Aldrich. ACV was obtained by fermentation (J. Keeping, O.C.M.S.). DTT was obtained from Lancaster. Ascorbic acid, iron sulphate and copper sulphate were obtained from Sigma-Aldrich. Radioactive chemicals were purchased from Amersham. Chloramphenicol and tetracycline were obtained from Sigma-Aldrich. ACA and ACAB were synthesised by Ms Alexandra Long (O.C.M.S.).

Determination of protein concentration

Protein concentrations were determined using Bradford Reagent[152]. This reagent was made up by mixing Coomassie Blue G250 (0.1 %, w/v), phosphoric acid 8.8% (v/v), ethanol (5% v/v) in Milli-Q water (stored at 4 °C). Bradford reagent (2 ml) was mixed with 40 µl protein solution in plastic cuvettes, followed by incubation at room temperature for 5-10 minutes before reading the absorption at 595 nm. The standard curve was obtained by mixing 2 ml of Bradford reagent with 40 µl of a stock solution of bovine serum albumin at 0.1-1.0 mg/ml.

Electrospray ionization mass spectroscopy (ESIMS)

Mass spectometric analyses were performed using electrospray ionisation on a Bio-Q triple quadrupole mass spectrometer (VG Instruments) and run by Dr Robin Aplin. Typically, 75-150 pmol of protein were dissolved in 15 µl of 50 % acetonitrile in water

and injected into the electrospray ionisation source. Scans of 3 s were accumulated covering a 800-1500 Da range and the spectra analysed with Mass Lynx 2.0 software (VG organic). Calibrations were performed separately by injections of horse heart myoglobin.

CD spectroscopy

Far UV circular dichroism spectra of wild-type and mutant IPNS were recorded with a Jasco-720 spectropolarimeter using 1 mm path length cuvettes at room temperature. The concentration of the protein was 4-6 μM in 25 mM phosphate buffer pH 7.0.

6.2 Experimental for Chapter 2 and 3

Molecular biology

General molecular biology procedures were performed as described by Sambrook *et al.*[153]. The enzymes for molecular biology were obtained from Pharmacia LKB and Promega, New England Biolabs (UK) Ltd.

Media and Solutions

LB medium/Litre

Bacto-typtone (10g), NaCl (10g), yeast extract (5g) were mixed in 1L Milli-Q and the pH was adjusted to 7 with NaOH before autoclaving at 121 °C, 15 psi, for 20 minutes.

For LB agar plates, 15 g bacto-agar was added to the LB medium before autoclaving. The appropriate antibiotic was added after cooling to 50 °C.

Chloramphenicol was added to a final concentration of 35 μg/ml tetracycline to a final concentration of 15 μg/ml.

2YT/Litre

Bacto-tryptone (16g), NaCl (10g), yeast extract (10g) were mixed with Milli-Q (900 ml) and the pH was adjusted to 7.0 with 5N NaOH. The final volume made up to 1 L with Milli-Q and autoclaved.

SOC medium/Litre

Bacto-tryptone (20g), NaCl (0.5 g), yeast extract (5g) and 250 mM KCl (10 ml) were dissolved in 900 ml Milli-Q. After the pH was adjusted to to 7.0 with 5N NaOH, Milli-Q was added to give a final volume of 990 ml and them autoclaved. After the solution had cooled to room temperature, 10 ml of sterile 1 M $MgCl_2$ and 20 ml of sterile 1 M glucose was added.

TE buffer/Litre

1 M TrisHCl pH 7.5 (10 ml) and 0.5 M EDTA (1 ml) were dissolved in Milli-Q (980 ml) before autoclaving.

TAE (50x)

Tris (121g), glacial acetic acid (28.5 ml) and EDTA (18 g) were mixed and the final volume was made up to 500 ml with Milli-Q.

Agarose gel loading buffer (6x)

Bromophenol blue (0.25% w/v), xylene cyanol (0.25% w/v), and Ficoll 400 (15% w/v) were mixed in Milli-Q.

Table 6.1: Synthetic oligonucleotides used for mutagenesis.

Selection primers

primer	mutation	sequence
SP-forward	Hind III to Mlu I	5'-GGC TGC AGC CAC GCG TGG CTG TTT TGG-3'
SP-reverse	Hind III to Mlu I	5'-CCA AAA CAG CCA CGC GTG GCT GCA GCC-3'

Sequencing primers

primer	sequence
SEQ-1	5'-.CT TAC CTG GAT CC-3'
SEQ-2	5'-AAG TAG CCA GTA TCG TCG G
SEQ-3	5'-AAC TAC TAT AAA GCG CCC-3'
SEQ-4	5'-GCC ATT GGG TTC TCG GGG-3'
SEQ-5	5'-CCA CTC TCC TAC GGC GAC-3'
SEQ-6	5'-GCT AAA TCC AAC TCC CG-3'

Target primers

primer	mutation	Sequence
pJB703-12	D216H	5'-GAG TGG CAT GAG CAC GTA TCC CTA ATG-3'
pJB703-11	D216E	5'-GAG TGG CAT GAG GAA GTA TCC CTA ATC-3'
pJB703-13	D216Q	5'-GAG TGG CAT GAG CAG GTA TCC CTA ATC-3'
pJB703-16	H214D	5'-GAT TAG GGA TAC ATC CTC GTC CCA CTC AAA ACT CAG-3'
pJB703-17	H214E	5'-GAT TAG GGA TAC ATC CTC TTC CCA CTC AAA ACT CAG-3'
pJB703-18	H214N	5'-GAT TAG GGA TAC ATC CTC GTT CCA CTC AAA ACT CAG-3'
pJB703-19	H270D	5'-C CCA TT T CAC CCG GTC GAT GGG CGC TTT ATA G-3'
pJB703-20	H270E	5'-C CCA TT T CAC CCG TTC GAT GGG CGC TTT ATA G-3'
pJB703-21	H270N	5'-C CCA TT T CAC CCG GTT GAT GGG CGC TTT ATA G-3'
pJB703-6	Q330D	5'-AAC AAG AAC GGC GAC ACC TAG AAG CGA GGG-3'
pJB703-3	Q330A	5'-AAC AAG AAC GGC GCT ACC TAG AAG CGA GGG-3'
pJB703-4	Q330L	5'-AAC AAG AAC GGC CTG ACC TAG AAG CGA GGG-3'
pJB703-7	G329	5'-ATC AAC AAG AAC GGC TAG ACC TAG AAG CGA-3
pJB703-8	I325	5'-CTG GTG AGT TTG ATC TAG AAG AAC GGC CAG-3'
pJB703-1	F211Y	5'-GGC ACC AAA CTG AGT TAC GAG TGG CAT GAG-3'
pJB703-2	F211M	5'-GGC ACC AAA CTG AGT ATG GAG TGG CAT GAG-3'
pJB703-5	F211L	5'-GGC ACC AAA CTG AGT CTG GAG TGG CAT GAG-3'
pJB703-9	F285Y	5'-CC CTG CCA TTC TAC GTC AAC CTG GG-3'
pJB703-10	F285L	5'-CC CTG CCA TTC CTG GTC AAC CTG GG-3'
pJB703-14	H214D/D216H	5'-CTG AGT TTT GAG TGG GAC GAG CAC GTA TCC CTA ATC-3'

Deprotection of oligonucleotides

Oligonucleotides were synthesised by Mrs Val Cooper (Dyson Perrins Laboratory) using an Applied Biosystem DNA synthesiser (model 380b or 394). The oligonucleotides were placed inside Falcon tubes containing ammonia solution, sealed tightly with parafilm and incubated at 55 °C for at least 15 hours. The Falcon tubes were cooled on ice for 20 minutes before opening. The deprotected oligonucleotides (0.36 ml) were placed inside an Eppendorf tube containing 36 μl of sodium acetate (3M, pH 5.5) and absolute ethanol (1 ml) was added. After incubation at -20 °C for 1 hour the tubes were centrifuged for 10 minutes at 10,000 rpm The pellets were washed twice with ethanol (80 % in Milli-Q) and air dried for 30 minutes. The dry pellets were dissolved in TE buffer (100 μl).

Transformation

The appropriate DNA (10 μl containing approximately 10 μg) was mixed with *E. coli* supercompetent *mutS* cells (90 μl) (Stratagene) in a pre-chilled 50 ml Falcon tube and placed on ice for 30 minutes. The mixtures were heat shocked at 42 °C for 45 seconds and placed on ice for 2 minutes. Freshly prepared SOC media (1 ml) was added and the mixture was incubated at 37 °C for 1 hour with shaking at 180 rpm Aliquots (100 μl) were spread on LB agar plates containing the appropriate antibiotic and incubated at 37°C overnight. SOC media (3 ml) containing the appropriate antibiotic was added to the cells and placed overnight in an incubator at 37 °C with shaking at 250 rpm For mutagenesis studies only the colonies from the second or the third transformation plates were used for screening mutants.

Quantification of DNA

The concentration of oligonucleotides were determined using the millimolar extinction coefficient ε_o. The value of ε_o was determined by the base composition of the oligonucleotide and summing the contributions of each base[153]:

Base	Contribution to ε_o ($mM^{-1}cm^{-1}$)
T	8.8
C	7.3
G	11.7
A	15.4

The concentration of the oligo is given by the equation:

$$\text{Concentration (mM)} = OD_{260} / \varepsilon_o$$

For genomic or plasmid DNA, the concentration was determined by measuring the absorption at $\lambda = 260$ nm. An OD_{260} of 1.0 is equivalent to 50 μg/ml for dsDNA.

Single stranded DNA preparation

The pJB703 plasmid was transformed into XL1-Blue competent cells. Single colonies were used to inoculate 4 x 5 ml 2TY containing chloramphenicol (35 μg/ml) and tetracycline (15 μg/ml). Cultures were grown in a shaker incubator (250 rpm) at 37 °C for 6 hours, or until the $OD_{600} = 0.1$. Helper phage R408 (Promega) (320 μl) was added to the cultures and grown overnight. 2 ml of overnight culture was centrifuged and purified using the Wizard™ single stranded DNA purification system (Promega).

Plasmid purification (miniprep)

Plasmid DNA was purified using the Wizard Plus Miniprep DNA Purification system (Promega).

Restriction enzyme digestion

Plasmid DNAs were digested with restriction enzymes for diagonostic purposes and to check that the correct restriction site had been made. 2 µl plasmid (300 µg/ml), 2 µl of recommended 10x buffer, 15 µl Milli-Q and 1 µl of restriction enzyme (10 U/µl) were mixed in an Eppendorf tube. The digestion was performed at 37 °C for 1 hour. 5 µl of the digested sample was run on minigels.

Minigel electrophoresis

DNA samples were analysed by electrophoresis on horizontal agarose minigel using submarine electrophoresis apparatus (Sigma). In general, 1 x TAE was used as the running buffer. The final concentration of the agarose was 0.80 % (w/v).

Site directed mutagenesis

In a total volume of 20 µl the following were added: mutant primer (12.5 pmoles, 1 µl), selection primer (12.5 pmoles, 1 ml), 10 x OPA^+ buffer (2 µl), single stranded DNA from above (16 µl) and annealed by heating at 100 °C (water bath) for 5 minutes followed by incubation at room temperature for 30 minutes. A nucleotide mix (7 µl) (2.86 mM each of dATP, dCTP, dGTP and dTTP; 4.34 mM ATP; 1.43 x OPA^+ buffer) and a reaction mix (3 µl)[FPLC *pure*® T4 DNA ligase (0.83-1.17 ku/ml); FPLC *pure*® T4 DNA polymerase (0.83-1.67 ku/ml; and T4 DNA Gene 32 Protein (0.2-0.28 mg/ml)

in aqueous buffer] were added. The mixture was incubated for 2 hours at 37 °C and the reaction stopped by heating for 15 minutes at 85 °C. The mixture was briefly centrifuged and kept on ice for the next stage.

Primary restriction digestion

To 30 µl of reaction mix was added 10 x buffer E (2 µl) Mill-Q (16 ml) and *Hin*dIII (2 µl) followed by incubation for 2 hours at 37 °C. Another 2 µl of *Hin*dIII was added and incubation continued for a further 2 hours.

Transformation into XL *mutS*

20 µl of digested reaction was mixed with 80 µl of XL *mutS* supercompetent cells (Stratagene), kept on ice for 30 minutes, and heat shocked for 45 seconds at 42 °C. The transformed cells were grown in SOC medium for 1 hour at 37 °C. 100 µl of transformed culture was spread onto chloramphenicol LB-agar plates and incubated overnight at 37 °C. To the remainder of the culture was added chloramphenicol (35 µg/ml) and incubated in the shaker (250 rpm) at 37 °C overnight.

Secondary restriction digestion and transformation into nm554

The following day 1.5 ml of the overnight cultures containing the transformants were used for plasmid purification. The plasmids were digested with *Hin*dIII as before and transformation into NM554 host cells was performed. Single colonies from NM554 were picked from chloramphenicol LB-agar plates and grown overnight for minipreps and DNA sequencing.

DNA sequencing

Sequencing reactions were performed using the Sequenase™ Version 2.0 DNA sequencing kit and [α-^{35}S] dATP from Amersham Life Sciences. The samples were stored at -20 °C until ready to load the sequencing gel.

DNA sequencing gel electrophoresis

Sequencing gels were run using Sequi-Gen Nucleic Acid Sequencing Cell (Bio-Rad, 21 x 50 cm model). Acrylamide gel used was of high grade ready made stock solution (SequaGel-6 from Flowgen). SequaGel-6 (48 ml) was mixed well with 12 ml buffer reagent (SequaGel-6™) in a beaker. Ammonium persulphate (10 %, 0.12 ml) was added to 15 ml of this solution and used to seal the bottom of the gel plates. The remaining solution (45 ml) was mixed with ammonium persulphate (10%, 0.36 ml) and poured in side the glass plates. The gel was allowed to polymerise for at least 3 h. Prior to loading the samples the gel was pre-run at 45 W for 40 minutes in 1x TBE buffer. Sequencing samples were heated at 75 °C for 2 minutes immediately before loading (2 μl) into each well. Electrophoresis was continued for 3 h at 45 W or until the bromophenol blue marker reached the bottom of the gel. The gel was immediately soaked in 5 % (v/v) acetic acid and 15 % (v/v) MeOH for 15 minutes in order to remove urea. After rinsing with water, the gel was transferred onto a Whatman 3MM filter paper and dried for 1-2 h at 50 °C under vacuum.

Autoradiography

Biomax MR film (Kodak) was used for autoradiography throughout this work. Exposure was usually performed for 2 days at room temperature. Films were developed

using Aculux developer for 5 minutes, rinsed briefly with running water and fixed with Ilford Hypam rapid fixer for 5 minutes.

Growth of cells

Wild-type and mutant IPNS clones were kept on chloramphenicol LB agar plates. Glycerol freezes were made from overnight growths in LB broth with appropriate antibiotic and stored at -80 °C in sterile glycerol (15 % final glycerol concentration). The original wild type IPNS (*A. nidulans*) expression plasmid, pJB703, used throughout this study was constructed by J. M. Blackburn, and the expression and growth of clones containing wild type were carried out in *Escherichia coli* strain NM554 as previously described[154].

Recombinant cells carrying the wild type or mutant IPNS (*A. nidulans*) plasmids were used to inoculate flasks of 2YT medium containing 35 mg/ml chloramphenicol. After overnight growth at 37° C cells were harvested by centrifugation and stored at -80°C.

Testing protein expression level

The recombinant cells were tested for expression of proteins. Typically 0.5g of wet cell pellet was lysed with 1.5 ml of 50 mM Tris pH 8 buffer and sonicated for 3 x 10s bursts on ice. The soluble material was collected by centrifugation (15,000 rpm, 10 minutes) of the lysed cells and analysed on SDS-PAGE.

Enzyme purification

Two purification protocols were used depending whether the protein was to be used for bioassays (protocol 1) or crystallisation (protocol 2):

Protocol 1: 2 g of wet cell paste was mixed with 6 ml lysis buffer (50 mM TrisHCl pH 8, 5 mM EDTA, 1 % (v/v) β-mercaptoethanol, 10 % (v/v) glycerol). The lysed cells were sonicated (4 x 10s) and mixed with polyethylineimine 0.01 % (w/v) and centrifuged at 15,000 rpm for 15 minutes. The soluble fraction was loaded onto a Resource Q column (6 ml) previously equilibriated with buffer B (25 mM TrisHCl pH 8.0, 1.0 M NaCl, 1 mM EDTA) followed by several column volumes of buffer A (25 mM TrisHCl pH 8.0). The bound protein was washed with 30 ml of buffer A before elution with a linear gradient of 0-50% buffer B (120 ml). The protein containing fractions (5 ml) were collected and analysed by SDS-PAGE. Protein preparations were desalted using a PD10 (Pharmacia) desalting column and concentrated to ~40 mg/ml in a ultrafiltration cell (Amicon) with PM10 membrane before storage.

Protocol 2: Crystallisation grade IPNS was purified from crude cell lysate using a three column purification as described elsewhere[155].

All protein purification procedures were performed at 4 °C and the purified protein was stored at -80 ° C with little loss of activity for up to 6 months.

IPNS activity

Activity was determined by hole plate assay or a more sensitive HPLC technique.

Hole plate assay

The specific activities of purified IPNS was determined by hole plate assay using *Staphylococcus aureus* N.C.T.C. 6571 as the indicator organism[154].

HPLC assay

This procedure was a modified version of the procedure described earlier[156]. The standard assay mixture contained in a final volume of 100 µl, 2 mM ACV, 4 mM DTT, 1 mM ascorbate, 0.10 mM $FeSO_4$, catalase (0.50 mg/ml), 50 mM Tris pH 8.0 and up to 10 µM (0.33 mg/ml) apo-enzyme. Incubations were terminated after 10 minutes at 28 °C by addition of an equal volume of methanol. The samples were centrifuged for 5 minutes at 11000 x *g* to remove any denatured protein and analysed immediately by HPLC or stored at -20 °C. HPLC analysis was carried out using an ODS C18 column (5 µm, 250 mm x 4.6 mm) and the mobile phase for optimal separation was a gradient of 2.5-45 % acetonitrile in 50 mM potassium phosphate pH 6.8. UV detection was at 220 nm at a sensitivity of 0.04 AUFS. Protein concentrations were determined by the method of Bradford using BSA as standard (*vide supra*). The amount of isopenicillin N produced in the HPLC assays was quantified with by comparison with a standard of synthetic isopenicillin N, calibrated by ^{1}H NMR (500 MHz) analysis.

Analysis of kinetic results

The Leonora program[79] was used to calculate the kinetic parameters K_m and V_{max} under the HPLC assay conditions. All initial velocities were calculated in duplicate and averaged for each calculation. Data was initially analysed using the Lineweaver-Burk Plot and good data (R>0.90) was used for further analysis.

α-KG turnover assay

The decarboxylation of α-KG was measured in purified recombinant wild-type and mutant IPNS enzymes following the procedure of Sabourin and Bierber[157]. Assays were

performed in a total incubation volume of 0.20 ml sealed inside a 5 ml tube fitted with vaccine caps. Each assay mix (in 50 mM Tris pH 7.5 buffer) contained the following cofactors: DTT (5 mM), ascorbate (5 mM), α-KG (2 mM), $FeSO_4$ (2 mM), ammonium sulphate (100 mM), penicillin N (10 mM). [1-^{14}C]-α-KG (NEN, Boston, MA, USA) was diluted with a cold α-KG stock solution to give 180,000 dpm per incubation. For the uncoupled turnover assay, the penicillin N was omitted. Enzyme (up to 26 μM) was added to initiate the reaction and the whole incubation was sealed (vaccine caps). Prior to adding the enzyme 0.20 ml hyamine hydroxide (inside a 0.5 ml unclosed microfuge tube) was placed inside each assay. All incubations were performed inside a shaker at 27 °C for 60 minutes (200 rpm). The reactions were stopped by the injection of 0.20 ml methanol to the incubation through the seal. The microfuge tube containing the radioactive hyamine hydroxide was transferred into a scintillation vial and mixed with 10 ml scintillation fluid (Optiphase Safe) before measuring the radioactivity.

^{1}H NMR studies

The ^{1}H NMR turnover experiments were performed as essentially described for the HPLC assays with the following modifications. The incubation was performed in a total volume of 1 ml containing the following: substrate (1-2 mM), DTT (4 mM), ascorbate (2 mM), $FeSO_4$ (1 mM), catalase (1 mg/ml) and enzyme (up to 260 μM). The assay was performed inside a shaker at 27 °C for 30 minutes (200 rpm) and terminated by the addition of 3 volumes of cold acetone. The mixture was centrifuged (3000 x *g*, 15 minutes) at 4 °C to remove protein debris and the supernatant was rotory evaporated to remove the acetone. The resultant solution (*ca.* 1 ml) was freeze-dried (overnight) and kept in the freezer (-20 °C) until the sample was needed for NMR measurements. The

freeze dried powder was dissolved into D_2O (0.60 ml) containing TSP internal standard (0.4 mM) and filtered into a NMR tube. 500 MHz ^1H NMR was measured in a 5 mm NMR tube (by Mrs Elizabeth McGuiness of the Dyson Perrins Laboratory) on a Bruker AM 500 spectrometer.

Anaerobic crystallisation

Crystallisation trials were performed at 17-20 °C under anaerobic conditions (<0.4 ppm O_2) in a glove box (Belle Technology) using the hanging-drop vapour-diffusion technique. All solutions except the protein were deoxygenated by repeated evacuation followed by argon flushing (repeated 3 times) prior to transfer to the anaerobic glove box. Solid reagents (ACV, ferrous sulphate and sodium dithionite), washed cover-slips and greased Linbro Plates were left inside the glove box for 16 h to further deoxygenate. Apo-IPNS mutant solutions (75 µl aliquots) were ported inside the glove-box and mixed by gentle pipetting to assist deoxygenation by diffusion.

A stock solution containing ferrous sulphate (5-50 mM), ACV (73.5 mM), and apo-protein (50 mg/ml, 1.35 mM) was then prepared by adding the ferrous sulphate solution [4 mg in 75 µl precipitant buffer (2.1 M $LiSO_4$ and 100 mM TrisHCl, pH 8.5)] and ACV (2 mg) to an aliquot of deoxygenated apo-IPNS mutant (75 µl) and used in random screening experiments using 6 µl drops. All drops were seeded by mixing with a microseed solution from crushed wild-type IPNS plate crystals (prepared by Dr Nicolai Burzlaff).

X-ray diffraction analysis

The crystals were withdrawn from the glove box then rapidly transferred to a cryoprotectant mother liquor (100 mM TrisHCl, pH 8.5, 20% (v/v) glycerol saturated at room temperature with lithium sulphate solution) and frozen using a cryostream (Oxford Cryosystems). To minimise radiation damage, oxidation or reaction in the crystals during data collection, data were collected at 100 K under a cold nitrogen stream from a cryostream. Data were processed by Dr Burzlaff.

ACV-NO spectroscopy

Protein (40 mg/ml), ACV-thiol (55 mM), TrisHCl pH 8.0 (2M) were ported inside the glove box and left inside with tops open to allow samples to deaerate for 30 minutes. Protein, buffer, iron and ACV were added to the cuvette in the same order to give final concentrations of one equivalent protein (0.3 mM), one equivalent iron (0.3 mM), five equivalents of ACV (1.5 mM) in 50 mM TrisHCl pH 8.0. The spectra were recorded of the anaerobic samples before and after either NO or O_2 (1 ml) was added to the sample through the rubber seal.

Iron concentration determination

The iron concentrations were measured following the procedure of Fish (1988)[158]. Reagent A was prepared fresh and used within 12 hours and Reagent B was prepared and stored at -20 °C. Sample (1 ml) was mixed with Reagent A (0.5 ml) and incubated at 60 °C for 2 hours followed by cooling on ice. Reagent B (100 μl) was added and mixed well before reading the absorption at 562 nm. A standard curve was obtained by using a standard stock solution of $FeSO_4$ solution (0-200 μM) in the above assay.

Reagent A	Reagent B
0.6 M HCl	80 mg ferrozine (Sigma)
2.25 % $KMnO_4$	80 mg neocuprine (Sigma)
in Milli-Q	8.8g ascorbic acid
	9.7 g ammonium acetate
	make up to 25 ml with Milli-Q

6.3 Experimental for Chapter 4 and 5

Pre-incubation experiments

IPNS was pre-incubated at a protein concentration of 1 mg/ml (26 μM) in buffer E (50 mM TrisHCl, pH 8.0) in a final volume of 1 ml. Combinations of iron (II) sulphate heptahydrate (final concentration up to 0.5 mM), sodium *L*-ascorbate (up to 25 mM), catalase (0.5 mg/ml), BSA (up to 5 mg/ml) were included as indicated. The order of addition of the components were buffer E, catalase or BSA (25 μl), *L*-ascorbate (25 μl of 1.0M solution), H_2O_2 (12 μl of 1.3 % v/v), Fe (II) (25 μl of 20 mM) and finally IPNS (25 μl). Samples 100 μl were removed and rapidly frozen (liquid nitrogen) and tested for IPNS activity as described above.

Anaerobic pre-incubations

Anaerobic pre-incubations experiments, at a dioxygen concentration of less than 0.4 ppm, were performed in a glove box. All solutions were prepared within the glove box. Reduced benzyl viologen remained coloured over periods greater than 6 hours. Frozen IPNS was kept on dry ice while being introduced into the glove box *via* a vacuum chamber port. The IPNS solution was then diluted with anaerobic buffer M. Incubations

were carried out at 20 °C at the same concentrations of iron, ascorbate and enzyme as used for aerobic pre-incubations. Samples (7.5 μl) were then removed at times indicated in the results section and frozen on dry ice. These samples were then removed from the glove box and individually assayed for IPN production over a 20 minutes incubation time. The frozen aliquots were transferred to the assay vials after rapid (<15 seconds) resuspension in 67.5 μl of argon-saturated buffer M.

Ethylene production assays

Ethylene production activity was measured essentially according to the method described by Zhang *et al.*[69] and references therein. IPNS, DAOCS (100-500 μg) or ACC oxidase (10-50 μg) was quickly pipetted into 1 ml of assay mix (3 mM sodium or calcium *L*-ascorbate, DTT 2 mM, 1 mM ACC, 15 mM NH_4HCO_3, 0.1 mM $FeSO_4$, 10% glycerol (v/v) in 0.1 M HEPES, pH 7.1) contained within an 8 ml glass vial. The ascorbate, bicarbonate, iron and DTT stock solutions were made up fresh on the day and care was taken to avoid direct mixing of the ascorbate and iron stock solutions before dilution. Catalase (500 μg) and BSA (100 μg) were included where indicated. ACC oxidase that had been frozen at high concentrations with glycerol was diluted and thoroughly mixed before addition to the assay mix. Upon addition of IPNS, DAOCS or ACC oxidase, the vial was quickly sealed with a rubber vaccine cap and the vial shaken at 27 °C for 1.3-2 hours. 1 ml of the headspace gas above the assay mix was then removed with a syringe and the syringe stopped with a rubber bung prior to injection onto a gas chromatograph (Pye Unicam Series 104 machine equipped with a Porapak R column [Phase Sep, Queensferry, Clwyd]). The temperature settings for the GC were: injector 120 °C, oven 80 °C, and detector 120 °C. Calibration of the GC was carried out

with 1 ml of ethylene standard (at 10 ppm). Peak heights rather than peak areas were used to quantitate amount of gas unless the peak shape of the sample deviated significantly from that of the standard. Activities were calculated using the following expression:

10 x (Sample peak height/calibration peak height) x (1000/μg ACC oxidase used in assay) x 6.9

The factor 6.9 represents the total volume (in ml) of the headspace gas. The activities are therefore reported as nl ethylene per mg ACC oxidase per incubation period (per 2 hours). Conversion of activities to units of nl ethylene per mg ACC oxidase per minute was not performed because of the non-linear production of ethylene with time. Activities for assays performed in the absence of bicarbonate or presence of catalase/BSA/DTT are indicated where shown.

For analysis of C2-C6 olefins a Haysep D GC column was used (1/8" O.D., 1X10 foot, stainless steel, 100-120 mesh, SGE). The column required additional support inside the oven with a metal supporting 'shelf' to prevent the high carrier gas back pressure from blowing the column end off the gas inlet. The oven temperature was 120 ^{o}C. Calibration was performed with a mixture of two to six carbon alkenes (Supelco).

Fragmentation of IPNS

IPNS was incubated as described for the pre-incubation experiments under aerobic conditions. Incubations were quenched by adding 2x SDS-PAGE sample buffer [50 mM Tris-HCl pH 6.8, 4 % (w/v) SDS, 18 % (v/v) glycerol, 0.001 % (w/v) Serva Blue G, 10 % (v/v) β-mercaptoethanol]. Samples were desalted twice, if necessary, using a PD10

desalting column (Pharmacia) or a gel filtration column (Pharmacia, superdex S75 10/30) into low salt buffer (10 mM Tris pH 8.0) for mass spectrometry.

SDS-PAGE

Tris-glycine gels were made according to the method of Laemmli[147]. Protein samples were mixed in 2x reducing gel sample buffer (glycerol 20% (v/v), β-mercaptoethanol 2% (v/v), SDS 2% (w/v), TrisHCl pH 6.8, 62.5 mM, bromophenol blue 0.2% (w/v) and heated for several minutes. at 100°C before loading. Gels were run for 60 minutes at a constant 30 mA and were stained in Coomassie Blue stain [Coomassie Brilliant Blue R250 0.25% (w/v) in methanol 50 % (v/v), acetic acid 10% (v/v)] followed by destaining [methanol 5% (v/v), acetic acid 7.5% (v/v)].

Tris-Tricine gels were run according to the method of Schägger and Jagow[148]. The following stock solutions were made:

Anode buffer (10x):	121.1g Tris base, adjust pH to 8.9 with HCl make up to a final volume of 500 ml with Milli-Q
Cathode buffer (10x):	60.55g Tris base, 89.58 g tricine, 5 g SDS, adjust pH to 8.25 with HCl and make up to a final volume of 500 ml
Acrylamide solution:	30 % (w/v)
Gel buffer (3x)	181.5 g Tris base, 1.5 g SDS, adjust pH to 8.45 make up to 500 ml with Milli-Q
50% (v/v) glycerol:	250 ml glycerol in 500 ml Milli-Q
Sample buffer:	3.6 ml 50% glycerol, 1 ml β-mercaptoethanol, 4 ml 10 % (w/v) SDS, 0.5 ml 1 M TrisHCl pH 6.8, 1 ml 10 % Serva Blue G (w/v), made up to 10 ml

12.5% running gel was made as follows: acrylamide solution (4.17 ml), 50% glycerol (2.12 ml), 3 x gel buffer (3.33 ml), Milli-Q (0.37 ml), TEMED (5 µl), 10% ammonium

persulphate (40 μl). 4 % stacking gel was made as follows: acrylamide solution (0.42 ml), 3 x gel buffer (0.78 ml), Milli-Q (1.93 ml), TEMED (3 μl), 10% ammonium persulphate (25 μl). Several gels were made and stored at 4 °C until required. Gels were run at 15-30 mA (depending on the thickness of the gel) until the dye front had reached the bottom of the gels and were then fixed in 50% Methanol and 10% acetic acid for 30 minutes and stained in Serva blue G (0.012 % w/v) in 10% acetic acid for 1-2 h. Destaining was achieved by shaking the gels in 10% acetic acid for 2 h.

N-Terminal sequence analyses

Fragmentation of IPNS was visualised by electrophoresis of samples (10-40 mg) on 12.5% Tris-glycine SDS-PAGE[147] or 12.5% Tris-tricine SDS-PAGE[148]. Cleaved fragments were blotted on to a Waters Immobilon Membrane in a Bio-Rad Mini Transblot cell at 0.3 A for 1 h in the presence of 10 mM 3-(cyclohexylamino)-1-propanesulfonic acid in 50% methanol (pH 11), and submitted for N-terminal sequencing by Edman degradation (by Mr A. C. Willis, of the O.C.M.S.).

Appendix A

Nucleotide Sequence of the aIPNS Gene (accession number M21882)

```
atgggttcag tcagcaaagc caatgttcca aagatcgatg tttctcccct 51
gtttggagac gaccaagcag ccaaaatgag agtagcccag caaatcgacg 101
ccgcttcgcg tgatactggg tttttctacg ccgtcaacca tgggatcaat 151
gtgcagcgac tctcgcagaa gaccaaggag tttcatatgt ctatcacacc 201
tgaggaaaag tgggaccttg cgattcgtgc ctacaacaaa gagcaccagg 251
accaagtccg tgccggatac tacctgtcca tccccgggaa aaaggcagtc 301
gagtccttct gctaccttaa cccgaacttc acgcccgatc atccccgtat 351
ccaggccaag actcccactc acgaggtaaa cgtgtggcca gacgagacca 401
agcaccctgg tttccaagac tttgccgagc agtattactg ggatgttttc 451
ggtctctctt ctgcactgct caagggctac gccttggcat taggcaaaga 501
ggagaatttc ttcgctcgcc acttcaagcc agacgatact cttgcctcgg 551
ttgtgctgat ccgctaccct tacctggatc cctaccccga ggctgctatc 601
aagacggcgg ccgacggcac caaactgagt tttgagtggc atgaggatgt 651
atccctaatc actgtgcttt accagtccaa cgtgcagaac ctgcaggtag 701
aaactgctgc cgggtatcaa gatatcgagg ccgacgatac tggctacttg 751
atcaactgcg gcagttacat ggcacatctc acaaacaact actataaagc 801
gcccatccat cgggtgaaat gggttaatgc agagcgccag tccctgccat 851
tcttcgtcaa cctgggatac gacagcgtga ttgatccatt tgatccccga 901
gaacccaatg gcaagtctga tcgggagcca ctctcctacg gcgactattt 951
gcaaaacggg ctggtgagtt tgatcaacaa gaacggccag acctag
```

Appendix B

Calibration curve for Tris-tricine SDS-PAGE. Molecular markers (horse-heart globin of known primary sequence) from Pharmacia LKB show: Globin (16949); Globin I + II (14404; Globin I (8159); Globin II (6214); Globin III (2512).

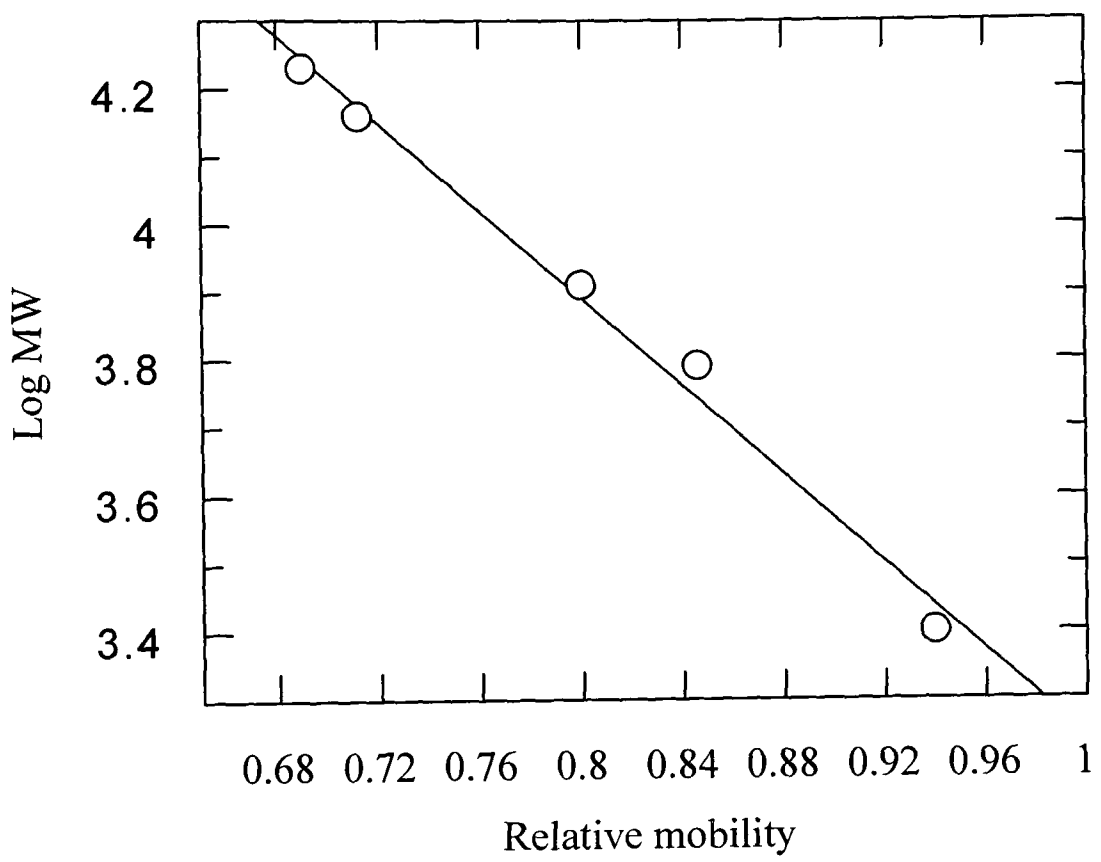

Appendix C

Analysis of inactivation data using first order [In $(A/A_o) = kt$ (top)] and second order rate equation [$1/A-1/A_o = k$ (bottom)]. Condition M (filled squares); condition F (open squares); condition F + BSA 0.5 mg/ml (open circles); condition F + catalase 0.5 mg/ml (filled circles).

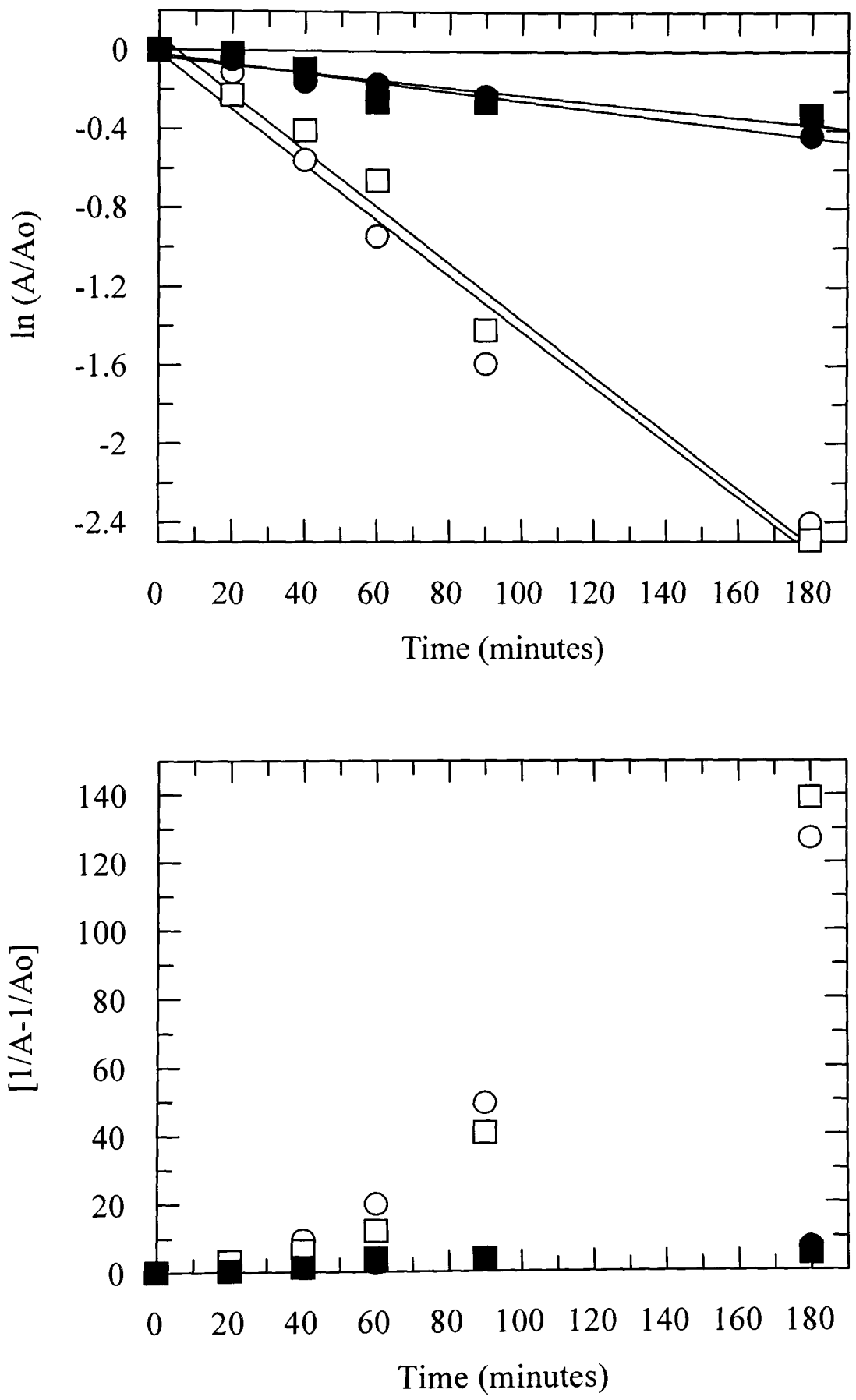

Appendix D

Effect of Ascorbate, Bicarbonate, DTT , α-ketoglutarate and Catalase on Ethylene production in ACCO, IPNS and REXH.

Key: (+) addition, (-) no addition
[1] Asc: sodium ascorbate; Bic : ammonium bicarbonate; Cat: catalase; a-KG: a-ketoglutarate.
[2] Average of more than three determinations

Assay Condition	Asc[1]	ACC	Fe(II)	Bic[1]	BSA	DTT	Cat[1]	αKG[1]	WT IPNS (nl/mg)	REXH (nl/mg)	ACCO (nl/mg)	Buffer only (nl)
7	-	+	+	-	+	+	+	-	-	-	-	6
8	-	+	+	+	+	+	-	-	120, 159	-	-	125 [2]
9	-	+	+	+	+	+	-	+	77	91	-	27
10	-	+	+	+	+	-	-	+	16	26	-	8.2
11	-	+	+	-	+	-	-	+	5.8	6.5	-	2.3
12	-	+	+	+	+	-	-	-	103	-	-	47
13	-	+	+	+	+	-	+	-	2.5	-	-	0.29
14	-	+	+	-	+	-	+	+	1	-	-	0.42

References

1. Singh, K.M. & Deopujari, S.W. "Experimental approach to the chemical evolution of iron containing enzymes: role of mixed ligand complexes of iron(II)" *Origins of Life and Evolution of the Biosphere* **16**, 496-497 (1986).

2. Cowen, J.P. & Bruland, K.W. "Metal deposits associated with bacteria: implications for iron and manganese marine biogeochemistry" *Deep Sea Research Part A: Oceanographic Research Papers* **32**, 253 et seq. (1985).

3. Bowen, H.J.M. *Environmental Chemistry of the Elements* (Academic Press, New York, 1979).

4. Halliwell, B. & Gutteridge, J.M.C. "Oxygen toxicity, oxygen radicals, transition metals and disease" *Biochemical Journal* **219**, 1-14 (1984).

5. Prasad, A.S. & Oberleas, D. (eds.) *Trace Elements in Human Health and Disease* (Academic Press, New York, 1976).

6. Aisen, P. & Listowsky, I. "Iron transport and storage proteins" *Annual Review of Biochemistry* **49**, 357-393 (1980).

7. Chase, Z. & Price, N.M. "Metabolic consequences of iron deficiency in heterotrophic marine protozoa" *Limnology and Oceanography* **42**, 1673-1684 (1997).

8. Theil, E.C. & Raymond, K.N. Transition metal storage, transport and biomineralization in *Bioinorganic Chemistry* (eds. Bertini, I., Gray, H.B., Lippard, S. & Valentine, J.) (University Science Books, Mill Valley, CA, 1994).

9. Theil, E.C. *Annual Review of Biochemistry* **55**, 289 (1987).

10. Cartwright, G.E. & Lee, G.R. "Anaemia" *British Journal of Haematology* **21**, 147 (1971).

11. Rodriguez-Matas, M.C., Campos, M.S., Lopez-Aliaga, I., Gomez-Ayala, A.E. & Lisbona, F. "Iron manganese interactions in the evolution of iron deficiency" *Annals of Nutrition and Metabolism* **42**, 96-109 (1998).

12. Quicho, F.A. & Lipscomb, W.N. "Carboxypeptidase A" *Advances in Protein Chemistry* **25**, 1-78 (1971).

13. Liljas, A., Kannan, K.K., Bergsten, P.C., Waara, I., Fridborg, K., Strandberg, B., Carlbom, U., Jarup, L., Lovgren, S. & Petef, M. "Crystal structure of human carbonic anhydrase at 2Å" *Nature New Biology* **235**, 131 (1972).

14. Vallee, B.L., Coleman, J.E. & Auld, D. "Zinc fingers, zinc clusters, and zinc twists in DNA binding protein domains" *Proceeding of the National Academy of Sciences USA* **88**, 999-1003 (1991).

15. Takano, T., Kallai, O.B., Swanson, R. & Dickerson, R.E. "X-ray crystal structure of cytochrome *c* from tuna" *Journal of Biological Chemistry* **248**, 5244 (1973).

16. Bertini, I., Gray, H.B., Lippard, S. & Valentine, J. (eds.) *Bioinorganic Chemistry* (University Science Books, California, 1994).

17. Fenna, R.E. & Matthews, B.W. "Chlorophyll arrangements in a bacteriochlorophyll protein from *Chlorobium limicola*" *Nature* **258**, 573-577 (1975).

18. Watenpaugh, K.D., Sieker, L.C. & Jensen, L.H. "X-ray crystal structure of rubredoxin from *Clostridium pasteurianum*" *Journal of Molecular Biology* **138**, 615 (1980).

19. Colman, P.M., Freema, H.C., Guss, J.M., Murata, M., Norris, V.A., Ramshaw, J.A.M. & Venkatappa, M.P. "X-ray crystal structure analysis of plastocyanin at 2.7 Å" *Nature* **272**, 319-324 (1978).

20. Bush, K. "Metallo β-lactamases: a class apart" *Clinical Infectious Diseases* **27**, S48-S53 (1998).

21. Brzozowski, A., Derewenda, Z., Dodson, E., Dodson, G., Grabowski, M., Liddington, R., Skarzynski, T. & Vallely, D. "Bonding of molecular oxygen to T state human hemoglobin" *Nature* **307**, 74-76 (1984).

22. Shaanan, B. "The iron oxygen bond in human oxyhemoglobin" *Nature* **296**, 683-684 (1982).

23. Anderson, B.F., Baker, H.M., Dodson, E.J., Norris, G.E., Rumball, S.V., Waters, J.M. & Baker, E.N. "Structure of human lactoferrin at 3.2 Å resolution" *Proceedings of the National Academy of Sciences USA* **84**, 1769-1773 (1987).

24. Roach, P.L., Clifton, I.J., Fulop, V., Harlos, K., Barton, G.J., Hajdu, J., Andersson, I., Schofield, C.J. & Baldwin, J.E. "Crystal structure of isopenicillin N synthase is the first from a new structural family of enzymes" *Nature* **375**, 700-704 (1995).

25. Stenkemp, R.E. "Haemerythrin" *Chemical Review* **94**, 715-726 (1994).

26. Rosenzweig, A.C., Frederick, C.A., Lippard, S.J. & Nordlund, P. "Crystal structure of a bacterial non-haem iron hydroxylase that catalyses the biological oxidation of methane" *Nature* **366**, 537-543 (1993).

27. Tainer, J.A., Getzoff, E.G., Richardson, J.S. & Richardson, D.C. "The crystal structure of Cu^{2+}-Zn^{2+} superoxide dismutase at 2 Å" *Nature* **306**, 284 (1983).

28. Messerschmidt, A., Ladenstein, R., Huber, R., Bolognesi, M., Avigliano, L., Petruzzelli, R., Rossi, A. & Finazziagro, A. "Refined crystal structure of ascorbate oxidase at 1.9 Å resolution" *Journal of Molecular Biology* **224**, 179-205 (1992).

29. Mandal, S.K. & Que, L. "Models for amide ligation in nonhaem iron enzymes" *Inorganic Chemistry* **36**, 5424-5425 (1997).

30. Zang, Y. & Que, L. "Structure and reactivity of Fe(II)-SAr complexes: relevance to the active site of isopenicillin N synthase" *Inorganic Chemistry* **34**, 1030-1035 (1995).

31. Whiting, A.K., Boldt, Y.R., Hendrich, M.P., Wackett, L.P. & Que, L. *Biochemistry* **35**, 160-170 (1996).

32. Nordlund, P., Dalton, H. & Eklund, H. "The active site structure of methane monooxygenase is closely related to the binuclear iron center of ribonucleotide reductase" *FEBS Letters* **307**, 257-262 (1992).

33. Ching, L. "Crystal structure of proline 3-hydroxylase" *in preparation* (1998).

34. Valegard, K., Van Scheltinga, A.C.T., Lloyd, M.D., Hara, T., Ramaswamy, S., Perrakis, A., Thompson, A., Lee, H.J., Baldwin, J.E., Schofield, C.J., Hajdu, J. & Andersson, I. "Structure of a cephalosporin synthase" *Nature* **394**, 805-809 (1998).

35. Olendorf, D.H., Lipscomb, J.D. & Weber, P.C. "The crystal structure of protocatechuate 3,4-dioxygenase" *Nature* **336**, 403-405 (1988).

36. Frazee, R.W., Orville, A.M., Dolbeare, K.B., Yu, H., Ohlendorf, D.H. & Lipscomb, J.D. "The axial tyrosinate Fe^{3+} ligand in protocatechuate 3,4-dioxygenase influences substrate binding and product release: evidence for new reaction cycle intermediates" *Biochemistry* **37**, 2131-2144 (1998).

37. Ahmed, M. & Focht, D.D. "Degradation of polychlorinated biphenyls by two species of *Achromobacter*" *Canadian Journal of Microbiology* **19**, 47-52 (1973).

38. Senda, T., Sugiyama, K., Narita, H., Yamamoto, T., Kimbara, K., Fukada, M., Sato, M., Yano, K. & Mitsui, Y. "Three dimensional structures of free form and two substrate complexes of an extradiol ring cleveage type dioxygenase, the BphC enzyme from *Pseudomonas* sp. strain KKS102" *Journal of Molecular Biology* **255**, 735-752 (1996).

39. Ford-Hutchinson, A.W., Gresser, M. & Young, R.N. "Lipoxygenases" *Annual Review of Biochemistry* **63**, 383-417 (1994).

40. Chasteen, N.D., Grady, J.K., Skorey, K.I., Neden, K.J., Riendeau, D. & Percival, M.D. "Characterization of the nonheme iron center of human 5-lipoxygenase by EPR, fluorescence, and ultraviolet-visible spectroscopy: redox cycling between ferrous and ferric states" *Biochemistry* **32**, 9763-9771 (1993).

41. Steczko, J., Donoho, G.P., Clemens, J.C., Dixon, J.E. & Axelrod, B. "Conserved histidine residues in soybean lipoxygenase: functional consequences of their replacement" *Biochemistry* **31**, 4053-4057 (1992).

42. Boyington, J.C., Gaffney, B.J. & Amzel, L.M. "The three-dimensional structure of an arachidonic acid 15-lipoxygenase" *Science* **260**, 1482-1486 (1993).

43. Minor, W., Steczko, J., Bolin, J.T., Otwinowski, Z. & Axelrod, B. "Crystallographic determination of the active site iron and its ligands in soybean lipoxygenase-1" *Biochemistry* **32**, 6320-6323 (1993).

44. Kramer, J.A., Johnson, K.R., Dunham, W.R., Sands, R.H. &. Funk, M.O. "Position 713 is critical for catalysis but not iron binding in soybean lipoxygenase-3" *Biochemistry* **33**, 15017-15022 (1994).

45. Fleming, A. "On the antibacterial action of cultures of *Penicillium*, with special reference to their use in the isolation of *B. influenzae*" *British Journal of Experimental Bacteriology* **10**, 226-236 (1929).

46. Levy, S.B. "The challenge of antibiotic resistance" *Scientific American* March (1998).

47. Arstein, H.R.V. & Morris, D. "ACVS" *Biochemical Journal* **76**, 357-361 (1960).

48. Banko, G., Demain, A. & Wolfe, S. "Non-ribosomal synthesis of ACV" *Journal of American Chemical Society* **109**, 2858-2860 (1987).

49. Baldwin, J.E. & Bradley, M. "Isopenicillin N synthase - mechanistic studies" *Chemical Reviews* **90**, 1079-1088 (1990).

50. Borovok, I., Landman, O., Kreisberg-Zakarin, R., Aharonowitz, Y. & Cohen, G. "Ferrous active site of isopenicillin N synthase: genetic and sequence analysis of the endogenous ligands" *Biochemistry* **35**, 1981-1987 (1996).

51. Tan, S.H. & Sim, T.S. "Functional analysis of conserved histidine residues in *Cephalosporium acremonium* isopenicillin N synthase by site-directed mutagenesis" *Journal of Biological Chemistry* **271**, 889-894 (1996).

52. Roach, P.L., Clifton, I.J., Hensgens, C.M.H., Shibata, N., Schofield, C.J., Hajdu, J. & Baldwin, J.E. "Structure of isopenicillin N synthase complexed with substrate and the mechanism of penicillin formation" *Nature* **387**, 827-830 (1997).

53. Chen, V.J., Orville, A.M., Harpel, M.R., Frolik, C.A., Surerus, K.K., Munck, E. & Lipscomb, J.D. "Spectroscopic studies of isopenicillin N synthase: a mononuclear nonheme Fe^{2+} oxidase with metal coordination sites for small molecules and substrate" *Journal of Biological Chemistry* **264**, 21677-21681 (1989).

54. Randall, C.R., Zang, Y., True, A.E., Que, L., Charnock, J.M., Garner, C.D., Fujishima, Y., Schofield, C.J. & Baldwin, J.E. "X-ray absorption studies of the ferrous active site of isopenicillin N synthase and related model complexes" *Biochemistry* **32**, 6664-6673 (1993).

55. Long, A. *D. Phil. Thesis* Oxford University (1998).

56. Baldwin, J.E., Abraham, E.P., Adlington, R.M., Chakravarti, B., Derome, A.E., Murphy, J.A., Field, L.D., Green, N.B., Ting, H.H. & Usher, J.J. "Penicillin biosynthesis - dual pathways from a modified substrate" *Journal of the Chemical Society-Chemical Communications* , 1317-1319 (1983).

57. Orville, A.M., Chen, V.J., Kriauciunas, A., Harpel, M.R., Fox, B.G., Munck, E. & Lipscomb, J.D. "Thiolate ligation of the active site Fe^{2+} of isopenicillin N synthase derives from substrate rather than endogenous cysteine - spectroscopic studies of site-specific Cys to Ser mutated enzymes" *Biochemistry* **31**, 4602-4612 (1992).

58. Rollins, M.J., Westlake, D.S., Wolfe, S. & Jensen, S.E. *Canadian Journal of Microbiology* **133**, 1196-1202 (1988).

59. Hanauskeabel, H.M. & Gunzler, V. "A stereochemical concept for the catalytic mechanism of prolylhydroxylase - applicability to classification and design of inhibitors" *Journal of Theoretical Biology* **94**, 421-455 (1982).

60. Lloyd, M.D., Valegard, K., Van Scheltinga, A.C.T., Hara, T., Ramaswamy, S., Perrakis, A., Thompson, A., Lee, H.J., Baldwin, J.E., Schofield, C.J., Hajdu, J. & Andersson, I. "Studies on the active site of deacetoxycephalosporin C synthase" *in preparation* (1998).

61. Prescott, A.G. "A dilemma of dioxygenases (or where biochemistry and molecular biology fail to meet)" *Journal of Experimental Botany* **44**, 849-861 (1993).

62. Burg, S.P. "The physiology of ethylene formation" *Annual Review of Plant Physiology* **13**, 265-302 (1962).

63. Yang, S.F. & Hoffman, N.E. *Annual Review of Plant Physiology* **35**, 155-189 (1984).

64. Smith, J.J., Zhang, Z.H., Schofield, C.J., John, P. & Baldwin, J.E. "Inactivation of 1-aminocyclopropane-1-carboxylate (ACC) oxidase" *Journal of Experimental Botany* **45**, 521-527 (1994).

65. Dong, J.G., Fernandezmaculet, J.C. & Yang, S.F. "Purification and characterization of 1-aminocyclopropane-1-carboxylate oxidase from apple fruit" *Proceedings of the National Academy of Sciences USA* **89**, 9789-9793 (1992).

66. Zhang, Z.H., Barlow, J.N., Baldwin, J.E. & Schofield, C.J. "Metal catalyzed oxidation and mutagenesis studies on the iron(II) binding site of 1-aminocyclopropane-1-carboxylate oxidase" *Biochemistry* **36**, 15999-16007 (1997).

67. Shaw, J.F., Chou, Y.S., Chang, R.C. & Yang, S.Y. *Biochemical Biophysical Research Communication* **225**, 697-700 (1996).

68. Lay, V.J., Prescott, A.G., Thomas, P.G. & John, P. "Heterologous expression and site-directed mutagenesis of the 1- aminocyclopropane-1-carboxylate oxidase from kiwi fruit" *European Journal of Biochemistry* **242**, 228-234 (1996).

69. Zhang, Z.H., Schofield, C.J., Baldwin, J.E., Thomas, P. & John, P. "Expression, purification and characterization of 1-aminocyclopropane-1-carboxylate oxidase from tomato in *Escherichia coli*" *Biochemical Journal* **307**, 77-85 (1995).

70. Barlow, J.N., Zhang, Z.H., John, P., Baldwin, J.E. & Schofield, C.J. "Inactivation of 1-aminocyclopropane-1-carboxylate oxidase involves oxidative modifications" *Biochemistry* **36**, 3563-3569 (1997).

71. Ming, L.J., Que, L., Kriauciunas, A., Frolik, C.A. & Chen, V.J. "NMR studies of the active site of isopenicillin N synthase, a nonheme iron(II) enzyme" *Biochemistry* **30**, 11653-11659 (1991).

72. Wang, Y. & Li, R. Accession number D78166 (Swissprot database, 1996).

73. Lee, M.H., Zhang, Z.H., McKinnon, C.H., Baldwin, J.E. & Crouch, C.P. "The C-terminal of rat 4-hydroxyphenylpyruvate is indispensible for enzyme activity" *FEBS Letters* **393**, 269--272 (1996).

74. Alber, T. "Mutational effects on protein stability" *Annual Review of Biochemistry* **58**, 765-798 (1989).

75. Deng, W.P. & Nicoloff, J.A. *Analytical Biochemistry* **200**, 81 (1992).

76. Shibata, N., Lloyd, M.D., Baldwin, J.E. & Schofield, C.J. "Adipoyl-6-aminopenicillanic acid is a substrate for deacetoxycephalosporin C synthase (DAOCS)" *Bioorganic & Medicinal Chemistry Letters* **6**, 1579-1584 (1996).

77. Jensen, S.E., Westlake, D.W.S. & Wolfe, S. *Journal of Antibiotics* **35**, 1026-1032 (1985).

78. Ramos, F.R., Lopez-Nieto, M.J. & Martin, J.F. "Isopenicillin N synthase of *Penicillium chrysogenum*, an enzyme that converts ACV to isopenicillin N." *Antimicrobial Agents Chemotherapy* **27**, 380-387 (1985).

79. Cornish-Bowden, A. *Analysis of Enzyme Kinetic Data* (Oxford University Press, Oxford, 1995).

80. Kriauciunas, A., Frolik, C.A., Hassell, T.C., Skatrud, P.L., Johnson, M.G., Holbrook, N.L. & Chen, V.J. "The functional role of cysteines in isopenicillin N synthase - correlation of cysteine reactivities toward sulfhydryl reagents with kinetic properties of cysteine mutants" *Journal of Biological Chemistry* **266**, 11779-11788 (1991).

81. Landman, O., Borovok, I., Aharonowitz, Y. & Cohen, G. "The glutamine ligand in the ferrous iron active site of isopenicillin N synthase of *Streptomyces jumonjinensis* is not essential for catalysis" *FEBS Letters* **405**, 172-174 (1997).

82. Que, L. & Ho, R.Y.N. "Dioxygen activation by enzymes with mononuclear non-haem iron active sites" *Chemical Reviews* **96**, 2607-2623 (1996).

83. Dubus, A. *personal communication* (1998).

84. Lange, S.J. & Que, L. "Oxygen activating nonhaem iron proteins" *Current Opinions in Chemical Biology* **2**, 159-172 (1998).

85. McCafferty, D.G., Lessard, I.A.D. & Walsh, C.T. "Mutational analysis of potential zinc-binding residues in the active site of the enterococcal *D*-Ala-*D*-Ala dipeptidase VanX" *Biochemistry* **36**, 10498-10505 (1997).

86. Myllyharju, J. & Kivirikko, K.I. "Characterization of the iron and 2-oxoglutarate binding sites of human prolyl 4-hydroxylase" *EMBO Journal* **16**, 1173-1180 (1997).

87. Goodwill, K.E., Sabatier, C., Marks, C., Raag, R., Fitzpatrick, P. & Stevens, R.C. "Crystal structure of tyrosine hydroxylase at 2.3 Å and its implications for inherited neurodegenerative diseases" *Nature Structural Biology* **4**, 578-585 (1997).

88. Whiting, A.K., Que, L., Saari, R.E., Hausinger, R.P. & Frederick, M.A. "Metal coordination environment of a Cu(II) substituted α-keto acid dependent dioxygenase that degrades the herbicide 2,4-D" *Journal of American Chemical Society* **119**, 3413-3414 (1997).

89. Robbins, A.H. & Stout, C.D. "Rubredoxins" *Proceedings of the National Academy of Sciences USA* **86**, 3639 (1989).

90. Bradley, M. *D. Phil. Thesis* Oxford University (1990).

91. Roach, P.L., Clifton, I.J., Hensgens, C.M.H., Shibata, N., Long, A.J., Strange, R.W., Hasnain, S.S., Schofield, C.J., Baldwin, J.E. & Hajdu, J. "Anaerobic crystallisation of an isopenicillin N synthase:Fe(II):substrate complex demonstrated by X-ray studies" *European Journal of Biochemistry* **242**, 736-740 (1996).

92. Lindstedt, S. & Rundgren, M. "Blue color, metal content, and substrate binding in 4-hydroxyphenylpyruvate dioxygenase from *Pseudomonas* sp. strain P.J. 874" *Journal of Biological Chemistry* **257**, 11922-11931 (1982).

93. Cooper, P.D. "Critical effect of oxygen tension on growth rate of animal cells in continuous suspended culture" *Nature* **182**, 1508-1509 (1958).

94. Gerschman, R., Gilbert, D.l., Nye, S.W., Dyer, P. & Fenn, W.O. "Oxygen poisoning and X-irradiation: a mechanism in common" *Science* **119**, 623-626 (1954).

95. Halliwell, B. & Gutteridge, J.M.C. "Role of iron in oxygen radical reactions" *Methods in Enzymology* **105**, 47-56 (1984).

96. Sawyer, D.T. & Valentine, J.S. "How super is superoxide ?" *Accounts of Chemical Research* **14**, 393-400 (1981).

97. Haber, F. & Weiss, J. "The catalytic decomposition of hydrogen peroxide by iron salts" *Proceedings of the Royal Society, London* **147**, 332-342 (1934).

98. Henle, E.S. & Lin, S. "Formation, prevention, and repair of DNA damage by iron/hydrogen peroxide" *Journal of Biological Chemistry* **272**, 19095-19098 (1997).

99. Lyras, L., Cairns, N.J., Jenner, A., Jenner, P. & Halliwell, B. "An assessment of oxidative damage to proteins, lipids, and DNA in brain from patients with Alzheimer's disease" *Journal of Neurochemistry* **68**, 2061-2069 (1997).

100. Berlett, B.S. & Stadtman, E.S. "Protein oxidation in aging, disease, and oxidative stress" *Journal of Biological Chemistry* **272**, 20313-20316 (1997).

101. Sawyer, D., Sobkowiak, A. & Matsushita, T. "Metal hydroperoxide induced activation of dioxygen for the oxygenation of hydrocarbons: oxygenated Fenton chemistry" *Accounts of Chemical Research* **29**, 409-416 (1996).

102. Walling, C. (ed.) *The nature of the primary oxidants in oxidation mediated by metal ions* 85-98 (Pergamon, 1982).

103. Sutton, H.C. & Winterbourn, C.C. "On the participation of higher oxidation states of iron and copper in Fenton reactions" *Free Radical Biology and Medicine* **6**, 53-60 (1989).

104. Rush, J.D. & Koppenol, W.H. "Oxidising intermediates in the reaction of ferrous-EDTA with hydrogen peroxide" *Journal of Biological Chemistry* **261**, 6730-6733 (1986).

105. Gutteridge, J.C., Maidt, L. & Poyer, L. "Superoxide dismutase and Fenton chemistry: reaction of ferric-EDTA complex and ferric-bipyridyl complex with hydrogen peroxide without the apparent formation of iron(II)" *Biochemical Journal* **269**, 169-174 (1990).

106. Stadtman, E.R. "Metal ion catalysed oxidation of proteins: biochemical mechanisms and biological consequences" *Free Radical Biology and Medicine* **9**, 315-325 (1990).

107. Halliwell, B. & Foyer, C.H. *Biochemical Journal* **155**, 697-700 (1976).

108. Shinar, E., Navok, T. & Chevion, M. "The analogous mechanism of enzymatic inactivation induced by ascorbate and superoxide in the presence of copper" *Journal of Biological Chemistry* **258**, 14778-14783 (1983).

109. Udenfriend, S., Clarke, C.T., Axelrod, J. & Brodie, B.B. *Journal of Biological Chemistry* **208**, 731-739 (1954).

110. Pogozelski, W.K., McNeese, T.J. & Tullis, T.D. "What species is responsible for strand scission in the reaction of Fe(II)-EDTA and H_2O_2 with DNA?" *Journal of American Chemical Society* **117**, 6428-6433 (1995).

111. Feig, A.L. & Lippard, S.J. "Reactions of nonheme iron(II) centers with dioxygen in biology and chemistry" *Chemical Reviews* **94**, 759-805 (1994).

112. Stadtman, E.R. "Oxidation of free amino acid residues in proteins by radiolysis and by metal-catalysed reactions" *Annual Review of Biochemistry* **62**, 797-821 (1993).

113. Chou, W.T., Tsai, W., Lin, C. & Chang, G. "Selective modification and affinity cleavage of pigeon liver malic enzyme by the copper ascorbate system" *Journal of Biological Chemistry* **270**, 25935-25941 (1995).

114. Levine, R.L. "Oxidative modification of glutamine synthetase" *Journal of Biological Chemistry* **258**, 11828-11833 (1983).

115. Wiseman, H. & Halliwell, B. "Damage to DNA by reactive oxygen and nitrogen species: role in inflammatory disease and progression to cancer" *Biochemical Journal* **313**, 17-29 (1996).

116. Stadtman, E.R. "Protein oxidation and aging" *Science* **257**, 1220-1224 (1992).

117. Halliwell, B. & Jenner, P. "Impaired clearance of oxidised proteins in neurodegenerative diseases" *Lancet* **351**, 1510 (1998).

118. Halliwell, B. & Gutteridge, J.M.C. "Lipid peroxidation in brain homogenates: the role of iron and hydroxyl radicals" *Journal of Neurochemistry* **69**, 1330 (1997).

119. Olson, T.S. & Dice, J.F. "Regulation of protein degradation rates in eukaryotes" *Current Opinion in Cell Biology* **1**, 1194-1200 (1989).

120. Varshavsky, A. "The N-end rule" *Cell* **69**, 725-735 (1992).

121. Fucci, L., Oliver, C.N., Coon, M.J. & Stadtman, E. "Inactivation of key metabolic enzymes by mixed-function oxidation reactions: possible implication in protein turnover and aging" *Proceedings of the National Academy of Sciences, USA* **80**, 1521-1525 (1983).

122. Rivett, A.J. "Preferential degradation of oxidatively modified forms of glutamine synthetase by intracellular mammalian proteases" *Journal of Biological Chemistry* **260**, 300-305 (1985).

123. Lawrence, C.C. *D. Phil. Thesis* Oxford University (1993).

124. Cooper, R.D.G. "The enzymes involved in the biosynthesis of penicillin and cephalosporin - structure and function" *Abstracts of Papers of the American Chemical Society* **206**, 3-ORGN (1993).

125. Myllyla, R., Majamaa, K., Gunzler, V., Hanauskeabel, H.M. & Kivirikko, K.I. "Ascorbate is consumed stoichiometrically in the uncoupled reactions catalysed by prolyl 4-hydroxylase" *Journal of Biological Chemistry* **259**, 5403-5405 (1984).

126. Nietfield, J.J. & Kemp, A. "The function of ascorbate with respect to prolyl 4-hydroxylase activity" *Biochemica Biophysica Acta* **657**, 159-167 (1981).

127. Rowe, C.J. *D. Phil. Thesis* Oxford University (1995).

128. Fujishima, Y. *D. Phil. Thesis* Oxford University (1992).

129. Pang, C.P., Chakravarti, B., Adlington, R.M., Ting, H.H., White, R.L., Jayatilake, G.S., Baldwin, J.E. & Abraham, E.P. "Purification of isopenicillin N synthetase" *Biochemical Journal* **222**, 789-785 (1984).

130. Castro, J.M., Liras, P., Laiz, L., Cortes, J. & Martin, J. "Purification and characterisation of the isopenicillin N synthase of *Streptomyces lactamdurans*" *Journal of Microbiology* **134**, 133-141 (1988).

131. Lange, T., Hedden, P. & Graebe, J.E. "Expression and cloning of a gibberellin 20 oxidase, a multifunctional enzyme involved in gibberellin biosynthesis" *Proceedings of the National Academy of Sciences USA* **91**, 8552-8556 (1994).

132. Britsch, L. & Grisebach, H. "Purification and characterisation of (2-*S*) flavanone-3-hydroxylase from *Pertunia hydrida*" *European Journal of Biochemistry* **156**, 569-577 (1986).

133. Yu, R., Kurata, T. & Arakawa, N. "The role of ascorbic acid in proline hydroxylation: the behavior of *L*-ascorbic acid in the prolyl 4-hydroxylase reaction" *Agricultural and Biological Chemistry* **52**, 729-733 (1988).

134. Lawlor, E.J., Elson, S.W., Holland, S., Cassels, R., Hodgson, J.E., Lloyd, M.D., Baldwin, J.E. & Schofield, C.J. "Expression in *Escherichia coli* of a clavaminic acid synthase isozyme- a trifunctional oxygenase involved in clavulanic acid biosynthesis" *Tetrahedron* **50**, 8737-8748 (1994).

135. Levine, R.L., Oliver, C.N., Fulks, R.M. & Stadtman, E.R. "Turnover of bacterial glutamine synthetases: oxidative inactivation precedes proteolysis" *Proceedings of the National Academy of Sciences USA* **78**, 2120-2124 (1981).

136. Cabiscol, E., Aguilar, J. & Ros, J. "Metal catalysed oxidation of Fe^{2+} dehydrogenases" *Journal of Biological Chemistry* **269**, 6592-6597 (1994).

137. Blanchard, J.S., England, S. & Kondo, A. "γ-Butryrobetaine hydroxylase- a unique protective effect of catalase" *Archives of Biochemistry and Biophysics* **219**, 327-334 (1982).

138. McCrae, D., Coker, J.A., Legge, R.L. & Thompson, J.E. "Bicarbonate/CO_2 facilitated conversion of 1-aminocyclopropane-1-carboxylic acid to ethylene in model systems and intact tissues" *Plant Physiology* **73**, 784-790 (1983).

139. Gibson, E.J. *D. Phil. Thesis* Oxford University (1997).

140. Ituriagagotia-Bueno, T., Gibson, E.J., Schofield, C.J. & John, P. "Inhibition of 1-aminocyclopropane-1-carboxylate oxidase by 2-oxoacids" *Phytochemistry* **43**, 343-349 (1996).

141. Fawcett, P.A., Usher, J.J., Huddleston, J.A., Bleany, R.C., Nisbet, J.J. & Abraham, E.P. *Biochemical Journal* **157**, 651-660 (1976).

142. Greiner, D.P., Hughes, K.A., Gunasekera, A.H. & Meares, C.F. "Binding of the σ70 protein to the core subunits of *Eschericia coli* RNA polymerase, studied by iron-EDTA protein footprinting" *Proceedings of the National Academy of Sciences USA* **93**, 71-75 (1996).

143. Barlow, J.N., Baldwin, J.E., Clifton, I.J., Hensgens, C.M.H., Hajdu, J., Hara, T., Hassan, A., John, P., Lloyd, M.D., Roach, P.L., Prescott, A., Robinson, J.K., Zhang, Z.H. & Schofield, C.J. "Studies on non-haem ferrous-dependent oxygenases and oxidases" *Biochemical Society Transactions* **25**, 86-90 (1997).

144. Rivett, A.J. & Levine, R.L. "Metal catalysed oxidation of *Escherichia coli* glutamine synthetase: correlation of structural and functional changes" *Archives of Biochemistry and Biophysics* **278**, 26-34 (1990).

145. Climent, I., Tsai, L. & Levine, R.L. "Derivatisation of γ-glutamyl semialdehyde residues in oxidised proteins by fluoresceinamine" *Analytical Biochemistry* **182**, 226-232 (1989).

146. Kim, K., Rhee, S.G. & Stadtman, E.A. "Nonenzymatic cleavage of proteins by reactive oxygen species generated by dithiothreitol and iron" *Journal of Biological Chemistry* **260**, 15394-15397 (1985).

147. Laemmli, U.K. "Cleavage of structural proteins during assembly of the head of bacteriophage T4" *Nature* **227**, 680-685 (1970).

148. Schagger, H. & Jagow, G.V. "Tricine sodium dodecyl sulphate polyacrylamide gel electrophoresis for the separation of proteins in the range from 1 to 100kDa" *Analytical Biochemistry* **166**, 368-379 (1987).

149. Ettner, N., Metzger, J.W., Lederer, T., Hulmes, J.D., Kisker, C., Hinrichs, W., Ellestad, G.A. & Hillin, W. "Proximity mapping of the tet repressor tetracycline Fe^{2+} complex by hydrogen peroxide mediated protein cleavage" *Biochemistry* **34**, 22-31 (1995).

150. Hassan, A. *D. Phil. Thesis* Oxford University (1998).

151. Barlow, J.N. *D. Phil. Thesis* Oxford University (1996).

152. Bradford, M.M. *Analytical Biochemistry* **72**, 248-254 (1976).

153. Sambrook, J., Fritsch, E.F. & Maniatis, T. *Molecular Cloning, A Laboratory Manual* (Cold Spring Harbor Laboratory, Cold Spring Harbor, New York, 1989).

154. Baldwin, J.E., Blackburn, J.M., Sutherland, J.D. & Wright, M.C. "High level soluble expression of isopenicillin N synthase isoenzymes in *E. coli*" *Tetrahedron* **47**, 5991-6002 (1991).

155. Roach, P.L., Schofield, C.J., Baldwin, J.E., Clifton, I.J. & Hajdu, J. "Crystallization and preliminary X-ray diffraction studies on recombinant isopenicillin N synthase from *Aspergillus nidulans*" *Protein Science* **4**, 1007-1009 (1995).

156. Sami, M., Brown, T.J.N., Roach, P.L., Schofield, C.J. & Baldwin, J.E. "Glutamine-330 is not essential for activity in isopenicillin N synthase from *Aspergillus nidulans*" *FEBS Letters* **405**, 191-194 (1997).

157. Sabourin, P.J. & Bieber, L.L. "Purification and characterisation of an α-ketoisocaproate oxygenase of rat liver" *Journal of Biological Chemistry* **257**, 7460-7467 (1982).

158. Fish, W. "Rapid colorimetric micromethod for the quantitation of complexed iron in biological samples" *Methods in Enzymology* **158**, 357-364 (1988).